# Resource Allocation in Future Green Wireless Networks: Applications and Challenges

by

Ha Vu TRAN

MANUSCRIPT-BASED THESIS PRESENTED TO ÉCOLE DE TECHNOLOGIE SUPÉRIEURE IN PARTIAL FULFILLMENT FOR THE DEGREE OF DOCTOR OF PHILOSOPHY
Ph.D.

MONTREAL, DECEMBER 12, 2019

ÉCOLE DE TECHNOLOGIE SUPÉRIEURE
UNIVERSITÉ DU QUÉBEC

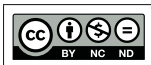

**BOARD OF EXAMINERS**

THIS THESIS HAS BEEN EVALUATED

BY THE FOLLOWING BOARD OF EXAMINERS

M. Georges Kaddoum, Thesis Supervisor
Département de génie électrique, École de Technologie Supérieure

M. Mohamed Faten Zhani, President of the Board of Examiners
Département de génie logiciel et des TI, École de Technologie Supérieure

M. Ghyslain Gagnon, Member of the jury
Département de génie électrique, École de Technologie Supérieure

Mme Gunes Karabulut Kurt, External Independent Examiner
Faculty of Electrical and Electronics Engineering, Istanbul Technical University

THIS THESIS WAS PRESENTED AND DEFENDED

IN THE PRESENCE OF A BOARD OF EXAMINERS AND THE PUBLIC

ON "DECEMBER 4, 2019"

AT ÉCOLE DE TECHNOLOGIE SUPÉRIEURE

## FOREWORD

This dissertation is written based on the author's PhD research outcomes under the supervision of Professor Georges Kaddoum from September 2015 to August 2019. This work is financially supported by the Natural Sciences and Engineering Research Council of Canada under Discovery Grant 435243-2013. The main theme of this dissertation focuses on the emerging topic of resource allocation for green communications for future networks. This dissertation is written as a monograph based on five published IEEE journal papers and two submitted IEEE journal papers as the first author.

In this dissertation, the first two chapters present the introduction and the literature review of green wireless communication networks. Futher, the next seven chapters are wrote based on my research journal papers. Finally, the conclusion and the recommendation for future work are given in the last chapter.

## ACKNOWLEDGEMENTS

Foremost, I would like to express my most genuine gratefulness to my doctoral supervisor, Professor Georges Kaddoum, for his support to my PhD study as well as for his patience, motivation, and encouragement. Actually, I think myself very lucky to have his guidance. He always shows unrivaled faith in my abilities and gives me the best atmosphere for doing research. Especially, he knows how to challenge and motivate me to show my best performance without putting any pressures. I would never have been able to complete my dissertation at its best without his guidance.

I would like to truly thank all my PhD committee members, Professor Mohamed Faten Zhani, and Professor Ghyslain Gagnon, for reviewing and giving many constructive comments for my dissertation. I would also like to thank Professor Gunes Karabulut Kurt for serving as the external examiner to my PhD defense.

I would like to sincerely thank Dr. Hung Tran and Professor Kien T. Truong for guiding me at the very first stage of my PhD with helpful advices and making remarkable contributions to my publications.

My sincere thanks go to my fellow labmates in LACIME. Especially, many thanks to Hamza Tayeb and Poulmanogo Illy for helping me translate the abstract into French.

I would like to take this oppurtunity to acknowlegde Professor Een-Kee Hong, Dr. Vu Van Thanh Le, Dr. Hieu Thanh Nguyen, and Dr. Dac-Binh Ha for guiding my research for the past several years and helping me to develop my background in mathematics, and wireless communications. I would like to thank my friend, Mr. Duc-Dung Tran, who has been collborating with me in many research papers.

Last but not least, my sincere thanks go to my parents, younger sister, and all family members for their endless support and encouragement. Most important than ever, I would never have been able to finish this long journey without my wife, Dr. Huong Thi Lan Nguyen. Thanks a million for her understanding when I must be apart from her right away after our marriage due

to taking up my PhD study in Canada while she was doing her PhD in South Korea. She has always been supporting, encouraging, cheering me up and stood by me through the good and bad time. Especially, no words could express my appreciation to her for bringing me “a little angel” in the next February.

**Allocation optimale des ressources dans les futures réseaux sans fil verts : Applications et défis**

Ha Vu TRAN

## RÉSUMÉ

Au cours des récentes dernières années, les réseaux sans fil vertes sont devenues un sujet émergent vu que l'empreinte carbone des technologies de l'information et de la communication (TIC) devrait, selon les prévisions, augmenter annuellement de 7,3%, puis dépasser 14% l'empreinte globale d'ici 2040. De plus, la croissance explosive des TICs, par exemple la cinquième génération de réseaux mobiles (5G), prévoit d'atteindre dix fois plus de durée de vie pour les batteries des appareils et mille fois plus de trafics de données dans les réseaux mobiles par rapport à la quatrième génération de réseaux mobiles (4G). Les demandes d'augmentation du débit de données et de la durée de vie des batteries tout en réduisant l'empreinte carbone des réseaux sans fil de nouvelles générations requièrent une utilisation plus efficace de l'énergie et bien d'autres ressources. Pour relever ce défi, les concepts de small-cell, energy harvesting, et les transferts sans fil de données et d'énergie électrique devraient être considérés comme solutions prometteuses pour reverdir le monde.

Dans cette thèse, les contributions techniques en termes de réduction du coût économique, de protection des environnements et de garantie de la santé humaine sont fournies. Plus spécifiquement, de nouveaux scénarios de communication sont proposés pour minimiser la consommation d'énergie et ainsi réduire les coûts économiques. De plus, des techniques de recueillement de l'énergie (EH) sont utilisées pour exploiter des ressources vertes disponibles afin de réduire l'empreinte carbone et ainsi protéger l'environnement. Dans les endroits où les appareils utilisateurs implémentés ne pourraient pas récupérer l'énergie directement des ressources naturelles, les stations de base pourraient récupérer et stocker l'énergie verte et ensuite utiliser cette énergie pour alimenter sans fil les appareils. Cependant, les techniques de transfert sans fil d'énergie électrique (WPT) devraient être utilisées de manière prudente pour éviter la pollution électromagnétique et ainsi garantir la santé humaine. Pour atteindre tous les aspects simultanément, cette thèse propose des schémas prometteurs pour la gestion et l'allocation optimale des ressources dans les réseaux futurs.

Dans la première partie, le chapitre 2 étudie principalement un schéma de minimisation de la puissance de transmission pour un réseau 2-tiers hétérogène sur des canaux à évanouissements selectifs en frequence. De plus, l'interconnexion de réseaux hétérogènes n'est pas capable de supporter un débit suffisant pour communiquer un échange d'informations entre deux tiers. Une idée novatrice est introduite dans laquelle la technique "time reversal (TR) beamforming" est utilisée sur une femtocellule, tandis que la technique "zero-forcing-based beamforming" est déployée sur une macrocellule. Ainsi, un schéma de minimisation de la puissance de liaison descendante est proposé et des solutions analytiques optimales sont fournies.

Dans la deuxième partie, les chapitres 3, 4 et 5 se concentrent sur le EH et le transfert sans fil d'informations et d'énergie électrique en utilisant des signaux fréquence radio (RF). Plus

précisément, le chapitre 3 présente un aperçu des progrès récents en matière de radiocommunications vertes et examine les technologies potentielles pour certains thèmes émergents sur les plateformes EH et WPT. Le chapitre 4 développe une nouvelle architecture intégrée de récepteurs d'information et d'énergie basée sur l'utilisation directe du courant alternatif pour le calcul. Il est des montré que l'approche proposée améliore non seulement la capacité de calcul, mais également l'efficacité énergétique par rapport à l'approche conventionnelle. En outre, le chapitre 5 propose un nouveau schéma d'allocation de ressources dans les réseaux de transfert sans fil simultané d'information et d'énergie électrique où trois problèmes cruciaux sont traités conjointement: l'amélioration de l'efficacité énergétique, la garantie d'équité des utilisateurs et l'atténuation de l'effet de réciprocité de canal non idéal. Par conséquent, de nouvelles méthodes permettant de déduire des solutions optimales et sous-optimales seront fournies.

Dans la troisième partie, les chapitres 6, 7 et 8 se concentrent sur le transfert simultané d'information par ondes lumineuses et énergie électrique (SWIPT) pour des applications intérieures, en tant que technologie complémentaire au SWIPT RF. Dans cette recherche, le chapitre 6 étudie un réseau à cellules ultra-petites de communication hybride radio fréquence/lumière visible dans lequel des émetteurs optiques acheminent l'information et l'énergie électrique en utilisant la lumière visible, tandis qu'un point d'accès radio fréquence travaille comme un système complémentaire de transfert d'énergie électrique. Ainsi, un nouveau schéma d'allocation de ressource exploitant la radio fréquence et la lumière visible pour le transfert d'énergie électrique est conçu. Le chapitre 7 propose l'utilisation du transfert d'énergie par ondes lumineuses pour permettre la mise en place future et durable des réseaux sans-fil basés sur le Federated Learning (FL). FL est une nouvelle technique de protection de la confidentialité des données pour entrainer des modèles d'apprentissage automatique partagés dans une approche distribuée. Toutefois, l'intégration d'appareils mobiles à contraintes énergétiques pour la construction des modèles d'apprentissage partagés peut réduire considérablement leur durée de vie. L'approche proposée peut prendre en charge le réseau sans fil basé sur le FL pour palier le problème de limitation d'énergie dans les appareils mobiles. Le chapitre 8 présente une nouvelle approche pour le transfert collaboratif d'énergie électrique par ondes lumineuses et radio fréquence pour les réseaux de communications sans fil. Les contraintes de puissance de transmission, fixées par les règles de sécurité, engendrent des défis importants pour améliorer la performance de transfert d'énergie électrique. Ainsi, l'étude de technologies complémentaires au SWIPT RF conventionnel est essentielle. Pour faire face à ce problème, ce chapitre propose une nouvelle technologie collaborative de transfert d'énergie électrique par ondes lumineuses et radio fréquence pour les réseaux sans fil de prochaine génération.

**Mots-clés:** communications vertes, réseau hétérogène, recueillement de l'énergie, transfert sans fil d'énergie électrique, Internet des objets.

**Resource Allocation in Future Green Wireless Networks: Applications and Challenges**

Ha Vu TRAN

## ABSTRACT

Over the past few years, green radio communication has been an emerging topic since the footprint from the Information and Communication Technologies (ICT) is predicted to increase 7.3% annually and then exceed 14% of the global footprint by 2040. Moreover, the explosive progress of ICT, e.g., the fifth generation (5G) networks, has resulted in expectations of achieving 10-fold longer device battery lifetime, and 1000-fold higher global mobile data traffic over the fourth generation (4G) networks. Therefore, the demands for increasing the data rate and the lifetime while reducing the footprint in the next-generation wireless networks call for more efficient utilization of energy and other resources. To overcome this challenge, the concepts of small-cell, energy harvesting, and wireless information and power transfer networks can be evaluated as promising solutions for re-greening the world.

In this dissertation, the technical contributions in terms of saving economical cost, protecting the environment, and guaranteeing human health are provided. More specifically, novel communication scenarios are proposed to minimize energy consumption and hence save economic costs. Further, energy harvesting (EH) techniques are applied to exploit available green resources in order to reduce carbon footprint and then protect the environment. In locations where implemented user devices might not harvest energy directly from natural resources, base stations could harvest-and-store green energy and then use such energy to power the devices wirelessly. However, wireless power transfer (WPT) techniques should be used in a wise manner to avoid electromagnetic pollution and then guarantee human health. To achieve all these aspects simultaneously, this thesis proposes promising schemes to optimally manage and allocate resources in future networks.

Given this direction, in the first part, Chapter 2 mainly studies a transmission power minimization scheme for a two-tier heterogeneous network (HetNet) over frequency selective fading channels. In addition, the HetNet backhaul connection is unable to support a sufficient throughput for signaling an information exchange between two tiers. A novel idea is introduced in which the time reversal (TR) beamforming technique is used at a femtocell while zero-forcing-based beamforming is deployed at a macrocell. Thus, a downlink power minimization scheme is proposed, and optimal closed-form solutions are provided.

In the second part, Chapters 3, 4, and 5 concentrate on EH and wireless information and power transfer (WIPT) using RF signals. More specifically, Chapter 3 presents an overview of the recent progress in green radio communications and discusses potential technologies for some emerging topics on the platforms of EH and WPT. Chapter 4 develops a new integrated information and energy receiver architecture based on the direct use of alternating current (AC) for computation. It is shown that the proposed approach enhances not only the computational ability but also the energy efficiency over the conventional one. Furthermore, Chapter 5 proposes a novel resource allocation scheme in simultaneous wireless information and power trans-

fer (SWIPT) networks where three crucial issues: power-efficient improvement, user-fairness guarantee, and non-ideal channel reciprocity effect mitigation, are jointly addressed. Hence, novel methods to derive optimal and suboptimal solutions are provided.

In the third part, Chapters 6, 7, and 8 focus on simultaneous lightwave information and power transfer (SLIPT) for indoor applications, as a complementary technology to RF SWIPT. In this research, Chapter 6 investigates a hybrid RF/visible light communication (VLC) ultra-small cell network where optical transmitters deliver information and power using the visible light, whereas an RF access point works as a complementary power transfer system. Thus, a novel resource allocation scheme exploiting RF and visible light for power transfer is devised. Chapter 7 proposes the use of lightwave power transfer to enable future sustainable Federated Learning (FL)-based wireless networks. FL is a new data privacy protection technique for training shared machine learning models in a distributed approach. However, the involvement of energy-constrained mobile devices in the construction of the shared learning models may significantly reduce their lifetime. The proposed approach can support the FL-based wireless network to overcome the issue of limited energy at mobile devices. Chapter 8 introduces a novel framework for collaborative RF and lightwave power transfer for wireless communication networks. The constraints on the transmission power set by safety regulations result in significant challenges to enhance the power transfer performance. Thus, the study of technologies complementary to conventional RF SWIPT is essential. To cope with this isue, this chapter proposes a novel collaborative RF and lightwave power transfer technology for next-generation wireless networks.

**Keywords:** green communication, heterogeneous networks, energy harvesting, wireless power transfer, and IoT.

## TABLE OF CONTENTS

## LIST OF TABLES

Page

## LIST OF FIGURES

## LIST OF ALGORITHMS

## LIST OF ABREVIATIONS

| | |
|---|---|
| 4G | the fourth generation |
| 5G | the fifth generation |
| AC | alternating current |
| ADC | analog-to-digital |
| AN | artifical noise |
| AP | access point |
| AWGN | additive white Gaussian noise |
| BS | base station |
| CEE | channel estimation error |
| CRN | cognitive radio network |
| CIR | channel impulse response |
| CSI | channel state information |
| DC | direct current |
| DRHSCN | disaster-resilient heterogeneous small cell network |
| EH | energy harvesting |
| EIRP | equivalent isotropically radiated power |
| ETSI | European Telecommunications Standards Institute |
| EMF | electromagnetic field |
| FBS | femtocell base station |

| | |
|---|---|
| FU | femtocell user |
| GSMA | Global Systems for Mobile Communications Association |
| H-CRAN | heterogeneous cloud access radio access networks |
| HetNet | heterogeneous network |
| HPN | high power node |
| ICF | interference channel |
| ICT | information and communication technology |
| ID | information decoding |
| IoT | internet of things |
| ISI | inter-symbol interference |
| ITU | international telecommunication union |
| MABC | multiple acces broadcast |
| MBS | macrocell base station |
| ML | machine learning |
| MMSE | minimum mean square error |
| mm-wave | milimeter wave |
| MIMO | multiple input multiple output |
| OFDMA | orthogonal frequency-division multiple access |
| OWC | optical wireless communication |
| RF | radio frequency |

| | |
|---|---|
| RRH | remote radio heads |
| SC | super capacitor |
| SCN | small-cell network |
| SINR | signal-to-interference-plus-noise ratio |
| SISO | single input single output |
| SLIPT | simultaneous lightwave information and power transfer |
| SWIPT | simultaneous wireless information and power transfer |
| TDBC | time division broadcast |
| TDD | time division duplex |
| TDMA | time division multiple access |
| TR | time reversal |
| VLC | visible light communication |
| WPT | wireless power transfer |
| WSN | wireless sensor network |
| ZF | zero forcing |

## LISTE OF SYMBOLS AND UNITS OF MEASUREMENTS

| | |
|---|---|
| $\mathbf{a}$ | vector |
| $\mathbf{A}$ | matrix |
| $\mathbf{A}^T$ | the transpose of matrix $\mathbf{A}$ |
| $\mathbf{A}^H$ | the transpose conjugate of matrix $\mathbf{A}$ |
| $\mathbf{A}^\dagger$ | Moore-Penrose generalized inverse of matrix $\mathbf{A}$, $\mathbf{A}^\dagger = \left(\mathbf{A}^T\mathbf{A}\right)^{-1}\mathbf{A}^T$ |
| $\mathrm{tr}\,(\mathbf{A})$ | trace of a matrix $\mathbf{A}$ |
| $\mathrm{diag}(\mathbf{A})$ | diagonal of matrix $\mathbf{A}$ |
| $\|\mathbf{A}\|_F$ | Frobenius norm |
| $\mathbb{R}_+^m$ | the sets of $m$-dimensional nonnegative real vector |
| $\mathbb{C}^{m\times n}$ | the sets of $m \times n$ complex matrix |
| $\Re\{.\}$ | the real part |
| $\Im\{.\}$ | the imaginary part |

# INTRODUCTION

## Motivation, problem statement, and research objective

Future wireless networks, e.g., the fifth generation (5G) networks, are expected to support multimedia applications to achieve 10-fold longer device battery lifetime and 1000-fold higher global mobile data traffic, which would surpass 100 ExaBytes (EB) by 2023 Ericsson (2017). This will escalate the power consumption by which leads to the increasing emission of the carbon footprint since existing wireless communication systems are mainly supplied by conventional carbon-based power sources.. More specifically, the overall carbon footprint from information and communication technology (ICT) services, e.g., computer, cell phone, and satellite networks, is predicted to triple in from 2007 to 2020 Fehske, A., Fettweis, G., Malmodin, J. & Biczok, G. (2011), and to exceed 14% of the global footprint by 2040, as shown in Fig. 0.1. In this context, resource management often faces a dilemma between network performance improvement and avoidance of the negative impacts on the natural environment and human health. Therefore, breakthroughs in information and power transfer to satisfy the wireless field are becoming more essential than ever due to the growing demand for more efficient exploitation of radio frequency (RF) resources. In this context, a challenging topic so-called *next-generation green wireless networks* has been emerged in which small-cell, energy harvesting (EH), and wireless information and power transfer (WIPT) concepts have been promoted as key enabling technologies to reduce the energy consumption and enhance the lifetime of future networks whereas exploiting green energy sources Agiwal, M., Roy, A. & Saxena, N. (2016); Buzzi, S., I, C.-L., Klein, T. E., Poor, H. V., Yang, C. & Zappone, A. (2016); Lu, X., Wang, P., D., N., Kim, D. I. & Han, Z. (2015b); Wu, Q., Li, G. Y., Chen, W., Ng, D. W. K. & Schober, R. (2017).

In 5G, the design of new cellular networks tends toward a large-scale deployment of small-cells, which can potentially realize significant energy savings Wu *et al.* (2017). Small-cell

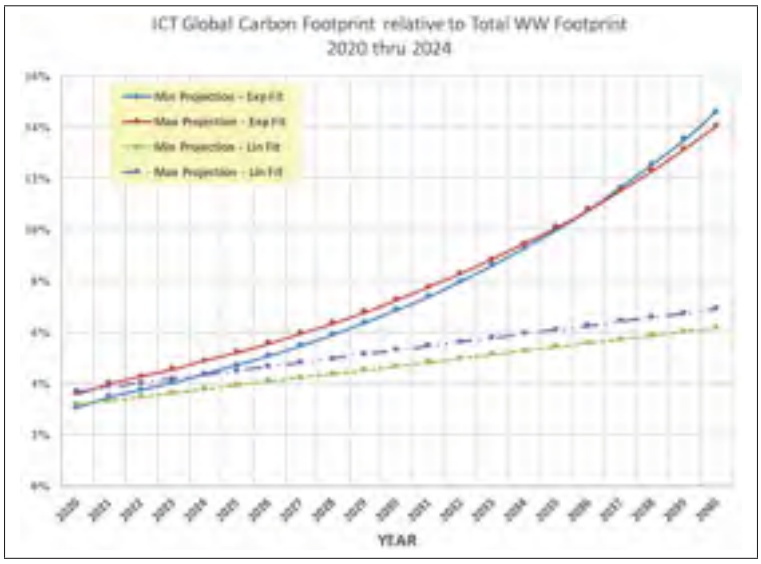


Figure 0.1 ICT footprint as a percentage of total footprint projected through 2040 using both an exponential and linear fits Taken from Belkhir, L. & Elmeligi, A. (2018)

networks (SCNs), which are low-power base stations (BSs) covering a short-range wireless access for mobile devices, can be classified into distinct types including femtocell, microcell, and picocell. It has been shown that the small-cell approach can attain a promising gain in terms of spectral and energy efficiencies due to low power consumption and good ubiquitous connectivities Agiwal *et al.* (2016); Hossain, E., Rasti, M., Tabassum, H. & Abdelnasser, A. (2014). Nevertheless, due to the network densification, multi-tier SCNs face the problems associated with the management of available resources to avoid resource collisions Buzzi *et al.* (2016). Therefore, the power allocation in the SCNs becomes more challenging compared to conventional single-tier networks.

Considering the SCNs, to further reduce the power consumption constituting the carbon footprint, EH has been considered as a promising solution Lu *et al.* (2015b); Wu *et al.* (2017). In principle, the EH paradigm harnesses green energy from natural sources, e.g., solar and wind, and converts it into electrical current used to supply wireless networks and prolong the lifetime of smart user devices. Thus, it decreases the overall footprint and then improves the quality

of the surrounding environment. Particularly, EH plays an extremely important role in various applications, including reducing battery replacement costs of wireless sensors working in toxic environments Ulukus, S., Yener, A., Erkip, E., Simeone, O., Zorzi, M., Grover, P. & Huang, K. (2015). Nevertheless, the performance of conventional EH is unstable. In more detail, the amount of harvested energy from natural resources, such as solar and wind, may vary randomly over time and depend on the locations and weather conditions which are not controllable, sustainable, and always available. For example, there is insufficient sunlight at night to generate energy, or it is difficult for indoor devices to harvest solar energy.

This motivated the use of a WIPT paradigm Clerckx, B., Zhang, R., Schober, R., Ng, D. W. K., Kim, D. I. & Poor, H. V. (2019) where base stations harvest-and-store green energy from outdoor and then wirelessly transfer energy to indoor devices using RF signals. Hence, battery-constrained terminal devices can receive information and energy from RF signals whenever it is necessary. Even though WIPT is a disruptive approach, the performance of RF wireless power transfer drastically suffers from path loss Clerckx *et al.* (2019); Niyato, D., Kim, D. I., Maso, M. & Han, Z. (2017). Besides, there exist tight restrictions imposed on the transmitted power since the intensity of microwave radiation can harm human health. Indeed, wireless devices must satisfy the equivalent isotropically radiated power (EIRP) requirement ruled by the Federal Communications Commission WHO (2007). For example, a maximum of 36 dBm EIRP is limited on the 2.4 GHz band.

The discussed issues regarding SCNs, EH, and WIPT are challenging the research community. Taking those issues into account, this dissertation aims to find solutions for the critical question of "how to minimize the power consumption and improve the lifetime of future networks while exploiting green energy sources and retaining electromagnetic pollution?" Different from the 4G network, future wireless communication systems are expected to be a mixture of various new system concepts, such as RF wireless power transfer (WPT), Li-Fi, Internet of Things

(IoT), etc.. Thus, the existing operational schemes also need to be renovated and/or redesigned to accommodate the advancements of new transmission technologies as well as network applications.

**Contributions and Outline**

The organization of this dissertation, which includes 8 chapters, is structured and detailed as follows. Chapter 1 presents the comprehensive literature review of SCNs, EH, and WIPT in the scope of next-generation green wireless networks. In this vein, these technologies and hence the trends for energy-aware communications are presented. Additionally, the review of related recent works is given.

Chapter 2 presents the first article studying an application of two different beamforming techniques and propose a novel downlink power minimization scheme for a two-tier heterogeneous network (HetNet) model. In this context, the time reversal (TR) technique is employed at a femtocell base station, whereby a zero-forcing-based algorithm is used at a macrocell base station, and the communication channels are subject to frequency selective fading. Additionally, the HetNet backhaul connection is unable to support a sufficient throughput for signaling and information exchange between two tiers. Given the considered HetNet model, a downlink power minimization scheme is proposed and closed-form expressions of the optimal solution are provided in two cases of perfect and imperfect channel estimation at TR-employed femtocell.

Chapter 3 presents the second article discussing potential technologies for the emerging topic of green radio communication where EH and WPT networks are evaluated as promising approaches. In this article, an overview of recent trends for future green networks on the platforms of EH and WPT is provided. By rethinking the application of RF-WPT, a new concept, namely green RF-WTP, is introduced. Accordingly, open challenges and promising combina-

tions among current technologies, such as small-cell, millimeter (mm) wave, and Internet of Things (IoT) networks, are discussed in details to seek solutions for the question of how to re-green the future networks?

Chapter 4 presents the third article developing a novel integrated information and energy receiver architecture for SWIPT networks inspired by the direct use of alternating current (AC) for computation. In this context, the AC computing method, in which wirelessly harvested AC energy is directly used to supply the computing block of receivers, enhances not only computational ability but also the energy efficiency over the conventional direct current (DC) one. Further, we aim to manage the trade-off between the information decoding (ID) and energy harvesting (EH) optimally while taking imperfect channel estimation into account. It results in a worst-case optimization problem of maximizing the data rate under the constraints of an EH requirement, the energy needed for supplying the AC computational logic, and a transmit power budget. Then, we propose a method to derive closed-form optimal solutions.

Chapter 5 presents the fourth article proposing a novel resource allocation scheme in SWIPT networks where three crucial issues: (i) power efficiency improvement, (ii) user-fairness guarantee, and (iii) non-ideal channel reciprocity effect mitigation, are jointly addressed. A resource allocation scheme jointly addressing such issues can be potentially devised by using the multi-objective optimization framework. However, the resulting problem might be complex to solve since the three issues hold different characteristics. Therefore, we propose a novel method to design the resource allocation scheme. In particular, the principle of our method relies on mathematically structuralizing the issues into a cross-layer multi-level optimization problem. On this basis, we then devise solving algorithms and closed-form solutions. Moreover, we propose a closed-form suboptimal solution to instantly adapt the CSI changes in practice while reducing computational burdens.

Chapter 6 presents the fifth article investigating the potential of RF and lightwave power transfer in a hybrid RF/visible light communication (VLC) ultra-small cell network. In the network, the optical transmitters play the primary role and are responsible for delivering information and power over the visible light, while the RF AP acts as a complementary power transfer system. Thus, we propose a novel collaborative RF and lightwave resource allocation scheme for hybrid RF/VLC ultra-small cell networks. The proposed scheme aims to maximize the communication quality-of-service provided by the VLC under a constraint of total RF and light energy harvesting performance, while keeping illumination constant and ensuring health safety. This scheme leads to the formulation of two optimization problems that correspond to the resource allocation at the optical transmitters and the RF AP. Both problems are optimally solved by appropriate algorithms. Moreover, we propose a closed-form suboptimal solution with high accuracy to tackle the optical transmitters' resource allocation problem, as well as an efficient semi-decentralized method.

Chapter 7 presents the sixth article proposing the use of lightwave power transfer to enable new possibilities for the sustainability of future Federated Learning (FL)-based wireless networks. FL has been recently presented as a new technique for training shared machine learning models in a distributed manner while respecting data privacy. However, implementing FL in wireless networks may significantly reduce the lifetime of energy-constrained mobile devices due to their involvement in the construction of the shared learning models. To handle this issue, we propose a novel approach at the physical layer based on the application of lightwave power transfer in the FL-based wireless network and a scheme design to manage the network's power efficiency. Hence, we formulate the corresponding optimization problem and then propose a method to obtain the optimal solution. Numerical results reveal that: with the infrared light transmit power of 4 W, a mobile device can process data and achieve the uplink rate of 40 kbps which is sufficient for doing FL tasks, without using the power from the device battery. Hence,

the proposed approach can support the FL-based wireless network to overcome the issue of limited energy at mobile devices.

Chapter 8 presents the seventh article introducing a novel framework for collaborative RF and lightwave power transfer for wireless communication networks. Relying solely on RF resources to cope with the expectations of next-generation wireless networks, such as longer device lifetimes and higher data rates, may no longer be possible. Thus, the investigation of technologies complementary to conventional RF SWIPT is of critical importance. In this chapter, we propose a novel collaborative RF and lightwave power transfer technology for future networks where both the RF and lightwave bands can be entirely exploited. We develop the corresponding system architecture, and design four corresponding collaborative communication and power transfer protocols in which the use of RF and lightwave can be combined and optimized over the time and power domains. Further, we show simulation results, and present potential future research directions.

For convenience, the big picture of this thesis is shown in Fig. 0.2.

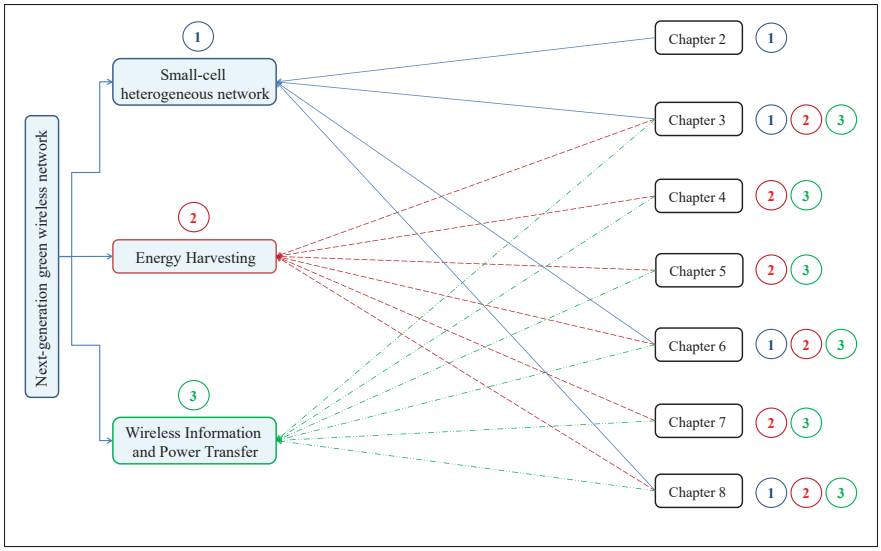


Figure 0.2 Paradigm of the thesis contributions.

**Author's Publications**

The outcomes of the author's PhD research are the articles listed below published and submitted in IEEE journals.

H-V. Tran, Georges Kaddoum, Panagiotis D. Diamantoulakis, Chadi Abou-Rjeily, and George K. Karagiannidis (2019), Ultra-small Cell Networks with Collaborative RF and Lightwave Power Transfer, *IEEE Transactions on Communications*, early access.

H-V. Tran and Georges Kaddoum (2019), Robust Design of AC Computing-enabled Receiver Architecture for SWIPT Networks, *IEEE Wireless Communications Letters*, 8(3), 801 - 804.

H-V. Tran, G. Kaddoum, and Kien T. Truong (2018), Resource Allocation in SWIPT Networks under a Nonlinear Energy Harvesting Model: Power Efficiency, User Fairness, and Channel Nonreciprocity, *IEEE Transactions on Vehicular Technology*, 67(9), 8466 - 8480.

H-V. Tran, and G. Kaddoum (2018), RF-wireless power transfer: Re-greening future networks, *IEEE Potentials Magazine*, 37(2), 35 - 41.

H-V. Tran, G. Kaddoum, H. Tran, and E.K. Hong (2017), Downlink optimization for heterogeneous networks with time reversal-based transmission under backhaul limitation, *IEEE Access*, 5, 755-770.

H-V. Tran, Georges Kaddoum, Hany Elgala, Chadi Abou-Rjeily, and Hemani Kaushal (2019), Lightwave Power Transfer for Federated Learning-based Wireless Networks, *OSA Optics Express*, under review.

H-V. Tran, Georges Kaddoum, Panagiotis D. Diamantoulakis, Chadi Abou-Rjeily, and George K. Karagiannidis (2019), Collaborative RF and Lightwave Power Transfer for Next-Generation Wireless Networks, *IEEE Communications Magazine*, under review.

Beside the above articles that contribute to the main contents of this dissertation, other publications that the author was involved in and which are not included in this dissertation are

D-D Tran, H-V. Tran (corresponding author), D-B Ha and G. Kaddoum (2019), Secure Transmit Antenna Selection Protocol for MIMO NOMA Networks over Nakagami-m channels, *IEEE Systems Journal*, early access.

G. Kaddoum, H-V. Tran, L. Kong, and M. Atallah (2017), Design of simultaneous wireless information and power transfer for short reference DCSK communication system, *IEEE Transactions on Communications*, 65(1), 431-443.

H-V. Tran, and G. Kaddoum (2018), Green cell-less design for RF wireless power transfer networks, *IEEE Wireless Communications and Networking Conference (WCNC)*, Barcelona, Spain.

H-V. Tran, G. Kaddoum, H. Tran, DD Tran, and DB Ha (2016), Time reversal SWIPT networks with an active eavesdropper: SER-Energy region analysis, *IEEE 84th Vehicular Technology Conference (VTC)*, Montreal, Canada.

H-V. Tran, Hung Tran, G. Kaddoum, Duc-Dung Tran, and Dac-Binh Ha (2015), Effective secrecy-SINR analysis of time reversal-employed systems over correlated multi-path channel, *11th IEEE International Conference on Wireless and Mobile Computing, Networking and Communications (WiMob)*, pp. 527-532.

DD. Tran, H-V. Tran, DB Ha, and G. Kaddoum (2018), Cooperation in NOMA networks under limited user-to-user communications: solution and analysis, *IEEE Wireless Communications and Networking Conference (WCNC)*, Barcelona, Spain.

Hung Tran, Quach Xuan Truong, H-V. Tran, Elisabeth Uhlemann (2017), Optimal Energy Harvesting Time and Power Allocation Policy in CRN Under Security Constraints from Eavesdroppers, *IEEE International Symposium on Personal, Indoor and Mobile Radio Communications (PIMRC)*, Montreal, Canada.

DD. Tran, H-V. Tran, DB Ha, H. Tran, and G. Kaddoum (2016), Performance analysis of two-way relaying system with RF-EH and multiple antennas, *IEEE 84th Vehicular Technology Conference (VTC)*, Montreal, Canada.

# CHAPTER 1

# LITERATURE REVIEW OF GREEN WIRELESS NETWORKS: SMALL-CELL, ENERGY HARVESTING, AND WIRELESS INFORMATION AND POWER TRANSFER

## 1.1 Small-Cell Networks

### 1.1.1 The Concept of Small-Cell Networks

Contemporarily, the world has witnessed the prompt development of wireless technologies. This appears with the exponentially increasing demands of heterogeneous wireless communication services over broadband channels. Thus, cellular networks have been developed to cope with the rising demand for high achievable throughput, seamless coverage, and reasonable installation costs. Nevertheless, this trend significantly increases the power consumption of wireless networks. Indeed, the energy cost and $CO_2$ emissions have been promptly growing due to the operation of cellular networks. Thus, this results in an emerging demand of energy saving in future wireless networks.

In 5G networks, the concept of small-cell networks has been considered as a promising solution to enhance the throughput and to overcome the drawbacks of traditional cellular networks Hossain *et al.* (2014); Xu, Z., Yang, C., Li, G., Liu, Y. & Xu, S. (2014), such as the inefficient usage of spectrum and power, dynamic spectrum access, and indoor coverage. In heterogeneous small-cell networks, the macrocell serves a large number of users in a wide area whereas densely deployed low-power cells, such as femtocells, picocells, and microcells, handle a substantially smaller number of users. Following this approach, not only the coverage range, throughput, and reliability but also power efficiency can be improved significantly Hossain *et al.* (2014); Liu, Y., Zhang, Y., Yu, R. & Xie, S. (2015); Wu *et al.* (2017).

### 1.1.2 Recent Approaches to Green Small-Cell Networks

#### 1.1.2.1 Energy-Efficient Small-Cell Networks

With restrictions applied on the maximum transmit power, this trend focuses on optimizing the resource allocation such that the transmit power is fully exploited to improve the energy efficiency of networks.

The problem of maximizing energy efficiency for downlink orthogonal frequency-division multiple access (OFDMA) in a HetNet scenario was addressed in Zhang, Z., Zhang, H., Zhao, Z., Liu, H., Wen, X. & Jing, W. (2013). In the system model, macrocell and femtocell work on different spectrums, thus there was no cross-tier interference. To reduce the complexity, power control and subchannel allocation were separated into two stages. The power control was formulated in terms of a non-cooperative game while the subchannel allocation had a common energy efficiency problem. On this basis, the authors solved the problems with a distributed algorithm. Obtained results indicate that the proposed algorithm had a lower complexity than Round-Robin Scheduling and the conventional noncooperative energy-efficient optimization algorithm.

In Venturino, L., Zappone, A., Risi, C. & Buzzi, S. (2015), the authors studied the problems of maximizing the global energy efficiency, the weighted sum of the energy efficiencies and exponentially-weighted multiplication of the energy efficiencies on each subcarrier for a cellular OFDMA network. In addition, the transmit power allocated for each subcarrier should not be larger than the ratio of total transmit power at the base station (BS) to the number of subcarriers. Accordingly, the algorithms to solve these problems was provided. Precisely, globally optimal solutions were given for the asymptotic noise-limited regime. The authors claimed that a proper reduction of the spectral efficiency might result in substantial energy saving in case of large values of the maximum transmit power.

A scenario of heterogeneous cloud access radio access networks (H-CRANs) was studied in Peng, M., Zhang, K., Jiang, J., Wang, J. & Wang, W. (2015). To mitigate interference and

enhance the energy efficiency, user association with remote radio heads (RRHs)/high power node (HPN) and the enhancement of traditional soft fractional frequency reuse (S-FFR) is considered. On this basis, the optimization problem of energy efficiency was formulated to address the resource allocation. The authors relaxed the original non-convex problem into a convex one; then they provided the closed-form solution using the Lagrange dual decomposition method. The paper showed that the H-CRAN system model and the resulting resource allocation could substantially improve the energy efficiency.

In Jiang, Y., Zou, Y., Guo, H., Tsiftsis, T. A., Bhatnagar, M. R., de Lamare, R. C. & Yao, Y.-D. (2019), the paper investigated an energy efficiency maximization problem for heterogeneous small-cell networks where a macro BS and a number of low-power small-cell stations serve a macro-cell user and small-cell users. The authors proposed a joint transmit power and channel bandwidth allocation scheme to maximize the energy efficiency of small cells constrained by transmit power and quality-of-service (QoS). Since the formulated optimization problem is nonconvex, the authors presented a novel two-tier algorithm to achieve optimal solutions. They demonstrated that their proposed approach outperforms conventional ones with respect to energy efficiency maximization.

#### 1.1.2.2 Transmit Power Minimization in Small-Cell Networks

In small-cell networks, minimizing the transmit power leads to a significant reduction of the overall power consumption at the base stations, hence leading to a power efficient design.

The work in Lakshminarayana, S., Assaad, M. & Debbah, M. (2015) focused on transmit power minimization under time average QoS constraints in an SCN where multiple users are served in each cell. On this basis, a stochastic optimization problem was formulated to find optimal downlink beamformers per each time slot. The authors tackled the problem by using Lyapunov optimization. They further investigated the impact of delays due to information exchange between small-cell BSs. Moreover, the authors considered additional constraints of channel state information (CSI) feedback, which result in a joint CSI feedback and beamforming optimiza-

tion scheme. Based on simulation results, they claimed that: in modern wireless applications, such as multimedia apps, where delay tolerance is adjustable, considering the time average QoS constraints might result in better power savings than using instantaneous QoS constraints.

In Bonnefoi, R., Moy, C. & Palicot, J. (2018), the authors studied the power control scheme and the cell discontinuous transmission issue in an SCN. They proposed a policy for energy consumption minimization at each BS for a multi-small-cell network. The simulation results showed that the proposed policy outperforms other policies. Additionally, it can provide a 6% performance gain in energy compared to a policy without power control. Furthermore, this gain can reach up to 11% when the maximum transmit power at each BS is decreased.

In Liu, Z., Zhang, P., Chan, K. Y., Ma, K. & Li, L. (2019), a two-tier femtocell network, where the communication environment is time-varying and the CSI is imperfect, was considered. The authors proposed a power control scheme in which a Fuzzy logic system is used to capture the instantaneous channel gain and the dynamics of the changing channel. Then, in contrast to previous existing methods, the proposed scheme does not require the knowledge of channel gain contribution. On this basis, a transmit power minimization is formulated under constraints of the transmission rate and a power budget. The authors solved this problem by an iterative fast-convergent algorithm. Simulation results show that the proposed scheme outperforms existing methods.

#### 1.1.2.3 Self-Organizing Small-Cell Networks

In cellular networks, the traffic load depends on the location and time. For instance, the traffic load might be higher in office areas compared with residential areas during the daytime, whereas the converse holds during nighttime. Thus, there always exist cells, that are either underloaded or overloaded. This motivates network-level management in which multiple BSs can coordinate with each other.

Specifically, since the BS operation consumes a significant amount of energy, selectively switching some BSs off according to their traffic load can be a promising approach for saving energy.

The coverage area of cells in sleep mode can be served by active neighbor cells. This approach is known as self-organizing networks introduced in the 3GPP standard (3GPP TS 32.521). In Americas, G. (2009), the different architecture approaches of self-configuring, self-optimizing, and self-healing were studied for the first time to save costs and enhance network performance and flexibility.

Moreover, the work in Jo, H.-S., Mun, C., Moon, J. & Yook, J.-G. (2010) proposed a novel coverage coordination scheme to deal with any unexpected handover of outdoor users. This scheme was based on the statistic of the interferences and desired signals of femtocell downlink transmission. Both the self-optimization and the self-configuration were considered for the pilot transmit power at a femtocell BS. Regarding self-configuration, the femtocell base station decides the amount of transmit power relying on the strength of interference from neighbor BSs to guarantee a nearly constant cell coverage. Further, the femtocell performs self-optimization to control the transmit power such that the femtocell signals are not leaked to the outdoor area while satisfying system performance.

The network architecture of disaster-resilient heterogeneous small cell networks (DRHSCNs) was described for the first time in Zhang, H., Jiang, C., Hu, R. Q. & Qian, Y. (2016). On this basis, self-optimizing techniques, in terms of capacity, mobility robustness, and coverage optimization, were proposed. Additionally, self-configuring methods regarding power, neighbor cell list, and physical cell ID were studied in DRHSCNs. Thus, according to detailed simulation results, the authors showed that the proposed techniques can improve the performance of the DRHSCNs significantly.

In Amiri, R., Almasi, M. A., Andrews, J. G. & Mehrpouyan, H. (2019), the authors studied the application of reinforcement learning to a self-organizing HetNet system model, including macrocells and denser small cells. A distributed power allocation based on Q-learning was proposed as a self-organization scheme. Extensive simulations with different learning configurations are conducted to illustrate the network performance. It was shown that the proposed

method can tackle the transmit power minimization problem in the network, whereas remarkably decreasing power usage and therefore the interference.

## 1.2 Energy Harvesting

### 1.2.1 The Concept of Energy Harvesting

The aim to exploit available green resources in order to reduce carbon footprint and then protect environments is a global trend towards re-greening the world. This motivates the utilization of EH to decrease the footprint due to the wireless network operation. EH is the process of harnessing energy from surrounding environments or mechanical sources (foot strike, finger strokes), and then converting the latter into electrical energy. The generated electrical current is then used to power wireless devices. Furthermore, EH has been recognized as a disruptive paradigm to extend the lifetime of wireless networks Ng, D. W. K. & Schober, R. (2015); Ulukus *et al.* (2015); Wu *et al.* (2017).

There are many reasons to support the applications of EH. For instance, in specific locations, such as Northern Canada and Africa, bringing fuels to such locations is a challenge. In general, each BS consumes on average 30,000 liters of diesel per year. The effort of transporting the fuel to the site can add a significant cost. As a solution, EH from renewable energy resources, such as solar and wind, is appealing in order to reduce the expenditure of networks as well as $CO_2$ emissions. Over the last few years, a project entitled "Green Power for Mobile" has been started by 25 companies under the Global Systems for Mobile Communications Association (GSMA) Gre (2014). The goal of this project is to exploit green energy sources in developing countries. 2.5 billion liters of diesel and 6.8 million tons of carbon emissions are expected to be cut annually. Although the implementation cost of network systems using renewable energy resources is expensive. Nevertheless, according to the report by GSMA, this cost can be compensated after less than three years of operation Gre (2014). This reveals that this green power technology can be a feasible and attractive solution in both technical and financial aspects.

### 1.2.2 Ambient Energy Sources

Demands for energy is scaling up day by day and therefore exploiting new and efficient energy resources is one of the primary trends today. In this subsection, we briefly present the characteristics of some primary energy sources.

#### 1.2.2.1 Solar Energy

Solar energy can be obtained by converting from sunlight into electricity using photovoltaic or concentrated solar EH techniques. In more details, the photovoltaic method exploits the photoelectric effect to transform sunlight into electrical current. On the other hand, the concentrated solar energy method is to focus light into a sharp beam resulting in a heat source. In fact, solar power is one of the most popular forms of EH. However, the drawback of this approach is that the energy is generated only when there exists a sufficient sunlight source. Indeed, the use of solar energy has been employed in many applications in wireless sensor networks Alippi, C. & Galperti, C. (2008); Hande, A., Polk, T., Walker, W. & Bhatia, D. (2007) and cellular networks Ng & Schober (2015); Wu *et al.* (2017).

#### 1.2.2.2 Wind Energy

Wind power has been considered as an efficient source of green energy over the last decade. Indeed, it even appears before petroleum economy. Wind power can be harvested by deploying wind turbine farms. Specifically, up to 800 MW can be achieved by a massive turbine farm, whereas 3 kW can be attained using small residential turbines. In principle, the wind turbine generator is responsible for converting mechanical energy into electrical energy. Additionally, the success of harnessing depends on two critical factors, i.e., wind direction and speed. The American Wind Energy Association evaluates that the wind turbines can generate electrical power sufficient for over 15 million homes in the USA. This energy is predicted to exceed the nation's electricity requirements by more than ten times Onl.

#### 1.2.2.3 Mechanical Energy

Mechanical energy is created according to the vibration effects, the motion of living beings, and noise. Thus, such energy can be harvested from three primary sources, which are machinery vibrations, human movements, and flow-induced vibrations. In this concern, piezoelectric materials are utilized to transform the mechanical energy into electrical current or voltage Ammar, Y., Buhrig, A., Marzencki, M., Charlot, B., Basrour, S., Matou, K. & Renaudin, M. (2005); Vijayaraghavan, K. & Rajamani, R. (2007). More specifically, this kind of materials helps convert the effects of pressure, vibrations, and forces into electricity. Particularly, piezoelectric materials are capable of producing an electrical charge when energy storage is available. However, the main disadvantage relies on their fragility and the potential leakage of charge.

#### 1.2.2.4 Thermal Energy

In principle, thermal energy harvesting exploits a temperature difference, such as the difference between the human body and the surrounding environment, to produce an electrical current. For instance, a device located on the human body can harvest the energy generated from the body using thermogenerators Mateu, L., Codrea, C., Lucas, N., Pollak, M. & Spies, P. (2006). In general, the phenomena of converting heat energy into electricity is the thermoelectricity. Nowadays, thermoelectric devices have been employed in various contexts, such as space and terrestrial applications. For example, the design of microstructured thermoelectric devices is investigated to address the concern of telecommunication systems in Bottner, H. & et al. (2004).

#### 1.2.2.5 Radio Frequency Energy

Radio signals belonging to a frequency range from 3 kHz to 300 GHz can be used to carry energy over the air. Different from the mentioned sources, the characteristics of RF sources can be listed as follows:

- RF sources are controllable and sustainable,

- The energy harvested at a receiver is foreseeable,
- The amount of harvested energy depends on the transmit power, propagation loss, and wavelength.

Therefore, the RF source is one of the most interesting candidates for future applications. In fact, it has been widely exploited in many interesting forms, such as wireless sensor networks, implanted body devices, and cellular networks Le, T., Kaddoum, G. & Shin, O. (2018); Lu, X., Niyato, D., Wang, P., Kim, D. I. & Han, Z. (2015a); Lu *et al.* (2015b); Ng & Schober (2015); Wu *et al.* (2017).

#### 1.2.2.6 Indoor Artificial Light Energy

Harvesting indoor artificial light energy is an attractive topic in recent years. It relies on that fact that indoor light sources, i.e., LED bulbs, provide "free" energy to wireless networks since no extra power is needed from the lighting system. Nevertheless, the intensity of indoor light is lower than that of the outdoor light, making the applications of indoor light EH challenging. In more detail, it is $10^4$ times less than the 1000 W/m$^2$ which is the intensity of 1-sun standard test conditions. Although the amount of achievable harvested indoor light energy is small, it is enough to supply wireless sensors, as demonstrated in Mathews, I., King, P. J., Stafford, F. & Frizzell, R. (2016). Moreover, a transparent solar panel named as Wysips Reflect, recently developed by Sunpartner Technologies wys (2019), can be integrated into phone screens. It promises to improve the indoor light EH performance substantially.

### 1.2.3 Energy Harvesting Architectures

Generally speaking, EH architectures can be classified into two types which are (i) Harvest-Use: Energy is harvested and then is used instantly, and (ii) Harvest-Store-Use: Energy is harvested as much as possible and then stored for future use.

#### 1.2.3.1 Harvest-Use Architecture

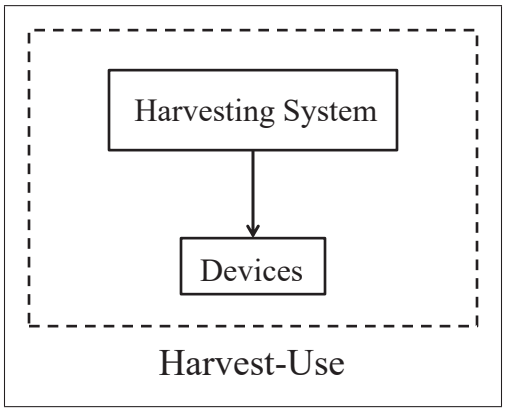


Figure 1.1 Harvest-Use Architecture

Fig. 1.1 illustrates the Harvest-Use architecture. In this case, the EH system directly supplies a device. Havest-Use EH systems can be implemented to exploit mechanical energy sources, i.e. pedaling, walking, etc. For example, piezoelectric materials which are placed in a shoe can deform to distinct extents when running or even walking. Then, the produced energy can be used to convey RFID signals with respect to tracking the shoe-wearer Shenck, N. & Paradiso, J. (2001); Starner, T. (1996).

To guarantee the operation of the devices, the power output of the EH system should be higher than the minimum working threshold. Otherwise, the devices would be disabled since there is not enough power supplied. As a consequence, the main drawback is that: the unanticipated fluctuations of harvested energy close to the threshold might yield the working devices to vacillate between ON and OFF states.

#### 1.2.3.2 Harvest-Store-Use Architecture

The Harvest-Store-Use architecture is shown in Fig. 1.2. The model is composed of a harvesting system and a component storing harvested energy. In fact, the energy storage is helpful when the harvested energy is more than the needed energy for the devices' usage. Such energy is stored for later uses when there is a lack of produced energy, or the devices need to

increase the working performance. The storage component might include two parts of primary and secondary storages. In this context, the secondary storage can be seen as a backup one. In particular, the Harvest-Store-Use system can make non-stable but foreseeable energy sources, such as solar and wind, more favorable in uses Raghunathan, V., Kansal, A., Hsu, J., Friedman, J. & Srivastava, M. (2005); Taneja, J., Jeong, J. & Culler, D. (2008).

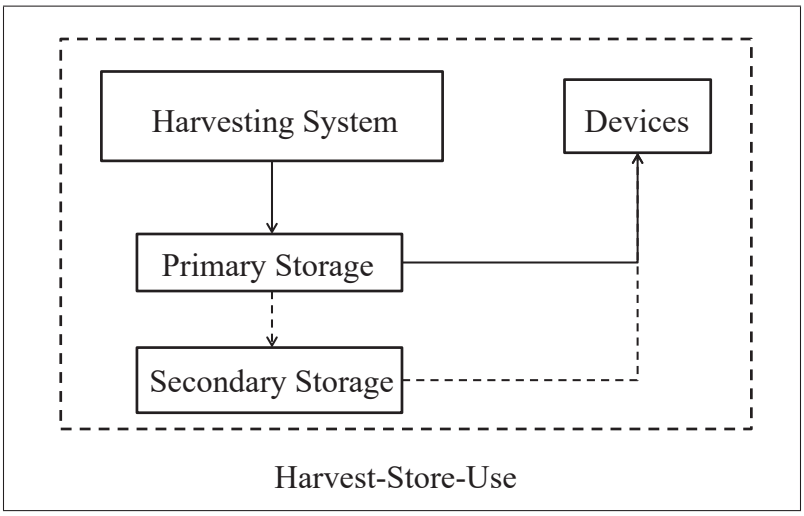


Figure 1.2 Harvest-Store-Use Architecture

Furthermore, the storage technology and recharge techniques are critical since they can affect system performance significantly. In EH systems, the rechargeable battery, which can be created by several technologies using chemical compositions, is the most suitable choice for the energy storage. In principle, it can be seen as a storage cell that can be recharged by reversing internal chemical reactions. Nowadays, there exist some popular rechargeable batteries, such as Lithium Ion (Li-ion), Nickel Cadmium (NiCd), Nickel Metal, Sealed Lead Acid (SLA), and Hydride (NiMH). Specifically, NiMH and Li-on, two kinds of batteries, can be evaluated as great choices for EH systems since they are immune from memory effect-loss on energy capacity, caused by shallow recharge referring to recharging a partially discharged battery.

### 1.2.4 Recent Trends for EH Networks

#### 1.2.4.1 EH Networks with Hybrid Natural and On-Grid Energy Sources

A hybrid energy source can be defined as a combination of a constant energy source and a harvesting energy source such as solar, wind, etc. Therefore, designing power allocation schemes for wireless systems with hybrid energy sources is challenging.

Considering a peer-to-peer communication where the EH transmitter is equipped with a hybrid energy supply, power allocation schemes in both online and offline fashions were proposed in Ahmed, E., Eltawil, A. M. & Sabharwal, A. (2013). The objective of the schemes is to minimize the contribution of the constant energy source. In this context, the energy harvested from the natural sources was fully exploited to transmit data packets over defined time slots. Regarding the power allocation scheme, this work shows that the offline fashion outperforms the online one.

In Ozel, O., Shahzad, K. & Ulukus, S. (2014), the authors studied the data transmission in an EH system model where a transmitter has hybrid storage with an inefficient battery and a super-capacitor (SC). The battery has unlimited capacity, whereas the SC has limited storage. The transmitter can choose either SC or battery to store the harvested energy. The consumed energy can be drained from the battery and SC at the same time. Given these settings, the authors provided solutions for the problems of offline throughput maximization in the cases of (i) a conventional point-to-point communication and (ii) an additive time-linear processing cost.

The work in Ng & Schober (2015) investigated the resource allocation problem addressing renewable energy harvesting, secure information, and power transfer in distributed antenna systems. The central processor plays the role of a core unit connected with all distributed remote radio heads. In this concern, backhaul connections are supposed to be capacity-limited. The authors assumed that the central processor is supplied by a constant energy source whereas the distributed RRHs are integrated with conventional energy harvesters. Particularly, the har-

vested energy can be shared between the RRHs and the central processor over a micropower grid. Hence, the RRHs can transmit information and energy to receivers over RF signals. On this basis, an optimization problem aiming to minimize the transmit power is formulated under Quality of Service (QoS) constraints in terms of efficient power transfer and secure communication. The authors provided an algorithm to solve this problem. Importantly, they concluded that the proposed system can save much more power than the conventional centralized one.

Considering downlink OFDMA networks with a non-ideal hybrid energy supply, to achieve the minimal grid energy cost, the utilization of a data buffer at user devices and an energy storage at a BS was proposed to adapt to the unstable nature of renewable energy sources in Chiang, P., Guruprasad, R. B. & Dey, S. (2018). Further, a low-complexity online management scheme relying on Lyapunov optimization is developed. It is able to give an asymptotically optimal performance bound without the knowledge of the stochastic distribution. The numerical results showed that the proposed approach can substantially reduce the grid power consumption and improve the QoS compared to other existing schemes.

To reduce the utilization of on-grid energy in HetNets supplied with hybrid energy sources, the authors in Fletscher, L. A., Suarez, L. A., Grace, D., Peroni, C. V. & Maestre, J. M. (2019) improved the energy efficiency over short- and long-timescale by using reactive and proactive management strategies. While there is no storage infrastructure available in the short-timescale case, a model predictive controller of the RF source behavior with storage support is considered in the other case. The proposed strategies were analyzed with the data of solar estimations and wind measurements from Valle de Aburra, Medellin, Colombia and from the Moscow region, Russian Federation, respectively. Numerical results show that: for the short-term case, the on-grid energy consumption can be reduced by up to 34%, which is better than other methods. Meanwhile, for the long-term case, using the model predictive controller can save up to 22% regarding the on-grid only macro-BS approach.

#### 1.2.4.2 EH Networks with RF Sources

Natural resources might not always be available for terminal devices to harvest energy. For instance, the locations or weather conditions play a crucial role in deciding how much energy can be harnessed. On the contrary, the user devices in RF-EH networks benefit from stable and controllable RF energy sources, e.g., base stations. In the following, some recent works on RF-EH networks are summarized.

Two relaying protocols were proposed for an RF-EH relay node in Nasir, A. A., Zhou, X., Durrani, S. & Kennedy, R. A. (2013). These protocols are based on time-switching and power-splitting with perfect CSI available at the destination node. Thus, the paper studied both the delay-limited and non-delay-limited transfers, and provided closed-form expressions of the outage capacity and the ergodic capacity. Further, the authors devised the optimal time-switching and power-splitting ratios for the two relaying protocols. On this basis, they claimed that considering the throughput performance, the relaying protocol based on time-switching outperforms the one based on power-splitting.

In Ju, H. & Zhang, R. (2014b), an extension of the harvest-then-transmit protocol was proposed to deal with the doubly near-far problem using user cooperation. The authors studied a two-user time division multiple access (TDMA) RF-EH network. Given this model, during the allocated time slot, the near user is responsible for using its harvested energy to forward the information of the distant user before conveying its own data. Thus, the time and power allocation schemes are optimized to maximize the weighted sum-rate. Using user cooperation, the authors show that the proposed scheduling scheme improves both the user fairness and throughput significantly.

The work in Krikidis, I., Sasaki, S., Timotheou, S. & Ding, Z. (2014a) investigated the configuration of the antenna array at the relay node over MIMO relay communication channels. A dynamic antenna switching scheme was proposed to schedule a number of the best channels for information decoding or EH while allocating the remaining channels for EH or information decoding. The closed-form outage probability expression for the proposed scheme was derived.

Further, the scheme was investigated in the case of co-channel interference and a zero-forcing receiver employed at the relay node.

A downlink scheduling scheme for an RF-EH network was studied in Morsi, R., Michalopoulos, D. S. & Schober, R. (2015). This scheme schedules a user for information reception and the others for harvesting energy in each time slot. Thus, the authors provided two schemes to manage the information and energy tradeoff. Specifically, the first scheme works based on the order of normalized SNR whereas the second one chooses the user according to throughput and SNR criteria. Both schemes were proven to attain user fairness regarding the EH performance. The work showed the tradeoff between the average EH performance and ergodic capacity under different the orders of SNR. Further, the closed-form expressions of the average harvested energy and capacity were derived for fading channels.

Particularly, the very recent work in Salman, E., Stanaćević, M., Das, S. & Djurić, P. M. (2018); Wan, T., Karimi, Y., Stanacevic, M. & Salman, E. (2017,1) proposed and developed a novel AC computing methodology for wireless powered-IoT devices. Conventionally, the computational logic component is supplied by DC, resulting in an AC-to-DC conversion loss. The proposed approach enables the direct use of AC for computation based on charge-recycling theory. It can decrease the energy consumption, one of the difficulties in realizing the global expandability of IoT.

## 1.3 Wireless Information and Power Transfer

### 1.3.1 The Concept of Wireless Information and Power Transfer

#### 1.3.1.1 Wireless Power Transfer

Conventional EH methods depend on ambient renewable energy sources, such as solar energy and wind energy, which are unstable and even unforeseeable in some situations. Thus, harvesting energy from intentionally generated electromagnetic (EM) sources is a promising al-

ternative approach. This motivates the concept of WPT initiated by Nikola Tesla in the 1910's. WPT can be defined as a method to convey the electrical energy from a source to wireless devices without using solid wires or conductors. Fig. 1.3 shows the principle of three main WPT techniques, namely inductive coupling, magnetic resonance coupling, and RF power transfer.

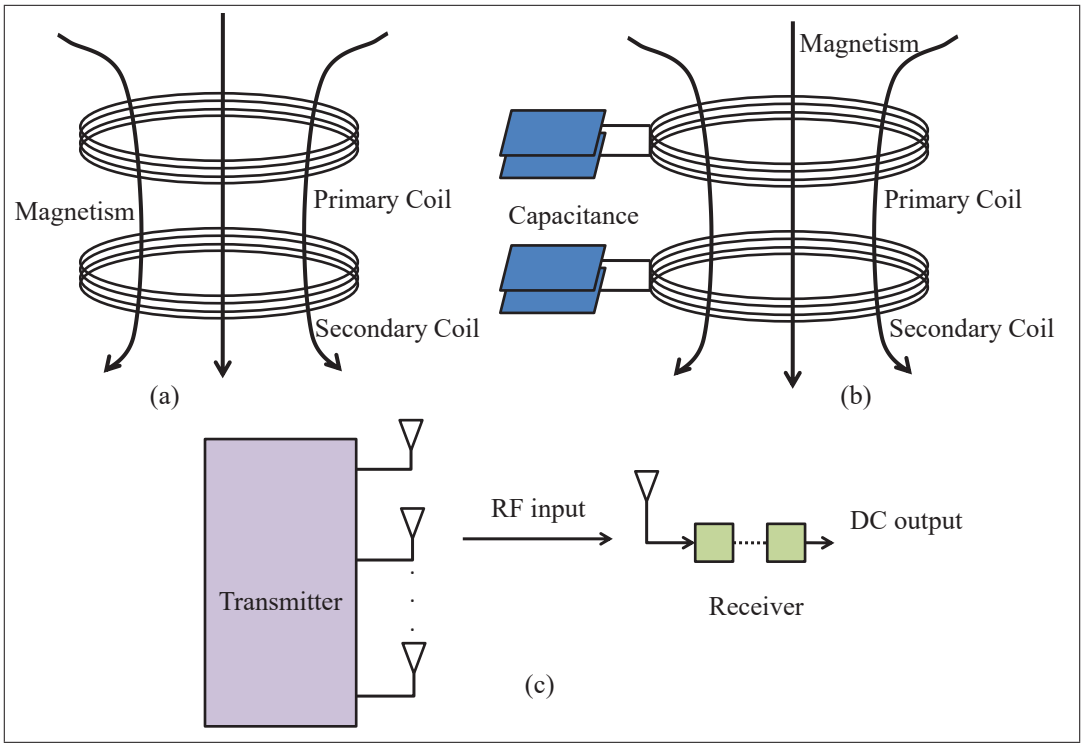


Figure 1.3 Wireless Charging Models: (a) inductive coupling, (b) magnetic resonance coupling, (c) RF wireless energy transfer

Considering the first two techniques, the inductive coupling technique Covic, G. A. & Boys, J. T. (2013) relies on the magnetic field induction that carries the energy between a primary coil and a secondary coil. Next, another technique, so-called the magnetic resonance coupling Kurs, A., Karalis, A., Moffatt, R., Joannopoulos, J. D., Fisher, P. & Soljacic, M. (2007), utilizes an evanescent-wave coupling to generate and transfer the electrical energy between two resonators. Each resonator is created by using an additional capacitance on an induction coil. In fact, both the inductive coupling and the magnetic resonance coupling techniques are used for the applications with near-field wireless transmissions. Therefore, they might not be suit-

able for mobile and remote replenishment/charging over a long range, such as wireless sensor networks and cellular networks.

Unlike the two above techniques, RF power transfer Visser, H. & Vullers, R. (2013) can be seen as a solution for far-field transmission. In this context, the RF signals with a frequency range between 3kHz and 300 GHz are used to carry the energy. On this basis, the RF power transfer is able to remotely recharge a number of wireless devices working in a wide area. However, the signal strength degrades according to the propagation loss, such as the transmission distance, fading effects, etc.

Furthermore, Table I shows a comparison between the three primary WPT techniques. We can observe that the RF WPT technique outperforms the others on the effective energy transfer distance. However, the main drawback is that it has low energy efficiency in RF-to-DC conversion due to the propagation loss.

Table 1.1 A comparison of three WPT techniques

| **WPT Techniques** | **Propagation** | **Charging Distance** | **Applications** |
|---|---|---|---|
| Inductive Coupling | Non-radiative | From a few millimeters to a few centimeters | Wireless sensor networks, mobile electronics (e.g, smart phones and tablets) |
| Magnetic Resonance Coupling | Non-radiative | From a few centimeters to a few meters | Mobile electronics, home appliances, cell phone charging, electric vehicle charging |
| RF Power Transfer | Radiative | Up to several kilometers. Typically, it depends on the performance of RF harvesting receiver, the fading effects, ect. | Cell phone charging, cellular networks, wireless sensors, implanted body devices, plug-in hybrid electric vehicle |

### 1.3.2 Wireless Information and Power Transfer

Indeed, WPT is a very promising technology and might bring many great conveniences for future wireless networks. However, it comes with some challenging problems, such as spectrum sharing between information transmission and power transfer. The reason for this is that the power transfer occupies a part of the spectrum used for the information transmission. To avoid the interference to information transmission, we can use orthogonal frequency channels to transmit information and energy at the same time. Nevertheless, this solution is inefficient.

To overcome the above problem, SWIPT is designed to save the spectrum by using the same waveform to convey the information and energy simultaneously. Its principle relies on the fact that any waveforms for the information signal also carry energy which can be converted to the electrical power. As a consequence, there exists a trade-off between the quality of decoded information and the amount of harvested energy.

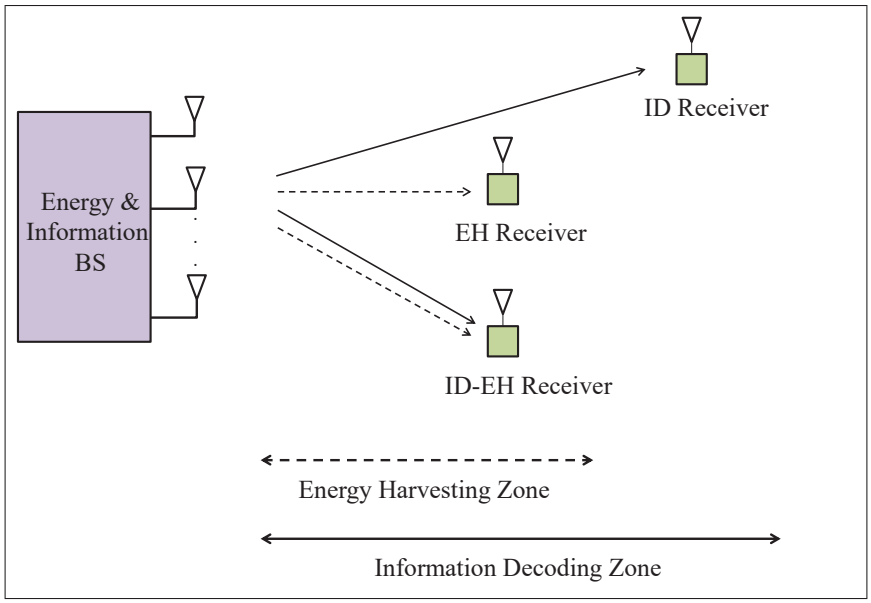


Figure 1.4 SWIPT System

A basic SWIPT network system, as illustrated in Fig. 1.4, consists of one multi-antenna transmitter able to transmit jointly the energy and information signals, one ID receiver, one EH

receiver, and one ID-EH receiver which is not only able to decode the information but also harvest the energy.

As shown in Fig. 1.4, the solid and dashed arrows represent the information and energy flows, respectively. Further, the solid and the dashed curves divide the network area into EH and ID zones. The reason for this is that the operating power level of EH is much higher than that of ID. More specifically, the specific ID and EH receivers work under much distinct power sensitivities, i.e., $-10$ dBm and $-60$ dBm for the energy and the information receivers, respectively Zhang, R. & Ho, C. K. (2013). The devices in the information zone can successfully decode the information sent by the transmitter, whereas the devices in the EH zone can do both harvesting and decoding efficiently.

### 1.3.3 SWIPT Receiver Architectures

In practice, there are two challenging issues when it comes to SWIPT systems. First, the current circuit designs cannot extract the RF energy from the decoded information signals. Any energy carried by the received RF signals is lost during the decoding process. Second, the conventional information receiver is optimal for information reception only, not for EH. This is due to a big gap that exists between power sensitivities of the ID and the EH receivers. Thus, the design of the receiver architecture plays a vital role in the achievable performance. In the following, we present an overview of receiver structures used in SWIPT systems.

#### 1.3.3.1 Antenna-Switching Receiver Architecture

Fig. 1.5 depicts a fundamental model of an antenna-switching receiver architecture. In this architecture, the energy harvester and the information decoder have their own separated antenna(s). Specifically, the antenna array is divided into two sets, and each set is connected to either the ID or the EH receivers. The most interesting feature of this architecture relies on its capability of conducting the EH and the ID processes independently. According to the various

CSIs observed at the antennas, the antenna-switching scheme can exploit the channel diversity and flexibly maximize either the performance of the ID or EH.

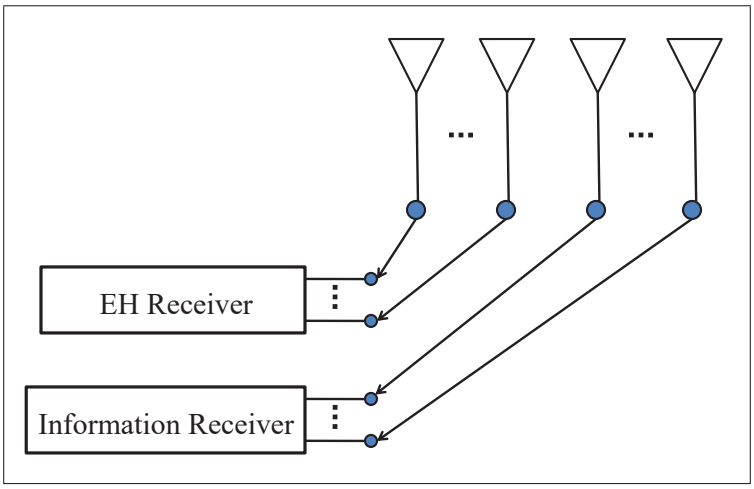


Figure 1.5 Antenna-switching receiver

#### 1.3.3.2 Time-Switching Receiver Architecture

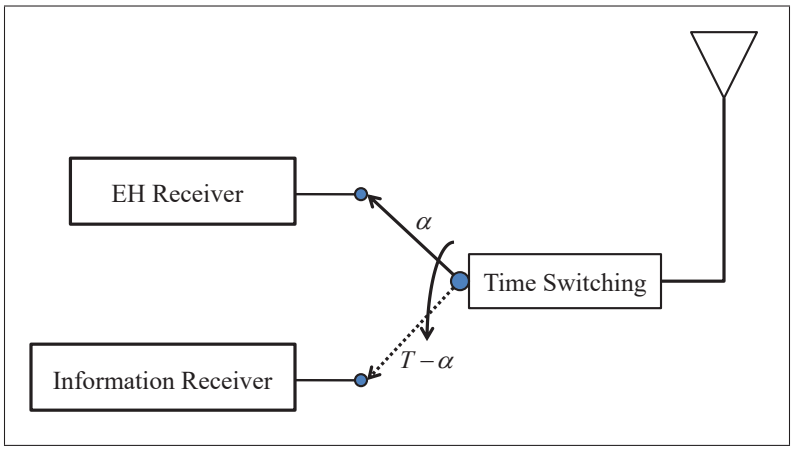


Figure 1.6 Time-switching receiver

A time-switching receiver architecture composed of an ID receiver, an EH receiver and a time-switcher is shown in Fig. 1.6. Its structure allows the wireless receiver to switch between the ID receiver or the EH receiver to obtain RF signals. At the transmitter side, the BS decomposes the transmission block into two separated time slots, one for conveying the energy and the other

for transmitting data. At each time slot, different transmit waveforms can be used to optimize either the energy or information transmission performances. Furthermore, the receiver can switch the working mode periodically between the harvesting energy and decoding information phases. Therefore, various rate-energy trade-offs could be achieved by adjusting the length of such time slots, i.e., the factor $\alpha$.

#### 1.3.3.3 Power-switching Receiver Architecture

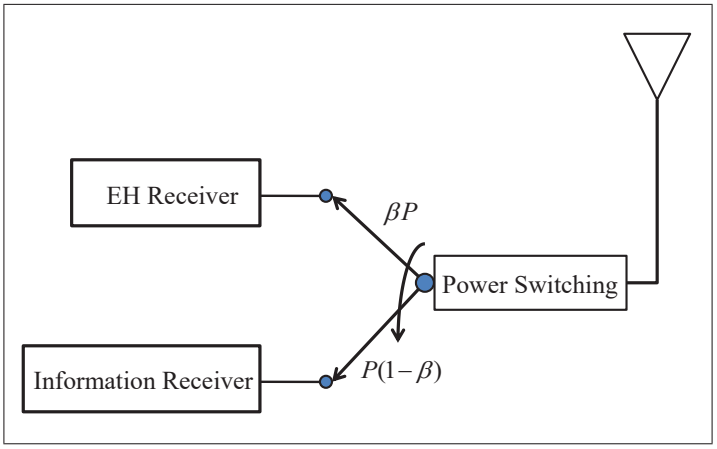


Figure 1.7 Power-switching receiver

The components of a power splitting receiver are illustrated as in Fig. 1.7. In the power-splitting architecture, the received RF signals are decomposed into two flows for the ID and EH receivers with different power levels. In this concern, one stream with power ratio $\beta$ $(0 \leq \beta \leq 1)$ is used for EH while the rest, with power ratio $(1-\beta)$, is used for ID. However, the BS cannot optimize the transmitted signals for both ID and the EH performanced at the same time where different rate-energy trade-offs are achieved by adjusting the value of $\beta$.

#### 1.3.3.4 Integrated Receiver Architecture

The work in Zhou, X., Zhang, R. & Ho, C. K. (2013) developed an integrated receiver (IntRx) architecture as shown in Fig. 1.8. Unlike the time-switching and power-switching receivers that process the RF signals in the RF band, the IntRx splits the signals after converting them

into DC. In this case, the information decoder does not need to install low pass filter which work as an RF band-to-baseband conversion module, since this operation has been integrated into the energy receiver. In more details, after passing through the dynamic power splitter, the baseband signal is sampled and then digitalized using an analog-to-digital converter (ADC). Thus, the integrated receiver architecture has a reduced form. Note that the dynamic power splitter can work as a time switcher or power splitter.

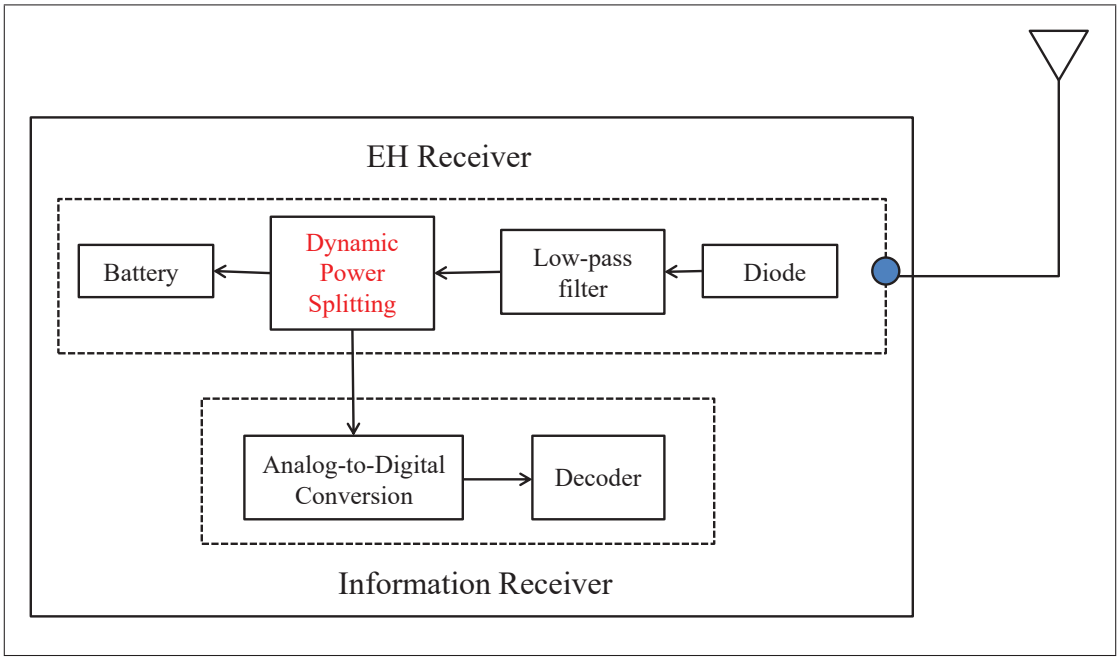


Figure 1.8 Integrated receiver

#### 1.3.3.5 Ideal Receiver Architecture

Some pioneer works in Fouladgar, A. & Simeone, O. (2012); Grover, P. & Sahai, A. (2010); Popovski, P., Fouladgar, A. & Simeone, O. (2013); Varshney, L. (2008) considered ideal receiver architectures to provide the theoretical upper bound of receiver's performance. In view of the ideal receiver architecture, they assume that the receiver can extract the RF energy from the decoded signals. However, this assumption is not feasible in practice. The existing circuit designs cannot extract RF energy from the decoded information carrier concurrently yet. In

other words, the total energy carried by the RF message-bearing signals is lost during the ID process.

#### 1.3.3.6 Comparison between Receiver Designs

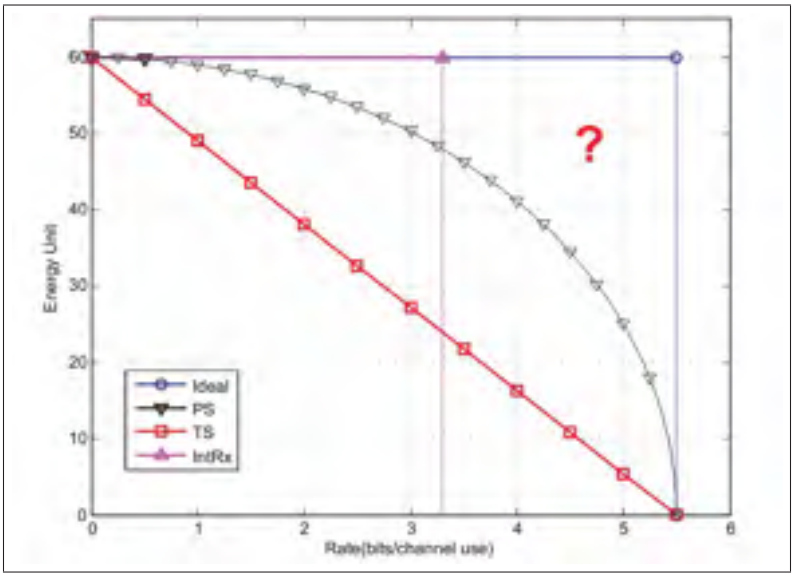


Figure 1.9 Comparison between receiver designs
Taken from Bi, S., Ho, C. & Zhang, R. (2015)

As shown in Fig. 1.9, the authors Bi *et al.* (2015) gave an example to illustrate the key characteristics of the rate-energy regions. Moreover, they investigated three practical receivers and one ideal receiver in a point-to-point additive white Gaussian noise (AWGN) channel. One can see that the rate-energy region of the ideal receiver is rectangular since no design tradeoff is involved in this case. A similar rate-energy region is also observed for IntRx. This is because the optimal strategy uses an infinitesimally small amount of DC for the ID and the remaining DC for the EH. The rate-energy region of the time-switching receiver is a straight line connecting the two optimal operating points for EH and ID, respectively. Compared to the time-switching receiver, the power-switching receiver has a strictly larger rate-energy region.

Indeed, the optimal EH-ID receiver is still unknown. It is unclear whether the non-trivial rate-energy region between the ideal and the introduced practical receivers could be achieved or

not, which is left for future exploration likely involving different domains, such as physics, circuits, and information theories.

### 1.3.4 Recent Works in terms of SWIPT Networks

#### 1.3.4.1 Beamforming Designs for SWIPT Networks

Due to the property of spatial multiplexing, multiple antennas and beamforming techniques can improve the power transfer efficiency significantly, while guaranteeing the high spectral efficiency of the information transmission. Indeed, beamforming has been considered as a key technique for feasible implementations of SWIPT networks.

For the first time, the work in Zhang & Ho (2013) addressed the beamforming optimization for SWIPT systems. The authors considered a SWIPT MIMO wireless broadcast system, including a BS and one or two active users. They assumed that the wireless channel is a quasi-static fading environment and the BS has perfect channel knowledge. For the scenario of two users, when a user obtains the information from the transmitter, the other one operates as a harvesting receiver. The work provided the optimal transmission strategy with the trade-off between the achieved information and energy. A semi-closed-form expression for the optimal covariance matrix is derived to satisfy rate-energy requirements. For the case of only one working user, the user harvests energy and decodes information using the same signal simultaneously. An outer bound for the achievable rate-energy region is shown for practical designs, such as time switching and power splitting. It is found that the performance bound cannot be generally achieved due to the fact that the EH receiver cannot decode the information directly. Furthermore, the wireless powered communication networks benefit from the interferences which increase the amount of harvested energy. Therefore, this leads to the issue of handling the compromise between information, harvested energy and interference.

Due to the distributed nature of wireless environments, the message-bearing signal can be easily eavesdropped and extracted by eavesdroppers. Therefore, secure transmission in MISO

SWIPT systems is an extremely important issue. In Ng, D., Lo, E. & Schober, R. (2014), a multiuser MISO SWIPT system which consists of a transmitter, multiple legitimate receivers, and multiple passive eavesdroppers was considered. The legitimate receivers were classified into two types, namely desired receivers and idle receivers. They are able to decode the information and harvest the energy from RF signals. Particularly, the authors treated the idle receivers as potential eavesdroppers due to secrecy issues. In this work, a dual use of both the artificial noise and the energy signals is proposed to enhance energy transfer efficiency and ensure communication security. In particular, when incomplete CSI of the eavesdroppers is available at the transmitter, the artificial noise and the energy signals are very useful in scaling down the signal performance at the eavesdroppers. The design of a resource allocation algorithm considering both artificial noise and energy signals is formulated as a non-convex optimization problem. Its objective function is to minimize the total transmit power, whereas the constraints take various requirements into account. To tackle this problem, the authors replaced a non-convex probabilistic constraint by a tractable convex deterministic one. The reformulated non-convex optimization problem is solved by a semidefinite programming-based resource allocation algorithm. Furthermore, a suboptimal scheme with low computational complexity is also provided.

Furthermore, accounting for exploiting the spatial degrees of freedom of the channel, the research in Timotheou, S., Krikidis, I., Karachontzitis, S. & Berberidis, K. (2015) investigated a new technique for MIMO SWIPT systems. In contrast to the well-known time-switching and power-switching approaches, their technique does not refer to the antenna elements Krikidis *et al.* (2014a); Liu, L., Zhang, R. & Chua, K.-C. (2013). Using singular value decomposition (SVD), the MIMO communication links can be transformed into eigenchannels that can convey either the information or the energy. Considering the practical assumption of imperfect CSI, the authors assumed that there exists channel estimation error in the decomposition process. This generates interference to the eigenchannels, and hence the interference between the eigenchannels is also addressed. Accordingly, the authors formulated an optimization problem minimizing the total transmit power with maximum power per eigenchannel, information, and energy constraints. The problem can be considered as a mixed-integer nonlinear program. The

authors provided the optimal solution as well as very close to optimal solutions with robust computational performance. An optimal polynomial complexity algorithm is further provided for the problem with no maximum power per eigenchannel constraint. Particularly, using Lagrange theory, a water filling-like procedure for the optimal power allocation is derived when the eigenchannel assignment is known. Then, a low polynomial complexity algorithm which induces a near-optimal solution for a broad range of parameter configurations is presented.

In another work, the authors Lee, H., Lee, S., Lee, K., Kong, H. & Lee, I. (2015) considered the beamforming optimization for SWIPT in MISO interference channels (IFCs). The system model consisted of an information transmitter, an information receiver, an energy transmitter, and an energy receiver. The paper proposed two cooperation categories. The first one considered a partial cooperation (PCoop) scheme, in which only CSI was available at transmitters and receivers (except the signal waveform). The second one addressed IFC with full signal cooperation (SCoop), where both the CSI and the signal waveforms were known by transmitters and receivers, was examined. They constituted the non-convex optimization problems for IFC-PCoop and IFC-SCoop, respectively, where the information rate was maximized under minimum required harvested energy constraints to obtain the Pareto boundary. To solve these problems, the original problem was separated into two subproblems with the introduction of two new parameters so-called energy splitting and power splitting metrics, for the IFC-PCoop and the IFCSC, respectively. Accordingly, the closed-form solutions were provided by using the line search method.

#### 1.3.4.2 Cooperative Relay Schemes in SWIPT Networks

The cooperative relaying technique is one of the best solutions to overcome the attenuation and fading effects by using the help of intermediate relay stations. By applying cooperative relaying, the network's reliability and efficiency can be improved. Therefore, this technique is highly useful in SWIPT networks where the path loss is one of the most important issues.

A SWIPT relay network, in which source-destination (S-D) pairs communicate with each other with the help of the assigned EH relays, was investigated in Chen, H. H., Li, Y., Jiang, Y., Ma, Y. & Vucetic, B. (2015). At each relay (R), the received signal was split into two streams dedicated for either information forwarding or energy harvesting. With the aim of improving network-wide performance, the authors used the game theory to develop a scheme of distributed power splitting for the considered system model. In this context, each S-R-D link was considered as a strategic player who tried to maximize the corresponding individual rate. Further, the formulated games were studied in terms of Nash equilibriums. After that, the authors studied the extension of mixed amplify-and-forward and decode-and-forward relays. To this end, they showed that the proposed algorithm can attain near-optimal solutions for the network-wide performance.

In Zeng, Y. & Zhang, R. (2016), the authors studied a wireless-powered amplify-and-forward relay system where a multi-antenna source node transmits information to a single-antenna destination node with the help of a multi-antenna full-duplex relay node. The proposed protocol can be described as follows. In the first phase, the source node transmits information to the relay node. In the second phase, at the same time, the relay forwards the amplified information signal to the destination and receives the energy signal from the source node. The proposed protocol takes two main advantages: (i) uninterrupted information transmission is guaranteed since there is no time and power-sharing/switching, and (ii) self-energy recycling is exploited, i.e., at the relay node, a part of the transmit signal interfering with the receive antennas can be harvested and re-used. Given the system model and the protocol, the authors devised the optimal power allocation and beamformers for the relay node. The paper showed that the protocol can achieve a significant throughput enhancement compared to the conventional time-switching relay protocol.

The authors Ding, Z., Krikidis, I., Sharif, B. & Poor, H. V. (2014) considered a SWIPT cooperative network in which decode-forward relays are randomly located. In the first scenario, one S-D pair and multiple EH relays were studied. Three different relay configurations were taken into account. Accordingly, by means of stochastic geometry, the performances regarding diver-

sity enhancement and outage probability are depicted. Based on analytical results, the authors claimed that wisely chosen EH relays can attain the same diversity gain as the self-powered relays. Nonetheless, the outage probability in the case of EH relays is higher than the one in the conventional case. In the second scenario, the authors considered the presence of multiple sources. In particular, such sources compete with each other in order to obtain the help of the EH relays. This competition is formulated as a coalition formation game. Accordingly, to address this problem, two game theory-based algorithms were proposed relying on different payoff functions.

#### 1.3.4.3 SWIPT Receiver Operation

In principle, ID-EH receivers use the same antenna array for both information reception and EH. Thus, most of the existing works follow the time-switching and power-splitting designs. Moreover, they have mainly investigated the trade-off in various circumstances to satisfy specific performance goals. In what follows, some recent works are summarized.

In Liu *et al.* (2013), a time-switching based policy for a time-varying fading channel was investigated. First, for the case with unknown CSI at the BS, a time-switching policy was proposed to leverage the ID and EH performances opportunistically. Second, when the CSI was available at the BS, the authors jointly designed a transmit power allocation and receiver policy. The policy coordinates the receiver to harvest energy when channel gain is higher than a preset threshold and to decode information otherwise. Some complexity-reduced policies were also provided, one of them works according to co-channel interference. Importantly, the authors concluded that optimal trade-off between ID and EH performances implies that allocating the best channels to energy transfer is preferred to information transmission.

The work in Zhou *et al.* (2013) developed an integrated receiver architecture by generalizing the time-switching and power-splitting cases. The receiver policy allows the RF signal to be dynamically split into two streams over time for ID and EH. Further, a special case of the policy, so-called on-off power-splitting, was proposed. In the off mode, all RF signals are fed

to the energy harvester. On the other hand, the receiver works as a power splitter in the on mode. Based on the analytical and simulation results, the authors concluded that the on-off is optimal for co-located and integrated receivers when circuit power consumption is taken into account.

The paper Zhou, X. (2014) investigated how to achieve the maximal ergodic capacity for a power-splitting receiver by designing a training phase. The authors proposed using a block-wise transmission scheme including training and transmission phases. On this basis, an optimal power-splitting scheme was designed for both phases to maximize the ergodic capacity whereas satisfying the EH requirements. Further, the authors provided non-adaptive/adaptive power-splitting schemes in which the splitting factors were fixed/adjusted in all blocks during the transmission phase. They showed that both schemes can achieve optimal solutions. In particular, the adaptive scheme outperforms the non-adaptive one with respect to the capacity where the performance gap is higher when more EH rate is required.

# CHAPTER 2

# DOWNLINK POWER OPTIMIZATION FOR HETEROGENEOUS NETWORKS WITH TIME REVERSAL-BASED TRANSMISSION UNDER BACKHAUL LIMITATION

Ha-Vu Tran[1], Georges Kaddoum[1], Hung Tran[2], and Een-Kee Hong[3]

[1] Department of Electrical Engineering, École de Technologie Supérieure,
1100 Notre-Dame west, Montreal, Canada H3C 1K3.
[2] School of Innovation, Design and Engineering,
Mälardalen University, Västerås, Sweden 721 23.
[3] School of Electronics and Information, Kyung Hee University,
Yongin, South Korea 449-701.

Paper published in *IEEE Access*, vol. 5, pp. 755-770, January 2017.

## 2.1 Introduction

Recently, heterogeneous network (HetNet) has been considered as a promising solution to enhance the throughput and to overcome the drawbacks of traditional cellular networks Buzzi *et al.* (2016); Hossain, E. & Hasan, M. (2015); Zahir, T., Arshad, K., Nakata, A. & Moessner, K. (2013), such as the inefficient usage of spectrum and dynamic spectrum access. According to the heterogeneous network (HetNet) concept, the macrocell serves a large number of users in a wide area while low power cells such as femtocells, picocells and microcells handle a smaller number of users. Following this approach, not only the coverage range is expanded but also the throughput and reliability can be improved significantly. More specifically, the works reported in Andrews, J., Claussen, H., Dohler, M., Rangan, S. & Reed, M. (2012); Buzzi *et al.* (2016); Hossain & Hasan (2015); Zahir *et al.* (2013) have investigated a HetNet model in which an original cellular network is decomposed into multi-tier networks, and each tier is responsible for a specific zone. These approaches have expanded the coverage ranges over the dead zones and hot zones of traditional cellular networks. Therefore, the *femtocell* is considered as one of the most cost-efficient provisioning for cellular network services Bennis, M., Giupponi, L., Diaz, E., Lalam, M., Maqbool, M., Strinati, E., De Domenico, A. & Latva-aho, M. (2011).

Regarding the radio environment, the signal power is often degraded due to path-loss effects and multipath propagation, and such an issue becomes more severe in the frequency selective fading. On the other hand, many techniques have been employed to mitigate the adverse effects of frequency selective channels such as: equalizers, multiple-input multipleoutput (MIMO) and time reversal (TR) techniques. When applied to wireless receivers, the first two techniques provide significant enhancement to the received signal-to-noise ratio (SNR). However, from the implementation point of view, these techniques are high-cost and require complex equipment which make them less interesting to be used at the subscriber end where limited energy and processing resources are the major constraints.

However, a special class of beamforming technique, namely the time reversal (TR), which was mainly used in acoustics and underwater communication systems, has been proposed in Bouzigues, M.-A., Siaud, I., Helard, M. & Ulmer-Moll, A.-M. (2013); Chen, Y., Wang, B., Han, Y., Lai, H.-Q., Safar, Z. & Liu, K. R. (2016b); Kaiser, T. & Zheng, F. (2010); Maaz, M., Helard, M., Mary, P. & Liu, M. (2015); Pitarokoilis, A., Mohammed, S. & Larsson, E. (2015); Siaud, I., Ulmer-Moll, A.-M., Bouzigues, M.-A. & Cassiau, N. (2015); Tran-Ha, V., Vu, Q.-D. & Hong, E.-K. (2015); Viteri-Mera, C. A., Teixeira, F. L. & Sainath, K. (2015) to wireless communications, e.g. ultra-wideband, large-scale antenna, and millimeter-wave systems. This techique provides a promising solution to save the processing cost and to combat the adverse effects of frequency selective fading channels. Benefiting from the reciprocal properties of wireless channels, the TR technique principles rely on using the time-reversed form of a channel impulse response (CIR) to pre-filter the transmitted signal which leads to the power convergence of this latter in the time and space domains at the receiver side. Specifically, the CIR at the transmitter side is estimated by virtue of a pilot signal sent from the receiver.

Particularly, some works have addressed the designs of TR beamforming. In Bouzigues *et al.* (2013), the authors have provided an analysis of the TR technique for green radio communications employed to WiFi-certified technologies. The work Viteri-Mera, C. A. & Teixeira, F. L. (2016) proposes three forms of space-time block diagonalization on the platform of the TR technique. Further, Yang *et.al.* Yang, Y.-H., Wang, B., Lin, W. & Liu, K. (2013) propose a

novel TR waveform to maximize the sum-rate of a multi-user system. In addition, the paper Yoon, E., Kim, S.-Y. & Yun, U. (2015) introduces a design of a TR-based waveform using predistortion to combat inter-symbol interference (ISI). In fact, encouraging results obtained in Bouzigues *et al.* (2013); Chen *et al.* (2016b); Maaz *et al.* (2015) show that the TR-based transmission is an ideal paradigm for green wireless communications. Moreover, the experiments in Henty, B. E. & Stancil, D. D. (2004); Nguyen, H. T., Pedersen, J., Kyritsi, P. & Eggers, P. (2006) confirm that the TR technique is feasible for broadband systems including femtocell networks.

In our paper, we focus on studying a realistic scenario of heterogeneous network (HetNet) system consisting of macrocell base station (MBS) and femtocell base station (FBS) and their users under backhaul limitation. The different channels in this network are subject to frequency selective fading. In our model, it is assumed that different cellular stations are equipped with multiple antennas whereas each receiver has one antenna due to the limited resources at the user end. Conventionally, a central controller, likely MBS, is responsible to compute the beamformers and power vectors for each base station (BS) located in the HetNet. Hence, this process requires a solid backhaul connections that must be always available to accommodate the central controller with all channel state information (CSI) of the different users located in different cells Andrews *et al.* (2012); Tolli, A., Pennanen, H. & Komulainen, P. (2011). However, in a realistic case that backhaul connection endures congestion in which obtaining sufficient amount of CSI might become infeasible. Therefore, given the system model, this work aims at seeking solutions for the question that *how to mitigate the frequency selectivity of fading channels, and to deal with the limited backhaul connection while taking the processing burden of the macrocell and the transmit power restriction of the femtocell network into account?* In the following, the potential proposed methods are discussed.

In this vein, one of our novelties consists of applying zero-forcing and TR techniques to MBS and FBS respectively to combat channel selectivity and to enhance network performance. In fact, zero-forcing is one of the most efficient beamforming techniques, and it is an interesting solution for macrocell networks Rozé, A., Hélard, M., Crussière, M. & Langlais, C. (2015);

Vu, Q.-D., Tran, L.-N., Farrell, R. & Hong, E.-K. (2016). However, in a femtocell working environment where FBS's transmit power is limited, zero-forcing might not be a promising approach due to the transmit power restriction and hardware limitation Peel, C., Hochwald, B. & Swindlehurst, A. (2005); Rozé *et al.* (2015); Zahir *et al.* (2013). In this case, the TR which offers an alternative low-cost beamforming technique, is proposed to provide a better system performance for femtocell networks.

Moreover, we propose a novel optimal power allocation method, assuming that the backhaul connection may only convey a limited throughput for signaling exchange. In single-tier multi-cell networks, the concept of cross-interference management has been introduced to deal with backhaul limitation Tolli *et al.* (2011). However, this approach might not be applied to multi-tier HetNets directly since macrocell users (MUs) and femtocell users (FUs) have different priorities. Besides, there are several previous works addressing the issue of backhaul limitation for HetNets Joeng, Y., Quek, T. Q. & Shin, H. (2011); Nguyen, D., Le, L. B. & Le-Ngoc, T. (2015). In principle, these works focus on splitting the conventional optimization problem into two subproblems (i.e. one for the macrocell and the other for the femtocell) in which solutions can be achieved with a reduced amount of required CSI. In our work, decoupling the original problem is adopted in a different manner to deal with backhaul limitation. In particular, the proposed scheme only requires the minimized cross-tier interference sent from the femtocell. This latter reduces the signaling overhead in the network compared with the scheme proposed in Joeng *et al.* (2011), and releasing the FUs from the task of measuring cross-interference caused by the MBS compared with the another work Nguyen *et al.* (2015). Moreover, importantly, our scheme can control the priority of MUs by using a preset threshold of the cross-tier interference that the MBS causes to the FUs. On this basis, the network operator can flexibly manage the overall network performance. Especially, we solve the considered macrocell and femtocell problems by devising optimal closed-form solutions which do not appear in the literature.

Furthermore, most of previous publications Bouzigues *et al.* (2013); Maaz *et al.* (2015); Viteri-Mera & Teixeira (2016); Yoon *et al.* (2015) address the designs of TR beamforming under

the assumption of perfect channel estimations. There are no existing works which consider the worst-case robust beamforming for the TR technique. Given this conern, the robust design is formulated into a non-convex problem. To transform such a problem into a tractable formulation to solve, the effects of channel estimation errors (CEE) on TR-based systems are analyzed in terms of the worst-case boundaries of desired signal and interference components. Especially, to tackle this case, a well-known Young's inequality Young, W. H. (1912) is able to bring an efficient solution dealing with the boundaries of ISI and co-tier interference. However, a novel tighter boundary formulation is derived to enhance the performance of power allocation strategy. On this basis, the robust optimization problem is relaxed into a convex problem that can be solved by closed-form expressions.

According to the discussed content, the main contributions of this work are summarized as follows

- The application of TR technique for the femtocell network is proposed,
- A novel downlink optimization method dealing with limited backhaul connections is provided,
- Closed-form optimal solutions are derived for both the downlink power minimization problems of macrocell and femtocell,
- A robust worst-case power allocation problem of TR-employed femtocell under the effects of imperfect CSI is analyzed.

Given this outline, the remainder of this paper is organized as follows: In Section 2.2, the system model is described. The beamforming designs for MBS and FBS are discussed in Section 2.3. In Section 2.4, the proposed power allocation manner is presented. In Section 2.5, the worst-case robust problem is formulated and analyzed. In Section 2.6, numerical results and discussions are provided. Finally, concluding remarks are put forward in Section 2.7.

*Notation:* The notation $\mathbb{R}_{+}^{m}$ and $\mathbb{C}^{m\times n}$ denote the sets of $m$-dimensional nonnegative real vector and $m \times n$ complex matrix, respectively. The boldface lowercase $\mathbf{a}$ and uppercase $\mathbf{A}$ indicate

vectors and matrices, respectively. The superscripts $\mathbf{A}^T$ and $\mathbf{A}^H$ represent the transpose and transpose conjugate, respectively. In addition, symbols $|.|$, $\|.\|$, and $\|.\|_1$ stand for the absolute value, vector Euclidean norm and vector $l_1$-norm, respectively. For a complex value, we denote $\Re\{.\}$ and $\Im\{.\}$ to be the real and imaginary part, respectively.

## 2.2 System Model

As shown in Fig. 2.1, a two-tier HetNet system including one MBS and one FBS is considered. For convenient notation, we denote the MBS as $\mathscr{B}_0$ and the FBS as $\mathscr{B}_1$. We assume that $\mathscr{B}_k$ ($k = \{0,1\}$) is equipped with $M_k$ antennas and serves $N_k$ users. On the other hand, FUs and MUs are equipped with a single antenna and a single tap diversity combiner.

Let $\mathbf{h}_{ij}^{kr} \in \mathbb{C}^{L\times 1}$ $(k,\ r = \{0,1\},\ \ 0 \le i \le M_k,\ 0 \le j \le N_r)$ denote the CIR between the $i^{\text{th}}$ transmission antenna of $\mathscr{B}_k$ and the $j^{\text{th}}$ user of $\mathscr{B}_r$. Moreover, $L$ denotes the maximum length of each CIR, and the superscript $k$ is used to represent superscript $kk$ for convenience in notation, (e.g. $\mathbf{h}_j^0$ is used to denote $\mathbf{h}_j^{00}$).

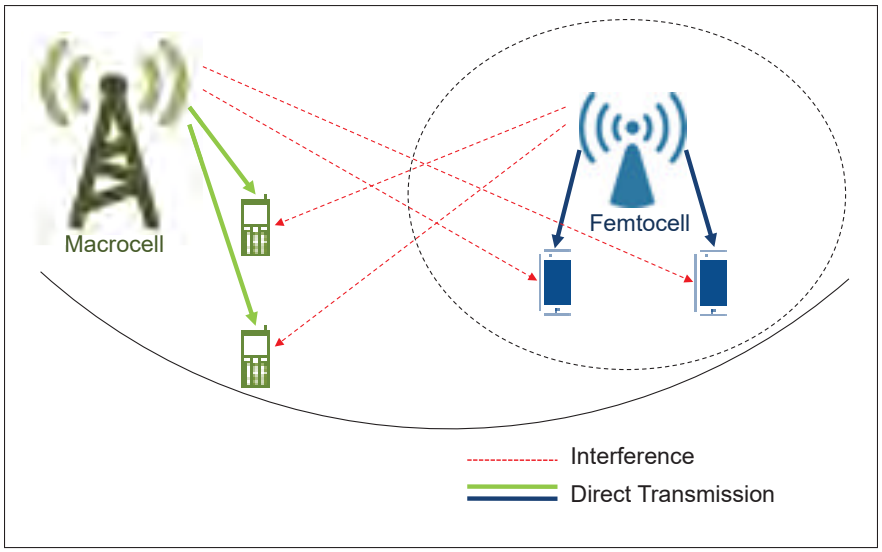


Figure 2.1 A two-tier system model including a macrocell and a femtocell

Therefore, the transmitted signals at $\mathscr{B}_0$ and $\mathscr{B}_1$ can be formulated, respectively, as

$$\mathbf{x}_n^0 = \sqrt{p_n^0}\left[\begin{array}{ccc} \mathbf{u}_{1n} & \ldots & \mathbf{u}_{M_0 n} \end{array}\right] s_n^0, (\mathbf{x}_n^0 \in \mathbb{C}^{L\times M_0}) \tag{2.1}$$

$$\mathbf{x}_j^1 = \sqrt{p_j^1}\left[\begin{array}{ccc} \mathbf{g}_{1j} & \ldots & \mathbf{g}_{M_1 j} \end{array}\right] s_j^1, (\mathbf{x}_j^1 \in \mathbb{C}^{L\times M_1}) \tag{2.2}$$

where $s_n^0$ and $s_j^1$ are scalars representing the unit power transmitted symbols for the $n^{\text{th}}$ MU and the $j^{\text{th}}$ FU, respectively. We define $\mathbf{p}^k = \left[\begin{array}{cccc} p_1^k & p_2^k & \ldots & p_{N_k}^k \end{array}\right]^T \in \mathbb{R}_+^{N_k\times 1}$ as the transmit power vector of the $\mathscr{B}_k$. Furthermore, $\mathbf{u}_{mn} \in \mathbb{C}^{L\times 1}$ is the beamformer for the $n^{\text{th}}$ MU used at the $m^{\text{th}}$ transmission antenna, and $\mathbf{g}_{ij} \in \mathbb{C}^{L\times 1}$ is the beamformer for the $j^{\text{th}}$ FU employed at the $i^{\text{th}}$ transmit antenna. Specifically, $\mathbf{u}_{mn}$ follows a zero-forcing-based algorithm whereas $\mathbf{g}_{ij}$ has the formulation of TR beamformer. The design of two such beamforming vectors is thoroughly discussed in Section 2.4.1 and Section 2.4.2.

In our paper, we consider the downlink communication scenario in which the MBS and the FBS transmit their signals to their corresponding users simultaneously and none of these communicate with its BS during this phase of communication. Accordingly, the received signal at the $n^{\text{th}}$ MU can be written as

$$\begin{aligned}\mathbf{y}_n^0 = &\sum_{m=1}^{M_0} \sqrt{p_n^0}\mathbf{u}_{mn} * \mathbf{h}_{mn}^0 s_n^0 + \sum_{\substack{n'=1\\ n'\neq n}}^{N_0}\sum_{m=1}^{M_0} \sqrt{p_{n'}^0}\mathbf{u}_{mn'} * \mathbf{h}_{mn}^0 s_{n'}^0 \\ &+ \sum_{j=1}^{N_1}\sum_{i=1}^{M_1} \sqrt{p_j^1}\mathbf{g}_{ij} * \mathbf{h}_{in}^{10} s_j^1 + \mathbf{n}_M, (\mathbf{y}_n^0 \in \mathbb{C}^{(2L-1)\times 1})\end{aligned} \tag{2.3}$$

where $\mathbf{n}_M$ is additive white Gaussian noise (AWGN), and $*$ is the convolution operator. It is noted that the first term in (2.3) is the received signal of the $n^{\text{th}}$ MU while the second term is the co-tier interference in the macrocell and the third term is the cross-tier interference from the femtocell.

Hence, at the $n^{\text{th}}$ MU, we define ${P_{(sig)}}_n^0$, ${P_{(isi)}}_n^0$, ${P_{(co)}}_n^0$, and ${P_{(cross)}}_n^0$ as the power of desired signal, ISI, co-tier interference power and cross-tier interference from femtocell, respectively,

as indicated in (2.4)-(2.7).

$$P_{(sig)_n^0} = \left| \left( \sum_{m=1}^{M_0} \sqrt{p_n^0}\mathbf{u}_{mn} * \mathbf{h}_{mn}^0 \right)[\alpha] \right|^2, \tag{2.4}$$

$$P_{(isi)_n^0} = \sum_{l \neq \alpha}^{2L-1} \left| \left( \sum_{m=1}^{M_0} \sqrt{p_n^0}\mathbf{u}_{mn} * \mathbf{h}_{mn}^0 \right)[l] \right|^2, \tag{2.5}$$

$$P_{(co)_n^0} = \sum_{\substack{n'=1 \\ n' \neq n}}^{N_0} \left\| \sum_{m=1}^{M_0} \sqrt{p_{n'}^0}\mathbf{u}_{mn'} * \mathbf{h}_{mn}^0 \right\|^2, \tag{2.6}$$

$$P_{(cross)_n^0} = \sum_{j=1}^{N_1} \left\| \sum_{i=1}^{M_1} \sqrt{p_j^1}\mathbf{g}_{ij} * \mathbf{h}_{in}^{10} \right\|^2, \tag{2.7}$$

where $\alpha$ represents the position of the selected tap.

Accordingly, the signal-to-interference-plus-noise ratio (SINR) at the $n^{\text{th}}$ MU can be formulated as

$$\begin{aligned} &\text{SINR}_n^0 \left( \alpha, \mathbf{p}^0, \{\mathbf{u}_{mn}\}_{n=1}^{N_0}, P_{(cross)_n^0} \right) \\ &= \frac{P_{(sig)_n^0}}{P_{(isi)_n^0} + P_{(co)_n^0} + P_{(cross)_n^0} + \|\mathbf{n}_M[\alpha]\|^2}, \end{aligned} \tag{2.8}$$

On the other hand, the received signal at the $j^{\text{th}}$ FU can be expressed as

$$\begin{aligned} \mathbf{y}_j^1 = &\sum_{i=1}^{M_1} \sqrt{p_j^1}\mathbf{g}_{ij} * \mathbf{h}_{ij}^1 s_j^1 + \sum_{\substack{j'=1 \\ j' \neq j}}^{N_1} \sum_{i=1}^{M_1} \sqrt{p_{j'}^1}\mathbf{g}_{ij'} * \mathbf{h}_{ij}^1 s_{j'}^1 \\ &+ \sum_{n=1}^{N_0} \sum_{m=1}^{M_0} \sqrt{p_n^0}\mathbf{u}_{mn} * \mathbf{h}_{mj}^{01} s_n^0 + \mathbf{n}_F, (\mathbf{y}_j^1 \in \mathbb{C}^{(2L-1)\times 1}) \end{aligned} \tag{2.9}$$

where $\mathbf{n}_F$ is AWGN. Here, the first term in (2.9) is the received signal for the $j^{\text{th}}$ FU, the second term is the co-tier interference in the femtocell, and the third term is the cross-tier interference from the macrocell.

Similarly, ${P_{(sig)}}_j^1$, ${P_{(isi)}}_j^1$, ${P_{(co)}}_j^1$, and ${P_{(cross)}}_j^1$, i.e. (2.10)-(2.13), represent the power of the desired signal, ISI, co-tier interference and cross-tier interference from macrocell, respectively.

$$ {P_{(sig)}}_j^1 = \left| \left( \sum_{i=1}^{M_1} \sqrt{p_j^1}\mathbf{g}_{ij} * \mathbf{h}_{ij}^1 \right) [\beta] \right|^2, \tag{2.10} $$

$$ {P_{(isi)}}_j^1 = \sum_{\substack{l=1 \\ l\neq\beta}}^{2L-1} \left| \left( \sum_{i=1}^{M_1} \sqrt{p_j^1}\mathbf{g}_{ij} * \mathbf{h}_{ij}^1 \right) [l] \right|^2, \tag{2.11} $$

$$ {P_{(co)}}_j^1 = \sum_{\substack{j'=1 \\ j'\neq j}}^{N_1} \left\| \sum_{i=1}^{M_1} \sqrt{p_{j'}^1}\mathbf{g}_{ij'} * \mathbf{h}_{ij}^1 \right\|^2, \tag{2.12} $$

$$ {P_{(cross)}}_j^1 = \sum_{n=1}^{N_0} \left\| \sum_{m=1}^{M_0} \sqrt{p_n^0}\mathbf{u}_{mn} * \mathbf{h}_{mj}^{01} \right\|^2, \tag{2.13} $$

where $\beta$ denotes the position of selected tap. Note that the problem of selecting the values of $\alpha$ and $\beta$ is discussed in the following Section IV.

Thus, the SINR of the $j^{\text{th}}$ FU can be expressed as

$$ \begin{aligned} &\text{SINR}_j^1 \left( \beta,\, \mathbf{p}^1,\, \{\mathbf{g}_{ij}^1\}_{i=1,j=1}^{M_1,N_1}, {P_{(cross)}}_j^1 \right) \\ &= \frac{{P_{(sig)}}_j^1}{{P_{(isi)}}_j^1 + {P_{(co)}}_j^1 + {P_{(cross)}}_j^1 + \|\mathbf{n}_F[\beta]\|^2}. \end{aligned} \tag{2.14} $$

## 2.3 Beamforming Designs for the MBS and the FBS

This section provides the beamforming designs for FBS and MBS over frequency selective fading channels. In more details, MBS uses a zero-forcing-based algorithm whereas FBS employs the TR technique.

### 2.3.1 Beamformer design following the zero-forcing technique for the MBS

It is well-known that the zero-forcing technique mainly aims to suppress the interference components. Also, such a technique leads to the fact that the desired signal strength might only reach a limited level. However, this issue can be overcome by using a high transmit power. Given this concern, the signal strength can be significantly improved whereas the interference is cancelled. Due to the avaibility of power at MBS, zero-forcing beamforming technique is preferred as an efficient solution in such an environment. On the other hand, user receivers take only one sample at a particular tap. For the $l^{\text{th}}$ case, we specifically treat the $l^{\text{th}}$ tap as the desired tap whereas the other taps can be considered as the ISI taps respectively. The corresponding beamformer must be designed following the zero-forcing scheme to suppress both ISI and co-tier interference. Thereupon, we obtain $(2L-1)$ relevant beamformers. Finally, we finger out the beamformer among these candidates that yields the best SINR at the user. In the following content, the zero-forcing-based algorithm is discussed in details.

Let us start with a beamforming design based on the well-known zero-forcing technique over macrocell environments by re-arranging values of $\left\{\mathbf{h}^0_{mn}[l]\right\}_{m=1}^{M_0}$ into a new form $\bar{\mathbf{h}}_{ln} \in \mathbb{C}^{1\times M_0}$ as follows

$$\bar{\mathbf{h}}_{ln} = \left[ \begin{array}{cccc} h^0_{1n}[l] & h^0_{2n}[l] & \ldots & \mathrm{h}^0_{M_0 n}[l] \end{array} \right]. \tag{2.15}$$

Further, we define a matrix $\bar{\mathbf{H}}_n \in \mathbb{C}^{(2L-1)\times M_0 L}$ as

$$\bar{\mathbf{H}}_n = \begin{bmatrix} \bar{\mathbf{h}}_{1n} & \mathbf{0} & & \mathbf{0} \\ \bar{\mathbf{h}}_{2n} & \bar{\mathbf{h}}_{1n} & & \\ \vdots & \bar{\mathbf{h}}_{2n} & & \\ \bar{\mathbf{h}}_{Ln} & \vdots & \ddots & \bar{\mathbf{h}}_{1n} \\ & \bar{\mathbf{h}}_{Ln} & & \bar{\mathbf{h}}_{2n} \\ & & \ddots & \vdots \\ \mathbf{0} & & & \bar{\mathbf{h}}_{Ln} \end{bmatrix}. \tag{2.16}$$

Note that the matrix $\bar{\mathbf{H}}_n$ is derived following the formulation of the Sylvester matrix of $(\mathbf{h}^0_{mn})^T$ [pp. 28, Trott, M. (2007)]. For each sampled tap $\bar{\alpha}^{\text{th}}$, let us define $\bar{\mathbf{u}}_{mn,\bar{\alpha}} \in \mathbb{C}^{L\times 1}$ as the $\bar{\alpha}^{\text{th}}$ candidate for the beamformer $\mathbf{u}_{mn}$.

On the basis of zero-forcing principle, the beamformer of MBS can be derived according to a computation as follows

$$\text{vec}([\bar{\mathbf{u}}_{1n,\bar{\alpha}} \quad \bar{\mathbf{u}}_{2n,\bar{\alpha}} \quad \dots \quad \bar{\mathbf{u}}_{M_0 n,\bar{\alpha}}]) = c_{n,\bar{\alpha}} \bar{\mathbf{H}}^{\dagger} \mathbf{z}_{n,\bar{\alpha}}, \tag{2.17}$$

where $\mathbf{z}_{n,\bar{\alpha}} = \begin{bmatrix} \mathbf{0}^T & \dots & \mathbf{0}^T & \mathbf{s}_{\bar{\alpha}} & \mathbf{0}^T & \dots & \mathbf{0}^T \end{bmatrix}^T$, in which $\mathbf{s}_{\bar{\alpha}}$ is the $n$-th vector of $\mathbf{z}_{n,\bar{\alpha}}$, $\bar{\mathbf{H}} = \begin{bmatrix} \bar{\mathbf{H}}_1^T & \bar{\mathbf{H}}_2^T & \dots & \bar{\mathbf{H}}_{N_0}^T \end{bmatrix}^T$, $c_{n,\bar{\alpha}}$ is a normalization factor, and $\mathbf{s}_{\bar{\alpha}} = \begin{bmatrix} 0 & \dots & 0 & 1 & 0 & \dots & 0 \end{bmatrix}^T \in \mathbb{R}_+^{(2L-1)\times 1}$ (the 1 is located at the $\bar{\alpha}^{\text{th}}$ index), and $(\cdot)^{\dagger}$ denotes Moore-Penrose pseudo-inverse operator.

Thus, the $\bar{\alpha}^{\text{th}}$ candidate for the beamformer component given in (2.1) can be represented as

$$[\bar{\mathbf{u}}_{1n,\bar{\alpha}} \quad \bar{\mathbf{u}}_{2n,\bar{\alpha}} \quad \dots \quad \bar{\mathbf{u}}_{M_0 n,\bar{\alpha}}] = \text{vec}^{-1}(c_{n,\bar{\alpha}} \bar{\mathbf{H}}^{\dagger} \mathbf{z}_{n,\bar{\alpha}}), \tag{2.18}$$

Specifically, in the case that the matrix $\bar{\mathbf{H}}$ has a right-inverse, the inteference components are completely cancelled. Hence, the received signal at $n^{\text{th}}$ MU can be simplified as

$$\mathbf{y}_n^0 = \sqrt{p_n^0} c_{n,\bar{\alpha}} \mathbf{s}_{\bar{\alpha}} s_n^0 + \sum_{j=1}^{N_1} \sum_{i=1}^{M_1} \sqrt{p_j^1} \mathbf{g}_{ij} * \mathbf{h}_{in}^{10} s_j^1 + \mathbf{n}_M, \tag{2.19}$$

On the other hand, for mathematical simplification, we define a factor $\Gamma_{n,\bar{\alpha}}$ shown in (2.20). This factor is to evaluate the ratio between the power of the main tap and that of the interferences. To this end, we present the details of the beamforming design in *Algorithm* 2.1 for a comprehensive idea.

Algorithm 2.1 Algorithm to solve $\mathbf{u}_{mn}$

1 Set $\bar{\alpha} = 1$.
2 **Loop**
3 Compute $\bar{\mathbf{u}}_{mn,\bar{\alpha}}$ by (2.17).
4 Calculate $\Gamma_{n,\bar{\alpha}}$ by (2.20).
5 Update $\bar{\alpha} \leftarrow \bar{\alpha} + 1$.
6 **Until** $\bar{\alpha} = 2L - 1$.
7 Find $\alpha$ with $\alpha = \arg\max_{\bar{\alpha}} \{\{\Gamma_{n,\bar{\alpha}}\}_{\bar{\alpha}=1}^{2L-1}\}$.
8 The chosen beamformer $\mathbf{u}_{mn}$ can be inferred from $\bar{\mathbf{u}}_{mn,\alpha}$.

$$\Gamma_{n,\bar{\alpha}} = \frac{\left| \left( \sum_{m=1}^{M_0} \bar{\mathbf{u}}_{mn,\bar{\alpha}} * \mathbf{h}_{mn}^0 \right) [\bar{\alpha}] \right|^2}{\sum_{l \neq \bar{\alpha}}^{2L-1} \left| \left( \sum_{m=1}^{M_0} \bar{\mathbf{u}}_{mn,\bar{\alpha}} * \mathbf{h}_{mn}^0 \right) [l] \right|^2 + \sum_{n' \neq n}^{N_0} \sum_{l=1}^{2L-1} \left| \left( \sum_{m=1}^{M_0} \bar{\mathbf{u}}_{mn,\bar{\alpha}} * \mathbf{h}_{mn'}^0 \right) [l] \right|^2 + 1}. \tag{2.20}$$

### 2.3.2 Time Reversal beamforming technique for the FBS

Unlike MBS, FBS is a low-power cellular station with limited hardware resources Andrews *et al.* (2012); Zahir *et al.* (2013). This limitation is due to the fact that the zero-forcing beam-

former includes the component of matrix inversion, with a huge computational burden that becomes extremely heavy in cases of many users and lengthy CIRs. Furthermore, the transmit power level of FBS is restricted Zahir *et al.* (2013). Therefore, the zero-forcing technique might not be an interesting solution for femtocell networks.

In this paper, we propose employing the TR technique to FBS to achieve a better system performance with a much reduced cost. Indeed, the location signature-specific property of the TR can be utilized to mitigate the ISI, the co-tier interference and the cross-tier interference to the macrocell Bouzigues *et al.* (2013); Yoon *et al.* (2015).

According to (2.2), the FBS beamformer can be expressed by

$$\left[ \begin{array}{ccc} \mathbf{g}_{1j} & \cdots & \mathbf{g}_{M_1 j} \end{array} \right] = \left[ \begin{array}{ccc} g_{1j}[1] & \cdots & g_{M_0 j}[1] \\ g_{1j}[2] & \cdots & g_{M_0 j}[2] \\ \vdots & \vdots & \vdots \\ g_{1j}[L] & \cdots & g_{M_0 j}[L] \end{array} \right]. \tag{2.21}$$

In TR principle, the time-reversed form of CIR is employed as FBS beamformer, thus each element of $\mathbf{g}_{ij}$ can be calculated as

$$g_{ij}[l] = \frac{h_{ij}^{1H}[L+1-l]}{\sqrt{\sum_{i=1}^{M_1} \left\| \mathbf{h}_{ij}^{1} \right\|^2}}. \tag{2.22}$$

Benefiting from the signal focalization property of the TR technique, FU receivers need only to select the central tap to take a sample, i.e. $\beta = L$. As one can evaluate, the TR technique has a much lower computational complexity in comparison to the zero-forcing one.

## 2.4 Proposed Power Allocation Approach

In this section, we propose a novel downlink power allocation scheme for the considered HetNet taking into account the fact that the backhaul connection is unable to convey all user CSI

from femtocell to macrocell. We start with briefly presenting the centralized power allocation approach in order to understand this concept and compare its performance to the proposed approach. In the centralized method, a central controller, likely MBS, is responsible of computing the beamforming and power allocation vectors for all BSs in the HetNet. Assuming that all the CSI of MUs and FUs are available at the MBS, the power control problem which minimizes the total transmit power of BSs with SINR constraints can be formulated as

$$\begin{aligned} \mathrm{OP}_0 : \min_{\mathbf{p^0},\mathbf{p^1}} \quad & \sum_{k=0}^{1}\sum_{r=1}^{N_k} p_r^k \\ \text{s.t.} \quad & \mathrm{SINR}_r^k \geq \gamma_r^k, (\ \forall k \in \{0,1\}; 1 \leq r \leq N_k), \end{aligned} \tag{2.23}$$

herein $\gamma_r^k$ is the preset threshold for the $r^{\text{th}}$ user of $\mathscr{B}_k$. Since we divide the downlink power allocation and the beamforming procedures into distinct processes, the optimization problem in (2.23) becomes convex on $\mathbf{p}^k$ and the optimal solution can be conveniently found Bengtsson, M. & Ottersten, B. (2001); Chandrasekhar, V., Andrews, J. G., Muharemovic, T., Chen, Z. & Gatherer, A. (2009).

Given this centralized approach, the femtocell needs to send all FU CSI to the macrocell via the backhaul link. Therefore, signaling overheads as well as computational burdens at the macrocell are heavy when the network size is large. However, in case of link congestion, obtaining sufficient CIR becomes intractable. Due to these drawbacks, a novel scheme is proposed for the considered HetNet. In this vein, the original optimization problem $\mathrm{OP}_0$ given in equation (2.23) is decomposed into two subproblems, i.e. MBS subproblem and FBS subproblem, to (i) share computational burden to all BSs and (ii) reduce the dependence on backhaul links. Different from previous works Joeng *et al.* (2011); Nguyen *et al.* (2015); Tolli *et al.* (2011), our proposed optimization method can perform as follows: (i) To reduce the amount of signaling information, the FBS computes first the beamforming vector for its own users, then optimizes the corresponding transmission power to mitigate the cross-tier interference to the MUs and finally transfers the minimized value of the cross-tier interference power to the MBS. (ii) Afterwards, the MBS initiates computing its own beamformer and power allocation vector once

it receives the specific information sent by the FBS. Hence, this method limits the signaling overhead since only a minimized value of the cross-tier interference power is required at the MBS side. In addition, the FUs are released from the task of measuring the cross-interference caused by the MBS. Importantly, our scheme can allow the operator to control the priority of MUs, shown in subsection 2.4.1. Furthermore, the optimal closed-form solutions are derived for such subproblems. A comparison between two the centralized and proposed approaches is shown in Fig. 2.2. In this regard, the required amount of signaling exchange between two tiers becomes much smaller (i.e. Table 2.1), and the proposed scheme can achieve near optimal performance. To this end, the subproblems for femtocell and macrocell are thoroughly discussed in the following subsections.

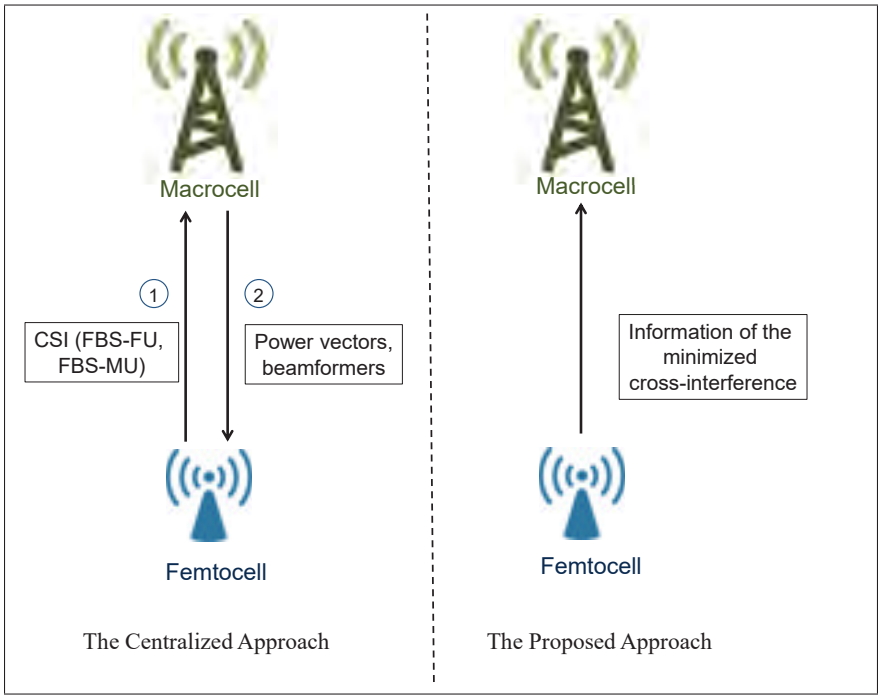


Figure 2.2 A comparsion between the approaches

### 2.4.1 Subproblem 1: Power allocation for the FBS

In HetNet, both MUs and FUs frequently endure the cross-tier interference, but MUs have a higher priority than FUs in communication such that optimization designs must satisfy MUs

Table 2.1 The CSI required at MBS

| **Kinds of CSI** | **Centralized approach** | **Proposed approach** |
|---|---|---|
| MBS - MU | required | required |
| MBS - FU | required | required |
| FBS - MU | required | not required |
| FBS - FU | required | not required |

quality of service (QoS). Therefore, to give priority to MUs, the femtocell should minimize the interference that it causes to MUs. On the other hand, to reduce the CSI sent to MBS, the femtocell starts the communication by providing an optimized power allocation with respect to a tolerable level of cross-tier interference that is set for each FU as ${P_{(tol)}}_j^{01}$. Accordingly, the downlink power control problem for the FBS can be interpreted as

$$\begin{aligned} \mathrm{OP}_1\colon \min_{\mathbf{p^1}} \quad & \sum_{j=1}^{N_1}\left(\sum_{n=1}^{N_0}\left\|\sum_{i=1}^{M_1}\mathbf{g}_{ij}*\mathbf{h}_{in}^{10}\right\|^2 p_j^1\right) \\ \text{s.t.} \quad & \mathrm{SINR}_j^1\left(L,\ \mathbf{p}^1,\ \left\{\mathbf{g}_{ij}\right\}_{i=1,j=1}^{M_1,N_1},\ {P_{(tol)}}_j^{01}\right) \geq \gamma_j^1. \\ & (1\leq j\leq N_1) \end{aligned} \tag{2.24}$$

Hence, the tolerable cross-tier interference implies that

$${P_{(cross)}}_j^1 = \sum_{n=1}^{N_0}\left\|\sum_{m=1}^{M_0}\sqrt{p_n^0}\mathbf{u}_{mn}*\mathbf{h}_{mj}^{01}\right\|^2 \leq {P_{(tol)}}_j^{01}. \tag{2.25}$$

Moreover, the inequality given in (2.25) is set as a constraint of the MBS's power allocation problem, i.e. see (2.34).

In fact, although MUs are primary users, there should be restrictions applied in the cross-interference that MBS cause to FUs due to flexible management for operators. Given this scheme, the operator might manage the priority level of MUs by adjusting the tolerable threshold, i.e. $\{{P_{(tol)}}_j^{01}\}$. This makes the proposed scheme more flexible than the previous works Joeng *et al.* (2011); Nguyen *et al.* (2015).

It is easy to see that the considered optimization problem requires the CSI at femtocells only, and the objective function aims to minimize the cross interference to MUs, i.e. $P_{(cross)_n^0}$. On the other hand, it is visible that the problem $\mathrm{OP}_1$ is a linear programming problem. Thus, the solution of problem $\mathrm{OP}_1$ is summarized in *Lemma* 1 below.

**Lemma 1.** Let $\mathbf{p}^{\star 1}$ denote the optimal value of $\mathbf{p}^1$. Based on preliminaries in [18.4 Bengtsson & Ottersten (2001)], [eq. (4) Chandrasekhar *et al.* (2009)], the closed-form expression of $\mathbf{p}^{\star 1}$ can be given by

$$\mathbf{p}^{\star 1} = \mathrm{diag}(\boldsymbol{\eta})^{-1} \left[\mathbf{I}_{N_1} - \mathrm{diag}(\boldsymbol{\eta})\mathbf{D}\left(\mathbf{B} \circ (\boldsymbol{\eta}^{-1}\mathbf{1}_{N_1\times 1}^T)\right)\right]^{-1}\mathbf{z}, \tag{2.26}$$

where $\circ$ denotes Hadamard product, $\mathbf{I}_{N_1}$ is an $N_1 \times N_1$ identity matrix, $\mathbf{B}$ is a $N_1 \times N_1$ matrix whose the $(j,\ j')^{\text{th}}$ entry is defined as

$$(\mathbf{B})_{j'j} = \begin{cases} 0, & j = j' \\ \left\| \sum\limits_{i=1}^{M_1} \mathbf{g}_{ij'} * \mathbf{h}_{ij}^1 \right\|^2, & j \neq j', \end{cases} \tag{2.27}$$

in addition,

$$\boldsymbol{\eta} = \frac{\hat{\boldsymbol{\eta}}}{\|\hat{\boldsymbol{\eta}}\|}, \tag{2.28}$$

in which each element of the vector $\hat{\boldsymbol{\eta}} \in \mathbb{C}^{N_1}$ is

$$\hat{\eta}_j = \sum_{n=1}^{N_0} \left\| \sum_{i=1}^{M_k} \mathbf{g}_{ij} * \mathbf{h}_{in}^{10} \right\|^2, \tag{2.29}$$

and $\mathbf{D}$ is a $N_1 \times N_1$ matrix which is presented by

$$\mathbf{D} = \mathrm{diag}\left\{ \frac{\gamma_1^1}{\varphi_1};\ \ldots;\ \frac{\gamma_{N_1}^1}{\varphi_{N_1}} \right\}, \tag{2.30}$$

where

$$\varphi_j = \left| \left( \sum_{i=1}^{M_1} \mathbf{g}_{ij} * \mathbf{h}_{ij}^1 \right) [L] \right|^2 - \gamma_j^1 \sum_{\substack{l=1 \\ l \neq L}}^{2L-1} \left| \left( \sum_{i=1}^{M_1} \mathbf{g}_{ij} * \mathbf{h}_{ij}^1 \right) [l] \right|^2, \tag{2.31}$$

and $\mathbf{z}$ is a vector $\mathbf{z} = [z_1 \; z_2 \; \ldots \; z_{N_1}]^T$ with each element given as

$$z_j = P_{(tol)j}^{01} + \|\mathbf{n}_F[L]\|^2 . \tag{2.32}$$

Proof: See Appendix I.1.

In the proposed scheme, when the femtocell tackles the optimization problem $\mathrm{OP}_1$, the value of $\left\{ P^{\star}_{(cross)n}{}^{0} \right\}_{n=1}^{N_0}$ given in equation (2.33) is sent to the macrocell instead of the information of $\mathbf{p}^{\star 1}$, $\left\{ \mathbf{h}_{ij}^1 \right\}_{i=1,\, j=1}^{M_1, N_1}$ and $\left\{ \mathbf{h}_{in}^{10} \right\}_{j=1, n=1}^{N_1, N_0}$ via the backhaul link.

$$P^{\star}_{(cross)n}{}^{0} = \sum_{j=1}^{N_1} \left\| \sum_{i=1}^{M_1} \sqrt{p_j^{\star 1}} \mathbf{g}_{ij} * \mathbf{h}_{in}^{10} \right\|^2 . \tag{2.33}$$

It is worth reminding that $\mathbf{h}_{in}^{10}$ denotes the CIR between the femtocell and the $n^{\text{th}}$ macrocell user. In other words, $\mathbf{h}_{in}^{10}$ is the local CSI of the femtocell network. In our paper, $\mathbf{h}_{in}^{10}$ is assumed to be available at the femtocell in both the centralized and the proposed approaches.

Therefore, in the proposed power allocation, one can conclude that the amount of overhead used for signaling information is significantly reduced.

### 2.4.2 Subproblem 2: Power loading problem for the MBS

In this part, we present our derivation methodology of the downlink power allocation for MBS. Our aim is to minimize the total transmit power with the interference constraint to FUs. To actively guarantee the performance for MU, the MBS computes the beamforming and power allocation vectors once it receives the signaling information of $\left\{ P^{\star}_{(cross)n}{}^{0} \right\}_{n=1}^{N_0}$ given by (2.33)

from the femtocell. Hence, the optimization problem involving the SINR and interference constraints is formulated as

$$\begin{aligned} \text{OP}_2\text{: } \min_{\mathbf{p^0}} \quad & \sum_{n=1}^{N_0} p_n^0 \\ \text{s.t.} \quad & \text{SINR}_n^0\left(\alpha, \mathbf{p}^0, \{\mathbf{u}_{mn}\}_{m=1,n=1}^{M_0,N_0}, P^{\star}_{(cross)}{}_n^0\right) \geq \gamma_n^0. \\ & \left\| \sum_{m=1}^{M_0} \sqrt{p_n^0}\mathbf{u}_{mn} * \mathbf{h}_{mj}^{01} \right\|^2 \leq P_{(tol)}{}_j^{01}, \end{aligned} \tag{2.34}$$

The above problem is a linear programming problem which can be solved by interior-point method. To reduce the computational burden, we aim at solving $\text{OP}_2$ by closed-form expressions. Since the objective function and the constrains of $\text{OP}_2$ are not differentiable, it is infeasible to solve $\text{OP}_2$ through its the Lagrangian dual. To deal with this issue, we endeavour to transform the problem $\text{OP}_2$ into an equivalent formulation solvable by the Lagrange multiplier method.

In this context, we start with applying the uplink-downlink duality property to the $\text{SINR}_n^0$ constraint of the $\text{OP}_2$. It is observed that the $\text{SINR}_n^0$ constraint can be considered as a function of $P_{(co)}{}_n^0$. According to the property of uplink-downlink duality, the virtual uplink $\text{SINR}_n^0$ derivation denoted by $\overline{\text{SINR}}_n^0$ has the same structure as $\text{SINR}_n^0$ expression, however, $P_{(co)}{}_n^0$ is replaced by $\overline{P}_{(co)}{}_n^0$, with

$$\overline{P}_{(co)}{}_n^0 = \sum_{\substack{n'=1 \\ n' \neq n}}^{N_0} \left\| \sum_{m=1}^{M_0} \sqrt{p_n^0}\mathbf{u}_{mn} * \mathbf{h}_{mn'}^0 \right\|^2. \tag{2.35}$$

$$\Delta_n = \frac{\sum_{l \neq \alpha}^{2L-1} \left| \left( \sum_{m=1}^{M_0} \mathbf{u}_{mn} * \mathbf{h}_{mn}^0 \right)[l] \right|^2 + \sum_{\substack{n'=1 \\ n' \neq n}}^{N_0} \left\| \sum_{m=1}^{M_0} \mathbf{u}_{mn} * \mathbf{h}_{mn'}^0 \right\|^2}{\left| \left( \sum_{m=1}^{M_0} \mathbf{u}_{mn} * \mathbf{h}_{mn}^0 \right)[\alpha] \right|^2}. \tag{2.36}$$

Since $\mathbf{p}_n^0$ is a non-negative vector, it can be re-written in the new form

$$\exp(\xi_n) = p_n^0. \tag{2.37}$$

On this basis, the inversion of $\overline{\text{SINR}}_n^0$ can be computed as

$$\left(\overline{\text{SINR}}_n^0\right)^{-1} = \Delta_n + \nabla_n \exp(-\xi_n), \tag{2.38}$$

where $\Delta_n$ is defined as in (2.36) and

$$\nabla_n = \frac{{P^{\star}_{(cross)}}_n^0 + \|\mathbf{n}_M\|^2}{\left|\left(\sum_{m=1}^{M_0} \mathbf{u}_{mn} * \mathbf{h}_{mn}^0\right)[\alpha]\right|^2}. \tag{2.39}$$

Without loss of generality, the problem $\text{OP}_2$ is reformulated into a more tractable formulation such as

$$\begin{aligned} \text{OP}_3\text{:} \min_{\{\xi_n\}_{n=1}^{N_0}} \quad & \sum_{n=1}^{N_0} \exp(\xi_n) \\ \text{s.t.} \quad & \log\left(\Delta_n + \nabla_n \exp(-\xi_n)\right) \leq \log \frac{1}{\gamma_n^0}, \\ & \left\| \sum_{m=1}^{M_0} \mathbf{u}_{mn} * \mathbf{h}_{mj}^{01} \right\|^2 \exp(\xi_n) \leq {P_{(tol)}}_j^{01}. \end{aligned} \tag{2.40}$$

Indeed, the problem $\text{OP}_3$ is convex and it is solvable by use of Lagrange multiplier method Grant, M. & Boyd, S. (2009). Considering the relationship between $\text{OP}_2$ and $\text{OP}_3$, it is clear that the optimal solution of $\text{OP}_2$ can be calculated according to that of $\text{OP}_3$, i.e. $p_n^{\star 0} = \exp(\xi_n^{\star})$ where $\xi_n^{\star}$ is the optimal solution of $\text{OP}_3$.

In the continuity, following Lagrange multiplier method, let $\{\mu_n\}$ and $\{\lambda_n\}$ be the dual variables associated with the SINR and interference constraints, respectively. After some mathe-

matical manipulations, the Lagrangian function of $OP_3$ can be given by

$$\begin{aligned}\mathscr{L}\left(\{\xi_n\},\{\mu_n\},\{\lambda_n\}\right) &= \sum_{n=1}^{N_0}\exp\left(\xi_n\right) \\ &+ \sum_{n}^{N_0}\mu_n\left(\log\left(\Delta_n+\nabla_n\exp\left(-\xi_n\right)\right)-\log\frac{1}{\gamma_n^0}\right) \\ &+ \sum_{n=1}^{N_0}\lambda_n\left(\left\|\sum_{m=1}^{M_0}\mathbf{u}_{mn}*\mathbf{h}_{mj}^{01}\right\|^2\exp\left(\xi_n\right)-{P_{(tol)}}_j^{01}\right).\end{aligned} \tag{2.41}$$

For convenience, we focus on the following simplified form of (2.41)

$$\begin{aligned}\mathscr{L}_n\left(\xi_n,\mu_n,\lambda_n\right) &= \exp\left(\xi_n\right)+\mu_n\log\left(\Delta_n+\nabla_n\exp\left(-\xi_n\right)\right) \\ &+ \lambda_n\left\|\sum_{m=1}^{M_0}\mathbf{u}_{mn}*\mathbf{h}_{mj}^{01}\right\|^2\exp\left(\xi_n\right).\end{aligned} \tag{2.42}$$

Accordingly, the dual function and the dual problem can explicitly be formulated as (2.43) and (2.44), respectively

$$\begin{aligned}\mathscr{D}\left(\{\xi_n\},\{\mu_n\},\{\lambda_n\}\right) &= \sum_{n=1}^{N_0}\min_{\xi_n}\mathscr{L}_n\left(\xi_n,\mu_n,\lambda_n\right) \\ &- \sum_{n=1}^{N_0}\mu_n\left(\log\frac{1}{\gamma_n^0}\right)-\sum_{n=1}^{N_0}\lambda_n\left({P_{(tol)}}_j^{01}\right),\end{aligned} \tag{2.43}$$

$$\begin{aligned}\underset{\{\mu_n\},\{\lambda_n\}}{\text{OP}_4:}\quad &\max\quad \mathscr{D}\left(\{\mu_n\},\{\lambda_n\}\right) \\ &\text{s.t.}\quad \{\mu_n\}\geq 0,\ \{\lambda_n\}\geq 0.\ \forall n\end{aligned} \tag{2.44}$$

It is a fact that the problem $OP_3$ is a convex optimization problem, thus strong duality holds, i.e. the duality gap between primal problem and dual problem is zero. According to Karush-Kuhn-Tucker condition, the optimal transmit power can be obtained through the first derivative

of the Lagrangian function with respect to $\xi_n$ as

$$\frac{\partial \mathscr{L}_n(\xi_n, \mu_n, \lambda_n)}{\partial \xi_n} = 0. \tag{2.45}$$

Specifically, the optimal solution $p_n^{\star 0}$ can be achieved by the closed-form derivation

$$\begin{aligned} p_n^{\star 0} &= \exp(\xi_n^{\star}) \\ &= \frac{2\mu_n \nabla_n \lambda_n^{-1} \left\| \sum_{m=1}^{M_0} \mathbf{u}_{mn} * \mathbf{h}_{mj}^{01} \right\|^{-2}}{\left( \nabla_n + \sqrt{\nabla_n^2 + \frac{4\nabla_n \Delta_n \mu_n}{\lambda_n \left\| \sum_{m=1}^{M_0} \mathbf{u}_{mn} * \mathbf{h}_{mj}^{01} \right\|^2}} \right)}. \end{aligned} \tag{2.46}$$

The final step in this method is to provide optimal Lagrangian multipliers, i.e. $\mu_n$ and $\lambda_n$ by solving the dual problem $\mathrm{OP}_4$. In this way, the optimal solution of $\mathrm{OP}_3$ is obtained once $\exp(\xi_n)$, $\mu_n$ and $\lambda_n$ are iteratively updated until convergence. The subgradient iteration algorithm is then applied to update the Lagrangian multipliers as

$$\mu_n(t) = [\mu_n(t-1) + \nu_n(t) X_1]^+, \tag{2.47}$$

$$\lambda_n(t) = [\lambda_n(t-1) + \kappa_n(t) X_2]^+, \tag{2.48}$$

where $\nu_n(t)$ and $\kappa_n(t)$ are step sizes, while $X_1$ and $X_2$ are defined as

$$X_1 = \log(\Delta_n + \nabla_n \exp(-\xi_n)) - \log \frac{1}{\gamma_n^0}, \tag{2.49}$$

$$X_2 = \left\| \sum_{m=1}^{M_0} \mathbf{u}_{mn} * \mathbf{h}_{mj}^{01} \right\|^2 \exp(\xi_n) - P_{(tol)_j}^{01}. \tag{2.50}$$

The subgradient iterative algorithm is ensured to converge to the optimal value with a sufficiently small step size Grant & Boyd (2009).

## 2.5 Worst-case Robust Optimization for TR Femtocell Network

In this section, we extend the downlink power minimization problem for the TR femtocell by considering imperfect CSI. It is worth noting that this work considers for the first time the worst-case robust optimization for TR femtocell network.

Accounting for error model, we assume that the maximum error quantity of the femtocell can be known, such that the imperfect CIR model can be referred to as

$$\hat{\mathbf{h}}_{ij}^{1} = \mathbf{h}_{ij}^{1} + \mathbf{e}_{ij}^{1}, \tag{2.51}$$

where $\mathbf{e}_{ij}^{1}$ represents a channel uncertainty defined by a feasible set as

$$\mathscr{F}_{ij}^{1} = \left\{ \mathbf{e}_{ij}^{1} \in \mathbb{C}^{L\times 1} : \left\| \mathbf{e}_{ij}^{1} \right\|^{2} \leq \psi \left\| \mathbf{h}_{ij}^{1} \right\|^{2} \right\}, \tag{2.52}$$

and $\psi$ is named as error factor. We also suppose that $\mathbf{h}_{ij}^{1}$ and $\mathbf{e}_{ij}^{1}$ are identically and independently distributed variables. Under the influence of CEE, we devise the robust optimization methodologies to guarantee the QoS requirement. Following the worst-case approach, the power allocation design of the femtocells may be formulated as

$$\begin{aligned} \mathrm{OP}_5\text{: } \min_{\mathbf{p}^1} \quad & \max_{\mathbf{e}_{in}^{10}} \sum_{j=1}^{N_1} \left( \sum_{n=1}^{N_0} \left\| \sum_{i=1}^{M_1} \hat{\mathbf{g}}_{ij} * \mathbf{h}_{in}^{10} \right\|^{2} p_j^{1} \right) \\ \text{s.t. } & \min_{\mathbf{e}_{ij}^{1}, \mathbf{e}_{ij'}^{1}} \mathrm{SINR}_j^{1} \left( L,\, \mathbf{p}^{1},\, \left\{ \hat{\mathbf{g}}_{ij}^{1} \right\}_{i=1,j=1}^{M_1,N_1}, {P_{(tol)}}_j^{01} \right) \geq \gamma_j^{1} \\ & \left( \mathbf{e}_{in}^{10} \in \mathscr{F}_{in}^{10}, \mathbf{e}_{ij}^{1} \in \mathscr{F}_{ij}^{1}, \mathbf{e}_{ij'}^{1} \in \mathscr{F}_{ij'}^{1} \right). \end{aligned} \tag{2.53}$$

Unluckily, the problem $\mathrm{OP}_5$ is intractable since the objective function and constraint include the convolution operator. However, it can be transformed into a convex one by approximating the latters. Indeed, one can see that it is challenging to obtain an exact closed-form SINR expression in the constraint.

To tackle this problem, we apply an approximation presented as (2.54) in which $\mathscr{P}l_{(sig)}{}_j^1$, $\mathscr{P}u_{(isi)}{}_j^1$ and $\mathscr{P}u_{(co)}{}_j^1$ are the worst-case lower-bound of central signal power, the worst-case upper-bound of ISI power, and worst-case upper-bound of co-tier interference power, respectively.

$$\min_{\mathbf{e}_{ij}^1,\mathbf{e}_{ij'}^1} \mathrm{SINR}_j^1\left(\beta,\ \mathbf{p}^1,\ \{\hat{\mathbf{g}}_{ij}^1\}_{i=1,j=1}^{M_1,N_1}, {P_{(tol)}}_j^{01}\right)$$
$$\approx \frac{\mathscr{P}l_{(sig)}{}_j^1\left(p_j^1,\hat{\mathbf{g}}_{ij}\right)}{\mathscr{P}u_{(isi)}{}_j^1\left(p_j^1,\hat{\mathbf{g}}_{ij}\right)+\mathscr{P}u_{(co)}{}_j^1\left(\{p_{j'}^1,\hat{\mathbf{g}}_{ij'}\}_{j'=1,j'\neq j}^{N_1}\right)+{P_{(tol)}}_j^{01}+\|\mathbf{n}_F[L]\|^2}. \tag{2.54}$$

$$\mathscr{P}l_{(sig)}{}_j^1 = \min_{\mathbf{e}_{ij}^1\in\mathscr{F}_{ij}^1}\left|\sum_{i=1}^{M_1}(\hat{\mathbf{g}}_{ij}*\mathbf{h}_{ij}^1)[L]\sqrt{p_j^1}\right|^2, \tag{2.55}$$

$$\mathscr{P}u_{(isi)}{}_j^1 = \max_{\mathbf{e}_{ij}^1\in\mathscr{F}_{ij}^1}\left\|\sum_{i=1}^{M_1}\hat{\mathbf{g}}_{ij}*\mathbf{h}_{ij}^1\right\|^2 - \mathscr{P}l_{(sig)}{}_j^1, \tag{2.56}$$

$$\mathscr{P}u_{(co)}{}_j^1 = \max_{\mathbf{e}_{ij'}^1\in\mathscr{F}_{ij'}^1}\sum_{\substack{j'=1\\j'\neq j}}^{N_1}\left\|\sum_{i=1}^{M_1}\sqrt{p_{j'}^1}\hat{\mathbf{g}}_{ij'}*\mathbf{h}_{ij}^1\right\|^2, \tag{2.57}$$

where $\hat{\mathbf{g}}_{ij}$ is the beamformer corresponding to the estimated channel $\hat{\mathbf{h}}_{ij}^1$, and it has a similar structure to $\mathbf{g}_{ij}$ shown in (2.22). Note that the derivation of $\mathscr{P}u_{(isi)}{}_j^1$ can be expressed as a substraction between the upper-bound of the power of all taps and the lower-bound of the power of central tap. Our aim is to derive such these boundaries into formulations that can be expressed in term of estimated values solely, e.g. $\hat{\mathbf{g}}_{ij}$, $\hat{\mathbf{h}}_{ij}^1$.

### 2.5.1 Worst-case lower-bound of signal power component

This part of the paper is dedicated to the derivation of the worst-case lower-bound of signal power given in equation (2.55).

With an erroneous channel estimation, the power of the central tap at the intended user becomes

$$\begin{aligned}
&\left|\sum_{i=1}^{M_1}\left(\hat{\mathbf{g}}_{ij} * \mathbf{h}_{ij}^1\right)[L]\right|^2 \\
&= \frac{\left|\sum\limits_{i=1}^{M_1}\left(\sum\limits_{l=1}^{L} h_{ij}^1[l]h_{ij}^{*1}[l] + \sum\limits_{l=1}^{L} e_{ij}^1[l]h_{ij}^{*1}[l]\right)\right|^2}{\sum\limits_{i=1}^{M_1}\left\|\hat{\mathbf{h}}_{ij}^1\right\|^2} \\
&= \frac{\left|\sum\limits_{i=1}^{M_1}\left(\left\|\mathbf{h}_{ij}^1\right\|^2 + (\mathbf{e}_{ij}^1)^H\mathbf{h}_{ij}^1\right)\right|^2}{\sum\limits_{i=1}^{M_1}\left\|\hat{\mathbf{h}}_{ij}^1\right\|^2},
\end{aligned} \tag{2.58}$$

where we have

$$\left\|\hat{\mathbf{h}}_{ij}^1\right\|^2 = \left\|\mathbf{h}_{ij}^1\right\|^2 + \left\|\mathbf{e}_{ij}^1\right\|^2 + 2\Re\left\{(\mathbf{e}_{ij}^1)^H\mathbf{h}_{ij}^1\right\}. \tag{2.59}$$

One can evaluate that while $\left\|\hat{\mathbf{h}}_{ij}^1\right\|^2$ is fixed, if $\left\|\mathbf{e}_{ij}^1\right\|^2$ increases then $\left\|\mathbf{h}_{ij}^1\right\|^2$ decreases. Considering (2.58), the increasing level of $(\mathbf{e}_{ij}^1)^H\mathbf{h}_{ij}^1$ is generally lower than the decreasing level of $\left\|\mathbf{h}_{ij}^1\right\|^2$. Therefore, the CEE effect monotonically reduces the power of desired signal, and the power focalization is decreased. *Lemma* 2 below determines $\mathscr{P}l_{(sig)_j^1}$ based on (2.58).

**Lemma 2.** The worst-case lower-bound on the signal power component can be stated as

$$\mathscr{P}l_{(sig)_j^1} = \left|\sum_{i=1}^{M_1}(\hat{\mathbf{g}}_{ij} * \hat{\mathbf{h}}_{ij}^1)[L]\right|^2 \frac{p_j^1}{\left(1-\sqrt{\psi}\right)^2}. \tag{2.60}$$

Proof: The proof is listed in Appendix I.2.

### 2.5.2 Worst-case upper-bound on the ISI power component

In order to find out worst-case upper-bound on the ISI term, the maximum of Euclidean norm of $\sum_{i=1}^{M_1} \hat{\mathbf{g}}_{ij} * \mathbf{h}_{ij}^1$, i.e. $\max_{\mathbf{e}_{ij}^1 \in \mathscr{F}_{ij}^1} \left\| \sum_{i=1}^{M_1} \hat{\mathbf{g}}_{ij} * \mathbf{h}_{ij}^1 \right\|^2$ needs to be discovered first. This problem is non-trivial since only the knowledge of the norm constraint of the estimation error is available, see (2.52). Fortunately, thanks to Young's inequality Young (1912), [eq (3.9.4) Bogachev & I., V. (2007)] the upper-bound can be derived. In this vein, the norm of convolution between the given two vectors can be bounded by Young's inequality as

$$\begin{aligned} \left\| \sum_{i=1}^{M_1} \hat{\mathbf{g}}_{ij} * \mathbf{h}_{ij}^1 \right\|^2 &\leq \hat{c} \sum_{i=1}^{M} \left\| \mathbf{h}_{ij}^1 \right\|^2 \left\| \hat{\mathbf{g}}_{ij} \right\|_1^2 \\ &+ \hat{c} \sum_{i=1}^{M_1} \sum_{\substack{i'=1 \\ i' \neq i}}^{M_1} \left\| \mathbf{h}_{ij}^1 \right\| \left\| \hat{\mathbf{g}}_{ij} \right\|_1 \left\| \mathbf{h}_{i'j}^1 \right\| \left\| \hat{\mathbf{g}}_{ij} \right\|_1, \end{aligned} \tag{2.61}$$

where $\|\cdot\|_1$ denotes the $l_1$–norm and $\hat{c}$ is a constant. One can see that the resulting boundary can be computed as a function of the norm of these two vectors only. Concerning the worst possible error case, based on the defined feasible set given in (2.52), we have

$$\begin{aligned} \max_{\mathbf{e}_{ij}^1 \in \mathscr{F}_{ij}^1} \left\| \sum_{i=1}^{M_1} \hat{\mathbf{g}}_{ij} * \mathbf{h}_{ij}^1 \right\|^2 &= \hat{c} \sum_{i=1}^{M_1} \frac{\left\| \hat{\mathbf{h}}_{ij}^1 \right\|^2 \left\| \hat{\mathbf{g}}_{ij} \right\|_1^2}{\left(1 - \sqrt{\psi}\right)^2} \\ &+ \hat{c} \sum_{i=1}^{M_1} \sum_{\substack{i'=1 \\ i' \neq i}}^{M_1} \frac{\left\| \hat{\mathbf{h}}_{ij}^1 \right\| \left\| \hat{\mathbf{g}}_{ij} \right\|_1 \left\| \hat{\mathbf{h}}_{i'j}^1 \right\| \left\| \hat{\mathbf{g}}_{i'j} \right\|_1}{\left(1 - \sqrt{\psi}\right)^2}. \end{aligned} \tag{2.62}$$

On the other hand, the objective function and $\mathscr{P} u_{(iui)_j^1}$ also contain the worst-case boundary of the norm of convolution between two vectors. It is a fact that the tight degree of the boundary plays an important role in limiting the waste of the transmit power allocation. For a long time, the designation of a value to the constant $\hat{c}$ in (2.61) that can improve the tightness of Young's inequality was a challenge for researchers. Eventually, Beckner Beckner, W. (1975) provided the best possible constant $\hat{c}$ and the work in Bobkov, S., Madiman, M. & Wang, L. (2011) generalized Young's inequality, the value of $\hat{c}$ designed by Beckner (1975); Bobkov *et al.*

(2011) has no effect in the case considered in our work, i.e. $\hat{c}$ is equal to 1. This motivates us to derive a tighter worst-case upper-bound on the ISI component through *Lemma* 3.

**Lemma 3.** Considering the worst-case boundary of the norm of convolution between two vectors, we introduce a new formulation as follows

$$\max_{\mathbf{e}_{ij}^{1}\in\mathscr{F}_{ij}^{1}}\left\|\sum_{i=1}^{M_1}\hat{\mathbf{g}}_{ij}*\mathbf{h}_{ij}^{1}\right\|^2=\sum_{i=1}^{M_1}\left\|\hat{\mathbf{g}}_{ij}*\tilde{\mathbf{h}}_{ij}^{\star 1}\right\|^2+\left|\sum_{i=1}^{M_1}\sum_{\substack{i=1\\ i'\neq i}}^{M_1}\left(\hat{\mathbf{g}}_{ij}*\tilde{\mathbf{h}}_{ij}^{\star 1}\right)^H\left(\hat{\mathbf{g}}_{i'j}*\tilde{\mathbf{h}}_{i'j}^{\star 1}\right)\right|. \tag{2.63}$$

in which,

$$\tilde{\mathbf{h}}_{ij}^{\star 1}=\frac{\left(\mathbf{\Phi}_{ij}^{\star 1}\right)\left\|\hat{\mathbf{h}}_{ij}^{1}\right\|}{\left(1-\sqrt{\psi}\right)}, \tag{2.64}$$

where $\mathbf{\Phi}_{ij}^{\star 1}$ can be obtained by computing the orthonormal eigenvector corresponding to the largest eigenvalue of the matrix $\left(\hat{\mathbf{G}}_{ij}\left(\hat{\mathbf{G}}_{ij}\right)^H\frac{\left\|\hat{\mathbf{h}}_{ij}^{1}\right\|^2}{\left(1-\sqrt{\psi}\right)^2}\right)$, and

$$\hat{\mathbf{G}}_{ij}\in\mathbb{C}^{(2L-1)\times L}=\begin{bmatrix}
\hat{g}_{ij}[1] & 0 & 0 & 0 & 0\\
\hat{g}_{ij}[2] & \hat{g}_{ij}[1] & \cdots & \vdots & \vdots\\
\hat{g}_{ij}[3] & \hat{g}_{ij}[2] & \cdots & 0 & 0\\
\vdots & \hat{g}_{ij}[3] & \cdots & \hat{g}_{ij}[1] & 0\\
\hat{g}_{ij}[L-1] & \vdots & \cdots & \hat{g}_{ij}[2] & \hat{g}_{ij}[1]\\
\hat{g}_{ij}[L] & \hat{g}_{ij}[L-1] & \vdots & \vdots & \hat{g}_{ij}[2]\\
0 & \hat{g}_{ij}[L] & \cdots & \hat{g}_{ij}[L-2] & \vdots\\
0 & 0 & \cdots & \hat{g}_{ij}[L-1] & \hat{g}_{ij}[L-2]\\
\vdots & \vdots & \vdots & \hat{g}_{ij}[L] & \hat{g}_{ij}[L-1]\\
0 & 0 & 0 & \cdots & \hat{g}_{ij}[L]
\end{bmatrix}. \tag{2.65}$$

Proof: Please refer to Appendix I.3.

Accordingly, the proposed upper-bound on $P_{(isi)}{}_j^1$ can be calculated as

$$\mathscr{P}u_{(isi)}{}_j^1 = \sum_{i=1}^{M_1} \left\| \sqrt{p_j^1}\hat{\mathbf{g}}_{ij} * \tilde{\mathbf{h}}_{ij}^{\star 1} \right\|^2 - \mathscr{P}l_{(sig)}{}_j^1 + \left| \sum_{i=1}^{M_1} \sum_{\substack{i=1 \\ i' \neq i}}^{M_1} \left( \sqrt{p_j^1}\hat{\mathbf{g}}_{ij} * \tilde{\mathbf{h}}_{ij}^{\star 1} \right)^H \left( \sqrt{p_{j'}^1}\hat{\mathbf{g}}_{i'j} * \tilde{\mathbf{h}}_{i'j}^{\star 1} \right) \right|. \tag{2.66}$$

### 2.5.3 Worst-case upper bound on the co-tier interference and objective function

Similarly, the upper bound on the co-tier interference may be presented as follows

$$\mathscr{P}u_{(co)}{}_j^1 = \sum_{\substack{j'=1 \\ j' \neq j}}^{N_1} \left( \sum_{i=1}^{M_1} \left\| \hat{\mathbf{g}}_{ij'} * \tilde{\mathbf{h}}_{ij}^{\star 1} \right\|^2 p_{j'}^1 \right) + \sum_{\substack{j'=1 \\ j' \neq j}}^{N_1} \left| \sum_{i=1}^{M_1} \sum_{\substack{i=1 \\ i' \neq i}}^{M_1} \left( \hat{\mathbf{g}}_{ij'} * \tilde{\mathbf{h}}_{ij}^{\star 1} \right)^H \left( \hat{\mathbf{g}}_{i'j'} * \tilde{\mathbf{h}}_{i'j}^{\star 1} \right) p_{j'}^1 \right|. \tag{2.67}$$

and the upper bound on the objective function is developed as

$$\begin{aligned} &\max_{\mathbf{e}_{in}^{10} \in \mathscr{F}_{in}^{10}} \sum_{j=1}^{N_1} \left( \sum_{n=1}^{N_0} \left\| \sum_{i=1}^{M_1} \hat{\mathbf{g}}_{ij} * \mathbf{h}_{in}^{10} \right\|^2 p_j^1 \right) \\ &= \sum_{j=1}^{N_1} \left( \sum_{n=1}^{N_0} \sum_{i=1}^{M_1} \left\| \hat{\mathbf{g}}_{ij} * \tilde{\mathbf{h}}_{in}^{\star 10} \right\|^2 p_j^1 \right) \\ &+ \sum_{j=1}^{N_1} \left| \sum_{n=1}^{N_0} \sum_{i=1}^{M_1} \sum_{\substack{i'=1 \\ i' \neq i}}^{M_1} \left( \hat{\mathbf{g}}_{ij} * \tilde{\mathbf{h}}_{in}^{\star 10} \right)^H \left( \hat{\mathbf{g}}_{i'j} * \tilde{\mathbf{h}}_{i'n}^{\star 10} \right) p_j^1 \right| \\ &= \Omega\left(\mathbf{p}^1\right). \end{aligned} \tag{2.68}$$

Following the worst-case approach and results from (A I-14) and (2.66), (2.67), and (2.68), the problem $\mathrm{OP}_6$ can be approximately relaxed as problem $\mathrm{OP}_6$

$$\begin{aligned} \mathrm{OP}_6\text{: } \min_{\mathbf{p^1}} \quad & \Omega\left(\mathbf{p}^1\right) \\ \text{s.t.} \quad & \frac{\mathscr{P} l_{(sig)}{}_j^1}{\mathscr{P} u_{(isi)}{}_j^1 + \mathscr{P} u_{(co)}{}_j^1 + P_{(tol)}{}_j^{01} + \|\mathbf{n}_F\|^2} \geq \gamma_j^k. \end{aligned} \tag{2.69}$$

This problem can be solved by the use of a similar approach adopted to tackle $\mathrm{OP}_1$.

## 2.6 Numerical Results

The impact of the proposed power allocation strategy on the system performance is analyzed in this section. Without other statements, the system parameters are set following the ITU-R channel model Hernandez, M., Li, H.-B., Dotlic, I. & Miura, R. (2012) which is applicable for vehicular and indoor communication environments where the macrocell and femtocell are implemented, respectively.

In the HetNet, the radii of MBS and FBS are $d_m = 300$ m and $d_f = 30$ m respectively. FBS is uniformly distributed in a circle of $d_{mf} = 100$ m far from MBS. MUs and FUs are also uniformly distributed in the served areas of MBS and FBS, respectively. Specifically, the marcocell, femtocell and the the cross-tier channels are considered as the ITU vehicular (Table 2.2), the ITU indoor (Table 2.3), the ITU outdoor to indoor (Table IV) models, repectively. Moreover, we assume that

- The outdoor link pathloss exponent is set to 4, thus each tap of MBS-to-MU links is $\mathscr{CN}(0, \left|\mathbf{h}_{mn}^0[l]\right|^2)$ where $\left|\mathbf{h}_{mn}^0[l]\right|^2 = \sigma_{0mn,l}^2/d_{0n}^4$ and $d_{0n}$ is the distance between MBS and the $n$-th MU ($0 \leq d_{0n} \leq d_m$).

- The indoor link pathloss exponent is set to 3, thus each tap of FBS-to-FU links is $\mathscr{CN}(0, \left|\mathbf{h}_{ij}^1[l]\right|^2)$ where $\left|\mathbf{h}_{ij}^1[l]\right|^2 = \sigma_{1ij,l}^2/d_{1j}^3$ and $d_{1j}$ is the distance between FBS and the $j$-th FU ($0 \leq d_{1j} \leq d_f$).

- The outdoor-to-indoor link pathloss exponent is set to 3.5, thus each tap of MBS-to-FU links is $\mathscr{CN}(0, \left|\mathbf{h}_{mj}^{01}[l]\right|^2)$ where $\left|\mathbf{h}_{mj}^{01}[l]\right|^2 = \sigma_{01mj,l}^2 / d_{01j}^{3.5}$ and $d_{01j}$ is the distance between MBS and the $j$-th FU ($0 \leq d_{01j} \leq d_f$).

- The indoor-to-outdoor links are assumed to be similar to the outdoor-to-indoor links.

It is worth noting that there exist no correlations between the channels and between their taps.

Table 2.2 ITU indoor office

| Tap | Relative Delay (ns) | Average Power (dBm) |
|---|---|---|
| 1 | 0 | 0 |
| 2 | 50 | -3 |
| 3 | 100 | -10 |
| 4 | 170 | -18 |
| 5 | 290 | -26 |
| 6 | 310 | -32 |

Table 2.3 ITU vehicular

| Tap | Relative Delay (ns) | Average Power (dBm) |
|---|---|---|
| 1 | 0 | 0 |
| 2 | 310 | -1 |
| 3 | 710 | -9 |
| 4 | 1090 | -10 |
| 5 | 1730 | -15 |
| 6 | 2510 | -20 |

Table 2.4 ITU outdoor to indoor and pedestrian

| Tap | Relative Delay (ns) | Average Power (dBm) |
|---|---|---|
| 1 | 0 | 0 |
| 2 | 110 | -9.7 |
| 3 | 190 | -19.2 |
| 4 | 410 | -22.8 |

For convenience, we set the SINR thresholds for FBS as $\left\{\gamma_j^1\right\}_{j=1}^{N_1} = \gamma_F$ and for MBS as $\left\{\gamma_n^0\right\}_{n=1}^{N_0} = \gamma_M$. In addition, the Gaussian noise power is set to $10^{-12}$ W and other parameters are adjusted as listed in Table 2.4.

Table 2.5 Important parameters

| **Parameters** | **System values** |
|---|---|
| Number of taps, $L$ | 6 |
| Number of antennas at MBS, $M_0$ | 4 |
| Number of antennas at FBS, $M_1$ | 4 |
| Number of users at MBS, $N_0$ | 2 |
| Number of users at FBS, $N_1$ | 2-4 |
| Tolerable level of cross-interference, $P_{(tol)_j^{01}}$ | -10 dBm |
| Bandwidth, $W$ | 20 MB |

### 2.6.1 The Proposed Power Allocation Strategy

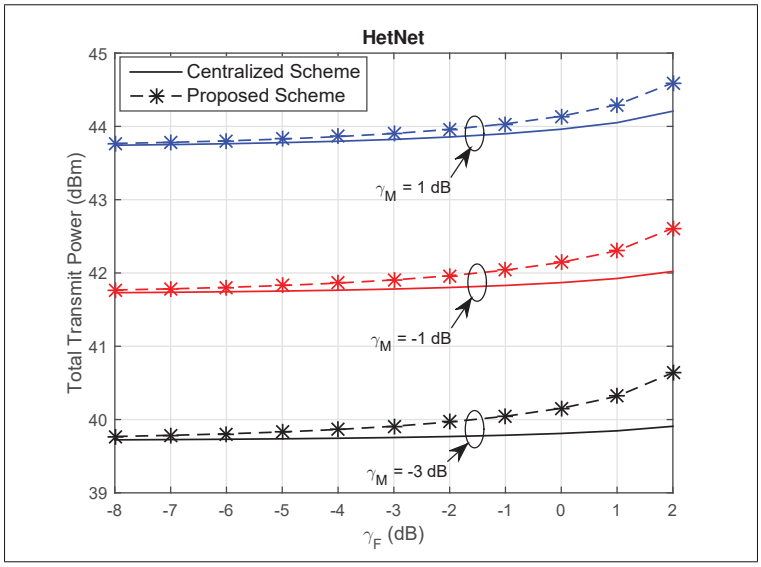


Figure 2.3 Performance of power allocation schemes

In Fig. 5.12, we investigate the transmit power of the HetNet system with the proposed optimization approach, and the scheme using centralized manner. The simulation is carried out with 1000 random locations of MBS, FBS and users in the considered HetNet environment. Since MUs are frequently located far from its own base station, the distance between MBS and MUs is much larger compared with the distance between FBS and FUs. Therefore, the amount of transmit power allocated for MUs constitutes a major part of the total transmit power of HetNet. As a result, the total transmit power slightly increases when the SINR threshold of

FUs scales up. Fig. 5.12 also shows the comparison between the centralized and the proposed approaches. In more details, the power gap at $\gamma_F = 2$ dB is roughly 0.6 dB, 0.5 dB and 0.4 dB in cases of $\gamma_M = 1$ dB, $-1$ dB and $-3$ dB, respectively. Furthermore, the gap scales up as the SINR threshold of FUs increases. This is because the FBS aims at minimizing the interference to MUs, instead of solely minimizing the transmit power as in the case of centralized approach. More specifically, the proposed scheme sacrifices an additional amount of transmit power for (i) a much smaller amount of required signaling information and (ii) a reduced interference to MU. Note that only $\left\{P^{\star}_{(cross)}{}^{0}_{n}\right\}_{n=1}^{N_0}$ is sent via backhaul to the macrocell instead of $\mathbf{p}^{\star 1}$, $\left\{\mathbf{h}^{1}_{ij}\right\}_{i=1,\,j=1}^{M_1,N_1}$ and $\left\{\mathbf{h}^{10}_{in}\right\}_{j=1,n=1}^{N_1,N_0}$, the signaling overhead is significantly reduced. Indeed, based on Fig. 5.12, one can conclude that the proposed optimization algorithm can achieve tight results to the centralized strategy which validates and verifies our strategy.

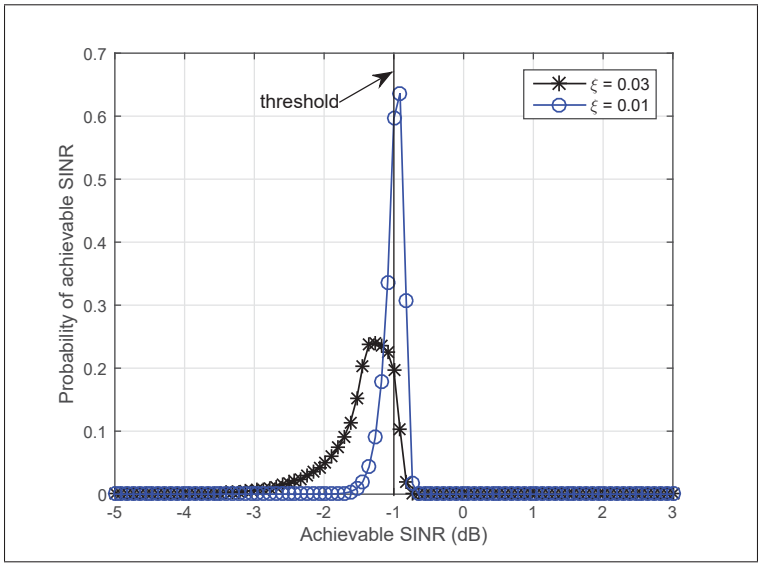


Figure 2.4 Impact of imperfect $\left\{\mathbf{h}^{10}_{in}\right\}_{j=1,n=1}^{N_1,N_0}$ on the performance at a MU

Moreover, in practice, obtaining the perfect information of cross channels, such as $\left\{\mathbf{h}^{10}_{in}\right\}_{i=1,n=1}^{M_1,N_0}$ and $\left\{\mathbf{h}^{01}_{mj}\right\}_{m=1,\,j=1}^{M_0,N_1}$, is a challenge. Although many previous works Chandrasekhar *et al.* (2009); Joeng *et al.* (2011); Nguyen *et al.* (2015) assume that the information is available at the base station or the computation node, this motivates us to further consider the impact of imper-

fect $\left\{\mathbf{h}_{in}^{10}\right\}_{j=1,n=1}^{N_1,N_0}$ on the SINR performance achieved at MUs. The latter represents the case in which FBS imperfectly estimate the CSI of $\left\{\mathbf{h}_{in}^{10}\right\}_{j=1,n=1}^{N_1,N_0}$, and then it sends the "inaccurate" information of minimized interference to MBS. In this concern, we use a general imperfect channel model as $\hat{\mathbf{h}}_{in}^{10} = \mathbf{h}_{in}^{10} + \mathbf{e}_{in}^{10}$, where $\mathbf{e}_{in}^{10}$ is a channel uncertainty and $\left\|\mathbf{e}_{in}^{10}\right\|^2 \leq \xi \mathbf{h}_{in}^{10}$. In fact, the inexact information of $\left\{\mathbf{h}_{in}^{10}\right\}_{j=1,n=1}^{N_1,N_0}$ might lead to the fact that the achieved SINR performance at each MU is not guaranteed to meet the preset threshold. In Fig. 2.4, the impact of imperfect CSI is shown in terms of the probability of the achievable SINR at a MU. As expected, given the threshold of $-1$ dB, it is clear that the outage probability increases when the error component scales up.

### 2.6.2 Comparison between TR and zero-forcing techniques

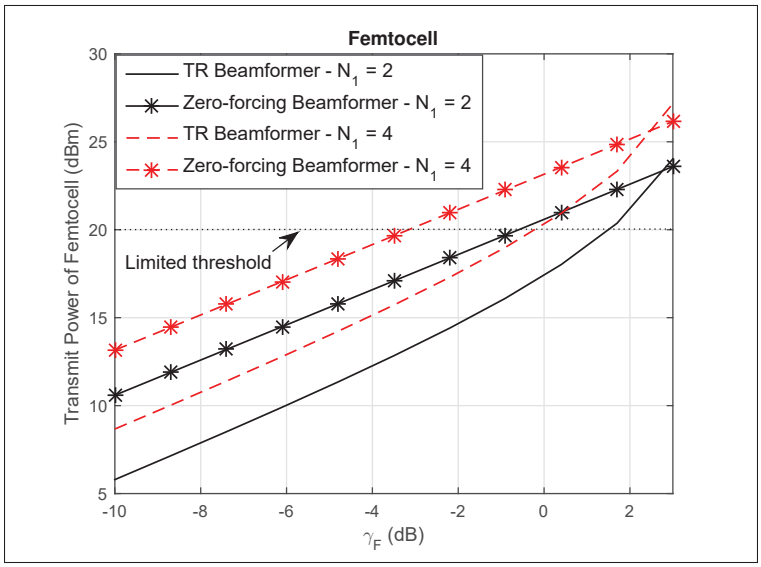


Figure 2.5 A comparison between TR and zero-forcing

In Fig. 2.5, we compare the effectiveness of TR-based beamformer with that of zero-forcing-based beamformer (*Algorithm* 1). Concerning channels, the ITU-R indoor model is still utilized, however, we arrange a distance of 15 meters between FBS and FUs. From Fig. 2.5, it is visible that for a transmit power range lower than 23 dBm and 25 dBm for cases of $N_1 = 2$ users and $N_1 = 4$ users, respectively, TR beamforming outperforms zero-forcing one and converse

holds for the entire transmit power regions. Specifically, it can be explained that zero-forcing scheme mainly deals with canceling the ISI, co-tier interference and cross-tier interference, whereas TR technique aims at both focusing signal power on the central tap, and reducing the ISI and co-tier interferences. As a result, the interference is ineliminable completely in TR-applying systems, and the interference power increases as transmit power scales up. Therefore, there exist working ranges in which either TR or zero-forcing techniques can dominate the other one regarding SINR metric. In practice, however, FBS is a low-power cellular station whose transmit power is limited to 20dBm in order to curb the effects of co- and cross-tier interferences Zahir *et al.* (2013). Indeed, in perspective of a small-cell system configured with a limited level of transmit power, such as femtocell operating environments, it can be concluded that the TR technique is more desirable than the zero-forcing.

### 2.6.3 Worst-case Optimization Problem and Performance of Proposed Upper-bounds

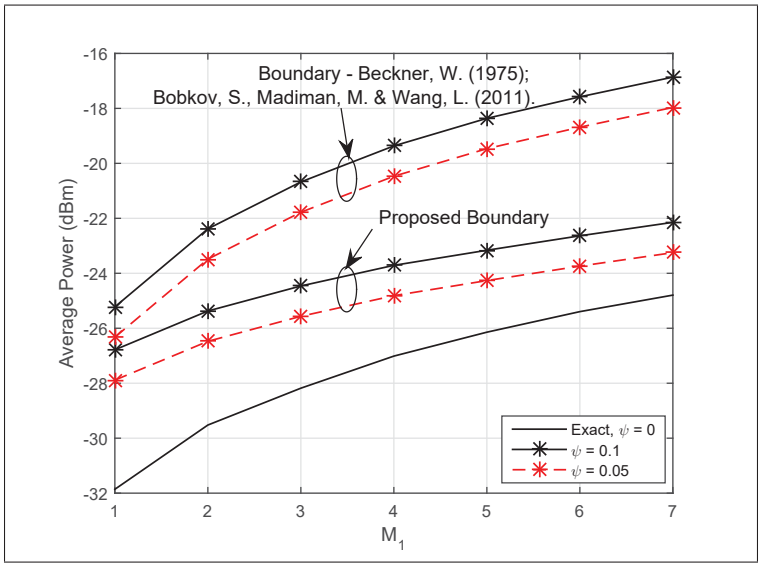


Figure 2.6 A comparison between worst-case upper-bounds

In subsection 2.5, we have proposed a novel worst-case upper-bound to provide a greater solution to the robust downlink power allocation for the TR femtocell. First, for simplicity, we observe the term $\left\| \sum_{i=1}^{M_1} \hat{\mathbf{g}}_{ij} * \mathbf{h}_{ij}^{1} \right\|^2$ to evaluate the performance of the proposed boundary and

Young's inequality-based boundary. Simulations are carried out in indoor channels with a fixed pathloss similar to the prior investigation. Fig. 2.6 clearly demonstrates that the proposed boundary is approximately 5dB tighter than Young's inequality-based boundary at $M_1 = 4$ for both cases of error factor $\psi = 0.05, 0.1$.

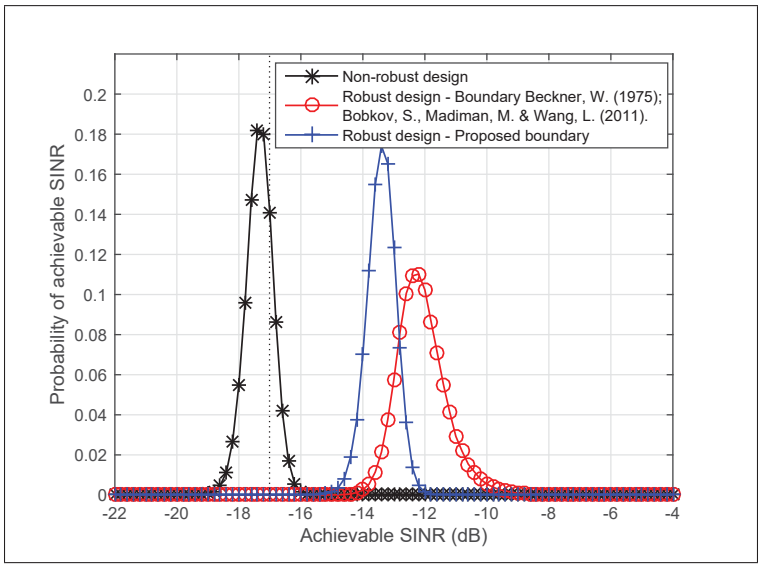


Figure 2.7 Probability distribution per a femtocell user

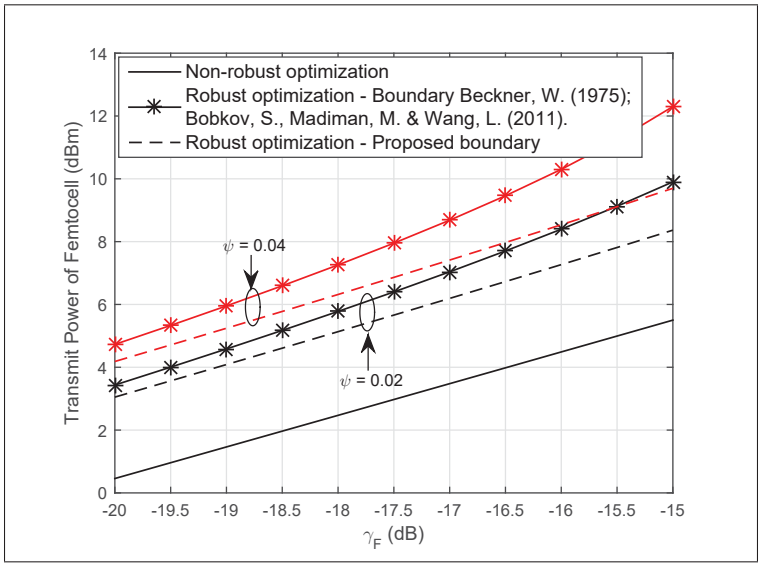


Figure 2.8 Transmit power of femtocell with worst-case upper-bounds

Concerning the worst case robust design, Fig. 2.7 and Fig. 2.8 demonstrate the transmission power in terms of worst-case approaches using: (i) the Young's inequality-based boundary as well as (ii) the proposed boundary, under similar error conditions. In more details, Fig. 2.7 exhibits the probability distribution of achievable SINR per FU obtained by non-robust design ($OP_1$) and robust design ($OP_6$). This result is achieved by use of 100000 randomly generated realizations for the simulation. For the channel error factor $\psi = 0.04$, our simulation shows that two robust designs can keep the outage probability equal to 0 by accounting the worst possible error case. Nevertheless, the probability distribution of the design employing the proposed boundary is closer to the preset threshold than that of Young's inequality-based design. It can be explained that FBS can save the radiated energy in obtaining the same desired SINR performance when applying the proposed boundary.

Moreover, as a reference, we plot the average transmit power of non-robust and robust manners in Fig. 2.8 and exhibit the amount of additional power that is needed to achieve a zero outage probability. It can be concluded that the advantage of our boundary makes the transmit power allocation more effective in the *worst-case approach* by curbing the waste of power transmission.

## 2.7 Conclusion

In this paper, we propose the application of TR technique to femtocell networks, and a novel power allocation scheme for the considered HetNet in which the backhaul connection provides only a limited throughput for signaling exchange. In perfect channel estimation cases, we tackle the beamformer designs and optimization problems of downlink power control for both macrocell and femtocell over frequency selective fading channels. Our analysis shows that the proposed allocation schemes require a higher increment in transmit power compared to the conventional approach but demands a lower amount of signaling exchange between the MBS and FBS. This important advantage makes our approach very promising to deal with limited backhaul connection drawbacks. Furthermore, under imperfect CSI assumption, we tackle the robust design following the worst-case approach. To relax the original formulation into

a solvable convex problem, the worst-case boundaries of concerning components are derived. In particular, we propose the novel tighter worst-case upper-bound of the ISI, co-tier interference and objective function to improve the system performance. Moreover, numerical results demonstrate that the TR technique outperforms the zero-forcing beamforming over femtocell working environments.

# CHAPTER 3

# RF-WIRELESS POWER TRANSFER: RE-GREENING FUTURE NETWORKS

Ha-Vu Tran[1], and Georges Kaddoum[1]

[1] Department of Electrical Engineering, École de Technologie Supérieure,
1100 Notre-Dame west, Montreal, Canada H3C 1K3.

Paper published in *IEEE Potentials Magazine*, vol. 37, issue 2, pp. 35-41, March-April, 2018.

## 3.1 Introduction

Over past few years, green radio communication has drawn much attention from the research community, and it has a strong impact on various aspects, such as telecom businesses, wireless technologies, and natural environments. Specifically, the cost of electricity and $CO_2$ emissions have been increasing due to wireless network operation. For instance, the number of base stations (BSs) is more than 4 million, and each BS consumes an average of 25 MWh/year (an estimated approximate of 80% of the total network's power consumption). Bearing in mind the environmental perspective, generating sufficient power to supply the networks causes a significant CO2 footprint. Particularly, the overall footprint of information and communication technology (ICT) services (e.g., computer, cell phone, and satellite networks) is predicted to triple by 2020.

Recently, in moving toward a future green world, energy-harvesting (EH) techniques have shown the potential to deal with the problem of energy inefficiency. There are two main advantages to this approach. First, the EH techniques harness green energy from natural sources, (e.g., solar and wind). As a result, it contributes to reducing the overall footprint and helps protect surrounding environments. Currently, the popularity of using conventional energy sources, e.g., diesel, still dominates the use of green sources. However, although the overall implementation cost of EH solutions is higher than that of conventional ones, this cost might be more palatable after several years of operation.

Another main challenge with future networks is prolonging the lifetime of smart user devices. Given this concern, EH networks have a tremendous advantage in various applications. For instance, EH is an efficient solution for reducing battery replacement costs in wireless sensor networks. Also, it can recharge the devices working in areas where the traditional power supply is infeasible (e.g., robotic devices working in toxic environments).

Nevertheless, the amount of harvested energy from natural resources, such as solar and wind, may vary randomly over time and depend on locations and weather conditions. So, harvesting energy from these sources is not controllable and sustainable. For instance, there exists insufficient sunlight at night to generate energy, and it is difficult for indoor devices to harvest solar energy. In this context, radio-frequency (RF) wireless power transfer (WPT) might be a promising approach to overcome such a drawback. In this article, we provide a comprehensive review to address the topic of regreening the future world.

## 3.2 Energy Harvesting and Green RF Wireless Power Transfer

In this section, an overview of EH models and a discussion on green RF wireless power transfer are shown.

### 3.2.1 EH Models

EH methodology might be described as harnessing energy from surrounding environments or thermal and mechanical sources and converting the latter into electrical energy. The generated electrical current can be used to supply devices by RF-WPT. Generally speaking, EH models can be classified into two architectures: harvest-use and harvest-store-use. In harvest-use, energy is harvested and is used instantly. With harvest-store-use, energy is harvested as much as possible and then stored for future use.

In the harvest-use architecture, the EH systems directly supply devices. To guarantee the operation of the devices, the power output of the EH systems should be higher than the threshold of minimum working requirements, otherwise, the devices would be disabled because there is

not enough power supplied. As a consequence, unanticipated fluctuation in harvesting capacity close to the threshold causes the working devices to vacillate in ON and OFF states.

The harvest-store-use model includes a component that stores harvested energy and also powers the connected devices. Thanks to the storage, the energy can be harvested until it is sufficient for supplying the devices. Moreover, such energy might be stored for later use when there is a lack of produced energy or if the devices need to increase their performance. The storage component might include primary and secondary storage. In this context, the secondary storage can be viewed as a backup. In particular, the harvest-store-use system can make nonstable but foreseeable energy sources, such as solar and wind, more favorable.

### 3.2.2 Green RF Wireless Power Transfer

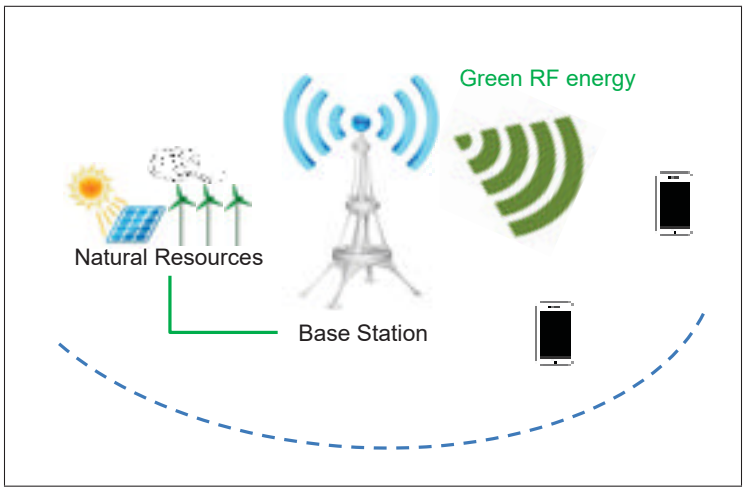


Figure 3.1 Green RF-WPT

Over the last decade, solar, wind, mechanical, and thermal energy have been the most efficient resources in generating green energy that can be used in wireless networks. However, the main drawback of such sources is a lack of stability. In the quest for an alternative solution, the research community has explored that radio signals belonging to a frequency range from 3 kHz to 300 GHz can be used to carry energy over the air. On this basis, a transmitter can proactively

recharge wireless devices by sending energy-bearing RF signals whenever it is necessary. This is the principle of the RF-WPT technique.

It is well known that EH is a green technique since it helps to reduce our carbon footprint. However, in a shared vision, the RF-WPT technique seems to be harmful to surrounding environments because it requires electricity to generate RF signals and causes electromagnetic pollution to the human body as well as interference to data transmission. By rethinking the role of the RF-WTP technique, we suggest that RF-WTP can be seen as green if

1) The RF signal carrying energy is generated using power harvested from green resources (for example, BSs are connected with outdoor energy harvesters to harvestand- store green energy and then use such energy to wirelessly recharge indoor devices using RF signals)

2) A tight restriction is applied for increasing the transmit power [i.e., following the equivalent isotropically radiated power (EIRP) requirement approved by the U.S. Federal Communications Commission].

In our work, the RF-WTP satisfying such two conditions is the so-called green RF-WTP. The characteristics of the green RF-WPT (Fig. 1) technique are as follows.

- The green RF-WPT technique plays a role as a bridge between green energy sources and energy-hunger devices,
- The energy harvested at a receiver is foreseeable,
- The amount of harvested energy belongs to transmit power, propagation loss, and wavelength.

It is expected that the green RF resource will be one of the most interesting candidates for future applications.

## 3.3 A Vision of Future Green and EH Networks

### 3.3.1 A predicted model of future green networks with EH

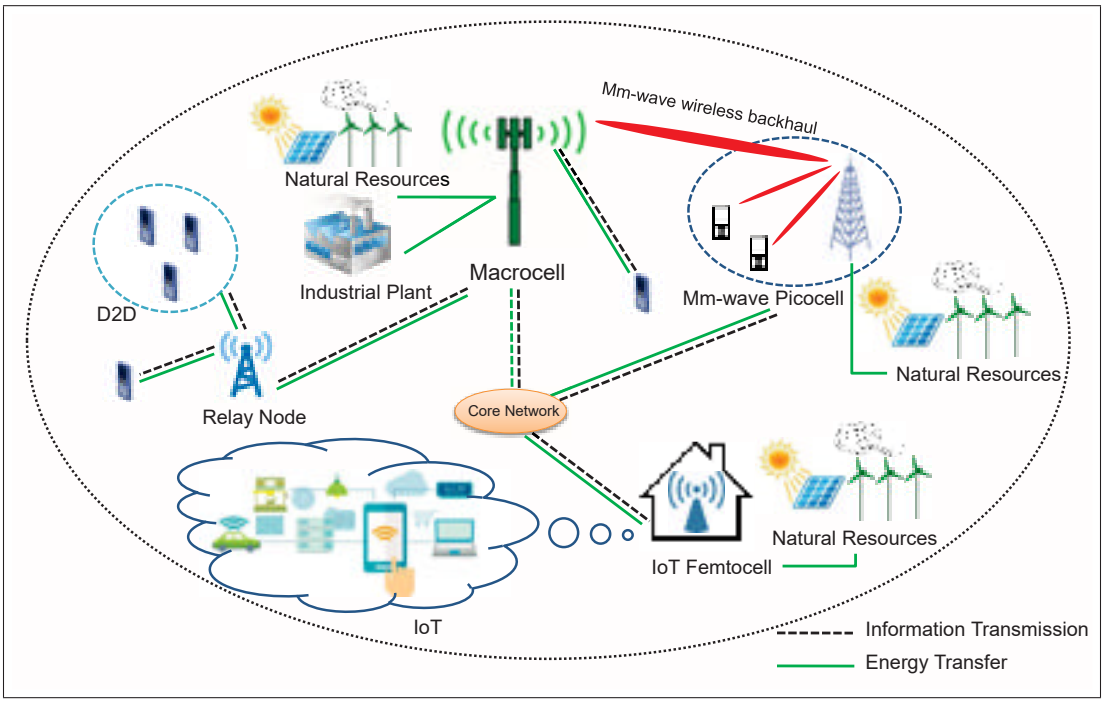


Figure 3.2 A Future Green Network

Future networks (e.g., fifth generation) are expected to support multimedia applications to achieve 1,000-fold-higher throughput, 1,000-fold-higher mobile data per unit area, and ten-fold-longer lifetime of devices over the fourth-generation networks. To adapt this progress, the design of new cellular networks tends to be a new form, embracing a large-scale deployment of small cells. Generally, the small cells can be classified into distinct types: femtocell, microcell, and picocell. The multitier HetNet attains a promising gain in terms of spectral and energy efficiencies due to low power consumption and good ubiquitous connectivities.

On the other hand, the development of wireless networks has exceeded the limits of power consumption, especially in cellular networks. Moreover, the energy cost and $CO_2$ emissions have been promptly growing due to network operation. This has inspired researchers with a challenging topic: future green wireless networks. As a promising solution, EH techniques

exploit natural sources and then contribute to reducing the overall footprint and extending the network lifetime. Nevertheless, natural resources may not always be available to all devices. For instance, it is difficult for indoor devices to harvest solar energy. This yields another trend - BSs connected with outdoor harvesters that can harvest and store green energy when natural resources are available. Then, BSs use such energy to wirelessly charge user devices using RF signals.

Another approach to future green networks is the concept of the green Internet of Things (IoT). The IoT is an emerging trend where billions of identified low-power devices (e.g., sensor nodes) are connected to each other without the need for human interaction. It can provide solutions to cut $CO_2$ emissions, reduce electromagnetic pollution, and improve energy efficiency. For instance, with the tracking of motion sensors, the lights in rooms would be turned off when no one is inside. Also, green IoT technology can monitor energy use in hightech buildings to reduce waste.

The green IoT is expected to enhance all technical, economical, and environmental benefits. In particular, IoT network architectures mainly rely on the platforms of wireless sensor networks (WSNs) and cooperative networks to connect devices together. In this area, battery recharging for a large number of IoT devices is challenging. Therefore, enabling the green IoT concept for future networks requires advanced solutions of prolonging a device's lifetime, resource management, and energy-efficient communication protocols.

Taking all of these challenges into account, in the following sections, we further discuss several potential concepts to move toward green future networks (Fig. 2). Specifically, challenges in implementing each concept are identified.

### 3.3.2 Green radio communications: Main concepts and discussions

#### 3.3.2.1 Full-duplex networks

As mentioned previously, indoor devices that might not harvest green energy directly can be wirelessly powered by RF signals sent from BSs. This has inspired a combination of the full-duplex and simultaneous wireless information and power transfer (SWIPT) techniques. At the same time, the devices can receive energy in the downlink transmission while conveying information in the uplink connections to boost spectral efficiency.

We will discuss two potential research issues of full-duplex SWIPT systems. First, the antennas at the full-duplex node are conventionally divided into transmit and receive sets. To improve the performance of SWIPT systems, an advanced form of the full-duplex technique that each antenna can simultaneously send information/energy and receive energy/information in the same frequency band is highly desirable. This approach mainly depends on new hardware designs and the innovation of self-interference cancellation techniques. Second, fullduplex the SWIPT small-cell BS can provide a promising approach regarding wireless backhauls in HetNets. In downlinks, the small-cell BS can receive information from the macrocell and transmit information/energy to users simultaneously. In uplinks, the small-cell BS can receive information/ energy and send information to the macrocell at the same time. On this basis, the small-cell BSs do not require a separate frequency band of backhaul connections. As a result, resources and implementing costs are reduced.

#### 3.3.2.2 Millimeter-wave networks

Benefitting from millimeter-wave (mm-wave) transmission, the overall electromagnetic field (EMF) exposure and power consumption per bit transmitted of networks are reduced due to a higher free-space attenuation at the mm-wave frequency, high-directive antennas, and short distance links. Therefore, mm-wave communication is considered a primary candidate for future green cellular networks. This approach is expected to achieve multigigabit data rates due

to large spectrum resources at an ultrahigh frequency band. Specifically, EH devices can extract energy from incident RF signals. Moreover, in mm-wave systems, many BSs are densely deployed to ensure proper coverage for ultrahigh frequency networks. This is attractive for EH devices to potentially harvest sufficient energy.

In ultrahigh-frequency bands, the mm-wave signals mainly suffer from the propagation loss, such as poor penetration and diffraction. To make mm-wave networks more favorable for SWIPT, beamforming techniques are a promising solution to increase the network coverage and system performance. Moreover, in mm-wave networks, although the small wavelength signals allow large antenna arrays to offer high beamforming gains, they require the alignment between transmit and receive beams to reach the highest possible performance. With these concerns, there is a nontrivial problem of the beamwidth design. In practice, the length of beam-searching overhead is directly proportional to the number of beamformer candidates. The narrower the beamwidth, the greater the number of beamformer candidates, and the longer the overhead. This leads the time of data transmission to be decreased. In constrast, a wider beamwidth means that it is easier for transmit and receive beams to be aligned, and the beam-searching process is sped up, however, the beamforming gain is reduced. Therefore, future works should consider the impact of beamwidth in various contexts to maximize the SWIPT system performance.

#### 3.3.2.3 Wireless sensor networks

Over the last few years, the trend toward WSNs is one of the most attractive options due to flexible installation and convenient maintenance. Accordingly, many standards such as WirelessHART, WIA-PA, and ISA100.11a have been proposed. Particularly, the IoT technology is mainly implemented on the WSN platform. With an integration of the IoT with sensors, sensor devices can be interconnected with the global Internet to provide solutions for future networks, such as reducing wasted energy in high-tech buidings.

Specifically, replacing or charging the batteries in IoT WSNs may take time and additional costs due to a large number of sensors, and this process becomes dangerous in hazardous environments. As a result, EH from natural resources and RF signals for WSNs have been considered a promising solution to prolong the sensor's lifetime.

The main distinction from conventional WSNs is that EH-WSNs require new criteria regarding information transfer and EH requirements. In fact, the network can fail to adapt the EH requirement while ensuring other system performances, such as throughput, delay, or packet loss. As a result, leveraging data transmission and EH is one of the critical concerns in designing EH-WSNs. Therefore, efficient resource allocation schemes should take this problem into account to achieve high energy efficiency for EH-WSNs.

#### 3.3.2.4 Cooperative relay networks

Recently, cooperative relay networks have been evaluated as one of the main core networks for the IoT technology where IoT nodes can communicate with each other and forward information and energy to remote nodes. Up until now, many mature research works of cooperative communication have clearly shown that the relay can be implemented not only to extend the coverage range but also to improve the performance of wireless communications. Furthermore, the concept of EH/WPT relay networks has been proposed and studied to enhance the lifetime of devices and overall performance of wireless networks. In cooperative EH/WPT relay networks, improving performance gain on the physical layer is one of the main research directions.

Considering the existing challenges, the enhancement for both spectral and energy efficiencies in cooperative relay networks with the green RF-WTP is remarkable. In this area, full-duplex or two-way relaying methods may be a promising solution. It is suggested that developed resource allocation schemes should consider the inf luence of incomplete channel state information (CSI) (e.g., the relay nodes have a partial users' CSI) and the energy status at the relay nodes

and users (e.g., the available energy, current power consumption, predicted energy harvested from natural resources or RF signals, among others) on system performance.

## 3.4 Future Research Issues

In the previous section, several challenges of each concept were presented. In future networks, since wireless communication systems are expected to be a mixture of various novel system concepts to enhance both the spectral and energy efficiencies, we discuss some interesting combinations of the existing concepts.

### 3.4.1 When full-duplex communications meet mm-wave SWIPT networks?

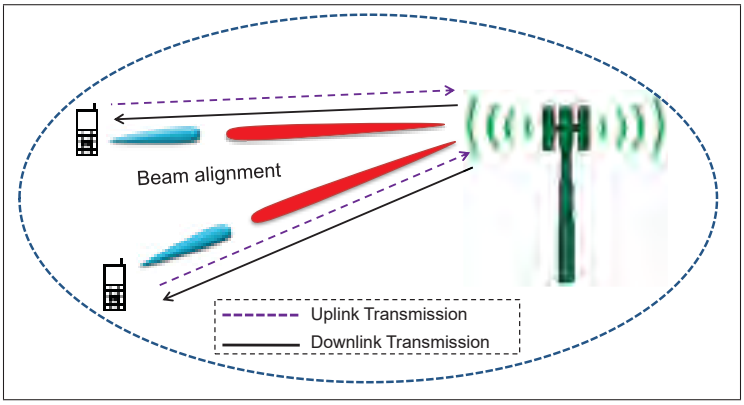


Figure 3.3 Mm-wave SWIPT networks with full-duplex communications

A combination of mm-wave and fullduplex SWIPT systems, as shown in Fig. 3.3, is interesting. Most of the recent research on ful l-duplex SWIPT systems mainly address the communications in conventional frequency bands. However, in mmwave frequency bands, there are two main challenges that must be discussed. First, the practical implementation of mm-wave full-duplex SWIPT should be investigated with a bandwidth of several gigahertz. Second, in mm-wave networks, the communication is inherently directional. Therefore, at both the transmission and reception sides, the directional antenna should be used. As a result, the node structure should be reconsidered according to the characteristics of mm-wave signals. To re-

duce the cost of antennas (i.e., parabolic antennas), one of the efficient solutions is to employ transmit and receive beams to limit self-interference. Therefore, the future objectives should address

- Studying how the beamwidth affects the beam alignment, beamforming gain and beam-searching process,
- Investigating the performance trade-off between self-interference and data transmission time,
- Properly allocating available resources to optimize system performance.

### 3.4.2 What are potential scenarios for SWIPT and EH HetNets with the full-duplex technique?

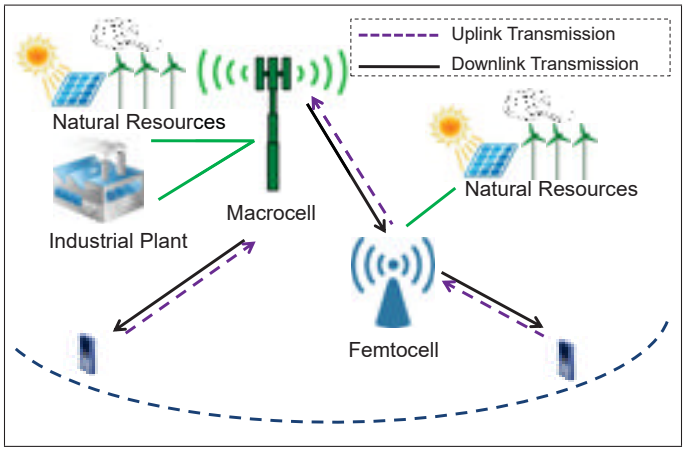


Figure 3.4 SWIPT and EH HetNets with the full-duplex technique

Full-duplex EH-SWIPT HetNets may bring a bright (however, challenging) approach. Given this concern, in Fig. 3.4, a macro cell BS harvests energy from natural sources and then communicates with a smallcell BS. On the other hand, whereas the small-cell BS receives information from the macro cell, it transmits information/energy to the users at the same time. In another case, the small cell BS transmits information to the macro cell while it receives information from the user simultaneously.

Given these scenarios, the system benefits from an enhanced spectral efficiency, however, many interference sources (e.g., self, intercell and intracell) appear due to full-duplex communications. Specifically, dealing with downlink-to-uplink interference is a big challenge, since the downlink power dominates the uplink one, in general. Therefore, using optimization frameworks, future works need to focus on

- Designing new self-interference cancellation techniques,
- Managing the downlink-to-uplink interference,
- Allocating resources to optimize the system performance in terms of the information and power transfer.

### 3.4.3 What are the main concerns of wirelessly powering Internet of Things networks?

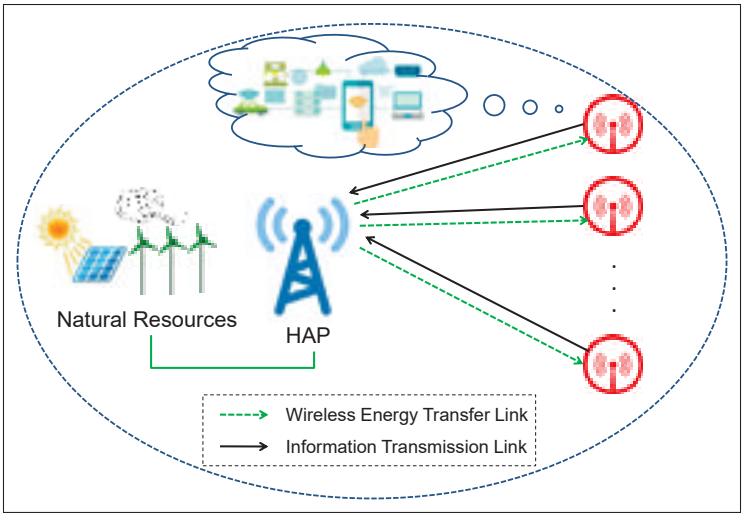


Figure 3.5 RF-WPT Internet of Things networks

Due to large-scale deployments of IoT networks, replacing or recharging a device's battery is one of the main challenges. Specifically, a large number of IoT sensors are implemented in indoor locations where natural resources might not be available to harvest. In this context, the green RF-WPT is a promising candidate for prolonging the lifetime of IoT low-power devices. This implies a scenario, as illustrated in Fig. 3.5, where a sink node is responsible for

harvesting energy from natural resources and then wirelessly transferring power to devices in a IoT wireless sensor network. In addition, the devices can communicate with each other. Given the model, some important concerns need to be addressed including

- Scheduling the power transfer to energy-hungry users according to the harvested energy at the sink node,
- Exploiting interference from ambient environments to improve the EH performance,
- Maximizing the information performance while satisfying EH requirements.

## 3.5 Concluding Remarks

In this article, we presented a review of the promising trends toward future green networks. Based on the platform of EH techniques, several potential concepts such as HetNet, mm-wave, and IoT networks, have been discussed. In particular, we focused on a promising architecture: the green RF-WPT, which plays a crucial role as a bridge between natural energy resources and smart energy-hungry devices. Accordingly, we have shown a vision of future green networks in which smart devices can be recharged by green resources even when they cannot harvest energy directly.

Furthermore, to facilitate the regreening process while adopting intensive system performance required in future networks, the combinations of techniques, such as SWIPT, mmwave, and full-duplex, can produce outstanding outcomes. It is expected that the green RF-WPT-based approaches can be one of the potential solutions for regreening the future ICT world.

**Read more about it**

A. Fehske, G. Fettweis, J. Malmodin, and G. Biczok (2011), The global footprint of mobile communications: The ecological and economic perspective, *IEEE Commun. Mag.*, 49(8), 55–62.

R. Mahapatra, Y. Nijsure, G. Kaddoum, N. U. Hassan, and C. Yuen (2016), Energy efficiency

tradeoff mechanism towards wireless green communication: A survey, *IEEE Commun. Surveys Tutorials*, 18(1), 686–705.

X. Lu, P. Wang, D. Niyato, D. I. Kim, and Z. Han (2015), Wireless networks with RF energy harvesting: A contemporary survey, *IEEE Commun. Surveys Tutorials*, 17(2), 757–789.

E. Hossain and M. Hasan (2015), 5G cellular: Key enabling technologies and research challenges, *IEEE Instrum. Meas. Mag.*, 18(3), 11–21.

A. Gupta and R. K. Jha (2015), A survey of 5G network: Architecture and emerging technologies, *IEEE Access*, 3, pp. 1206–1232.

H-V. Tran, G. Kaddoum, H. Tran, DD Tran, and DB Ha (2016), Time reversal SWIPT networks with an active eavesdropper: SER-Energy region analysis, *IEEE 84th Vehicular Technology Conference (VTC)*, Montreal, Canada.

G. Kaddoum, H-V. Tran, L. Kong, and M. Atallah (2017), Design of simultaneous wireless information and power transfer for short reference DCSK communication system, *IEEE Transactions on Communications*, 65(1), 431-443.

H-V. Tran, G. Kaddoum, H. Tran, and E.K. Hong (2017), Downlink optimization for heterogeneous networks with time reversal-based transmission under backhaul limitation, *IEEE Access*, 5, 755-770.

Internet of things: Wireless sensor networks, White Paper, IEC. [Online]. Available: http:// www.iec.ch/whitepaper/pdf/iecWPinternetofthings- LR-en.pdf

C. Zhu, V. C. M. Leung, L. Shu, and E. C.-H. Ngai (2015), Green Internet of things for smart world, *IEEE Access*, 3, 2151–2162.

# CHAPTER 4

# ROBUST DESIGN OF AC COMPUTING-ENABLED RECEIVER ARCHITECTURE FOR SWIPT NETWORKS

Ha-Vu Tran[1], and Georges Kaddoum[1]

[1]Department of Electrical Engineering, École de Technologie Supérieure,
1100 Notre-Dame west, Montreal, Canada H3C 1K3.

Paper published in *IEEE Wireless Communications Letters*, vol. 8, issue 3,
pp. 801 - 804, June 2019.

## 4.1 Introduction

Internet of Things (IoT) has been known as an innovative platform for which billions of identified low-power devices, such as sensor nodes, are connected to each other without the need for human interactions Al-Fuqaha, A., Guizani, M., Mohammadi, M., Aledhari, M. & Ayyash, M. (2015). It is expected that the number of connected IoT devices will exceed 50 billion by 2021 Sorrell, S. (2018). This gives rise to the challenging issue of replacing the batteries for IoT devices since this task is very time consuming and expensive. Among wireless power transfer approaches using electromagnetic waves Lu *et al.* (2015b), RF simultaneous wireless information and power transfer (SWIPT) technology, which can support far-field transmission Krikidis, I., Timotheou, S., Nikolaou, S., Zheng, G., Ng, D. W. K. & Schober, R. (2014b), have opened up the opportunity for wirelessly recharging and then prolonging the lifetime of IoT networks Clerckx *et al.* (2019); Krikidis *et al.* (2014b); Lu *et al.* (2015b); Tran, H.-V. & Kaddoum, G. (2018a); Zhang & Ho (2013); Zhou *et al.* (2013).

In SWIPT networks, the integrated information and energy receiver architecture of wireless devices, such as power-splitting, and time-switching architectures, plays a critically important role in managing the fundamental trade-off between information decoding (ID) and energy harvesting (EH) performances. Conventionally, the RF signals directed to an energy harvester, having an AC voltage, is rectified to obtain the form of a direct current (DC) voltage. This DC

can be used to supply wireless devices. However, the rectified voltage amplitude, determining the computational ability of devices, is often low Wan *et al.* (2017). Motivated by this issue, E. Salman *et al.* have recently developed a promising approach for computing circuits, that can be directly powered by AC in Salman *et al.* (2018); Wan *et al.* (2017). On this basis, not only the computing efficiency's energy is improved but the part of AC-to-DC conversion loss for computing blocks is also eliminated. The promise of the approach has been demonstrated in previous works Salman *et al.* (2018); Wan *et al.* (2017). However, this approach calls for the redesign of existing architectures and managing strategies at the receiver.

In this work, we propose a novel receiver architecture, based on power splitting, which enables AC computing for the SWIPT ID-EH receiver. Accordingly, we consider a SWIPT system model where a multi-antenna transmitter conveys information and energy wirelessly to a single antenna receiver using RF signals. With the proposed architecture, we aim to derive a strategy to handle the fundamental trade-off between ID and EH performances optimally while accounting for imperfect downlink channel estimation. Hence, it raises an interesting problem on optimizing robust beamformers at the transmitter side and the power splitting ratios for the information decoder, the energy harvester, and the AC computational logic at the receiver side. Also, the data rate is maximized under the constraints of an EH requirement, the energy needed for supplying the AC computational logic, and a transmit power budget. The resulting problem is difficult to solve because it has the form of convex-convex ratio maximization with multi-variable coupling in the constraints. Then, we propose a method to tackle such a problem using closed-form optimal solutions. The main contributions of this work can be summarized by

- Proposing the information and energy receiver architecture with AC computational logic for SWIPT networks,
- Developing closed-form optimal solutions to solve the optimization problem.

## 4.2 System Model

We consider a SWIPT network where an $M$-antenna transmitter aims to recharge one single-antenna receiver over RF signals. Particularly, the device can decode information and harvest energy from RF signals. Moreover, it is integrated with a recently proposed AC computational logic Salman *et al.* (2018), directly supplied by AC.

More specifically, the high-level architecture of the device can be represented as in Fig. 4.1. The obtained RF signal is split into two flows for ID and EH. Different from conventional energy harvesters Lu *et al.* (2015b); Zhou *et al.* (2013), the EH module in Fig. 4.1 includes not only a voltage multiplier to convert AC to DC but also signal conditioning blocks to produce the required AC signals for AC computational logic Salman *et al.* (2018). Further, the energy management block is responsible for handling the task of energy distribution to the ID and the control blocks. Based on the amount of harvested RF energy, the management block decides to draw energy from the storage or to convey excessive energy to the storage for future use.

According to Fig. 4.1, we propose an RF EH receiver architecture with AC computational logic, based on power splitting, as shown in Fig. 4.2. Compared with the conventional power-splitting architecture Lu *et al.* (2015b); Zhou *et al.* (2013), the proposed one has an extra splitter to direct the AC energy to the AC computational logic.

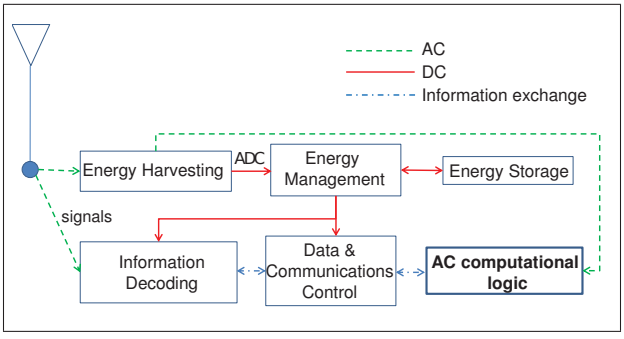


Figure 4.1 Integrated ID and EH Receiver with AC computing

We assume imperfect channel state information (CSI) is estimated at the transmitter, denoted by $(\hat{\mathbf{h}})^H$ (i.e., $\hat{\mathbf{h}} \in \mathbb{C}^M$). Similar to Le, T. A., Vien, Q.-T., Nguyen, H. X., Ng, D. W. K. & Schober,

R. (2017), the channel model can be modelled as

$$\mathbf{h} = \hat{\mathbf{h}} + \mathbf{e}, \tag{4.1}$$

where $\mathbf{h}$ is the actual channel, $\mathbf{e}$ represents a channel uncertainty defined by $\mathbf{e} \in \mathbb{C}^M$ with $\|\mathbf{e}\|^2 \leq \psi \left\|\hat{\mathbf{h}}\right\|^2$, where $\psi$ is named as an error factor. Thus, the received signal is

$$y = (\mathbf{h})^H \mathbf{w} s + n_0, \tag{4.2}$$

where $\mathbf{w} \in \mathbb{C}^{M\times 1}$ is the beamforming vector, $s$ is the complex-valued signal with unit power, modeled as an independent and identically distributed random variable ($s \in \mathbb{C}$) Clerckx *et al.* (2019), and $n_0$ is the additive white Gaussian noise (AWGN), i.e. $n_0 \sim \mathscr{CN}(0, \sigma_0^2)$.

According to the architecture given in Fig. 4.2, the data rate (in bps/Hz) can be computed as

$$R = \log\left(1 + \frac{\left|(\mathbf{h})^H \mathbf{w}\right|^2}{\sigma_0^2 + \frac{\sigma_1^2}{1-\rho}}\right), \tag{4.3}$$

where $\sigma_1^2$ is the variance of the AWGN noise introduced by the information decoder, and $\rho$ $(0 < \rho < 1)$ is a power spitting ratio. Hence, the AC signal power dedicated for supplying the AC computational logic is

$$\mathtt{SP}_{AC} = \rho(1-\phi)\left|(\mathbf{h})^H \mathbf{w}\right|^2, \tag{4.4}$$

where $\phi$ $(0 < \phi < 1)$ is a power spitting ratio. Further, we consider the non-linear EH model for DC Boshkovska, E., Ng, D. W. K., Zlatanov, N., Koelpin, A. & Schober, R. (2017); Clerckx, B. & Bayguzina, E. (2016); Tran, H.-V., Kaddoum, G. & Truong, K. T. (2018); Xiong, K., Wang, B. & Liu, K. J. R. (2017), thus the DC EH performance can be calculated as

$$\mathtt{EH}_{DC} = \frac{\frac{\mathtt{M}^{EH}}{1+e^{-\mathtt{a}(\hat{\mathtt{EH}}_{DC}-\mathtt{b})}} - \frac{\mathtt{M}^{EH}}{1+e^{\mathtt{ab}}}}{1 - \frac{1}{1+e^{\mathtt{ab}}}}, \tag{4.5}$$

where $\hat{\mathtt{EH}}_{DC} = \rho\phi \left|(\mathbf{h})^H \mathbf{w}\right|^2$, and $\mathtt{M}^{EH}$ is a constant representing the maximum harvested energy at a user when the RF EH circuit meets saturation. In addition, `a` and `b` are constants regarding circuit specifications Boshkovska *et al.* (2017); Clerckx & Bayguzina (2016); Tran *et al.* (2018); Xiong *et al.* (2017).

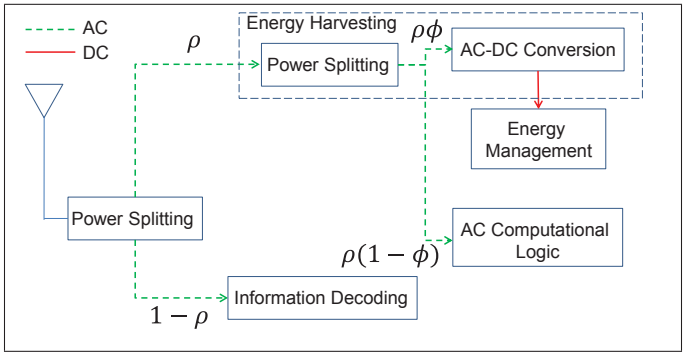


Figure 4.2 Power splitting-based EH receiver architecture with AC computing

## 4.3 Problem Formulation and Proposed Solution

### 4.3.1 Worst-case Problem Formulation

We aim at maximizing the data rate, subject to the constraints of the energy directed to the energy management unit, the energy dedicated for the AC computational logic, and transmit power. Accordingly, the corresponding optimization problem can be formulated as follows:

$$\mathrm{OP}_1: \quad \max_{\mathbf{w},\rho,\phi} \quad \min_{\mathbf{e}} R \tag{4.6a}$$

$$\text{s.t.:} \quad \min_{\mathbf{e}} \mathtt{SP}_{AC} \geq \theta \tag{4.6b}$$

$$\min_{\mathbf{e}} \mathtt{EH}_{DC} \geq \varepsilon, \tag{4.6c}$$

$$|\mathbf{w}|^2 + P_{circ} \leq P, \tag{4.6d}$$

$$0 < \phi < 1, \tag{4.6e}$$

$$0 < \rho < 1, \tag{4.6f}$$

where constraint (7.9b) is to ensure that the energy directed to the AC computational logic is larger than the threshold $\theta$. Also, constraint (7.9c) implies that the energy conveyed to the management unit is larger than the threshold $\varepsilon$. Further, $P_{circ}$ is circuit power consumption, and the transmit power is limited by a budget, denoted by $P$, through constraint (7.9e).

In this context, we denote $\mathbf{w}^\star$, $\phi^\star$ and $\rho^\star$ as the optimal values of $\mathbf{w}$, $\rho$, and $\phi$, respectively. Different from the previous works Clerckx *et al.* (2019); Zhang & Ho (2013), problem $\mathrm{OP}_1$ has one more variable and one more constraint due to taking the AC computing into account, resulting in an intractable form of maximization of the ratio of two convex functions. Furthermore, variables $\mathbf{w}$, $\rho$, and $\phi$ are coupled in constraints (7.9b) and (7.9c). Hence, solving $\mathrm{OP}_1$ is challenging.

### 4.3.2 Proposed Closed-form Optimal Solution

To solve $\mathrm{OP}_1$, we need to have the expressions of $\min\limits_{\mathbf{e}} R$, $\min\limits_{\mathbf{e}} \mathtt{SP}_{AC}$, and $\min\limits_{\mathbf{e}} \mathtt{EH}_{DC}$ first. Based on (4.3), (4.4), and (6.14), the expressions can be obtained through finding $\min\limits_{\mathbf{e}} \left|(\mathbf{h})^H\mathbf{w}\right|^2$, computed below

$$\min_{\mathbf{e}} |(\mathbf{h})^H\mathbf{w}|^2 = (1-\sqrt{\psi})^2|(\hat{\mathbf{h}})^H\mathbf{w}|^2, \tag{4.7}$$

when $\mathbf{e} = -\sqrt{\psi}\hat{\mathbf{h}}$. By substituting (4.7) into (7.9a), (7.9b), and (7.9c), the expressions of these constraints are then achieved.

Further, to deal with the difficulty of solving problem $\mathrm{OP}_1$ mentioned in subsection III.A, we propose a two-step method to deal with it as follows. First, we find the closed-form derivation of the optimal beamformer $\mathbf{w}^\star$ while considering $\phi$ and $\rho$ as constants. Second, we substitute the derivation of $\mathbf{w}^\star$ into the problem and then optimize $\rho$ and $\phi$. More details are depicted subsequently.

#### 4.3.2.1 Finding $\mathbf{w}^\star$ for a given $\phi$ and $\rho$

In the first step, we aim to solve problem $\text{OP}_1$ while treating $\phi$ and $\rho$ as constants. For convenience, we reformulate constraints (7.9b) and (7.9c) respectively as

$$|(\hat{\mathbf{h}})^H \mathbf{w}|^2 \geq \frac{\theta}{\rho(1-\phi)(1-\sqrt{\psi})^2}, \tag{4.8}$$

and

$$|(\hat{\mathbf{h}})^H \mathbf{w}|^2 \geq \frac{\bar{\varepsilon}}{\rho\phi(1-\sqrt{\psi})^2}, \tag{4.9}$$

where $\bar{\varepsilon} = \mathtt{b} - \frac{1}{\mathtt{a}}\ln\left(\frac{e^{\mathtt{ab}}(\mathtt{M}^{EH}-\varepsilon)}{e^{\mathtt{ab}}\varepsilon+\mathtt{M}^{EH}}\right)$.

Since log is an increasing function, problem $\text{OP}_1$ can be equivalently represented as

$$\begin{aligned} \text{SubOP}_1\text{:} \quad & \max_{\mathbf{w}} \quad |(\hat{\mathbf{h}})^H \mathbf{w}|^2 \\ \text{s.t.:} \quad & (4.8),\ (4.9),\ (7.9e),\ \text{and}\ (7.9f). \end{aligned} \tag{4.10}$$

For given constants $\phi$, $\rho$, $\theta$, and $\bar{\varepsilon}$, it can be seen that $\text{SubOP}_1$ is feasible if and only if there is a large enough value of $P$ which allows $|(\hat{\mathbf{h}})^H \mathbf{w}|^2$ to satisfy constraints (4.8) and (4.9).

We continue solving $\text{SubOP}_1$ by assuming that $\text{SubOP}_1$ is feasible. It implies that constraints (4.8) and (4.9) are satisfied and then can be neglected. Therefore, $\text{SubOP}_1$ simply becomes the maximization of $|(\hat{\mathbf{h}})^H \mathbf{w}|^2$ with $|\mathbf{w}|^2 = P - P_{circ}$. Thus, $\mathbf{w}^\star$ can be computed by the following closed-form expression

$$\mathbf{w}^\star = \sqrt{P - P_{circ}}\mathbf{v}, \tag{4.11}$$

where $\mathbf{v}$ is the orthonormal eigenvector corresponding to the largest eigenvalue $\lambda_{\text{largest}}\left(\hat{\mathbf{h}}(\hat{\mathbf{h}})^H\right)$. Thus, we can draw a significant remark as follows

**Remark 1.** *It is found that the optimal beamformer* $\mathbf{w}^\star$ *can be derived as a closed-form expression not including* $\rho$ *and* $\phi$*. In other words, we could have* $\mathbf{w}^\star$ *without solving* $\rho^\star$ *and* $\phi^\star$*.*

#### 4.3.2.2 Finding $\rho^\star$ and $\phi^\star$ with solved $\mathbf{w}^\star$

In the second step, by substituting $\mathbf{w}^\star$ into problem $\mathrm{OP}_1$, we then find $\rho^\star$ and $\phi^\star$. Initially, for convenience, let $(1-\sqrt{\psi})^2\left|(\hat{\mathbf{h}})^H\mathbf{w}^\star\right|^2 = (1-\sqrt{\psi})^2(P-P_{circ})\left|(\hat{\mathbf{h}})^H\mathbf{v}\right|^2 = \Gamma$, where $\Gamma$ is a constant. Next, we reformulate constraints (7.9b) and (7.9c), respectively, as

$$\rho \geq \frac{\theta}{\Gamma(1-\phi)}, \tag{4.12}$$

and

$$\rho \geq \frac{\bar{\varepsilon}}{\phi\Gamma}. \tag{4.13}$$

By combining (4.12) and (4.13), we have

$$\rho \geq \max\left\{\tfrac{\theta}{\Gamma(1-\phi)}, \tfrac{\bar{\varepsilon}}{\phi\Gamma}\right\}. \tag{4.14}$$

Considering objective (7.9a), the objective can be seen as maximizing $1-\rho$. Furthermore, maximizing $1-\rho$ with $0<\rho<1$ is equivalent to minimizing $\rho$. Accordingly, also taking (4.14) into account, problem $\mathrm{OP}_1$ can be equivalently transformed into $\mathrm{OP}_2$ as

$$\begin{aligned} \mathrm{OP}_2\text{:}\quad & \min_{\phi} \quad \max_{\phi}\left\{\tfrac{\theta}{\Gamma(1-\phi)}, \tfrac{\bar{\varepsilon}}{\phi\Gamma}\right\} \\ \text{s.t.:}\quad & \text{(7.9f)}. \end{aligned} \tag{4.15}$$

In general, problem $\mathrm{OP}_2$ is still in an intractable formulation to solve. However, since $0 < \phi < 1$ and the objective function is in the form of $\max\left\{f(\frac{1}{1-\phi}), g(\frac{1}{\phi})\right\}$, we have found an interesting property for problem $\mathrm{OP}_2$, presented as follows.

**Lemma 1.** The optimal value of $\phi$, denoted by $\phi^\star$, should satisfy the equation below

$$\frac{\theta}{(1-\phi^\star)\Gamma} = \frac{\bar{\varepsilon}}{\Gamma\phi^\star}. \tag{4.16}$$

Proof: See Appendix II.1.

Thus, according to *Lemma* 1, the closed-form optimal solutions of $\mathrm{OP}_2$ can be calculated as

$$\phi^\star = \frac{\bar{\varepsilon}}{\theta + \bar{\varepsilon}}, \tag{4.17}$$

and then

$$\rho^\star = \frac{\bar{\varepsilon}}{\Gamma\phi^\star}. \tag{4.18}$$

To this end, we provide an important remark below

**Remark 2.** It can be seen that every step solving $\mathrm{OP}_1$ is derived without the loss of generality. Then, our method does not yield any optimality loss. Notably, it is clear that our closed-form solutions only require simple calculations.

For the extension of multiple users, since the closed-form solution of beamformers may not be achieved, it is suggested that an iterative algorithm may be required to update one variable while fixing the others until convergence.

## 4.4 Numerical Results

In this section, the number of transmit antenna is set to $M = 4$, and the receiver is located 4m far away from the transmitter. Specifically, the channels between the transmitter and the user are

assumed to have Rician distribution in which the Rician factor is set to 6 dB and the pathloss exponent factor is set to 2.6. Moreover, we set $\sigma_0^2 = -111$ dBm and $\sigma_1^2 = 35$ dBm. Regarding the nonlinear EH model, we set $\mathtt{M}^{EH} = 3.9$ mW, $\mathtt{a} = 1500$ and $\mathtt{b} = 0.0022$ Boshkovska *et al.* (2017); Xiong *et al.* (2017). Particularly, we set $\theta = 0.04764$ mW and $\theta = 0.00027$ mW Salman *et al.* (2018) which are the energy needed for supplying conventional DC computing and AC computing blocks, respectively. The simulation is carried out using 10000 channel realizations.

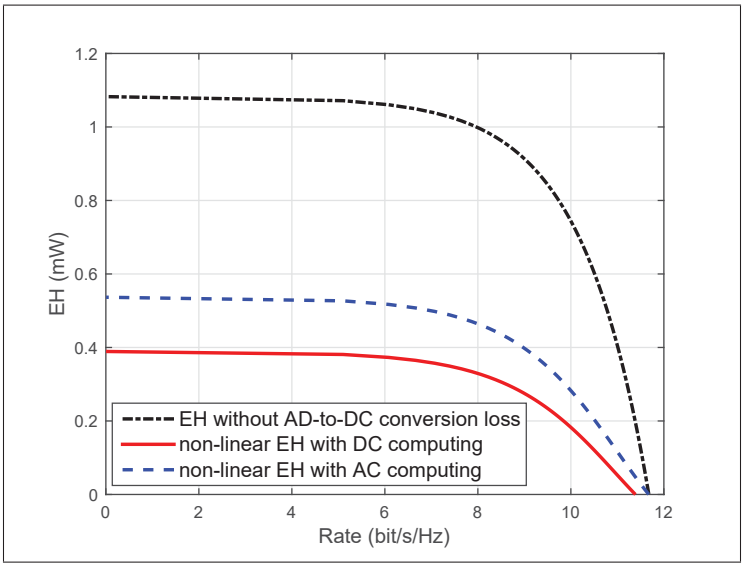


Figure 4.3 Rate-Energy region, $P_0 = P - P_{circ} = 10$ dBm, $\psi = 0$

In Fig. 4.3, a performance comparison between the conventional architecture and the one with AC computing is shown under the perfect CSI condition, for a fair observation. It is observed that using the proposed AC computing-enabled architecture results in a significantly larger rate-energy region. It can be explained by the facts that (i) there is no AC-DC conversion needed for the AC computational logic, and (ii) supplying the AC computing block also requires less energy than the DC computing one. This outcome is consistent with the measurement results in Salman *et al.* (2018); Wan *et al.* (2017) where the AC computing outperforms the DC one.

Fig. 4.4 presents the impact of channel error factor $\psi$ on the data rate in the cases with AC and DC computing blocks. It can be seen that the data rate increases as the transmit power scales

up. Further, at the same transmit power, addressing a higher $\psi$ results in a lower data rate. It is because all the constraints require more energy to be satisfied, and then less energy is dedicated to the ID purpose.

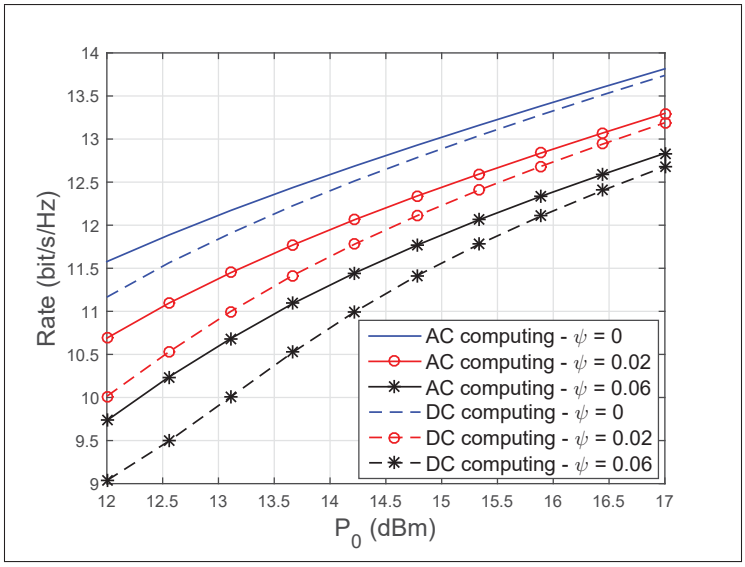


Figure 4.4 Impact of imperfect CSI, $P_0 = P - P_{circ}$ and $\varepsilon = 0.2$

## 4.5 Conclusion

In this work, we proposed a novel integrated information and energy receiver architecture, based on power splitting, to enable the AC computing methodology for SWIPT users. Accounting for the imperfect CSI, we devised the robust strategy to maximize the data rate under the constraints of the harvested AC and DC energies and the transmit power budget. We provided a simple closed-form optimal solution to the problem to facilitate the solving process. The numerical results indicate that the proposed architecture significantly improves the rate-energy region. Therefore, it can be evaluated as one of the principal candidates in developing smarter IoT devices with more powerful computational capability and longer lifetime.

# CHAPTER 5

# RESOURCE ALLOCATION IN SWIPT NETWORKS UNDER A NON-LINEAR ENERGY HARVESTING MODEL: POWER EFFICIENCY, USER FAIRNESS, AND CHANNEL NON-RECIPROCITY

Ha-Vu Tran[1], Georges Kaddoum[1], and Kien T. Truong[2]

[1] Department of Electrical Engineering, École de Technologie Supérieure,
1100 Notre-Dame west, Montreal, Canada H3C 1K3.
[2] Wireless Systems and Applications Laboratory, Posts and Telecommunications Institute of Technologies, Hanoi, Vietnam.

Paper published in *IEEE Transactions on Vehicular Technology*, vol. 67 , issue 9,
pp. 8466 - 8480, September 2018.

## 5.1 Introduction

The explosive progress of information and communication technologies (ICT), such as the fifth generation (5G) networks, has resulted in a tremendous demand for energy to prolong the lifetime of devices in wireless networks Buzzi *et al.* (2016); Gupta, A. & Jha, R. K. (2015b); Hossain & Hasan (2015). Energy harvesting (EH) techniques can be a promising solution, however, one of the main drawbacks of conventional EH networks is the dependence on unstable energy resources, such as solar and wind energy. To overcome this issue, a radio frequency (RF) wireless power transfer technique has been proposed due to the fact that the RF signals having a frequency range from 3 kHz to 300 GHz can be used to carry energy Grover & Sahai (2010); Lu *et al.* (2015b); Niyato *et al.* (2017). In RF wireless power transfer (WPT) networks, a transmitter can proactively convey RF signals to recharge energy-hungry devices whenever necessary. Especially, by integrating RF wireless power transfer techniques into traditional wireless communications, the research community has witnessed the prompt development of simultaneous wireless information and power transfer (SWIPT) technique Buzzi *et al.* (2016); Hossain & Hasan (2015); Lu *et al.* (2015b); Niyato *et al.* (2017). Over past few years, the SWIPT technique has showed its bright potential of prolonging the lifetime of wireless devices in many applications, such as cellular, wireless sensor, cognitive radio and Internet-of-Things

networks Kaddoum, G., Tran, H.-V., Kong, L. & Atalla, M. (2017); Le *et al.* (2017); Lu *et al.* (2015b); Tran & Kaddoum (2018a); Tuan, P. V. & Koo, I. (2017).

In SWIPT networks, the performance of RF energy transfer drastically suffers from path loss. In this concern, resource allocation, whose the principle relies on taking advantages of users' diversity to improve the system performance under limited availabe resources, is one of the key solutions. In Shi, Q., Liu, L., Xu, W. & Zhang, R. (2014); Zhang & Ho (2013), the authors have addressed beamforming optimization for SWIPT systems. Recently, researchers have developed a non-linear EH model for which analytical EH results tightly match the measured ones in practical systems Boshkovska, E., Ng, D. W. K., Zlatanov, N. & Schober, R. (2015); Boshkovska *et al.* (2017). More specifically, Boshkovska *et al.* (2017); Jiang, R., Xiong, K., Fan, P., Zhang, Y. & Zhong, Z. (2017) have shown a scheme of joint time and power allocation and a scheme of joint beamforming optimization and power splitting for SWIPT networks, respectively, taking a non-linear EH model into account. In Xiong *et al.* (2017), the authors have investigated rate-energy trade-off behaviour for MIMO SWIPT networks under a non-linear EH model.

In recent years, several articles Chingoska, H., Hadzi-Velkov, Z., Nikoloska, I. & Zlatanov, N. (2016); Diamantoulakis, P. D. & Karagiannidis, G. K. (2017); Diamantoulakis, P. D., Pappi, K. N., Karagiannidis, G. K., Xing, H. & Nallanathan, A. (2017); Ju, H. & Zhang, R. (2014a); Tuan & Koo (2017) have exploited the property of channel reciprocity to develop resource allocation schemes for SWIPT and wireless powered communication (WPC) networks. According to channel reciprocity, reversed time division duplex (TDD)-based systems can benefit from the fact that the downlink CSI can be achieved by estimating the uplink channels. One of the main advantages of applying TDD to SWIPT systems is that the energy consumption of channel estimation at user receivers is reduced and then the user lifetime can be prolonged consequently. In practice, the antennas at the transmitter and receiver sides have distinct RF chains, and need to be calibrated. However, imperfectly calibrating these antennas can impair the channel reciprocity. Thus, designing robust beamformers taking this issue into account is

one of the primary solutions. To the best of our knowledge, there has been little prior work on the impact of non-ideal channel reciprocity for SWIPT systems.

Furthermore, in conventional communication systems, it is well-known that the users with the worse channel quality consumes more energy for uplink transmissions than the ones with the better channel condition. Indeed, this phenomenon becomes more prominent in WPC networks where distant users who are often associated with worse channel quality not only have less chance to harvest suffcient energy but also spend more energy for uplink transmission than near users do. Some earlier papers Ju & Zhang (2014a); Liu, L., Zhang, R. & Chua, K.-C. (2014); Mishra, D., De, S. & Krishnaswamy, D. (2017); Tabassum, H., Hossain, E., Ogundipe, A. & Kim, D. I. (2015) have studied this phenomenon under the doubly near-far effect point of view. More specifically, most of them have dealt with the unfairness between distant and near users in WPCNs by jointly managing power transfer in downlinks and information transmission in uplinks. Particularly, in those works, the user fairness is improved following channel gains. Nevertheless, this might result in inflexible fairness controls for network operators. The issue of user fairness in WPCNs has inspired us to rethink the resource allocation in SWIPT networks. So far, to the best of our knowledge, most of the previous works Boshkovska *et al.* (2017); Jiang *et al.* (2017); Le *et al.* (2017); Shi *et al.* (2014); Tuan & Koo (2017); Xiong *et al.* (2017); Zhang & Ho (2013) only address the management of downlink SWIPT to meet ID and EH targets without further prediction of energy demands. In practical SWIPT networks however, after receiving information and harvesting energy in downlinks, the users might need to send pilot and information-bearing signals to the BS via uplinks. Similar to WPCNs, this raises an issue of user unfairness in SWIPT networks, referring that distant users spend more energy to connect to the BS than near users do. Therefore, this motivates us to take into account such an issue when designing resource allocation schemes for downlink SWIPT networks. In fact, considering a practical SWIPT network with a non-linear EH model, flexibly guaranteeing the user fairness between users located at different communication ranges while minimizing transmit power and taking the non-ideal channel reciprocity into account is a challenge.

In this paper, we address the above issues for a SWIPT system under a non-linear EH model in which a multi-antenna BS and multiple single-antenna users are considered. Each user employs a power splitter to coordinate the processes of information decoding (ID) and EH. In this model, downlink CSI is estimated at the BS side via an uplink TDD scheme to exploit the channel reciprocity. Moreover, the channels are assumed to be flat fading. Specifically, this work focuses on designing a novel resource allocation scheme able to jointly *(i)* save energy by minimizing transmit power, *(ii)* account for the user fairness by maximizing the weighted sum of the coverage probability of EH (under the calibration error), and *(iii)* mitigate the non-ideal channel reciprocity by minimizing the effect of calibration error on ID performance. Recently, multi-objective optimization has been promoted as an efficient approach to handle resource allocation in SWIPT networks Bjornson, E., Jorswieck, E. A., Debbah, M. & Ottersten, B. (2014); Marler, R. & Arora, J. (2004); Ng, D. W. K., Lo, E. S. & Schober, R. (2016); Sun, Y., Ng, D. W. K., Zhu, J. & Schober, R. (2016). However, since the considered objectives (i.e. *(i)*, *(ii)* and *(iii)*) have different characteristics, the algorithms in previous works Ng *et al.* (2016); Sun *et al.* (2016) based on the weighted Tchebycheff method Marler & Arora (2004) might not be adopted for the considered SWIPT system.

In this work, we propose a novel method in which such objectives are structured on a cross-layer multi-level optimization problem. In our method, objectives *(i)* and *(iii)* can be addressed by a physical-layer optimization problem with a multi-level structure. More specifically, objectives *(i)* and *(iii)* are formulated into a first-level and a second-level problems, respectively. Besides, objective *(ii)* is transformed into a set of constraints of the physical-layer problem whose threshold values are designed by an upper-layer optimization problem. The overall problem formulation would be thoroughly presented in section III. On this basis, we reformulate the upper-layer problem into a quadratic optimization problem, and then solve it using a closed-form optimal solution. After that, considering the multi-level problem, we develop a manner to relax the second-level problem into a set of constraints of the first-level one. Accordingly, the resulting multi-level problem is convex and can be conveniently tackled by solvers Grant & Boyd (2009). In practice, the CSI changes with time, due to user mobility, yielding

the need of updating and resolving the problem. Thus, to maintain a stable system performance while reducing computational burdens at the BS, we further propose a closed-form suboptimal solution to tackle the problem. Our main contributions can be stated as follows

- Proposing a novel resource allocation scheme for SWIPT networks based on structuralizing multiple objectives with different characteristics into the cross-layer multi-level optimization approach,
- Deriving the closed-form approximate expressions of the average SINR, and the coverage probability of EH under the effect of the non-ideal channel reciprocity,
- Developing a method to solve the cross-layer multi-level optimization problem,
- Providing a closed-form suboptimal solution with low complexity to deal with time-varying channels.

The remainder of this paper is organized as follows: In Section 5.2, the system model is described. The overall idea of the proposed resource allocation scheme is discussed in Section 5.3. In Section 5.4, optimal and suboptimal solutions of the cross-layer multi-level optimization problem are presented. In Section 5.5, numerical results and discussions are provided. Finally, concluding remarks are put forward in Section 5.6.

*Notation:* The notation $\mathbb{R}_+^m$ and $\mathbb{C}^{m\times n}$ represent the sets of $m$-dimensional nonnegative real vector and $m \times n$ complex matrix, respectively. The boldface lowercase $\mathbf{a}$ and uppercase $\mathbf{A}$ denote vectors and matrices, respectively. The superscripts $\mathbf{A}^T$ and $\mathbf{A}^H$ indicate the transpose and transpose conjugate, respectively. Moreover, symbols $|.|$, and $\|.\|$ stand for the absolute value, vector Euclidean norm, respectively.

## 5.2 System Model

Consider a multiuser SWIPT system when an $M$-antenna BS serves $N$ single-antenna users. The users are randomly located in the cell area such that some users have more severe channel conditions than the other. For example, the users located far from the BS experience higher

distance-dependent path-losses than those located near the BS. This might lead to a form of the doubly near-far problem in which distant users not only have less chance to harvest energy but also spend more energy for uplink transmission than near users do. In fact, the effort to improve the EH performance for distant users can lead to some diffculties in managing the ID performance of the overall system since near users might be exposed to denser interference than distant users. Thus, resource allocation is the key solution to this issue.

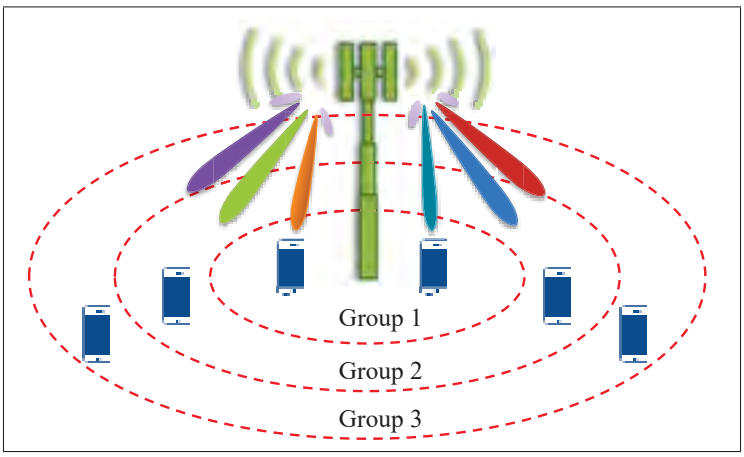


Figure 5.1 An illustration of the SWIPT system including 3 groups of users

Therefore, to take into account the doubly near-far problem in providing fairness among users in the cell, we divide the users into $G$ disjoint groups, based on communication ranges, as illustrated in Fig. 5.1. Here, group $g$, $g = 1, \cdots, G$, has $N_g$ users is assigned a unique priority parameter $b_g$. The advantage of prioritizing users can be described as follows. In the previous works of Ju & Zhang (2014a); Liu *et al.* (2014); Tabassum *et al.* (2015), the EH performance of a user is improved according to channel gains. In practice, however, the channel gain approach may not meet the energy demands exactly, it may offer less or more energy than required. For instance, farthest users whose batteries run out faster may need to harvest more energy than the amount estimated by the channel-gain-based approach. Additionally, when a user is exposed to RF radiation over safety limits, this issue might be diffcult to manage using the channel-gain-based approach. In the approach proposed in this work, the network operator can take other concerns into account and then flexibly manage the priority to balance system performance.

### 5.2.1 Channel Model of Non-ideal Reciprocity

We assume that the channels are flat-fading. Let $\mathbf{h}_n^g \in \mathbb{C}^{M\times 1}$ and $\mathbf{u}_n^g \in \mathbb{C}^{M\times 1}$ be the downlink channel vector and the uplink channel vector between the BS and user $n$, $n = 1,\cdots,N_g$, in the group $g$, respectively. According to 3GPP (2009), the downlink and uplink channels can be respectively modelled as

$$\mathbf{h}_{m,n}^g = t_m v_{m,n}^g \bar{r}_n^g, \tag{5.1}$$

$$\mathbf{u}_{m,n}^g = r_m v_{m,n}^g \bar{t}_n^g, \tag{5.2}$$

where $v_{n,m}^g$, $m = 1,\cdots,M$, is the wireless channel coefficient between transmit antenna $m$ of the BS and user $n$ in group $g$; $t_m$ and $r_m$ are the equivalent transmit and receive antenna gains of antenna $m$ of the BS, respectively; $\bar{t}_n^g$ and $\bar{r}_n^g$ are the equivalent receive and transmit circuit gains of user $n$ in group $g$, respectively.

Let us define $c_{m,n}^g$ such that $\dfrac{\mathbf{h}_{m,n}^g}{\mathbf{u}_{m,n}^g} = \dfrac{t_m \bar{r}_n^g}{r_m \bar{t}_n^g} = c_{m,n}^g$. If antennas are perfectly calibrated, then $c_{1,n}^g = c_{2,n}^g = \cdots = c_{M,n}^g = \tilde{c}_n^g$, where $\tilde{c}_n^g$ is a constant number 3GPP (2009). In this case, channel reciprocity holds and the BS is able to estimate the downlink channels based on uplink pilots perfectly. In fact, some papers on TDD channel reciprocity observe that the difference between the uplinks and downlinks, i.e. $\tilde{c}_n^g$, does not affect the designs of beamforming/precoding/detector in multi-user multi-input multi-output (MIMO) systems Vieira, J., Rusek, F. & Tufvesson, F. (2014).

However, there are always hardware calibration errors in practice. Thus, according to one of the most common approaches 3GPP (2009), the downlink channels can be modelled considering calibration errors as follows

$$\mathbf{h}_n^g = (\mathbf{I}_M + \mathbf{C}_n^g)\mathbf{u}_n^g, \tag{5.3}$$

where $\mathbf{I}_M$ is an $M \times M$ identity matrix, and $\mathbf{C}_n^g = \text{diag}\{c_{1,n}^g, c_{2,n}^g, \cdots, c_{M,n}^g\}$ is a matrix presenting calibration errors and $c_{m,n}^g \sim \mathscr{CN}(0, \sigma_{cal}^2)$.

In practice, users may have more than one antenna. Thus, we provide a brief discussion on the extension of channel model as follows. Since both the BS and users are equipped multiple antennas, the hardware calibration might be complex. In light of 3GPP (2009), to reduce the compexity, it is suggested calibration be mainly performed at the BS side while the antennas at the user side are pre-calibrated such that $\frac{\bar{r}^g_{n,l}}{\bar{t}^g_{n,l}} = \lambda^g_n \ (\forall l)$ where the index $l$ indicates antenna $l$ at a user and $\lambda^g_n$ is a constant. Hence, we obtain an expression $\frac{\mathbf{h}^g_{m,n,l}}{\mathbf{u}^g_{m,n,l}} = \frac{t_m \bar{r}^g_{n,l}}{r_m \bar{t}^g_{n,l}} = c^g_{m,n}$. Note that index $l$ does not appear in $c^g_{m,n}$ since antenna $l$ has been pre-calibrated. Then, similar to the case of single-antenna user, the channel model can be formulated as

$$[\mathbf{h}^g_{n,1} \quad ... \quad \mathbf{h}^g_{n,L}] = (\mathbf{I}_M + \mathbf{C}^g_n)[\mathbf{u}^g_{n,1} \quad ... \quad \mathbf{u}^g_{n,L}]. \tag{5.4}$$

### 5.2.2 Signal Model

On the downlink, the received signal at user $n$ in group $g$ could be expressed as

$$\begin{aligned} y^g_n = (\mathbf{h}^g_n)^T \mathbf{w}^g_n s^g_n + \sum_{\substack{n'=1 \\ (n' \neq n)}}^{N_g} (\mathbf{h}^g_n)^T \mathbf{w}^g_{n'} s^g_{n'} \\ + \sum_{\substack{g'=1 \\ (g' \neq g)}}^{G} \sum_{n=1}^{N_g} (\mathbf{h}^g_n)^T \mathbf{w}^{g'}_n s^{g'}_n + n_0, \end{aligned} \tag{5.5}$$

where $\mathbf{w}^g_n$ is the beamforming vector for user $n$ in group $g$, and $s^g_n$ is the unit power transmit symbol. The first term is the desired signal, the second term is the interference in the same group, the third term is the interference from the other groups, and the fourth term $n_0$ is the additive white Gaussian noise (AWGN), i.e. $n_0 \sim \mathscr{CN}(0, \sigma^2_0)$.

Further, the received signal at user $n$ in group $g$ is split to the information decoder and the energy harvester by a power spitter, which divides an $\rho^g_n \ (0 \leq \rho^g_n \leq 1)$ portion of the signal power to the information decoder, and the remaining $(1 - \rho^g_n)$ portion of power to the energy

harvester. As a result, the signal split to the information decoder is expressed as

$$y_n^{\mathrm{ID},g} = \sqrt{\rho_n^g} y_n^g + n_1, \tag{5.6}$$

where $n_1$ is the AWGN introduced by the ID, i.e. $n_1 \sim \mathscr{CN}(0, \sigma_1^2)$. Due to calibration errors, the BS has imperfect downlink CSI, and the instantaneous signal-to-interference-plus-noise ratio (SINR) values are not available. Alternatively, to evaluate ID performance, the average SINR at user $n$ in group $g$ can be given by

$$\mathbb{E}\left[\mathtt{SINR}_n^g\right] \triangleq \frac{\mathbb{E}\left[\rho_n^g \left|(\mathbf{h}_n^g)^T \mathbf{w}_n^g\right|^2\right]}{\mathbb{E}\left[\rho_n^g \left(\mathscr{I}_n^g + |n_0|^2\right) + |n_1|^2\right]}, \tag{5.7}$$

where $\mathscr{I}_n^g$ is the interference component which can be presented as below

$$\mathscr{I}_n^g = \sum_{\substack{n'=1 \\ (n' \neq n)}}^{N_g} \left|(\mathbf{h}_n^g)^T \mathbf{w}_{n'}^g\right|^2 + \sum_{\substack{g'=1 \\ (g' \neq g)}}^{G} \sum_{n'=1}^{N_g} \left|(\mathbf{h}_n^g)^T \mathbf{w}_{n'}^{g'}\right|^2. \tag{5.8}$$

It is worth noting that we apply a relaxation for computing the average SINR given in (5.7) due to further conveniences.

### 5.2.3 Non-Linear Energy Harvesting Model

Further, the signal split to the energy harvester is

$$y_n^{\mathrm{EH},g} = \sqrt{(1-\rho_n^g)} y_n^g. \tag{5.9}$$

Conventionally, in linear EH models, the harvested energy, denoted by $\mathtt{E}_n^g$, can be computed as a linear function of input energy, i.e. $\mathtt{E}_n^g = \xi_n^g \hat{\mathtt{E}}_n^g$ in which $\xi_n^g$ $(0 \leq \xi_n^g \leq 1)$ is the energy

conversion efficiency and $\hat{\mathrm{E}}_n^g$ is the input energy defined by

$$\hat{\mathrm{E}}_n^g = (1-\rho_n^g) \sum_{g'=1}^{G} \sum_{n'=1}^{N_g} \left| (\mathbf{h}_n^g)^T \mathbf{w}_{n'}^{g'} \right|^2 . \tag{5.10}$$

Note that the contribution of $n_0$ and $n_1$ is neglected Ng *et al.* (2014); Zhang & Ho (2013).

However, in practice, it has been shown that the RF energy conversion efficiency varies with different levels of input energy. The linear model is only proper for the specific scenario when the received powers at users are constant. Thus, in this work, we consider a non-linear EH model that can give more accurate results to practical systems. According to Boshkovska *et al.* (2017); Jiang *et al.* (2017); Xiong *et al.* (2017), the non-linear model can be described as

$$\mathrm{E}_n^g = \frac{\frac{\mathtt{M}^{EH}}{1+e^{-\mathtt{a}(\hat{\mathrm{E}}_n^g - \mathtt{b})}} - \frac{\mathtt{M}^{EH}}{1+e^{\mathtt{ab}}}}{1 - \frac{1}{1+e^{\mathtt{ab}}}}, \tag{5.11}$$

where $\mathtt{M}^{EH}$ is maximum harvested energy at a user when the EH circuit meets saturation. In addition, $\mathtt{a}$ and $\mathtt{b}$ are constants regarding circuit specifications, e.g. the resistance, capacitance, and diode turn-on voltage Boshkovska *et al.* (2017); Jiang *et al.* (2017); Xiong *et al.* (2017).

In this work, to characterize the chance of harvesting energy at a user, the coverage probability of harvested energy regarding calibration errors Upton, G. & Cook, I. (2014) is given by

$$\mathscr{P}r\left(\mathrm{E}_n^g \geq \theta_n^g\right), \tag{5.12}$$

where $\theta_n^g$ is a threshold.

## 5.3 Problem Formulation and Proposed Approach

This section describes the overall idea of the proposed resource allocation scheme and presents the related problem formulation.

We start with discussing the considered objectives for resource allocation in the SWIPT system. First, one of the important objectives is transmit power saving, namely objective *(i)*. Second, the overall EH performance should be maximized taking the user fairness into account, namely objective *(ii)*. Third, the effect of non-ideal channel reciprocity on ID performance should be minimized, namely objective *(iii)*. To handle this task, although multi-objective optimization seems to be promising Bjornson *et al.* (2014); Marler & Arora (2004), directly applying it might bring non-trivial computing difficulites. For instance, one of the most popular methods, so-called *weighted sum method* Marler & Arora (2004), might not be a suitable choice since the characteristic of the objectives are not the same. Indeed, the metrics of objectives $(i)$, $(ii)$, and $(iii)$ are Watt(s), percentage(s), and dB. This leads to difficulties of choosing weighted values Marler & Arora (2004). Further, another multi-objective optimization method, namely *lexicographic method* Marler & Arora (2004), can deal with this drawback. However, the resulting problem is highly complex and hard to solve.

In this work, we propose a novel method o jointly solve these objectives. In fact, objective *(ii)* can be represented by maximizing the weighted sum of coverage probability of EH according to the group priorities. In this concern, distant users with a higher priority can be managed to have more chance to harvest energy than near users. Thus, our idea exploits this point and then proposes a cross-layer design in terms of a cooperation between the physical and the upper layers. In this concern, objectives *(i)* and $(iii)$ are jointly formulated into the physical-layer problem. Besides, objective *(ii)* is translated into the EH coverage probability constraints of the physical-layer problem whose threshold values are planned by an upper-layer optimization problem, namely $\mathrm{OP}_2$. After solving $\mathrm{OP}_2$, the designed plan of the thresholds is conveyed to the physical layer. The proposed approach has many advantages, of which we include three. First, the issue of dissimilarity of characteristics between the objectives can be properly relaxed when the objective *(ii)* is separately tackled at the upper layer. Second, the computation burden is shared between the processing units of the layers. Third, network operators can flexibly manage the user fairness and balance the system performance since they can check the designed

plan before conveying it to the processing unit at the physical layer. The detailed formulation is shown below.

Accounting for problem $\mathrm{OP}_2$, we consider a realistic situation where the network operator has an existing serving plan regarding the thresholds of the EH coverage probability constraints. This plan might be created according to user demands or registered Quality of Service (QoS) only. It does not take the user fairness into account. Thus, re-designing the plan is to address this task. Moreover, in practice, the network operator might not want the new plan to deviate too much from an existing plan. In this concern, the first aim is to maximize the weighted sum of the threshold with the purpose of guaranteeing the user fairness, whereas the second one is to minimize the 0-norm of the difference between the existing plan and the re-designed one. Thus, based on the user-prioritized system model, re-designing the plan can be represented by a multi-objective optimization problem as follows

$$\mathrm{OP}_2 : \max_{\{\alpha_n^g\}} \quad \sum_{g=1}^{G}\sum_{n=1}^{N_g} b^g \alpha_n^g \quad \& \quad \min_{\{\alpha_n^g\}} \quad \|\boldsymbol{\alpha} - \mathbf{q}\|_0 \tag{5.13a}$$

$$\text{s.t.:} \quad \sum_{g=1}^{G}\sum_{n=1}^{N_g} \alpha_n^g = \sum_{g=1}^{G}\sum_{n=1}^{N_g} q_n^g, \tag{5.13b}$$

$$0 \leq \alpha_n^g \leq 1, \quad \forall g, n, \tag{5.13c}$$

in which, $\{q_n^g\}$ and $\{\alpha_n^g\}$ represent the threshold values of coverage probabilites set in the existing and desired plans, respectively. Also, $\boldsymbol{\alpha} = [\alpha_1^1 \dots \alpha_N^G]^T$ and $\mathbf{q} = [q_1^1 \dots q_N^G]^T$. It is worth mentioning that $b_g$ is the priority factor associated with group $g$. Additionally, constraint (5.13b) is to keep the total coverage probability (i.e. the total offered QoS of the system) given in the two plans equal.

Considering the physical-layer problem, on one hand, objective *(i)* can be formulated by minimizing total transmit power. On the other hand, to combat the channel reciprocity effect on the ID performance (i.e. objective $(iii)$), it is desirable to design robust beamformers to maximize the average SINR obtained at each user. However, since the beamforming vectors for multiple users in the expression of the average SINR are coupled. This might make this multi-

objective problem intractable. Thus, we propose an alternative manner to manage objectives $(i)$ and $(iii)$ using a multi-level structure. More specifically, the first-level problem, namely $\mathrm{OP}_1$, is to account for objective *(i)*, whereas the second-level problem, namely $\mathrm{SL}_1$, is to address objective $(iii)$. However, even in this case, achieving the beamformers such that the beam direction and beam power are jointly optimized is difficult. Thus, considering problem $\mathrm{SL}_1$, it is suggested that only the beam directions of beamformers are designed to maximize the average signal-to-leakage ratio (SLR) on calibration errors at each user with setting the average SINR as constraints. In this concern, specifically, SLR beamforming is also known by another name, transmit minimum mean square error (MMSE) beamforming [Remark 3.2, Bjornson, E. & Jorswieck, E. (2013)]. Its principle relies on minimizing the effect of calibration errors on the desired signal performance. Besides, it is well-known that the leakage or the interference can be useful in improving EH performance. Thus, the SLR criterion might be non-preferred to EH. In fact, dealing with non-ideal channel reciprocity to improve ID performance, in its nature, affects the EH performance. This can be seen as a performance trade-off between ID and EH. However, benefting from the cross-layer approach, the EH performance can be guaranteed through the thresholds designed by upper-level problem $\mathrm{OP}_2$.

For further concerns, detailed problem formulations can be presented as follows

$$\mathrm{OP}_1: \quad \min_{\{\mathbf{w}_n^g, \rho_n^g\}} \quad \sum_{g=1}^{G} \sum_{n=1}^{N_g} \|\mathbf{w}_n^g\|^2 \tag{5.14a}$$

$$\text{s.t.:} \quad \{\mathbf{w}_n^g\} \in \mathscr{F}, \tag{5.14b}$$

$$\mathbb{E}\left[\mathtt{SINR}_n^g\right] = \gamma_n^g, \quad \forall g, n, \tag{5.14c}$$

$$\mathscr{P}r\left(\mathtt{E}_n^g \geq \theta_n^g\right) \geq \alpha_n^g, \quad \forall g, n, \tag{5.14d}$$

$$0 < \rho_n^g < 1, \quad \forall g, n, \tag{5.14e}$$

where $\{\gamma_n^g\}$, $\{\theta_n^g\}$, and $\{\alpha_n^g\}$ are the thresholds of the average SINR, the EH, and the coverage probability of EH, respectively. In particular, the values of $\{\alpha_n^g\}$ are designed by the upper layer, i.e. problem $\mathrm{OP}_2$, such that the weighted sum of the threshold values is maximized. $\{\alpha_n^g\}$ can be affected by the method used to solve multi-objective problem $\mathrm{OP}_2$, determined by

network operators. Additionally, the values of $\{\gamma_n^g\}$ and $\{\theta_n^g\}$ can be also assigned by network operators. In practice, the network operators can determine these thresholds based on several concerns, such as user requests and the registered QoS at the user side. Further, $\mathscr{F}$ is a set defined by the second-level problem $\mathrm{SL}_1$.

Regarding the formulation of second-level problem $\mathrm{SL}_1$, the beamformer should be designed to maximize the average SLR at each user. Accordingly, problem $\mathrm{SL}_1$ can be formulated as below

$$\mathrm{SL}_1 : \left\{ \max_{\mathbf{w}_n^g} \quad \overline{\mathrm{SLR}}_n^g \right\}, \quad \forall n, g \tag{5.15}$$

where

$$\overline{\mathrm{SLR}}_n^g = \tag{5.16}$$

$$\frac{(\mathbf{w}_n^g)^H \mathbb{E}\left[\mathbf{h}_n^g (\mathbf{h}_n^g)^H\right] \mathbf{w}_n^g}{(\mathbf{w}_n^g)^H \mathbb{E}\left[\sum\limits_{\substack{n'=1 \\ (n' \neq n)}}^{N} \mathbf{h}_{n'}^g (\mathbf{h}_{n'}^g)^H + \sum\limits_{\substack{g'=1 \\ (g' \neq g)}}^{G} \sum_{n=1}^{N} \mathbf{h}_n^{g'} (\mathbf{h}_n^{g'})^H\right] \mathbf{w}_n^g}. \tag{5.17}$$

in which, the numerator includes the desired signal power while the denominator consists of the total interference power. In principle of the multi-level problem Caramia, M. & Dell'Olmo, P. (2008), constraint (7.9b) implies that any optimal solutions $\{\mathbf{w}_n^g\}$ of the first-level problem must belong to the set of the optimizers of second-level problem $\mathrm{SL}_1$, i.e. $\mathscr{F}$. In other words, optimal beamformers, i.e. $\{\mathbf{w}_n^{\star g}\}$, should have the beam directions designed by problem $\mathrm{SL}_1$. For convenience, responsibility of each problem and an illustration of the overall proposed scheme are shown in Figs. 5.2 and 5.3, respectively.

## 5.4 Solutions to the Cross-Layer Multi-Level Optimization Problem

This section is to present a novel method to tackle the cross-layer multi-level problem.

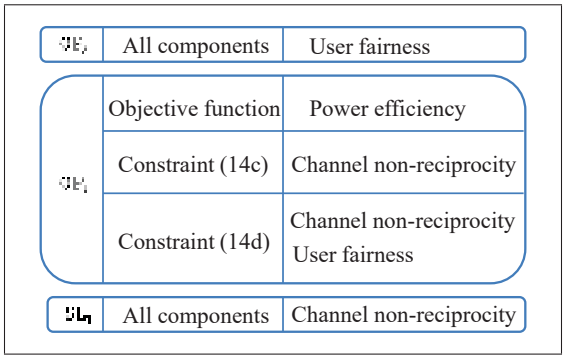


Figure 5.2 Responsibility for each objective function and each constraint

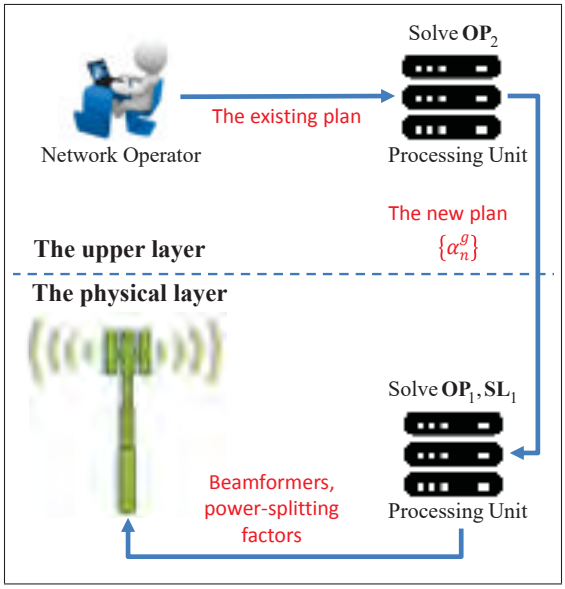


Figure 5.3 The proposed resource allocation scenario

### 5.4.1 Solving Upper-Layer Problem $\mathbf{OP}_2$

On one hand, it is obvious that our aim is to design a new serving plan taking the user fairness into account. This is hence formulated into $\mathrm{OP}_2$ which is a multi-objective optimization problem. Due to the aim of the new plan, the first objective, i.e. maximizing the weighted-sum of the coverage probabilities, should be treated more importantly than the second objective, i.e. minimizing the difference between the two plans.

On the other hand, actually, solving a single-objective problem with the $l_0$-norm is difficult. This is even more challenging when considering this issue in the form of a multi-objective problem. In principle, the $l_0$-norm handles the plan difference through the number of dissimilar elements between the two plans. However, this approach results in a strongly NP-hard problem which is highly complex and computationally intractable to solve Baraniuk, R. (2007); Ge, D., Jiang, X. & Ye, Y. (2011). The main difficulty is due to the sparsity property of the $l_0$-norm. Several previous works proposed methods to relax the $l_0$-norm into a higher-order norm problem Chen, F. & Zhang, Y. (2013); Iordache, M.-D., Bioucas-Dias, J. M. & Plaza, A. (2014). However, it is still difficult to adopt directly those methods to the multi-objective problem.

As discussed, since the second objective is less important than the first one, our idea is to exploit this point to relax the sparsity property required in the second objective and then make problem $\mathrm{OP}_2$ more tractable. In this concern, we propose minimizing the $l_2$-norm of the plan difference as an alternative approach. In fact, the $l_2$-norm might not measure the sparsity of the plan difference, however, it can measure the sum of the plan difference which the $l_0$-norm might not do. Particularly, the previous work [Agarwal, D., Chen, B.-C., Elango, P. & Wang, X. (2012), pp. 488] managed the plan difference by minimizing the squared variance (i.e. a form of the $l_2$-norm) between the two plans. Thus, we focus on minimizing the squared variance, instead of minimizing the $l_0$-norm of the plan difference. Accordingly, problem $\mathrm{OP}_2$ is reformulated as follows

$$\mathrm{OP}_2 : \max_{\{\alpha_n^g\}} \quad \sum_{g=1}^{G}\sum_{n=1}^{N_g} b^g \alpha_n^g \quad \& \quad \min_{\{\alpha_n^g\}} \quad \sum_{g=1}^{G}\sum_{n=1}^{N_g} (\alpha_n^g - q_n^g)^2 \tag{5.18a}$$

$$\text{s.t.:} \quad \sum_{g=1}^{G}\sum_{n=1}^{N_g} \alpha_n^g = \sum_{g=1}^{G}\sum_{n=1}^{N_g} q_n^g, \tag{5.18b}$$

$$0 \leq \alpha_n^g \leq 1, \quad \forall g, n. \tag{5.18c}$$

Based on suggested methods given in Marler & Arora (2004), multi-objective problem $\mathrm{OP}_2$ can be solved by using the weighted-sum approach. In this regard, we introduce a parameter $R$ $(0 < R < 1)$ to represent the relative importance between the two objectives. Hence, $\mathrm{OP}_2$ can be re-written as

$$\begin{aligned} \mathrm{OP}_{2-1}: \max_{\alpha_n^g} \quad & (1-R)\sum_{g=1}^{G}\sum_{n=1}^{N_g} b^g \alpha_n^g - R\sum_{g=1}^{G}\sum_{n=1}^{N_g}(\alpha_n^g - q_n^g)^2 \\ \text{s.t.:} \quad & (5.18b), (5.18c). \end{aligned} \tag{5.19}$$

By modifying $R$, a trade-off between the objective functions can be evaluated. On this basis, a resource allocation scheme can be reasonably designed, according to network requirements. To derive the closed-form solution, the Lagrangian function is derived as

$$\begin{aligned} &\mathscr{L}^{s2}\left(\boldsymbol{\alpha}, \mu^{s2}, \boldsymbol{\delta}_1^{s2}, \boldsymbol{\delta}_2^{s2}\right) \\ &= -\boldsymbol{\alpha}^T \mathbf{f} + R\boldsymbol{\alpha}^T\boldsymbol{\alpha} + \mu^{s2}\left(\boldsymbol{\alpha}^T \mathbf{1}_{NG} - \sum_{g=1}^{G}\sum_{n=1}^{N_g} q_n^g\right) \\ &+ \sum_{g=1}^{G}\sum_{n=1}^{N_g}(q_n^g)^2 + (\boldsymbol{\delta}_1^{s2})^T(\boldsymbol{\alpha} - \mathbf{1}_{NG}) - (\boldsymbol{\delta}_2^{s2})^T\boldsymbol{\alpha}. \end{aligned} \tag{5.20}$$

where $\mathbf{f} = \left[f_1^1 \ldots f_{N_G}^1 \ldots f_1^G \ldots f_{N_G}^G\right]^T \in \mathbb{C}^{NG\times 1}$ in which $f_n^g = (1-R)b^g + 2Rq_n^g$,

$\boldsymbol{\alpha} = \left[\alpha_1^1 \ldots \alpha_{N_G}^1 \ldots \alpha_1^G \ldots \alpha_{N_G}^G\right]^T \in \mathbb{C}^{NG\times 1}$, $\mu^{s2} \in \mathbb{R}$, $\boldsymbol{\delta}_1^{s2} \in \mathbb{R}^{NG\times 1}$ and $\boldsymbol{\delta}_2^{s2} \in \mathbb{R}^{NG\times 1}$ are dual variables. After some manipulations, the optimal solution, i.e. $\boldsymbol{\alpha}^\star$, can be obtained by

$$\boldsymbol{\alpha}^\star = \frac{1}{2R}\left(\mathbf{f} - \mu^{s2}\mathbf{1} - \boldsymbol{\delta}_1^{s2} + \boldsymbol{\delta}_2^{s2}\right). \tag{5.21}$$

By substituting $\boldsymbol{\alpha}^\star$ into the Lagrangian function, we can obtain the dual problem. To make mathematical presentation favorable, we re-arrange the dual variables into only one vector, and

then re-write the above equation in a more convenient form as follows

$$\boldsymbol{\alpha}^{\star} = \frac{1}{2R}\left(\mathbf{f} + \mathbf{B}\mathbf{d}\right), \tag{5.22}$$

in which $\mathbf{B} = [-\mathbf{1}_{NG} \quad -\mathbf{I}_{NG} \quad \mathbf{I}_{NG}]$ and $\mathbf{d} = \left[\mu^{s2} \quad (\boldsymbol{\delta}_1^{s2})^T \quad (\boldsymbol{\delta}_2^{s2})^T\right]^T$. Next, we plug $\boldsymbol{\alpha}^{\star}$ back into the Lagrangian function given in (5.20). After some manipulations, we have

$$\mathscr{L}^{s2}\left(\boldsymbol{\alpha}^{\star}, \mu^{s2}, \boldsymbol{\delta}_1^{s2}, \boldsymbol{\delta}_2^{s2}\right) = \mathbf{s}^T\mathbf{d} - \frac{1}{4R}\left(\mathbf{f} + \mathbf{B}\mathbf{d}\right)^T\left(\mathbf{f} + \mathbf{B}\mathbf{d}\right), \tag{5.23}$$

where $\mathbf{s} = \left[-\left(\sum_{g=1}^{G}\sum_{n=1}^{N_g} q_n^g\right) \quad -\mathbf{1}_{NG}^T \quad \mathbf{0}_{NG}^T\right]^T$. Accordingly, the dual problem can be formulated as

$$\min_{\mathbf{d}} \quad \mathbf{s}^T\mathbf{d} - \frac{1}{4R}\left(\mathbf{f} + \mathbf{B}\mathbf{d}\right)^T\left(\mathbf{f} + \mathbf{B}\mathbf{d}\right) \tag{5.24a}$$

$$\text{s.t.} \quad \mathbf{d} \succeq 0. \tag{5.24b}$$

Since problem $\text{OP}_{2-1}$ is quadratic convex and all constraints are convex, there never exists a duality gap Boyd, S. & Vandenberghe, L. (2004).

In order to transform (5.24) into a more tractable form, we let $\hat{\mathbf{B}} = \mathbf{B}^T\mathbf{B}/R$ and $\hat{\mathbf{f}} = \mathbf{s} - \mathbf{B}^T\mathbf{f}/R$. On this basis, the above problem can be represented in the well-known form as

$$\min_{\mathbf{d}} \quad \frac{1}{4}\mathbf{d}^T\hat{\mathbf{B}}\mathbf{d} - \hat{\mathbf{f}}^T\mathbf{d} \tag{5.25a}$$

$$\text{s.t.} \quad \mathbf{d} \succeq \mathbf{0}. \tag{5.25b}$$

Indeed, problem (5.25) is derived in a convex formulation. However, due to nonnegativity constraint (5.25b), there might not exist analytical solutions of optimal $\mathbf{d}^{\star}$. Hence, an iterative algorithm would be needed. Conventionally, gradient iteration algorithm is applied to update the Lagrangian multipliers. However, the work of Sha, F., Lin, Y., Saul, L. K. & Lee, D. D. (2007) has proven that multiplicative updates can enhance the value of the problem objective

at each iteration and hence monotonically converge to the optimal solution. This motivates us to construct an algorithm in terms of multiplicative updates to tackle the problem (5.25). Then, we define $\hat{\mathbf{B}}^{\bullet}$ and $\hat{\mathbf{B}}^{\circ}$ as follows

$$\hat{B}_{ij}^{\bullet} = \begin{cases} \hat{B}_{ij} & \text{if} \quad \hat{B}_{ij} \geq 0, \\ 0 & \text{if} \quad \text{otherwise}, \end{cases} \tag{5.26}$$

$$\hat{B}_{ij}^{\circ} = \begin{cases} |\hat{B}_{ij}| & \text{if} \quad \hat{B}_{ij} \leq 0, \\ 0 & \text{if} \quad \text{otherwise}, \end{cases} \tag{5.27}$$

On this basis, the iterations of multiplicative updates can be shown as

$$d_i \leftarrow d_i \left( \frac{\hat{f}_i + \sqrt{\hat{f}_i^2 + (\hat{\mathbf{B}}^{\bullet}\mathbf{d})_i (\hat{\mathbf{B}}^{\circ}\mathbf{d})_i}}{(\hat{\mathbf{B}}^{\bullet}\mathbf{d})_i} \right), \quad \forall i. \tag{5.28}$$

The convergence of the iterative algorithm is ensured Sha *et al.* (2007). Through achieving optimal solution $\mathbf{d}^{\star}$, the optimal values of Lagrangian multipliers, i.e. $\mu^{\star s2}, \boldsymbol{\delta}_1^{\star s2}, \boldsymbol{\delta}_2^{\star s2}$, can be conveniently found. As a result, optimal value $\boldsymbol{\alpha}^{\star}$ is determined.

### 5.4.2 Solving Second-Level Problem $\mathrm{SL}_1$

In fact, the beamforming vector can be decomposed into two components which are the beam power and the beam direction. In the mathematical presentation, this can be shown as

$$\mathbf{w}_n^g = \sqrt{p_n^g}\boldsymbol{v}_n^g, \quad \forall g, n, \tag{5.29}$$

where $\left\|\boldsymbol{v}_n^g\right\|^2 = 1$. Without loss of generality, we can eleminate parameter $p_n^g$ at both the numerator and denominator of the average SLR given in (5.16). Accordingly, problem $\mathrm{SL}_1$ can

be equivalently reformulated as below

$$\mathrm{SL}_1 : \left\{ \max_{\boldsymbol{v}_n^g} \quad \overline{\mathrm{SLR}}_n^g \right\}, \quad \forall n, g \tag{5.30a}$$

$$\text{s.t.:} \|\boldsymbol{v}_n^g\|^2 = 1, \quad \forall g, n, \tag{5.30b}$$

where

$$\overline{\mathrm{SLR}}_n^g = \tag{5.31}$$

$$\frac{(\boldsymbol{v}_n^g)^H \mathbb{E}\left[\mathbf{h}_n^g (\mathbf{h}_n^g)^H\right] \boldsymbol{v}_n^g}{(\boldsymbol{v}_n^g)^H \mathbb{E}\left[\sum\limits_{\substack{n'=1 \\ (n' \neq n)}}^{N} \mathbf{h}_{n'}^g (\mathbf{h}_{n'}^g)^H + \sum\limits_{\substack{g'=1 \\ (g' \neq g)}}^{G} \sum_{n=1}^{N} \mathbf{h}_n^{g'} (\mathbf{h}_n^{g'})^H\right] \boldsymbol{v}_n^g}. \tag{5.32}$$

To gain insight into problem $\mathrm{SL}_1$, we analyze the average channel gains on calibration errors, shown as follows

$$\mathbb{E}\left[\mathbf{h}_n^g (\mathbf{h}_n^g)^H\right] = \mathbb{E}\left[(\mathbf{I}_M + \mathbf{C}_n^g)\mathbf{u}_n^g ((\mathbf{I}_M + \mathbf{C}_n^g)\mathbf{u}_n^g)^H\right], \tag{5.33a}$$

$$= \hat{\mathbf{U}}_n^g + \hat{\mathbf{U}}_n^g \bar{\mathbf{C}}_n^g, \tag{5.33b}$$

$$= \mathbf{A}_n^g, \tag{5.33c}$$

where $\hat{\mathbf{U}}_n^g \in \mathbb{C}^{M \times M} = \mathbf{u}_n^g (\mathbf{u}_n^g)^H$, and $\bar{\mathbf{C}}_n^g \in \mathbb{R}^{M \times M} = \mathbb{E}\left[\mathbf{C}_n^g (\mathbf{C}_n^g)^H\right] = \mathrm{diag}\left\{\sigma_{cal}^2, \sigma_{cal}^2, ..., \sigma_{cal}^2\right\}$.

In light of the above result, the average SLR can be re-written as

$$\overline{\mathrm{SLR}}_n^g = \frac{(\boldsymbol{v}_n^g)^H \mathbf{A}_n^g \boldsymbol{v}_n^g}{(\boldsymbol{v}_n^g)^H \left(\sum\limits_{\substack{n'=1 \\ (n' \neq n)}}^{N} \mathbf{A}_{n'}^g + \sum\limits_{\substack{g'=1 \\ (g' \neq g)}}^{G} \sum_{n=1}^{N} \mathbf{A}_n^{g'}\right) \boldsymbol{v}_n^g}. \tag{5.34}$$

Relying on the Rayleight-Ritz quotient Parlett, B. N. (1998), the optimal values of $\{\boldsymbol{v}_n^g\}$ to maximize the average SLR can be given by

$$\boldsymbol{v}_n^{\star g} = \boldsymbol{\Phi}_n^g, \tag{5.35}$$

where $\boldsymbol{\Phi}_n^g$ can be obtained by computing the orthonormal eigenvector corresponding to the largest eigenvalue of the matrix pair $\left( \mathbf{A}_n^g, \sum\limits_{\substack{n'=1 \\ (n'\neq n)}}^{N} \mathbf{A}_{n'}^g + \sum\limits_{\substack{g'=1 \\ (g'\neq g)}}^{G} \sum\limits_{n=1}^{N} \mathbf{A}_n^{g'} \right)$.

### 5.4.3 Analysis of non-linear EH and ID performances on Non-Ideal Channel Reciprocity

In this subsection, we present the closed-form expressions of the coverage probability of EH, and the average SINR under the calibration errors.

First, we analyze constraint (7.9d). In light of previous work Xiong *et al.* (2017) and (5.10), (6.14) and (5.12), the formulation regarding the non-linear EH model can be dealt with as follows

$$\mathscr{P}r\left(\mathrm{E}_n^g \geq \theta_n^g\right) = \mathscr{P}r\left( \sum_{g'=1}^{G} \sum_{n'=1}^{N_g} \left| (\mathbf{h}_n^g)^T \mathbf{w}_{n'}^{g'} \right|^2 \geq \frac{\hat{\theta}_n^g}{(1-\rho_n^g)} \right), \tag{5.36}$$

where

$$\hat{\theta}_n^g = \mathtt{b} - \frac{1}{\mathtt{a}} \ln\left( \frac{e^{\mathtt{ab}}(\mathrm{M}^{EH} - \theta_n^g)}{e^{\mathtt{ab}}\theta_n^g + \mathrm{M}^{EH}} \right). \tag{5.37}$$

According to (5.29) and (5.36), constraint (7.9d) can be represented by

$$\mathscr{P}r\left( - \sum_{g'=1}^{G} \sum_{n'=1}^{N_g} p_{n'}^{g'} \left| (\boldsymbol{v}_{n'}^{g'})^T \mathbf{h}_n^g \right|^2 \geq \frac{\hat{\theta}_n^g}{(\rho_n^g - 1)} \right) \leq 1 - \alpha_n^{\star g}. \tag{5.38}$$

It is worth reminding that $\alpha_n^{\star g}$ is the optimal value of $\alpha_n^g$ derived in subsection IV.A.

Indeed, the distribution of $\mathbf{h}_n^g$ under the calibration errors is $\mathscr{CN}(\mathbf{u}_n^g, \sigma_{cal}^2 \hat{\mathbf{U}}_n^g)$, where $\hat{\mathbf{U}}_n^g = \text{diag}\{|\mathbf{u}_n^g[1]|^2, ..., |\mathbf{u}_n^g[M]|^2\}$. This leads to the fact that it is difficult to obtain the exact closed-form expression of (5.38). Additionally, the expression should be derived in a favorable formulation to the concept of the convex optimization. Therefore, this motivates us to provide an approximation of (5.38) through *Lemma* 1.

**Lemma 1.** The closed-form approximate derivation of constraint (7.9d) can be given by

$$\begin{aligned}
&\boldsymbol{\varphi}_n^g(\{p_n^g\}, \rho_n^g) \\
&= \sum_{g'=1}^{G} \sum_{n'=1}^{N_g} \sqrt{\left(1/(1-\alpha_n^{\star g}) - 1\right) \text{var}\left[|(\boldsymbol{\nu}_{n'}^{g'})^T \mathbf{h}_n^g|^2\right]}\, p_{n'}^{g'} \\
&- \sum_{g'=1}^{G} \sum_{n'=1}^{N_g} \mathbb{E}\left[\left|(\boldsymbol{\nu}_{n'}^{g'})^T \mathbf{h}_n^g\right|^2\right] p_{n'}^{g'} - \frac{\hat{\theta}_n^g}{(\rho_n^g - 1)} \leq 0.
\end{aligned} \tag{5.39}$$

Proof: See Appendix III.1.

It can be observed that the above constraint is convex over variables $\{p_n^g\}$ and $\rho_n^g$ since the term $-\frac{\hat{\theta}_n^g}{(\rho_n^g - 1)}$ is convex (i.e. the second-order condition Boyd & Vandenberghe (2004)). Further, it is clear that such a closed-form derivation is a function of the expectation and variance of $|(\boldsymbol{\nu}_{n'}^{g'})^T \mathbf{h}_n^g|^2$ for which the closed-form expressions are provided in *Lemma* 2.

**Lemma 2.** The closed-form expressions of the expectation and variance of $\left|(\boldsymbol{\nu}_{n'}^{g'})^T \mathbf{h}_n^g\right|^2$ can be derived respectively as follows

$$\mu_{n'n}^{g'g} = \mathbb{E}\left[\left|(\boldsymbol{\nu}_{n'}^{g'})^T \mathbf{h}_n^g\right|^2\right] = \text{tr}\left(\mathbf{V}_{n'}^{g'} \hat{\mathbf{U}}_n^g \sigma_{cal}^2\right) + (\mathbf{u}_n^g)^H \mathbf{V}_{n'}^{g'} \mathbf{u}_n^g, \tag{5.40}$$

$$\upsilon_{n'n}^{g'g} = \text{var}\left[\left|(\boldsymbol{\nu}_{n'}^{g'})^T \mathbf{h}_n^g\right|^2\right] = \text{tr}\left(\mathbf{V}_{n'}^{g'} \hat{\mathbf{U}}_n^g \sigma_{cal}^2\right)^2 + 2\sigma_{cal}^2 (\mathbf{u}_n^g)^H \mathbf{V}_{n'}^{g'} \hat{\mathbf{U}} \mathbf{V}_{n'}^{g'} \mathbf{u}_n^g. \tag{5.41}$$

Proof: See Appendix III.2.

Second, we take constraint (7.9g) into account. On the basis of (5.7), the average SINR can be computed by *Lemma* 3 as follows

**Lemma 3.** According to (5.7), the closed-form derivation of the approximate average SINR can be given by

$$\mathbb{E}\left[\mathtt{SINR}_n^g\right] \triangleq \frac{\rho_n^g \mu_{nn}^{gg} p_n^g}{\rho_n^g \left(\bar{\mathscr{I}}_n^g + \sigma_0^2\right) + \sigma_1^2}. \tag{5.42}$$

where $\bar{\mathscr{I}}_n^g = \sum\limits_{\substack{n'=1 \\ (n'\neq n)}}^{N_g} \mu_{n'n}^{gg} p_{n'}^g + \sum\limits_{\substack{g'=1 \\ (g'\neq g)}}^{G} \sum\limits_{n'=1}^{N_g} \mu_{n'n}^{g'g} p_{n'}^{g'}$.

Proof: By substituting (5.40) into (5.7), we obtain (5.42) as in *Lemma* 3.

### 5.4.4 Optimal and Sub-optimal Solutions for the Problem $\mathrm{OP}_1$

Since problem $\mathrm{SL}_1$ has been relaxed, and the closed-form derivations regarding the EH and SINR metrics have been provided; problem $\mathrm{OP}_1$ given by (5.18) can be reformulated as

$$\begin{aligned}
\min_{\{p_n^g, \rho_n^g\}} \quad & \sum_{g=1}^{G} \sum_{n=1}^{N_g} p_n^g, \\
\text{s.t.:} \quad & \{\mathbf{w}_n^g\} \in \mathscr{F}, \quad \mathscr{F} \triangleq \left\{ \mathbf{w}_n^g | \mathbf{w}_n^g = \sqrt{p_n^g} \boldsymbol{\nu}_n^{\star g}, (\forall g, n) \right\}, \\
& \sum_{\substack{n'=1 \\ (n'\neq n)}}^{N_g} \mu_{n'n}^{gg} p_{n'}^g + \sum_{\substack{g'=1 \\ (g'\neq g)}}^{G} \sum_{n'=1}^{N_g} \mu_{n'n}^{g'g} p_{n'}^{g'} + \frac{1}{\gamma_n^g} \mu_{nn}^{gg} p_n^g \\
& = \sigma_0^2 + \frac{\sigma_1^2}{\rho_n^g}, \quad \forall g, n, \\
& \boldsymbol{\varphi}_n^g(\{p_n^g\}, \rho_n^g) \leq 0, \quad \forall g, n, \\
& 0 < \rho_n^g < 1, \quad \forall g, n, \\
& p_n^g \geq 0, \quad \forall g, n.
\end{aligned} \tag{5.43}$$

It can be observed that problem (5.43) is not convex due to the equality symbol in the second constraint. However, given the problem, the second constraint can be relaxed by replacing the

equality symbol by an inequality one (i.e. $\geq$). Hence, the resulting problem becomes convex and easy to solve Grant & Boyd (2009).

In practice, since the CSI changes with time, the BS needs to update the CSI and then resolve the problem to maintain the system performance. However, this task might bring a heavily computational burden. Therefore, a sub-optimal solution that can be achieved with a much reduced complexity plays an important role. In the following, we present a method resulting in a closed-form sub-optimal solution.

First, we simplify problem (5.43) by setting $\rho_n^g = \rho \ (\forall g,n)$. This implies that all users employ the same power-splitting factor. In fact, this system configuration has been adopted for multi-user SWIPT networks Ng *et al.* (2014). Thus, the resulting problem of (5.43) can be given by

$$
\begin{aligned}
\min_{\{p_n^g\},\rho} \quad & \sum_{g=1}^{G}\sum_{n=1}^{N_g} p_n^g, \\
\text{s.t.:} \quad & \{\mathbf{w}_n^g\} \in \mathscr{F}, \quad \mathscr{F} \triangleq \left\{ \mathbf{w}_n^g | \mathbf{w}_n^g = \sqrt{p_n^g}\boldsymbol{\nu}_n^{\star g}, (\forall g,n) \right\}, \\
& \sum_{\substack{n'=1 \\ (n'\neq n)}}^{N_g} \mu_{n'n}^{gg} p_{n'}^g + \sum_{\substack{g'=1 \\ (g'\neq g)}}^{G}\sum_{n'=1}^{N_g} \mu_{n'n}^{g'g} p_{n'}^{g'} + \frac{1}{\gamma_n^g}\mu_{nn}^{gg} p_n^g \\
& = \sigma_0^2 + \frac{\sigma_1^2}{\rho}, \quad \forall g,n, \\
& \boldsymbol{\varphi}_n^g(\{p_n^g\},\rho) \leq 0, \quad \forall g,n, \\
& 0 < \rho < 1, \quad \forall g,n, \\
& p_n^g \geq 0, \quad \forall g,n.
\end{aligned} \tag{5.44}
$$

Second, we propose a method to facilitate the speed of solving problem (5.44). Obviously, the more the variables and constraints are, the longer is the computation time required for finding solutions is. Thus, a novel transformation for problem (5.44) in which only one variable of $\rho$ exists is proposed.

Our idea can be explained by eliminating the variable of $\mathbf{p}$ ($\mathbf{p} = [p_1^1 ... p_N^G]^T$) as follows. We start with considering the second constraint of problem (5.44). By representing this constraint in terms of a matrix formulation [Bengtsson & Ottersten (2001), 18.4], [Chandrasekhar *et al.* (2009), eq. (2)], [Tran, H.-V., Kaddoum, G., Tran, H. & Hong, E.-K. (2017), eq. (26)] , the value of $\mathbf{p}$ should satisfy

$$\mathbf{p} = (\mathbf{I} - \mathbf{L}\boldsymbol{\Upsilon})^{-1}\boldsymbol{\Delta}(\sigma_0^2 + \sigma_1^2\bar{\boldsymbol{\rho}}), \tag{5.45}$$

where

$$\mathbf{L} \in \mathbb{C}^{NG\times NG} = \text{diag}\{\gamma_1^1, \ldots, \gamma_N^1, \ldots, \gamma_1^G, \ldots, \gamma_N^G\}. \tag{5.46}$$

Moreover, $\boldsymbol{\Upsilon} \in \mathbb{C}^{NG\times NG}$ is a zero-diagonal matrix with

$$(\boldsymbol{\Upsilon})_{(k-1)G+m,(g-1)G+n} = \frac{\Xi_{m,n}^{k,g}}{\Xi_{m,m}^{k,g}}, \tag{5.47}$$

where

$$\Xi_{m,n}^{k,g} = \text{tr}\left(\boldsymbol{\nu}_m^k(\boldsymbol{\nu}_m^k)^H\mathbf{U}_n^g(\sigma_{cab}^2 + 1)\right). \tag{5.48}$$

In addition, $\boldsymbol{\Delta}$ is a diagonal matrix, in which

$$\boldsymbol{\Delta} = \text{diag}\left\{\frac{1}{\Xi_{1,1}^{1,1}}, \ldots, \frac{1}{\Xi_{m,m}^{g,g}}, \ldots, \frac{1}{\Xi_{M,M}^{G,G}}\right\}\mathbf{L}. \tag{5.49}$$

Also,

$$\bar{\boldsymbol{\rho}} = \frac{\mathbf{1}_{NG}}{\rho}. \tag{5.50}$$

For convenience, we re-express (5.45) in terms of vector components as

$$p_n^g = \Lambda_{g,n}(1/\rho), \quad \forall g,n, \tag{5.51}$$

where function $\Lambda_{g,n}(1/\rho)$ can be obtained by the $((g-1)G+n)^{\text{th}}$ row of the matrix $(\mathbf{I}-\mathbf{L}\boldsymbol{\Upsilon})^{-1}\boldsymbol{\Delta}(\sigma_0^2+\sigma_1^2\bar{\boldsymbol{\rho}})$.

Moreover, since $0<\rho<1$, the constraint $p_n^g \geq 0 \quad (\forall g,n)$ can be replaced by $(\mathbf{I}-\mathbf{L}\boldsymbol{\Upsilon})^{-1} \succeq 0$ Bambos, N., Chen, S. C. & Pottie, G. J. (2000). Now, we subsitute (5.51) into the problem (5.44) and then obtain the new formulation as

$$\min_{\rho} \quad \sum_{g=1}^{G}\sum_{n=1}^{N_g} \Lambda_{g,n}(1/\rho), \tag{5.52a}$$

$$\text{s.t.:} \quad \boldsymbol{\varphi}_n^g(\{\Lambda_{g,n}(1/\rho)\}, 1/\rho) \leq 0, \tag{5.52b}$$

$$0<\rho<1, \tag{5.52c}$$

$$(\mathbf{I}-\mathbf{L}\boldsymbol{\Upsilon})^{-1} \succeq 0. \tag{5.52d}$$

Furthermore, to reduce computational burden, we aim at solving the above problem using closed-form solution through *Lemma 4* as follows.

**Lemma 4.** Without loss of generality, constraint (5.52b) can be transformed into a convex form as follows

$$(\boldsymbol{\mu}_n^g - \boldsymbol{\upsilon}_n^g)^T \mathbf{a}\sigma_0^2\rho^2 - \kappa_n^g\rho - (\boldsymbol{\mu}_n^g - \boldsymbol{\upsilon}_n^g)^T \mathbf{a}\sigma_1^2 \leq 0, \tag{5.53}$$

in which,

$$\mathbf{a} = (\mathbf{I} - \mathbf{L}\boldsymbol{\Upsilon})^{-1}\boldsymbol{\Delta}\mathbf{1}_{NG}, \tag{5.54a}$$

$$\boldsymbol{\mu}_n^g = [\mu_{1n}^{1g} ... \mu_{Nn}^{Gg}]^T, \tag{5.54b}$$

$$\bar{\alpha}_n^g = (1/(1-\alpha_n^{\star g}) - 1), \tag{5.54c}$$

$$\boldsymbol{\upsilon}_n^g = [\sqrt{\bar{\alpha}_n^g \upsilon_{1n}^{1g}} ... \sqrt{\bar{\alpha}_n^g \upsilon_{Nn}^{Gg}}]^T, \tag{5.54d}$$

$$\kappa_n^g = (\boldsymbol{\mu}_n^g - \boldsymbol{\upsilon}_n^g)^T \mathbf{a}(\sigma_0^2 - \sigma_1^2) - \hat{\theta}_n^g. \tag{5.54e}$$

By replacing (5.52b) by (5.53), problem (5.52) is convex. Thus, the closed-form solution of problem (5.52) can be given by

$$\rho^\star = \min_{\substack{1\le n\le N \\ 1\le g\le G}} \left\{ \frac{\kappa_n^g + \sqrt{(\kappa_n^g)^2 + 4((\boldsymbol{\mu}_n^g - \boldsymbol{\upsilon}_n^g)^T \mathbf{a})^2 \sigma_0^2 \sigma_1^2}}{2(\boldsymbol{\mu}_n^g - \boldsymbol{\upsilon}_n^g)^T \mathbf{a} \sigma_0^2} \right\}, \tag{5.55}$$

Proof: See Appendix III.3.

Based on the proof of *Lemma* 4 in Appendix C, the feasibility of problem (5.52) can be checked through two conditions as below. The problem is feasible if and only if

$$(\mathbf{I} - \mathbf{L}\boldsymbol{\Upsilon})^{-1} \succeq 0, \tag{5.56}$$

and

$$\boldsymbol{\mu}_n^g \ge \boldsymbol{\upsilon}_n^g. \tag{5.57}$$

In practice, since the variance of calibration errors is much smaller than 1, i.e. $\sigma_{cal}^2 \ll 1$, condition (6.7) could be neglected for simplicity.

In summary, the principle of our method relies on exploiting the problem structure of (5.44) to reduce the number of variables. Specifically, the equality constraint is utilized to eliminate

variable $\mathbf{p}$ without loss of generality. Since $\mathbf{p}$ can be calculated as a function of $\rho$, i.e. $\mathbf{\Lambda}(\rho)$, the objective function and the constraints are transformed in terms of $\rho$ and $\mathbf{\Lambda}(\rho)$. In this concern, the equality constraint causing some difficulties due to its nonconvexity is also eliminated. As aforementioned, problem (5.52) is convex over $\rho$, thus the optimal value of $\rho$ can be conveniently obtained.

## 5.5 Numerical Results

In this section, the performance of the proposed resource allocation strategy is analyzed. Without loss of generality, we assume that there exist 6 users classified into 3 groups. Specifically, group 1 includes three users (i.e. users 1, 2, and 3) located 1.5 meters far away from the BS. Group 2 consists of two users (i.e. users 4, and 5) located 3.5 meters far away from the BS. Also, group 3 contains one user whose distance to the BS is 5.5 meters (i.e. user 6). The users are randomly located in the defined ranges. Channels are assumed to have Rician distribution in which Rician factor is set to 2 dB and pathloss exponent factor is set to 2.6, i.e. in offices with soft partition Rappaport, T. & Sandhu, S. (1994). Regarding the nonlinear EH model, we set $\mathtt{M}^{EH} = 24$ mW, $\mathtt{a} = 150$ and $\mathtt{b} = 0.014$ Boshkovska *et al.* (2017); Jiang *et al.* (2017). For convenience, we set the SINR thresholds as $\gamma_n^g = \gamma$, the EH thresholds as $\theta_n^g = \theta$, and the variance of calibration error as $\sigma_{cal}^2 = 0.01$. Other parameters are listed in Table I. The simulation is carried out using 1000 channel realizations. In each iteration, results are averaged on 100000 random calibration errors.

Table 5.1 Important parameters

| **Parameters** | **System values** |
|---|---|
| Number of antennas at the BS, $M$ | 6 |
| AWGN, $\sigma_0^2$ | $10^{(-12)}$ W |
| AWGN, $\sigma_1^2$ | $10^{(-8)}$ W |
| The existing plan of EH, $[q_1^1 q_2^1 q_3^1 q_1^2 q_2^2 q_1^3]$ | [0.9 0.9 0.9 0.8 0.8 0.7] |
| Group priorities, $[b_1^1 b_2^1 b_3^1 b_1^2 b_2^2 b_1^3]$ | [0.1 0.1 0.1 0.2 0.2 0.3] |

### 5.5.1 Designing the serving plan at the upper layer

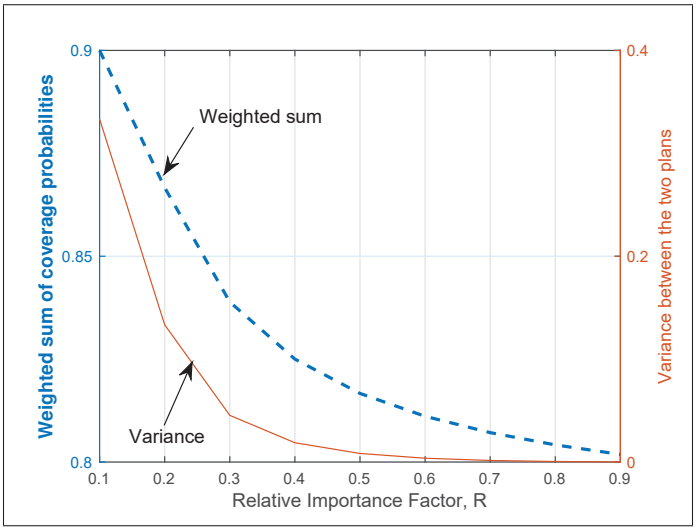


Figure 5.4 The trade-off between the two objectives

In this work, one of the main goals is to maximize the weighted sum of the coverage probability of EH. This can be achieved by designing a new serving plan through the upper-level optimization problem $OP_2$. Thus, by using the method mentioned in subsection IV.A to solve $OP_2$, the trade-off between the two objectives is analysed and shown in Fig. 5.4. As observed, increasing the factor $R$ represents that minimizing the variance between the two plans is being preferred over maximizing the weighted sum of the coverage probabilities, i.e. the higher $R$, the lower the weighted sum of the probabilities and the lower the variance. Based on this result, the network operator can select an appropriate value of $R$ for system setting according to specific network situations.

Additionally, in Fig. 5.5, the varying trend for the coverage probabilities at each user in the new plan, i.e. $\{\alpha_n^g\}$, is illustrated with respect to $R$. When $R$ is close to 1, the values of $\{\alpha_n^g\}$ are close to $\{q_n^g\}$, the original plan. When $R$ tends to 0, this means the trend for maximizing the weighted sum of $\{\alpha_n^g\}$ becomes more important. Thus, the user with a higher priority is allocated with a higher coverage probability in the new plan. This implies that distant users may have more chances to harvest sufficient energy than nearer ones.

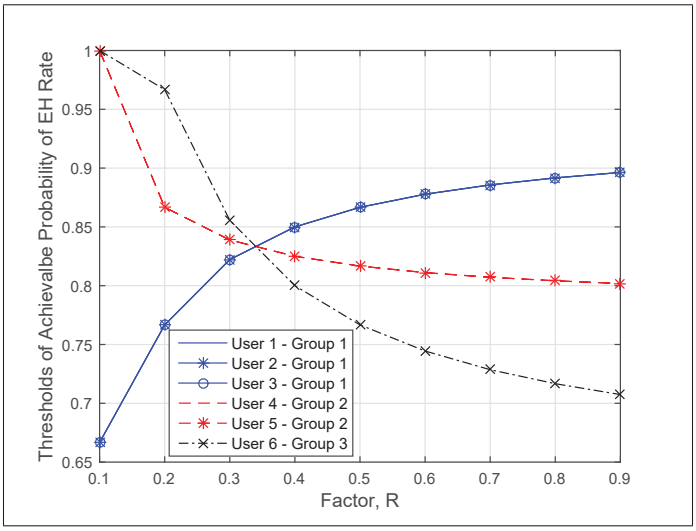


Figure 5.5 Variation of the coverage probability of EH at each user

### 5.5.2 Performance of the proposed resource allocation scheme

In this section, by setting $R = 0.3$, we obtain the new plan as $[\alpha_1^{\star 1}\alpha_2^{\star 1}\alpha_3^{\star 1}\alpha_1^{\star 2}\alpha_2^{\star 2}\alpha_1^{\star 3}] = [0.8 \quad 0.8 \quad 0.8 \quad 0.85 \quad 0.85 \quad 0.9]$.

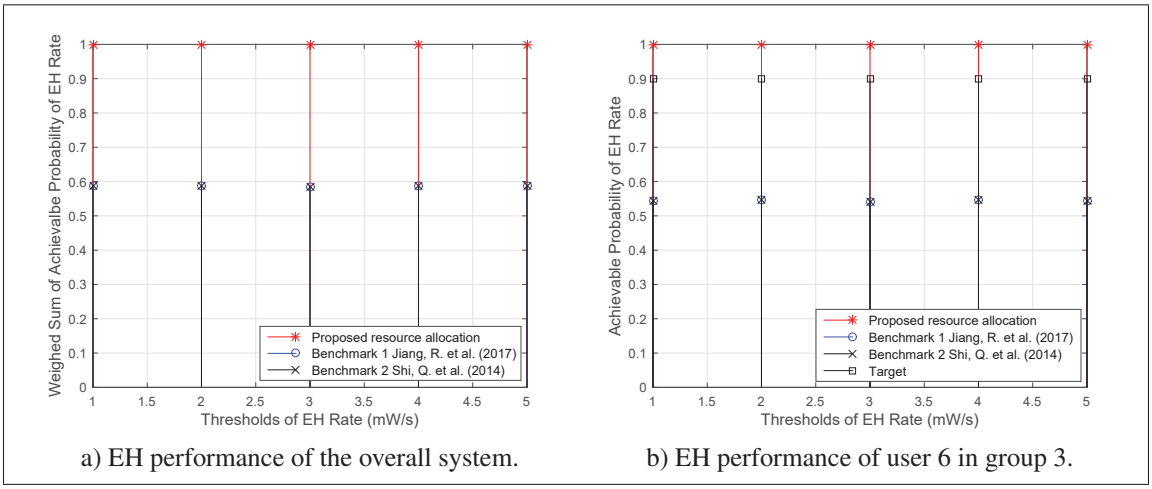


a) EH performance of the overall system. b) EH performance of user 6 in group 3.

Figure 5.6 EH performance enhancement ($\gamma = 2$ dB)

Accordingly, Figs. 8.1a-8.1b show the performance enhancement by a comparison between the proposed resource allocation scheme and the benchmarks Jiang *et al.* (2017); Shi *et al.* (2014).

In this simulation, it is worth noting that, for a fair comparison, the scheme in benchmark Shi *et al.* (2014) considering a linear EH model is adopted to the nonlinear EH model. It can be seen that the two benchmarks achieve the same performance since they consider similar optimization problem and instantaneous EH and SINR constraints. As observed, the weighted sum of the probability can achieve approximately 1 and 0.6 in the cases of the proposed approach and the benchmarks, respectively. This represents a significant overall improvement of the EH performance for the considered overall system. Furthermore, in the following, we investigate the EH performance achieved at user 6, as shown in Fig. 8.1b. Given this concern, our resource allocation scheme can guarantee the coverage probability of EH rate above the preset target. On the other hand, in the case of the benchmarks, the probability performance at user 6 is 0.54 because the user is far from the BS. It is worth noting that the trend for the probabilities keeps constant over various EH rates. This is because the values of the probabilities mainly depend on the variance of calibration error, i.e. $\sigma_{cal}^2$, which is unchanged in this simulation. The result with different value of $\sigma_{cal}^2$ is shown in Fig. 5.7.

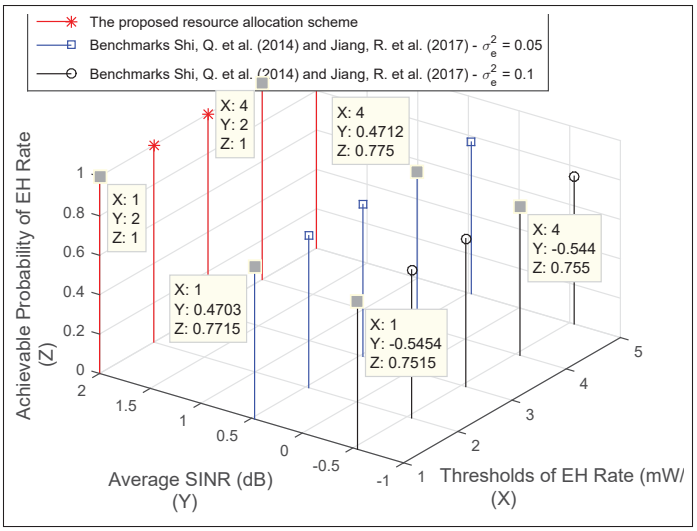


Figure 5.7 The performance of EH and SINR at user 1 ($\gamma = 2$ dB)

In the continuity, the effectiveness of our scheme on combating the non-channel reciprocity property is shown in Fig. 5.7. On one hand, the average SINR on the calibration error can be

ensured to reach SINR threshold $\gamma$ by applying the proposed resource allocation. This can be explained by the fact that the second level problem $\mathrm{SL}_1$ produces robust beamformers to deal with the non-channel reciprocity property efficiently. On the other hand, the SINR performance does not meet the requirement by employing the benchmarks. The more the SINR is reduced when the more the calibration error is considered. Based on Figs. 8.1a, 8.1b and 5.7, it can be concluded that not only the user fairness but the effect of the non-ideal channel reciprocity can also be properly managed.

Fig. 5.8 provides a comparison in terms of the transmit power between the proposed resource allocation scheme, the existing benchmarks and a baseline. To highlight the effect of nonlinear and linear EH models, we show the transmit power for the proposed scheme and the benchmarks Jiang *et al.* (2017); Shi *et al.* (2014). Note that the energy conversion effciency is set to 0.5 when considering the linear EH model. Here, we can evaluate the mismatch between the linear EH model and the practical nonlinear EH model. In particular, it is observed that the proposed scheme sacrifices 2.7 dB more than the benchmarks in both of the models to maintain the required ID and EH performances. Further, a comparison with a baseline that consists of the well-known zero-forcing beamformer is shown. A gap of approximately 2.9 dB between the baseline and the proposed resource allocation scheme exists. This is because the interference caused by the SLR beamformer can be useful for EH performance. So, the proposed scheme requires less transmit power to achieve the same targeted system performance than the baseline does.

Additionally, the closed-form approximate expressions of the average SINR and the coverage probability of EH, shown in *Lemmas* 1 and 3, play an important role in the performance of the proposed scheme. In Fig. 5.9, the tightness of the approximations is verified. It is evaluated that there exists a gap of approximately 1.9 dB regarding the transmit power. Since the exact closed-form expressions are not available, using the derived approximation can be an efficient choice.

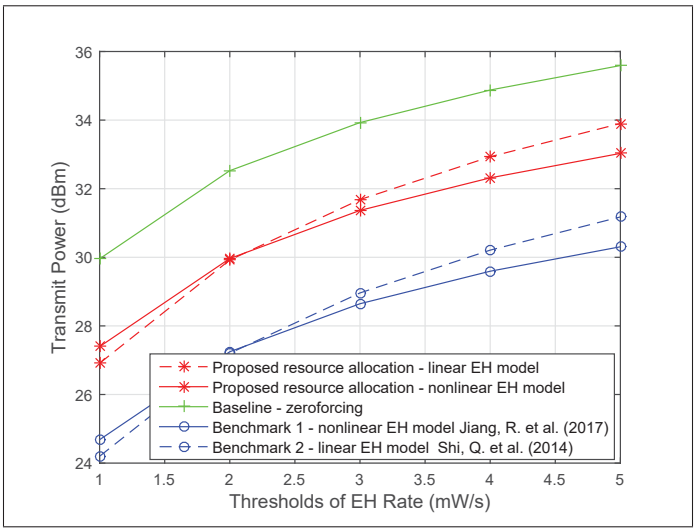


Figure 5.8 A comparison between the proposed scheme and others

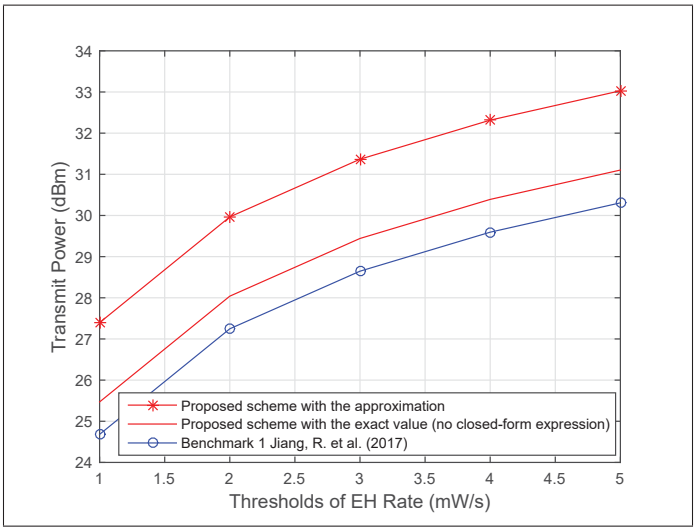


Figure 5.9 Performance with the approximations

### 5.5.3 Performance loss due to user mobility, and the suboptimal solution

This part of the simulation is to investigate performance loss due to the user mobility, and then highlight the role of the suboptimal solution. Assuming that users 1, 4, and 6 are moving, Fig. 5.10 depicts the system performance loss due to the user mobility in each group. In the

simulation and for the sake of convenience, we consider a mobility scenario in which each user moves to a new random location keeping its distance to the BS unchanged. In other words, the corresponding propagation loss and the assigned user group are unaffected. Particularly, since the actual CSI is unknown at the BS, this inspires us to simulate user mobility using a correlation model. In this concern, the difference between the actual CSI and the estimated one at the BS can be measured by correlation coefficients. Thus, the simulation can be carried out by generating CSI correlated with the estimated CSI. In fact, the motion of the users can lead the estimated CSI at the BS to be outdated promptly. The latter results in a non-trivial reduction of the SINR and EH performances. On this basis, Figs. 5.10 and 5.11 indicate the average SINR degrade with respect to the correlation where the smaller correlation implies the higher user mobility and yields the higher average SINR loss. Further, Figs. 5.10 and 5.11 illustrate a reduction of the achievable coverage probability of EH rate at each user. Especially, it seems that the EH performance at user 1 unchanged even when there is no correlation between the actual and estimated CSI. Besides, it can be observed that the shorter the distance between the users and the BS is, the worse the SINR performance is at each moving user. This is because nearer users are exposed by denser interferences compared to farther users.

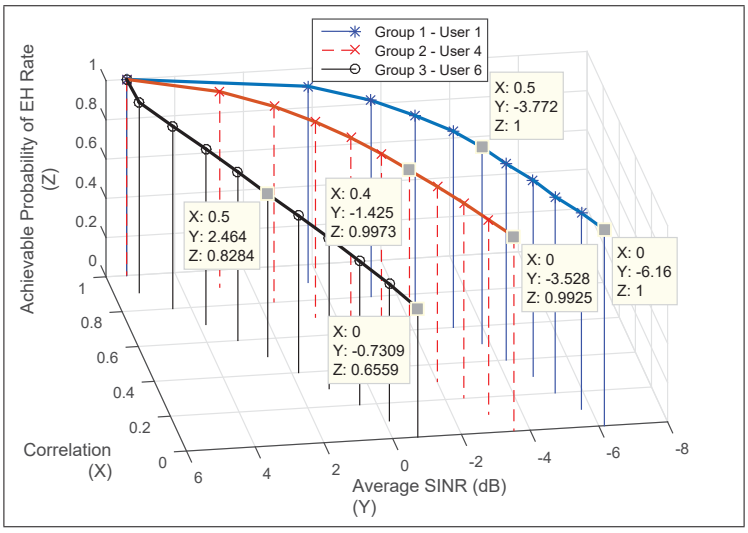


Figure 5.10 Performance loss of the average SINR and the EH

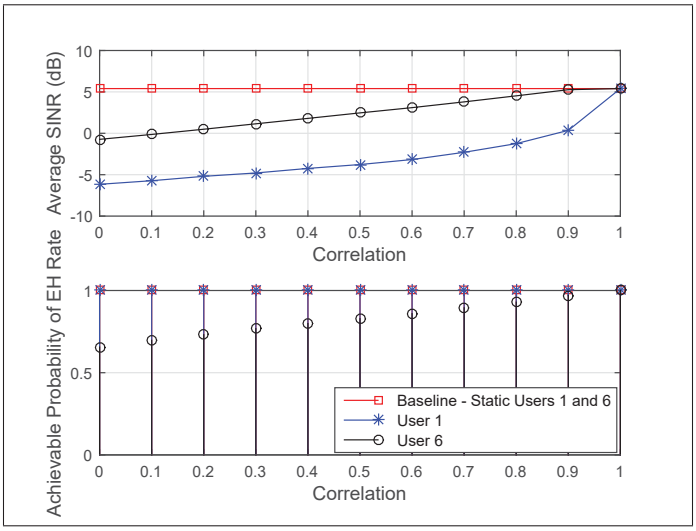


Figure 5.11 Performance loss at near and far users

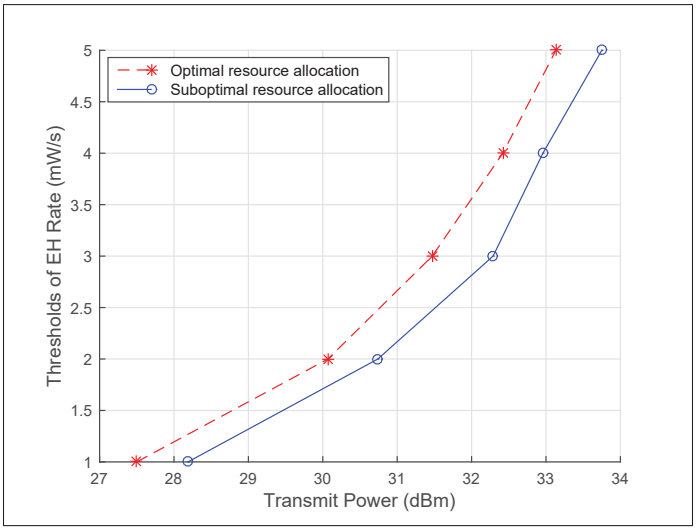


Figure 5.12 A comparison between the optimal and suboptimal solutions ($\gamma = 5$)

As shown in Fig. 5.10, the system performance decreases significantly due to the user mobility. When the users move, the BS should update the CSI and then re-compute the power vectors, the beamformers and the power-splitting factors. This task might bring a heavily computational burden to the BS, especially in the case where the user mobility is high. Thus, the proposed suboptimal solution for which its closed-form derivation provided in this work can be very well

considered as an efficient alternative approach. In this concern, Fig. 5.12 shows a performance comparison between the optimal and suboptimal solutions. On this basis, it can be evaluated that there exists a power gap of approximate 0.75 dBm between two approaches. Indeed, using the suboptimal approach implies sacrificing an additional amount of transmit power, however, this also significantly reduces computational burden.

## 5.6 Conclusion

In this paper, we propose a novel approach to allocate resources for the SWIPT system under a nonlinear EH model, in which multiple critical requirements, such as minimizing transmit power, maximizing the weighted sum of coverage probability of EH and minimizing the effect of calibration error on the ID performance, need to be concurrently managed. Such requirements are mathematically structured on the cross-layer multi-level formulation where the upper-layer and physical layer problems are devised. On this basis, we provide the algorithms and the closed-form solutions to tackle these problems. The obtained numerical results show that not only the user fairness but the effect of the non-ideal channel reciprocity can also be properly managed using the proposed resource allocation scheme. A comparison between the proposed scheme, the existing benchmarks, and the baseline has been provided to highlight the effectiveness of our work. Particularly, the results imply that when users are moving, farther users can obtain a better SINR performance than nearer users. This is because the nearer users are more susceptible to interferences. To this end, the suboptimal solution can be considered as an efficient alternative to maintain the system performance in the case of fast time-varying channels.

# CHAPTER 6

# ULTRA-SMALL CELL NETWORKS WITH COLLABORATIVE RF AND LIGHTWAVE POWER TRANSFER

Ha-Vu Tran[1], Georges Kaddoum[1], Panagiotis D. Diamantoulakis[2], Chadi Abou-Rjeily[3], and George K. Karagiannidis[2]

[1] Department of Electrical Engineering, École de Technologie Supérieure, 1100 Notre-Dame west, Montreal, Canada H3C 1K3.
[2]Department of Electrical and Computer Engineering, Aristotle University of Thessaloniki, Thessaloniki, Greece 541 24.
[3]Department of Electrical and Computer Engineering of the Lebanese American University, Beirut, Lebanon.

Paper published in *IEEE Transactions on Communications*, May 2019, early access.

## 6.1 Introduction

To cope with the exponentially growing demand for data traffic, the design of future cellular networks, i.e., the fifth generation (5G) networks, is tending to a new form, embracing a large-scale deployment of small cells Gupta & Jha (2015b); Hossain & Hasan (2015). In this context, a potential paradigm shift of 5G networks appeared, so-called optical attocell networks, developed on the platform of visible light communication (VLC), lifting the small cell concept to a new level of ultra-small cells Chen, C., Basnayaka, D. A. & Haas, H. (2016a); Chen, Z., Basnayaka, D. A. & Haas, H. (2017); Haas, H. (2017). In particular, the advantages of this optical network are related to the fact that the visible light spectrum is 1000-fold wider than the entire radio frequency (RF) spectrum. Moreover, artificial light sources, i.e., light emitting diode (LED) bulbs, can be densely deployed in indoor areas, such as houses, offices, etc., with a conveniently lower cost than their RF counterparts, i.e., WiFi access points Ayyash, M., Elgala, H., Khreishah, A., Jungnickel, V., Little, T., Shao, S., Rahaim, M., Schulz, D., Hilt, J. & Freund, R. (2016); Pathak, P. H., Feng, X., Hu, P. & Mohapatra, P. (2015).

Furthermore, while moving toward future networks, another main challenge is prolonging the network lifetime. More specifically, the lifetime of mobile devices is expected to be 10-fold

longer, while the overall network power consumption should not exceed 10 percent of the current usage Hossain & Hasan (2015); Niyato *et al.* (2017). To cope with these expectations, energy harvesting (EH), wireless power transfer (WPT), and simultaneous wireless information and power transfer (SWIPT) can be considered as primary solutions Clerckx *et al.* (2019); Hossain & Hasan (2015); Lu *et al.* (2015b); Niyato *et al.* (2017); Tran & Kaddoum (2018a). Particularly, SWIPT, when properly optimized, can result in significant gains in terms of spectral efficiency, time delay, energy consumption, and interference management, by superposing information and power transfer Krikidis *et al.* (2014b); Timotheou, S., Krikidis, I., Zheng, G. & Ottersten, B. (2014).

While RF WPT is a well explored technology, recently, along with the development of VLC Arnon, S. (2015); Kavehrad, M. (2010); Ma, H., Lampe, L. & Hranilovic, S. (2015); Mossaad, M. S. A., Hranilovic, S. & Lampe, L. (2015); Wang, Z., Tsonev, D., Videv, S. & Haas, H. (2015), optical WPT and EH from artificial light have gained increasing attention from the research community Basnayaka, D. A. & Haas, H. (2017); Carvalho, C. & Paulino, N. (2014); Diamantoulakis, P. D., Karagiannidis, G. K. & Ding, Z. (2018); Fakidis, J., Videv, S., Kucera, S., Claussen, H. & Haas, H. (2016); Mathews *et al.* (2016); Nasiri, A., Zabalawi, S. A. & Mandic, G. (2009); Pan, G., Ye, J. & Ding, Z. (2017); Rakia, T., Yang, H.-C., Gebali, F. & Alouini, M.-S. (2016); Tabassum, H. & Hossain, E. (2018). It has been shown that wireless users in VLC EH networks can benefit from the illumination, data communication and light EH simultaneously. In the literature, there are some fundamental works providing measurement results regarding optical wireless power transfer Fakidis *et al.* (2016) as well as EH from indoor artificial light Carvalho & Paulino (2014); Mathews *et al.* (2016); Nasiri *et al.* (2009). Further, the work in Rakia *et al.* (2016) has considered a dual-hop hybrid VLC/RF communication system; the relay harvests energy over the VLC first-hop link by taking the DC component out of the received signal and uses this energy for retransmitting the signal over the RF second-hop link. Some scenarios of hybrid VLC/RF networks with multiple RF access points (APs) and multiple optical transmiters have been studied and analyzed in Basnayaka & Haas (2017); Tabassum & Hossain (2018). In Pan *et al.* (2017), the authors have proposed a secure scheme in

which the harvested energy from indoor artificial light via downlinks is used for uplink communication. Moreover, the framework of simultaneous lightwave information and power transfer was introduced for the first time in Diamantoulakis *et al.* (2018). Particularly, according to Diamantoulakis *et al.* (2018); Pan *et al.* (2017), the light energy harvested in VLC systems is around 1.5 mW which can provide enough operating energy for low-power devices, such as IoT sensors Torfs, T., Sterken, T., Brebels, S., Santana, J., van den Hoven, R., Spiering, V., Bertsch, N., Trapani, D. & Zonta, D. (2013). However, it might only supply 11% of the energy needed to smartphones. Precisely, a smartphone requires an EH rate of 13.69 mW[1]. Indeed, the energy demand is more than the energy offered by conventional VLC systems. Nevertheless, it is noted that the indoor light provides *free* energy since no extra power is needed from the lighting system. Moreover, a transparent solar panel named as Wysips Reflect, recently developed by Sunpartner Technologies wys (2019), can be integrated into phone screens. It promises to remarkably enhance the light EH performance. Therefore, the previous works wys (2019); Basnayaka & Haas (2017); Carvalho & Paulino (2014); Diamantoulakis *et al.* (2018); Fakidis *et al.* (2016); Mathews *et al.* (2016); Nasiri *et al.* (2009); Pan *et al.* (2017); Rakia *et al.* (2016); Tabassum & Hossain (2018) have shown the promising performance of using visible light for communications and power transfer.

Nevertheless, in VLC systems, there are three major issues of EH from indoor light. First, the amount of indoor light energy is limited. This is due to the fact that the intensity of LED light is lower than the one of solar light, even in well-illuminated areas, such as drafting tables or workshops Mathews *et al.* (2016). Second, during the non-working time at night, LED bulbs in office buildings are often turned off or dimmed to save energy. Thus, the EH performance is significantly decreased. Third, the illumination in indoor living environments should respect eye safety standards. Therefore, LED light bulbs might not change flexibly their emitting directions or optical beamforming to maximize the EH performance. Different from visible light, RF is more flexible, and its well-known application, RF WPT, has been well studied in

[1] In the provision of continuous services, it is expected that smartphones can always be rechared with sufficient energy for the phone call service. According to **?**, a phone consumes 1054.3 mW averaged over 77 seconds for a call which corresponds that 13.69 mW of harvested power is needed.

the literature Boshkovska *et al.* (2015,1); Clerckx & Bayguzina (2016); Jiang *et al.* (2017); Ju & Zhang (2014a); Kaddoum *et al.* (2017); Ku, M.-L., Li, W., Chen, Y. & Liu, K. J. R. (2016); Liu *et al.* (2014); Niyato *et al.* (2017); Tabassum *et al.* (2015); Tran, H.-V. & Kaddoum, G. (2018b); Tran, H. V. & Kaddoum, G. (2019); Tran *et al.* (2018); Xiong *et al.* (2017). Thus, a combination between optical and RF WPTs can provide an efficient solution in both power and data transmisions, since it becomes evident that RF and lightwave wireless power transfer approaches are complementary rather than competing technologies. Indeed, the cooperation between the two technologies seems to be a particularly promising direction that can fundamentally extend the efficacy of single-band WPT (i.e., either RF or lightwave), while respecting the power constraints per band for safety and consistent illumination reasons.

Motivated by the aforementioned issues, in this paper, we consider a hybrid RF/VLC network consisting of multiple optical transmitters, one multi-antenna RF AP, and multiple terminal devices. Each optical transmitter, composed of multiple LED elements, can generate multiple narrow beams simultaneously, known as optical angle-diversity transmitters Chen *et al.* (2017). This configuration in terms of spatial division can enhance the bandwidth resource and eliminate intercell interference in attocell networks Chen *et al.* (2017). Further, each terminal device is equipped with one single antenna and one photodetector. We assume that the devices have a multi-homing capability that allows to aggregate resources received from the optical transmitters and the RF AP Kashef, M., Ismail, M., Abdallah, M., Qaraqe, K. A. & Serpedin, E. (2016). Due to the limitations of light EH, the network can fail to ensure the desirable light EH performance while guaranteeing information decoding (ID) performance. On this basis, this work aims at proposing a novel collaborative RF and lightwave resource allocation scheme to enhance the EH performance of the overall network.

In the proposed scheme, the optical transmitters play the primary role and are responsible for delivering both information and energy over only visible light while the RF AP is a helper which is liable for transferring wireless power using RF. In the system model, the communication quality of service (QoS) is maximized for all users, in terms of VLC signal-to-noise ratios (SNRs), under a constraint of the sum of light and RF EH performance at each user, while

keeping illumination constant and ensuring health safety in the network area. In this concern, the RF AP is configured to minimize its power budget while contributing a certain amount of the RF EH performance to the overall network. Thus, we formulate two corresponding optimization problems associated with the group of the optical transmitters and the RF AP, whose solving process are tightly related to each other. Hence, we devise algorithms to handle and optimally solve the two problems. Moreover, to reduce the computational burden, we derive a closed-form suboptimal solution to the problem of the group of the optical transmitters. Finally, considering the case where each optical transmitter is capable of calculating the suboptimal solution using the low complex closed-form expression, we further propose a semi-decentralized method to further facilitate the solving process.

In summary, the main contributions of our work can be summarized as follows:

- Proposing a novel collaborative RF and lightwave resource allocation scheme for hybrid RF/VLC ultra-small cell networks with simultaneous power and data transmission,
- Devising algorithms to solve the optimization problems of the optical transmitters and the RF AP optimally,
- Providing a closed-form suboptimal solution with high accuracy and low complexity to the problems of the optical transmitters,
- Developing a semi-decentralized method to tackle the problems of the network.

The remainder of this paper is organized as follows: In Section 6.2, the system model is presented. The proposed collaborative resource allocation scheme and its formulation are shown in Section 6.3. The optimal and the suboptimal solutions are given in Section 6.4. In Section 6.5, numerical results are provided and discussed. Finally, the conclusion is put forward in Section 6.6.

## 6.2 System Model

### 6.2.1 Optical Angle-diversity Transmitters with Color Allocation

In this work, we consider the optical transmitters composed of multiple LED elements which can generate multiple narrow beams simultaneously as in Chen *et al.* (2017). Each LED element points in a distinct direction. The angle diversity transmitter, whose layout is described in Chen *et al.* (2017), covers the same area and provides the same white illumination as conventional single-element transmitters. However, since the beam of each LED element can interfere with the others, multi-color white LED lamps, e.g. RGB white LEDs, can be a promising candidate to overcome this issue. Specifically, one of the three colors is selected to convey communication data whereas the others are used to keep illumination constant. Since the three colors are orthogonal, the interference can be canceled by properly selecting a color for each LED element. Further, the unselected colors operate at zero alternating current (AC) and non-zero direct current (DC) bias. Consequently, they have no impact on the information detection of neighboring receivers.

Given the use of the optical angle-diversity with color allocation, we consider a system model consisting of one RF AP with $M_T$ antennas, $\mathscr{O}$ optical transmitters with $M_I$-element angle-diversity, and $J$ terminal devices, as shown in Fig. 6.1. The optical transmitters are placed on the ceiling to provide illumination and communication at the same time. Each multi-homing terminal device is equipped with a single antenna and a solar panel. We assume that each device is served by an optical transmitter.

In Fig. 6.1, an illustration of the network with 7-element angle diversity optical transmitters is shown where the information-carrying colors are interleavedly allocated to circular areas to eliminate interference. Further, to avoid inter-transmitter interference, two vertically consecutive transmitters are adjusted to guarantee a shift of $\frac{360}{M_I}$ degrees between them. Particularly, it is worth noting that the light intensity or the radiance angle at half-power in the covered area is the same regardless of the values of $M_I$ Chen *et al.* (2017). Under this condition, increasing

the number of elements $M_E$ improves the spectral efficiency and increases the number of users able to be simultaneously served Chen *et al.* (2017), however, it does not impact the lightwave WPT performance.

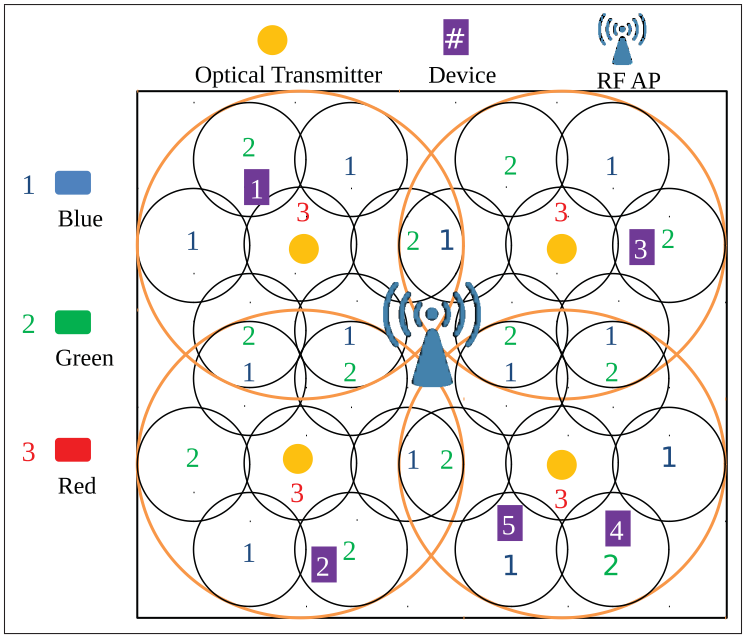


Figure 6.1 An illustration of the network with color allocation

### 6.2.2 VLC Channel Model

The total received optical power at a receiver can be composed of line-of-sight (LOS) and non-line-of-sight (NLOS) components. However, the contribution of the second component is much smaller than that of the first one Diamantoulakis *et al.* (2018); Pan *et al.* (2017). In this work, for simplicity, we consider only the VLC channels with the LOS component. Thus, the VLC channel between LED element $i$ $(1 \leq i \leq M_I)$ of optical transmitter $o$ $(1 \leq o \leq \mathscr{O})$ and the photodetector of device $j$ $(1 \leq j \leq J)$, denoted by $h_{oi,j}$, can be given as Diamantoulakis *et al.* (2018); Pan *et al.* (2017)

$$h_{oi,j} = \frac{Ar_j(m_i+1)}{2\pi d_{oi,j}^2} \cos^{m_{oi}}(\phi_{oi,j}) T_s(\psi_{oi,j}) g(\psi_{oi,j}) \cos(\psi_{oi,j}), \tag{6.1}$$

where $Ar_j$ is the active area of the photodetector, $d_{oi,j}$ is the distance between the LED element to the photodetector of device $j$, $\phi_{oi,j}$ is the irradiation angle, $\psi_{oi,j}$ is the incident angle of light radiation, $T_s(\psi_{oi,j})$ is the optical band-pass filter gain of transmission, $m_{oi}$ is the Lambert's mode number, and $g(\psi_{oi,j})$ is the optical concentrator gain. The different parameters of the VLC channel are shown in Fig. 6.2. Furthermore, $\phi_{oi,1/2}$ is the LED semi-angle at half-power, and $\psi_{oi,j,c} \leq \pi/2$ is the field of view (FOV). These two paramteters are used to compute $m_{oi}$ and $g(\psi_{oi,j})$ Diamantoulakis *et al.* (2018); Pan *et al.* (2017).

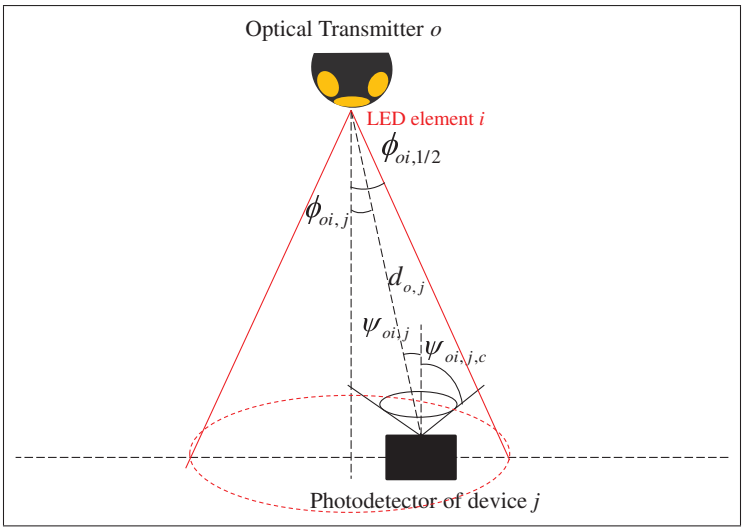


Figure 6.2 Visible light communication channel

### 6.2.3 RF Channel Model

In this paper, we consider the Rician channel model for RF links. The transmission channel between the RF AP and device $j$ is given by

$$\mathbf{g}_j = \sqrt{\frac{R}{1+R}}\mathbf{g}_{j,0} + \sqrt{\frac{1}{1+R}}\mathbf{g}_{j,1}, \tag{6.2}$$

where $\mathbf{g}_{j,0} \in \mathscr{CN}^{M_T \times 1}$ denotes the line of sight component, $\mathbf{g}_{j,1} \in \mathscr{CN}^{M_T \times 1}$ represents the non-line of sight fading component, and $R$ is the Rician factor.

### 6.2.4 Signal Models

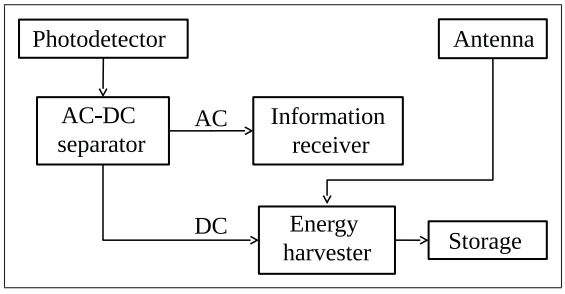


Figure 6.3 The receiver structure of the device with a multi-homing capability
Adapted from Kashef *et al.* (2016)

We consider a receiver structure of the device with a multi-homing capability, as shown in Fig. 6.3.

#### 6.2.4.1 Visible Light Communication

Considering the transmitted optical signals, one of the three colors in $\mathbb{S} = \{\text{Blue, Green, Red}\}$, denoted by $\mathtt{s} \in \mathbb{S}$, is selected to convey communication data whereas the others, denoted by $\mathtt{c} \in \bar{\mathbb{S}}$ ($\bar{\mathbb{S}} = \mathbb{S} \backslash \{\mathtt{s}\}$), are used to keep illumination constant. The optical signal from LED element $i$ of optical transmitter $o$ to device $j$ can be expressed as

$$x_{oi,j} = N_{\mathtt{s}} V_{\mathtt{s}} [A^{\mathtt{s}}_{oi,j} s_{oi,j} + B^{\mathtt{s}}_{oi,j}] h_{oi,j} + \sum_{\mathtt{c} \in \bar{\mathbb{S}}} N_{\mathtt{c}} V_{\mathtt{c}} B^{\mathtt{c}}_{oi,j} h_{oi,j}, \tag{6.3}$$

where $N_{\mathtt{s}}$ and $N_{\mathtt{c}}$ are the numbers of LEDs at each element dedicated for the selected and other colors, respectively. $V_{\mathtt{s}}$ and $V_{\mathtt{c}}$ are the LED voltages of the selected and the other colors, respectively. Additionally, $s_{oi,j}$ denotes the modulated electrical signal with zero mean and a unity variance Chen *et al.* (2016a), $A^{\mathtt{s}}_{oi,j}$ is the AC component of the selected color associated with $s_{oi,j}$, $B^{\mathtt{s}}_{oi,j}$ and $B^{\mathtt{c}}_{oi,j}$ represent the DC bias components used for the selected and the other colors respectively. In this concern, $B^{\mathtt{s}}_{oi,j} \in [I_L, I_H]$ and $B^{\mathtt{c}}_{oi,j} \in [I_L, I_H]$, where $[I_L, I_H]$ are the minimum and the maximum input bias currents. Further, to mitigate the effect of clipping

distortion, the limitation applied on $A^{\mathtt{s}}_{oi,j}$ can be shown as

$$A^{\mathtt{s}}_{oi,j} \leq \min\left\{B^{\mathtt{s}}_{oi,j} - I_L, I_H - B^{\mathtt{s}}_{oi,j}\right\}. \tag{6.4}$$

To ensure white illumination, the average light intensity of the three colors should be the same

$$N_{\mathtt{s}} V_{\mathtt{s}} (A^{\mathtt{s}}_{ij} \mathbb{E}\left[s_{oi,j}\right] + B^{\mathtt{s}}_{oi,j}) = N_{\mathtt{c}} V_{\mathtt{c}} B^{\mathtt{c}}_{oi,j} \quad (\forall \mathtt{c} \in \bar{\mathbb{S}}, \forall o, \forall i, \forall j). \tag{6.5}$$

Particularly, since $\mathbb{E}\left[s_{oi,j}\right] = 0$ Chen *et al.* (2016a), the intensity is determined by the DC component, therefore we have the following condition

$$N_{\mathtt{s}} V_{\mathtt{s}} B^{\mathtt{s}}_{oi,j} = N_{\mathtt{c}} V_{\mathtt{c}} B^{\mathtt{c}}_{oi,j} \quad (\forall \mathtt{c} \in \bar{\mathbb{S}}, \forall o, \forall i, \forall j). \tag{6.6}$$

In particular, for convenience, we generalize $N_{\mathtt{s}} = \{N_{\mathtt{c}}\} = N_{LED}$ $(\forall \mathtt{c} \in \bar{\mathbb{S}})$, and $V_{\mathtt{s}} = \{V_{\mathtt{c}}\} = V_{LED}$ $(\forall \mathtt{c} \in \bar{\mathbb{S}})$. Thus, condition (6.6) can be simplified as

$$B^{\mathtt{s}}_{oi,j} = B^{\mathtt{c}}_{oi,j} = B, \quad (\forall \mathtt{c} \in \bar{\mathbb{S}}, \forall o, \forall i, \forall j). \tag{6.7}$$

Since the AC component is used for the ID, the SNR expression can be derived as

$$\mathtt{SNR}^{\mathtt{s}}_{oi,j} = \frac{\left(\nu N_{LED} V_{LED} h_{oi,j} A^{\mathtt{s}}_{oi,j}\right)^2}{\sigma^2}, \tag{6.8}$$

where $\nu$ is photodetector responsivity and $\sigma^2$ is the noise power.

#### 6.2.4.2 VLC Energy Harvesting

It is obvious that the VLC signals include the DC component, which is separated and then conveyed to the energy harvester, as shown in Fig. 6.3. The VLC harvested energy at device $j$

can be computed as Diamantoulakis *et al.* (2018)

$$\mathtt{EH}_j^{VLC} = f I_{j,G} V_{j,c}, \tag{6.9}$$

where $f$ is the fill factor Li, C., Jia, W., Tao, Q. & Sun, M. (2011), and $I_{j,G}$ is the light generated current. Particularly, since the three colored lights contribute to the EH performance and a device can benefit from multiple light sources, $I_{j,G}$ can be calculated as

$$I_{j,G} = 3\nu N_{LED} V_{LED} B \sum_{o}^{\mathscr{O}} \sum_{i}^{M_I} h_{oi,j}, \tag{6.10}$$

and $V_{j,c}$ is the open circuit voltage, computed as

$$V_{j,c} = V_0 \ln\left(1 + \frac{I_{j,G}}{I_D}\right), \tag{6.11}$$

where $V_0$ is the thermal voltage and $I_D$ is the dark saturation current.

#### 6.2.4.3 RF Wireless Power Transfer and Energy Harvesting

On the other hand, RF signals beamed to device $j$ can be given by

$$x_j^{RF} = s_j^{RF} \mathbf{g}_j^H \mathbf{w}_j, \tag{6.12}$$

where $s_j^{RF}$ is the unit energy signal and $\mathbf{w}_j \in \mathbb{C}^{M_T \times 1}$ is the beamforming vector.

Thus, the RF harvested energy input at device $j$ can be expressed as

$$\hat{\mathtt{EH}}_j^{RF} = \sum_{j'=1}^{J} \left| \mathbf{g}_j^H \mathbf{w}_{j'} \right|^2. \tag{6.13}$$

Considering conventional linear RF EH models, the actual harvested energy, denoted by $\mathtt{EH}_j^{RF}$, can be computed as a linear function of the input energy, i.e. $\mathtt{EH}_j^{RF} = \xi_j^{RF} \hat{\mathtt{EH}}_j^{RF}$ in which $\xi_j^{RF}$ $(0 \leq \xi_j^{RF} \leq 1)$ is the energy conversion efficiency. Nevertheless, in practice, the RF energy

conversion efficiency is not a constant, its value depends on the strength of the input energy. Hence, a practical non-linear RF EH model is considered in this work. Based on Boshkovska *et al.* (2015,1); Clerckx & Bayguzina (2016); Jiang *et al.* (2017); Ku *et al.* (2016); Tabassum *et al.* (2015); Xiong *et al.* (2017), the non-linear model is

$$\mathtt{EH}_j^{RF} = \frac{\dfrac{\mathtt{M}^{EH}}{1+e^{-\mathtt{a}(\hat{\mathtt{EH}}_j^{RF}-\mathtt{b})}} - \dfrac{\mathtt{M}^{EH}}{1+e^{\mathtt{ab}}}}{1-\dfrac{1}{1+e^{\mathtt{ab}}}}, \tag{6.14}$$

where $\mathtt{M}^{EH}$ is a positive constant representing the maximum harvested energy at a user when the RF EH circuit meets saturation. In addition, $\mathtt{a}$ and $\mathtt{b}$ are positive constants related to the circuit's specifications, e.g. the resistance, capacitance, and diode turn-on voltage Boshkovska *et al.* (2015,1); Clerckx & Bayguzina (2016); Jiang *et al.* (2017); Xiong *et al.* (2017).

## 6.3 Problem Formulation

In this section, we explain the aim of the proposed resource allocation scheme and then show the corresponding problem formulation.

In VLC systems, there are some major limitations on the light EH performance. First, indoor light EH might be limited, compared with outdoor solar light EH Mathews *et al.* (2016). Second, the light EH performance might not be stable during non-working times, such as at night. Third, at the transmitter side, the transmit power and the light beam of the LED elements might not be flexibly changed due to maintaining consistent illumination, a very important criteria. These limitations lead to the fact that the VLC network can fail in managing a high information performance whereas ensuring the EH requirement.

Thus, we propose the combination of optical and RF WPTs to overcome these drawbacks. In this regard, the group of optical transmitters aims to (i) maximize the minimum of the VLC SNRs under a total EH constraint at each user. Meanwhile, the RF AP intends to (ii) minimize its transmit power while contributing a certain amount of RF EH performance to the

overall network to help improve the achievable VLC SNR performance. In this work, since our main goal is to improve the VLC performance, we prioritize objective (i) over objective (ii). Therefore, we propose a scheme in which, first, the group of optical transmitters actively allocates resources to achieve objective (i) without considering objective (ii) and then decides the amount of RF EH contributed by the RF AP. Second, the RF AP should allocate RF energy to each user according to the RF EH requirement.

To achieve this, there should be a central processing unit in the hybrid RF/VLC network to handle the scheme. In the first step, the optical transmitters convey the information of $\{h_{oi,j}\}$ to the central unit, responsible of tackling the problem for the group of the optical transmitters, namely $\mathrm{OP}_1$, given as

$$\mathrm{OP}_1:$$

$$\max_{\{B,A^{\mathtt{s}}_{oi,j},\mathtt{EH}^{RF}_j\}} \min \frac{\alpha_{oi,j}\left(\nu N_{LED} V_{LED} h_{oi,j} A^{\mathtt{s}}_{oi,j}\right)^2}{\sigma^2}, \tag{6.15a}$$

$$\text{s.t.:} \quad \mathtt{EH}^{VLC}_j + \mathtt{EH}^{RF}_j \geq \theta, \quad (\forall j) \tag{6.15b}$$

$$B^{\mathtt{s}}_{oi,j} = B, \quad (\forall o, \forall i, \forall j) \tag{6.15c}$$

$$A^{\mathtt{s}}_{oi,j} \leq I_H - B^{\mathtt{s}}_{oi,j}, \quad (\forall o, \forall i, \forall j) \tag{6.15d}$$

$$\frac{I_L + I_H}{2} \leq B \leq I_H, \tag{6.15e}$$

$$\mathtt{EH}^{RF}_j \leq \theta^{RF}, \quad (\forall j) \tag{6.15f}$$

where $\{\alpha_{oi,j}\} \in \{0;1\}$ with $\alpha_{oi,j} = 1$ indicating that LED element $i$ of optical transmitter $o$ serves user $j$ which are known as a priori, and these values are determined by the operator according to the users' geographical position. Further, $\theta$ is the preset threshold of the total EH. Constraint (6.15c) ensures that the transmit power of the three colors is the same for the white illumination. Further, the restriction on $A^{\mathtt{s}}_{oi,j}$, given in (6.4), implies that there are two possible values of $B^{\mathtt{s}}_{oi,j}$ resulting in the same $A^{\mathtt{s}}_{oi,j}$. These two values fall in two ranges, $I_L \leq B^{\mathtt{s}}_{oi,j} < \frac{I_L+I_H}{2}$ and $\frac{I_L+I_H}{2} \leq B^{\mathtt{s}}_{oi,j} \leq I_H$, respectively. As mentioned earlier, the indoor light EH in its nature is limited. Since we aim to exploit the light energy and maintain a reasonable illumination in the

covered area, we only consider the values of $B$ in the higher range (i.e. $\frac{I_L+I_H}{2} \leq B^{\mathbf{s}}_{oi,j} \leq I_H$) as feasible solutions. Thus, constraints (6.15d) and (6.15e) are formulated. Moreover, $\theta^{RF}$ is the threshold of the RF EH that the RF AP contributes to each user. In this context, it is well-known that the efforts to convey energy wirelessly might lead to RF pollution, resulting in human health issues. There is a restriction on the RF absorption rate applied to the human body IEE (2005); Tran & Kaddoum (2018b). Accordingly, this issue is also imposed through (6.15f).

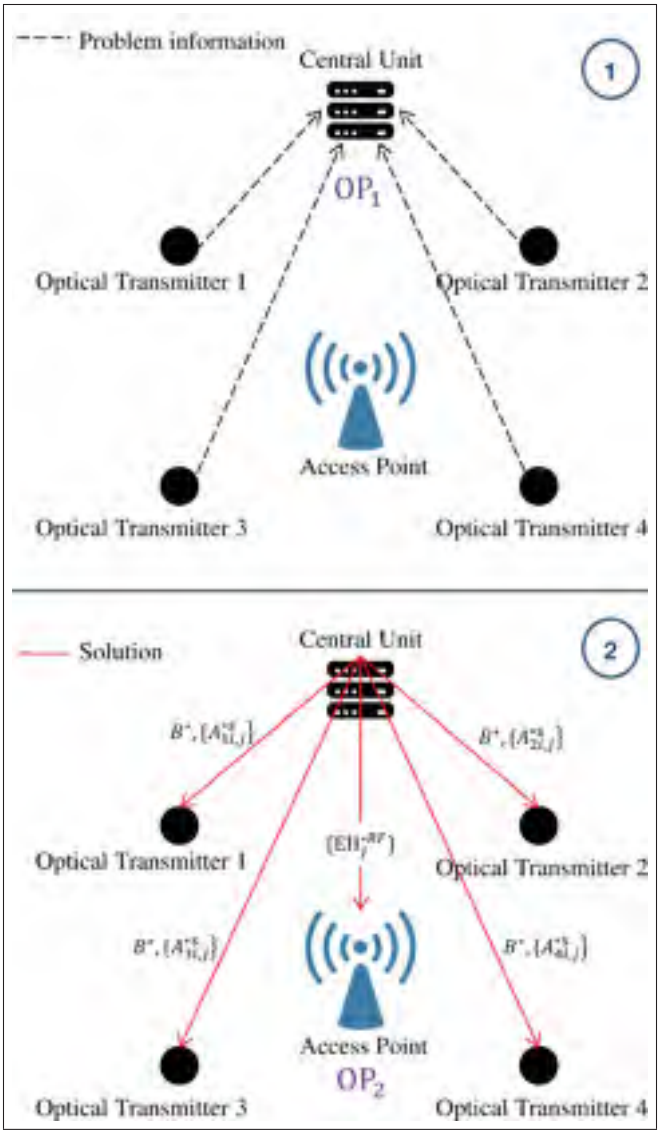


Figure 6.4 The scenario of solving problems $OP_1$ and $OP_2$

**Remark 1.** The solution of $\mathrm{OP}_1$, which is optimal in terms of the initial objective (i.e., max-min SNR), also maximizes the VLC SNR for any user in the network. This is because an increase of the SNR for any user directly leads to higher SNRs for all users (due to equal DC component for each LED element). On this basis, choosing the max-min SNR objective for managing QoS implies maximizing the sum and the minimum achievable throughput of the network, with the latter being an increasing function of the SNR for each user Lapidoth, A., Moser, S. M. & Wigger, M. A. (2009). This is an important observation, since these objectives are the most commonly used, when the channel knowledge is available at the transmitter.

Next, in our scheme, the central unit tackles problem $\mathrm{OP}_1$ and then distributes the optimal values, $B^{\star}$ and $\{A^{\star \mathtt{s}}_{oi,j}\}$, to each optical transmitter while conveying the optimal values $\{\mathtt{EH}^{\star RF}_{j}\}$ to the RF AP. Therefore, the RF AP is responsible of allocating the energy resources such that the RF EH at each user achieves $\{\mathtt{EH}^{\star RF}_{j}\}$ obtained from $\mathrm{OP}_1$. The optimization problem of the RF AP, namely $\mathrm{OP}_2$, is

$$\mathrm{OP}_2: \quad \min_{\mathbf{w}_j} \quad \sum_{j=1}^{J} \left\|\mathbf{w}_j\right\|^2 \tag{6.16a}$$

$$\text{s.t.:} \quad \mathtt{EH}^{RF}_{j} \geq \mathtt{EH}^{\star RF}_{j}, \quad (\forall j) \tag{6.16b}$$

where $\mathtt{EH}^{\star RF}_{j}$ is the optimal value of $\mathtt{EH}^{RF}_{j}$, obtained from solving problem $\mathrm{OP}_1$. For convenience, Fig. 6.4 shows that how problems $\mathrm{OP}_1$ and $\mathrm{OP}_2$ are handled.

**Remark 2.** In realistic scenarios, when the network needs to update solutions, the network operator can exclude $B$ from re-solving $\mathrm{OP}_1$ and include it again whenever necessary (i.e., when it is suitable to change the illumination level to increase/decrease system performance). This helps to actively maintain the constant lighting level in covered areas. This further highlights the crucial role of RF AP in fulfilling performance requirements under the changes of the network.

In general, it is difficult to solve problem $\mathrm{OP}_1$. In this regard, considering the objective function, the maximization of a convex function is not a convex problem. Further, constraint (6.15b)

is nonconvex since it can be seen that $\mathtt{EH}_j^{VLC}$ is concave while $\mathtt{EH}_j^{RF}$ is convex (i.e. the second-order condition Boyd & Vandenberghe (2004)). Therefore, problem $\mathrm{OP}_1$ is nonconvex. Furthermore, problem $\mathrm{OP}_2$ is nonconvex because constraint (6.16b) has the form of a convex function larger than a constant. To overcome these issues, we propose novel methods to solve these problems optimally and suboptimally, presented in the next section.

## 6.4 Proposed Solutions

This section presents our methods to tackle problems $\mathrm{OP}_1$ and $\mathrm{OP}_2$. First, we propose a method to decompose problem $\mathrm{OP}_1$ without the loss of optimality and then solve the corresponding subproblems. Second, we tackle problem $\mathrm{OP}_2$. Lastly, we derive a suboptimal solution with low complexity and then introduce a semi-decentralized approach to handle $\mathrm{OP}_1$ and $\mathrm{OP}_2$.

### 6.4.1 Decomposing Problem $\mathrm{OP}_1$ without Loss of Optimality

In light of *Remark* 1, it is worth emphasizing that since all the DC components of the LED elements are the same, increasing the VLC SNR for any user leads to increasing the VLC SNR for all users. On this basis, considering problem $\mathrm{OP}_1$, there is an interesting characteristic, given in *Proposition* 1 below

**Proposition 1.** Constraint (6.15b) implies that, to improve the VLC SNR, the contribution of VLC EH to the overall EH performance should be lowered through increasing RF EH. Since maximizing the minimum of VLC SNRs is equivalent to maximizing the VLC SNR at the user with the worst VLC SNR, the RF EH allocated to the user with the worst VLC SNR determines the value of $B$ for all the users.

Proof: See Appendix IV.1.

Based on *Proposition* 1, we propose an approach to decompose problem $\mathrm{OP}_1$ into two subproblems without loss of optimality. The resource allocation can be divided into two stages: First, considering user $\bar{j}$ (where $\bar{j}$ is the user with the worst VLC SNR), the optimal values of

$\{\mathtt{EH}_{\bar{j}}^{RF}\}$ denoted by $\{\mathtt{EH}_{\bar{j}}^{\star RF}\}$, need to be determined. Second, by replacing $\{\mathtt{EH}_{\bar{j}}^{RF}\}$ by $\{\mathtt{EH}_{\bar{j}}^{\star RF}\}$ in $\mathrm{OP}_1$, the optimal values of $\{A_{oi,j}^{\mathtt{s}}\}$ and $B$ are then found. It is clear that the optimality of this decomposition is preserved.

To excute the first stage, we omit the parts unrelated with $\{\mathtt{EH}_{\bar{j}}^{RF}\}$ in $\mathrm{OP}_1$. Accordingly, the corresponding problem, namely SubRF, can be formulated as

$$\text{SubRF:} \max_{\{B,A_{oi,j}^{\mathtt{s}},\mathtt{EH}_{\bar{j}}^{RF}\}} \frac{\left(\nu N_{LED} V_{LED} h_{oi,\bar{j}} A_{oi,\bar{j}}^{\mathtt{s}}\right)^2}{\sigma^2}, \tag{6.17a}$$

$$\text{s.t.:} \quad \mathtt{EH}_{\bar{j}}^{VLC} + \mathtt{EH}_{\bar{j}}^{RF} \geq \theta \tag{6.17b}$$

$$\mathtt{EH}_{\bar{j}}^{RF} \leq \theta^{RF}, \tag{6.17c}$$

In the second stage, we substitute $\{\mathtt{EH}_{\bar{j}}^{\star RF}\}$ into $\mathrm{OP}_1$. The resulting problem, namely SubVLC, can be written as

$$\text{SubVLC:} \max_{B,A_{oi,j}^{\mathtt{s}},\mathtt{EH}_{j}^{RF}} \min \frac{\alpha_{oi,j}\left(\nu N_{LED} V_{LED} h_{oi,j} A_{oi,j}^{\mathtt{s}}\right)^2}{\sigma^2}, \tag{6.18a}$$

$$\text{s.t.:} \quad \mathtt{EH}_{\bar{j}}^{VLC} \geq \theta - \mathtt{EH}_{\bar{j}}^{\star RF}, \tag{6.18b}$$

$$\mathtt{EH}_{j}^{VLC} \geq \theta - \mathtt{EH}_{j}^{RF}, (\forall j, j \neq \bar{j}) \tag{6.18c}$$

$$A_{oi,j}^{\mathtt{s}} \leq I_H - B, (\forall o, \forall i, \forall j) \tag{6.18d}$$

$$\frac{I_L + I_H}{2} \leq B \leq I_H. \tag{6.18e}$$

Generally, since the principle of optimally allocating the resources is unveiled through *Remark* 1 and *Proposition* 1, it is obvious that $\mathtt{EH}_{\bar{j}}^{\star RF}$, the optimal solution of problem SubRF, is also the optimal one of problem $\mathrm{OP}_1$. Thus, the optimality of our method is guaranteed.

### 6.4.2 Solution to Sub-problem SubRF

To solve problem SubRF, we start with finding the feasible range of $\mathtt{EH}_{\bar{j}}^{VLC}$ through its maximum and minimum, denoted as $\{\max \mathtt{EH}_{\bar{j}}^{VLC}\}$ and $\{\min \mathtt{EH}_{\bar{j}}^{VLC}\}$, respectively. It is clear that, according to (6.7), $\mathtt{EH}_{\bar{j}}^{VLC}$ in problem SubRF achieves its maximum when $\{A_{oi,\bar{j}}^{\mathtt{s}}\} = 0$ and $B = I_H$. Thus, we have

$$\max \mathtt{EH}_{\bar{j}}^{VLC} = f\hat{I}_{\bar{j}G} V_0 \ln(1 + \frac{\hat{I}_{\bar{j},G}}{I_D}), \tag{6.19}$$

where

$$\hat{I}_{\bar{j},G} = 3\nu N_{LED} V_{LED} I_H \sum_{o}^{\mathscr{O}} \sum_{i}^{M_I} h_{oi,\bar{j}}. \tag{6.20}$$

Next, $\mathtt{EH}_{\bar{j}}^{VLC}$ in problem SubRF achieves the minimum when $\{A_{oi,\bar{j}}^{\mathtt{s}}\}$ reach the maximum, i.e., (6.4). In more details, the maximum of $\{A_{oi,\bar{j}}^{\mathtt{s}}\}$ and the corresponding values of $B$ in problem SubRF can be computed, respectively, as follows

$$\hat{A}_{oi,\bar{j}}^{\mathtt{s}} = \frac{I_H + I_L}{2}, \tag{6.21}$$

$$\bar{B} = \frac{I_H - I_L}{2}. \tag{6.22}$$

Based on (6.21) and (6.22), $\min \mathtt{EH}_{\bar{j}}^{VLC}$ can be given by

$$\min \mathtt{EH}_{\bar{j}}^{VLC} = f\bar{I}_{\bar{j},G} V_0 \ln(1 + \frac{\bar{I}_{\bar{j},G}}{I_D}), \tag{6.23}$$

where

$$\bar{I}_{\bar{j},G} = 3\nu N_{LED} V_{LED} \bar{B} \sum_{o}^{\mathscr{O}} \sum_{i}^{M_I} h_{oi,\bar{j}}. \tag{6.24}$$

In general, the feasibility of problem SubRF can be confirmed using the condition below. Problem SubRF is feasible if and only if

$$\theta - \max \mathtt{EH}_{\bar{j}}^{VLC} \leq \theta^{RF}. \tag{6.25}$$

After some mathematical calculations, the optimal solution can be computed as follow

$$\mathtt{EH}_{\bar{j}}^{\star RF} = \min\{\theta - \min \mathtt{EH}_{\bar{j}}^{VLC}, \theta^{RF}\}. \tag{6.26}$$

### 6.4.3 Optimal Solution to Sub-problems SubVLC

One can observe that sub-problem SubVLC is subject to the class of maximizing a convex function. Conventionally, the sub-problem can be solved by applying successive convex approximation (SCA) methods Beck, A., Ben-Tal, A. & Tetruashvili, L. (2010). However, this approach can bring a significant computational burden. In this work, we show a method to transform the sub-problem into a convex formulation by exploiting the sub-problem's characteristics.

According to *Proposition* 1, solving SubVLC can be achieved by tackling two alternative sub-problems, namely $\text{SubVLC}_{\bar{j}}$ and $\text{SubVLC}_{j}$, with respect to user $\bar{j}$ and the other users, respectively. Thus, the optimization problem associated with user $\bar{j}$ can be formulated as

$$\text{SubVLC}_{\bar{j}}: \max_{B, A_{oi,\bar{j}}^{\mathtt{s}}} \quad \frac{\left(\nu N_{LED} V_{LED} h_{oi,\bar{j}} A_{oi,\bar{j}}^{\mathtt{s}}\right)^2}{\sigma^2} \tag{6.27a}$$

$$\text{s.t.:} \quad \mathtt{EH}_{\bar{j}}^{VLC} \geq \theta - \mathtt{EH}_{\bar{j}}^{\star RF}, \tag{6.27b}$$

$$A_{oi,\bar{j}}^{\mathtt{s}} \leq I_H - B, \tag{6.27c}$$

$$\frac{I_L + I_H}{2} \leq B \leq I_H. \tag{6.27d}$$

Further, the optimization problem with respect to the other users $(\forall j, j \neq \bar{j})$ is

$$\text{SubVLC}_j: \quad \max_{A^{\mathtt{s}}_{oi,j}} \quad \frac{\alpha_{oi,j}\left(\nu N_{LED} V_{LED} h_{oi,j} A^{\mathtt{s}}_{oi,j}\right)^2}{\sigma^2} \tag{6.28a}$$

$$\text{s.t.:} \quad A^{\mathtt{s}}_{oi,j} \leq I_H - B^{\star}. \tag{6.28b}$$

It is worth noting that $B^{\star}$ is the optimal value of $B$, obtained from solving sub-problem SubVLC$\bar{j}$. Also, we obtain

$$\mathtt{EH}^{\star RF}_{j} = \theta - \mathtt{EH}^{VLC}_{j}(B^{\star}). \tag{6.29}$$

We start with solving SubVLC$_{\bar{j}}$. According to (6.8), maximizing $\mathtt{SNR}^{\mathtt{s}}_{oi,\bar{j}}$ can be achieved by maximizing $A^{\mathtt{s}}_{oi,\bar{j}}$. Moreover, considering constraints (6.18c) and (6.18d), one can observe the relationship between $A^{\mathtt{s}}_{oi,\bar{j}}$, and $B$. Constraint (6.18d) always holds with equality at the optimal values of $\{A^{\mathtt{s}}_{oi,\bar{j}}\}$. Hence, maximizing $A^{\mathtt{s}}_{oi,\bar{j}}$ is equivalent to minimizing $B$. In light of this discussion, solving problem SubVLC$_{\bar{j}}$ can be equivalently reformulated into two steps. First, the optimal solution of $B$, denoted by $B^{\star}$, in problem SubVLC$_{\bar{j}}$ can be found by solving the problem below

$$\min_{B} \quad B \tag{6.30a}$$

$$\text{s.t.:} \quad \mathtt{EH}^{VLC}_{\bar{j}} \geq \theta_j - \mathtt{EH}^{\star RF}_{\bar{j}}, \tag{6.30b}$$

$$\frac{I_H - I_L}{2} \leq B \leq I_H. \tag{6.30c}$$

Second, the optimal value of $A^{\mathtt{s}}_{oi,\bar{j}}$ in sub-problem SubVLC$_{\bar{j}}$ can be given by

$$A^{\star\mathtt{s}}_{oi,\bar{j}} = I_H - B^{\star}. \tag{6.31}$$

Following (7.3) and (7.4), constraint (6.30b) needs to be represented into a more tractable form, given by

$$\ln\left(1+\frac{I_{\bar{j},G}(B)}{I_D}\right) \geq \frac{\theta_{\bar{j}} - \mathtt{EH}_{\bar{j}}^{\star RF}}{fV_0 I_{\bar{j},G}(B)}, \tag{6.32}$$

where, for convenience, $I_{\bar{j},G}(B)$ denotes that $I_{\bar{j},G}$ is a function of $B$. Accordingly, replacing (6.30b) by (7.20), problem (6.30) becomes convex. In particular, solving problem (6.30) can be achieved by a bisection-based algorithm as follows

Algorithm 6.1 Algorithm to find $B^\star$

1 Set $B_{min} = \dfrac{I_H - I_L}{2}$, $B_{max} = I_H$, and a solution accuracy $\varsigma \geq 0$.
2 **Repeat**
3 *If* constraint (7.20) is satisfied with $B = \frac{B_{min}+B_{max}}{2}$
4 *then* $B_{min} = B$
5 *Else* $B_{max} = B$.
6 **Until** $B_{max} - B_{min} \leq \varsigma$.
7 The output $B$ is the desired solution.

After obtaining $B^\star$, we consider sub-problem SubVLC$_j$. It can be seen that constraint (6.27b) holds optimality with equality. Therefore, the optimal solution SubVLC$_j$ can be calculated as

$$A_{oi,j}^{\star \mathtt{s}} = I_H - B^\star, \quad (\forall j, j \neq \bar{j}). \tag{6.33}$$

Combining (6.31) and (6.33), for all users, we have

$$A_{oi,j}^{\star \mathtt{s}} = I_H - B^\star, \quad (\forall j). \tag{6.34}$$

For convenience, a flowchart of handling problem OP$_1$ is shown in Fig. 6.5.

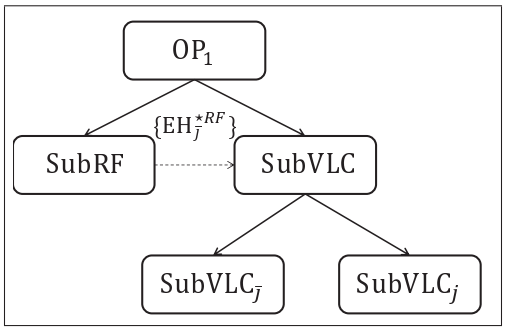


Figure 6.5 Flowchart of handling $\mathrm{OP}_1$.

### 6.4.4 Solution to Problem $\mathrm{OP}_2$

In this subsection, we propose an efficient method to solve $\mathrm{OP}_2$.

To deal with problem $\mathrm{OP}_2$, first, we can transform the constraint into a more tractable form based on Jiang *et al.* (2017). Next, by defining $\mathbf{W}_j = \mathbf{w}_j \mathbf{w}_j^H$ and $\mathbf{G}_j = \mathbf{g}_j (\mathbf{g}_j)^H$, problem $\mathrm{OP}_2$ can be equivalently reformulated as

$$\min_{\{\mathbf{W}_j\}} \quad \sum_{j=1}^{J} \mathrm{tr}(\mathbf{W}_j) \tag{6.35a}$$

$$\text{s.t.:} \quad \sum_{j'=1}^{J} \mathrm{tr}(\mathbf{W}_{j'} \mathbf{G}_j) \geq \bar{\theta}_j, \quad (\forall j), \tag{6.35b}$$

$$\mathbf{W}_j \succeq 0, \quad (\forall j), \tag{6.35c}$$

$$\mathrm{Rank}(\mathbf{W}_j) = 1, \quad (\forall j). \tag{6.35d}$$

in which, from (6.14),

$$\bar{\theta}_j = \mathtt{b} - \frac{1}{\mathtt{a}} \ln \left( \frac{e^{\mathtt{ab}} (\mathtt{M}^{EH} - \mathtt{EH}_j^{\star RF})}{e^{\mathtt{ab}} \mathtt{EH}_j^{\star RF} + \mathtt{M}^{EH}} \right). \tag{6.36}$$

The constraint $\mathrm{Rank}(\mathbf{W}_j) = 1$ is set to guarantee that $\mathbf{W}_j = \mathbf{w}_j \mathbf{w}_j^H$ holds after optimizing $\mathbf{W}_j$.

Problem $\mathrm{OP}_2$ has been transformed into a form of semi-definite programming (SDP). Also, it is still non-convex due to the rank-one constraint. However, we can demonstrate that the rank-one condition always holds in problem $\mathrm{OP}_2$ through *Lemma* 1 as follows

**Lemma 5.** Considering problem (6.35), the constraint of rank one condition, i.e. $\mathrm{Rank}(\mathbf{W}_j) = 1\ (\forall j)$, always does hold.

Proof: See Appendix IV.2.

Accordingly, we can omit constraint (6.35d) and then tackle (6.35) using SDP solvers, such as CVX Grant & Boyd (2009).

### 6.4.5 Suboptimal Solution to SubVLC and Proposed Semi-Decentralized Approach

In the continuity, to facilitate the solving process and to reduce the computational burden at the central control unit, we present a suboptimal solution to sub-problem $\mathrm{SubVLC}_j$ through *Lemma* 2 below

**Lemma 6.** The closed-form suboptimal solution to problem SubVLC, denoted by $A_{oi,j}^{\times \mathbf{s}}$ and $B^{\times}$, can be calculated by

$$B^{\times} = \min\left\{\max\{\Upsilon, I_L\}, I_H\right\}, \tag{6.37}$$

$$A_{oi,j}^{\times \mathbf{s}} = I_H - B^{\times}, \quad (\forall j) \tag{6.38}$$

where

$$\Upsilon = \frac{\theta - \mathtt{EH}_{\bar{j}}^{\star RF}}{3\nu N_{LED} V_{LED} f V_0 \mathscr{W}\left(\frac{\theta - \mathtt{EH}_{\bar{j}}^{\star RF}}{f V_0 I_D}\right) \sum_{o}^{\mathscr{O}} \sum_{i}^{M_I} h_{oi,\bar{j}}}, \tag{6.39}$$

where $\mathscr{W}(.)$ is the Lambert function.

Proof: See Appendix IV.3.

Indeed, the suboptimal solution can be calculated with low complexity. Assuming that each optical transmitter is capable of computing the suboptimal solution of SubVLC$_j$ (i.e., it is equipped with a micro controller), we propose a semi-decentralized approach for the network as follows.

Instead of solving OP$_1$, the control unit solves only problem SubRF and then distributes the information of $\mathtt{EH}_{\bar{j}}^{\star RF}$ and $h_{\bar{j}}$ $\left(h_{\bar{j}} = \sum_{o}^{\mathscr{O}} \sum_{i}^{M_I} h_{oi,\bar{j}}\right)$ to the optical transmitters and the RF AP. Afterwards, each optical transmitter tackles its own problem SubVLC$_j$ by using the closed-form expression provided in *Lemma* 2. Also, the RF AP solves problem OP$_2$ to get the optimal beamformers.

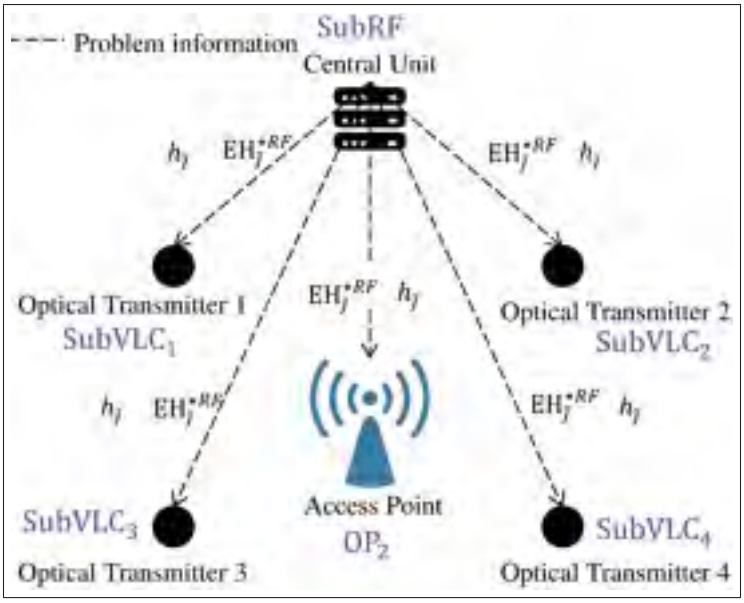


Figure 6.6 An example of the proposed decentralized scenario

For convenience, our decentralizing method is illustrated in Fig. 6.6. The advantages of this approach can be listed as: (i) all the computation burden is no longer put on the control unit but shared between the optical transmitters, (ii) the optical transmitters can adapt to the changes of the networks (i.e. users' position) instantly, and (iii) since the Lambert function $\mathscr{W}(.)$ is a simple well-known function and is easy to compute within nano seconds using average CPUs Fukushima, T. (2013), it can be seen that the closed-form suboptimal solution has low com-

plexity. The performance of this approach relies on the sub-optimality of the solution which is verified in the numerical section.

## 6.5 Numerical Results

Regarding the simulation, we consider a hybrid RF/VLC network consisting of one 6-antenna RF AP, four 7-angle-diversity optical transmitters and five user devices. We consider an office environment, as shown in Fig. 6.1, with a size of $5 \times 5 \times 3$ m$^3$. The locations of the four optical transmitters are $(1.5, 1.5, 3)$, $(1.5, 3.5, 3)$, $(3.5, 3.5, 3)$, and $(3.5, 1.5, 3)$, respectively. The distance between the transmitters and the receiver plane is 2 meters. The RF AP is located at $(2.5, 2.5, 3)$.

Regarding VLC channels, based on pioneering works Chen *et al.* (2017); Diamantoulakis *et al.* (2018); Pan *et al.* (2017); Rakia *et al.* (2016), we set $T_s(\psi_{oi,j}) = 1$ , $\phi_{oi,1/2} = 17^\circ$, $n = 1.5$, $\psi_{oi,j,c} = 60^\circ$, $I_L = 2$ mA, $I_H = 12$ mA, $B = I_H$, $I_D = 10^{-9}$ A, $\sigma^2 = 10^{-15}$ . The distances between the five users and their corresponding optical transmitters are 2.05 m, 2.10 m, 2 m, 2.11 m, and 2.08 m, respectively. Particularly, similar to Chen *et al.* (2017), with $\phi_{oi,1/2} = 17^\circ$ for each LED element, the 7-element angle-diversity transmitters are designed to have a LED semiangle at half-power equal to $60^\circ$ which is equivalent to the one in conventional single-element transmitters. Further, according to Wysips Reflect wys (2019), a solar pannel can be integrated into the phone screen, thus we can set $Ar_j = 85$ cm$^2$ (i.e. the screen size of a Samsung Galaxy S8). Also, $\nu = 0.4$, and $f = 0.75$. In addtion, we also set the number of LEDs as $N_{LED} = 40$ and the LED voltage as $V_{LED} = 2.25$ V Larimore, B. (2013). All the optical transmitters have the same settings.

Additionally, considering the RF channels, we set the Rician factor $R = 6$ dB and the exponent path loss factor to 2.6, suitable for office environments Rappaport & Sandhu (1994). Also, we investigate the system performance for $\theta^{RF} \leq 6$ mW which is the limit for human health safety Tran & Kaddoum (2018b). Regarding the nonlinear RF EH model, we set $\mathtt{M}^{EH} = 24$ mW, $\mathtt{a} = 150$ and $\mathtt{b} = 0.014$ based on the mathematical analysis of the practical nonlinear RF

EH model provided in Boshkovska *et al.* (2015,1); Jiang *et al.* (2017); Xiong *et al.* (2017). On this basis, the numerical results are shown and discussed as follows.

Fig. 6.7 exhibits the VLC SNR-EH regions for all the users without the help of the RF AP. It is obvious that a user with a shorter VLC transmission distance has a larger VLC SNR-EH region. Particularly, as observed, the minimum VLC EH is always larger than zero for all users. This can be explained by the restriction applied on the values of the AC components $\{A^{\mathbf{s}}_{oi,j}\}$, mathematically represented by (6.4), which implies that the maximum $\{A^{\mathbf{s}}_{oi,j}\}$ is less than $I_L$, and therefore $\{B^{\mathbf{s}}_{oi,j}\}$ is always positive. On this basis, the VLC EH is always greater than zero for all users.

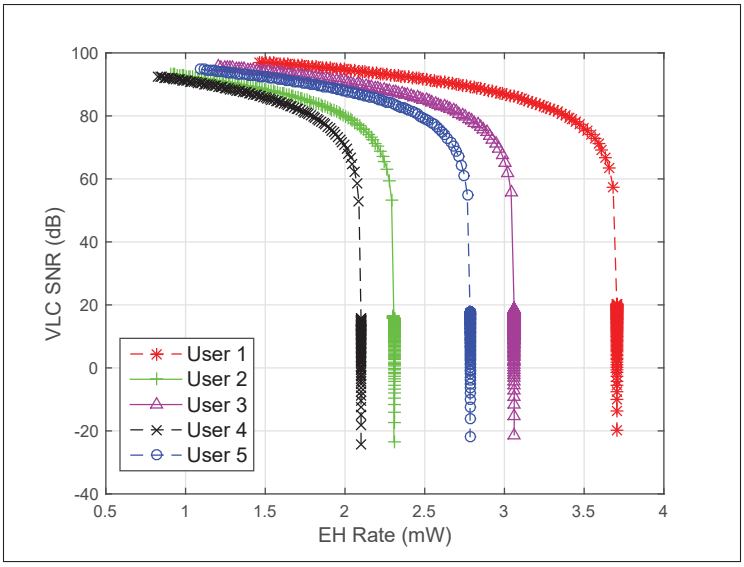


Figure 6.7 SNR-EH region at each user

In Fig. 6.8, the outperformance of the collaborative RF and lightwave resource allocation is shown. We explore the SNR-EH region of problem $\mathrm{OP}_1$ over threshold $\theta$. Without the help of the RF AP, solving problem $\mathrm{OP}_1$ becomes infeasible when $\theta$ is larger than 2.1 mW/s. This is because user 4 has the lowest SNR range and its maximum VLC EH is 2.1 mW, as observed from Fig. 6.7. One can see that the SNR-EH region is significantly enlarged when a higher level of $\theta^{RF}$ is given by the RF AP. In fact, the greater the amount of RF wireless power is, the

more extensive the feasible region is. This implies a significant outperformance of the hybrid approach over the pure VLC one.

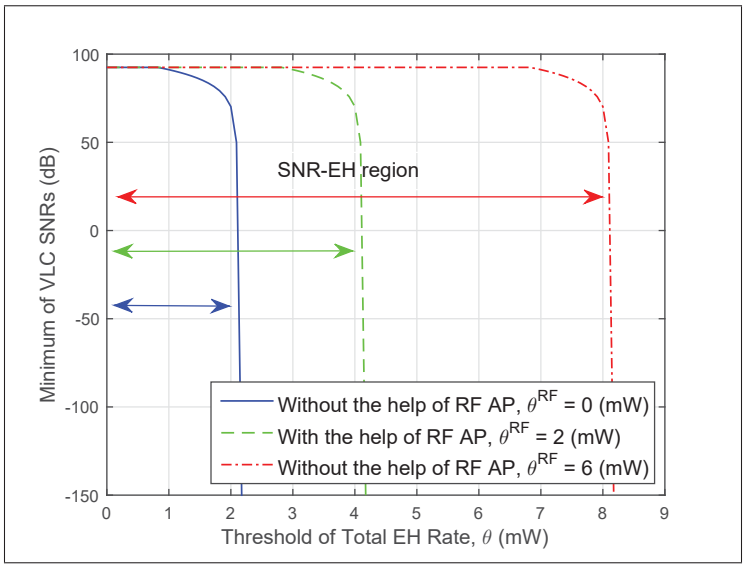


Figure 6.8 Outperformance of the hybrid RF and lightwave power transfer network

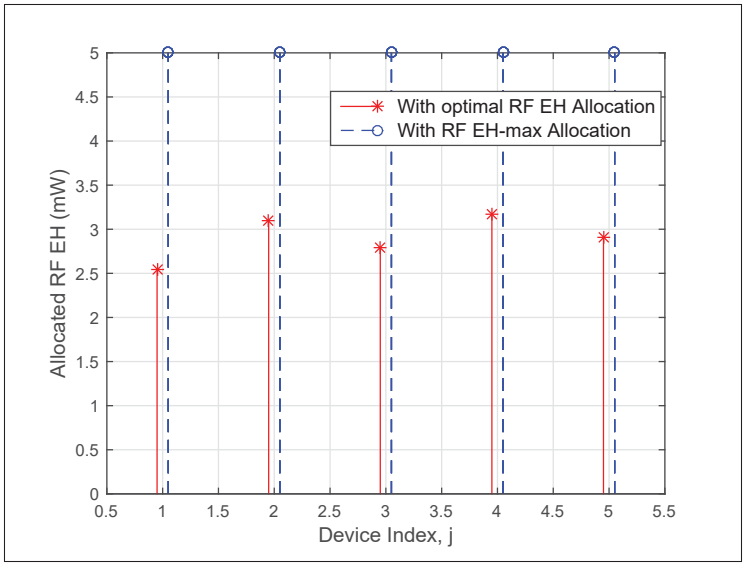


Figure 6.9 Impact of EH rate allocation, $\theta^{RF} = 5$ and $\theta = 4$

In Fig. 6.9, the importance of problem SubRF regarding the EH rate allocation is highlighted. Indeed, the manner of allocating all possible RF EH budget, termed as RH EH-max allocation, to each user is wasteful. Fig. 6.9 shows the optimal RH EH needed at each user to achieve the same minimum VLC SNR performance. In general, the optimal RF EH allocation can help avoid the transfer of redundant wireless power. It directly results in saving a significant amount of RF transmit power, which is clarified in the next simulation.

Fig. 6.10 illustrates the amount of transmit power at the RF AP spent to supply the users with the preset EH threshold $\theta^{RF}$. In this simulation, the impact of the EH models and the RF EH allocation on transmit power is revealed. It is obvious that employing the optimal RH EH allocation leads to more power saving. Regarding the linear EH model, the energy conversion efficiency is set to 0.5. In this concern, it is observed that the power efficiency of the non-linear EH model is considerably higher than the idealistic linear model, which indicates the suitability of the proposed analysis for the applications of practical systems.

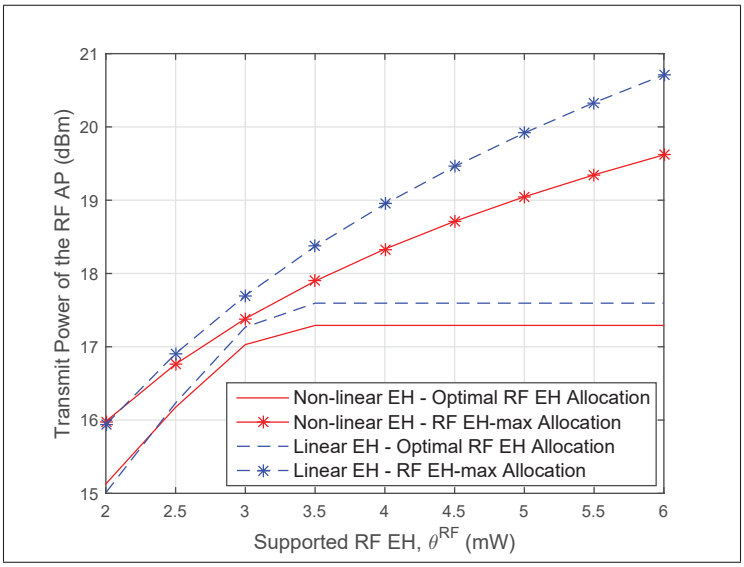


Figure 6.10 Transmit power at the RF AP

Fig. 6.11 presents the effectiveness of the suboptimal solution given in Lemma 2 of $\{\text{SubVLC}_j\}$. As observed, the suboptimal minimum of SNRs is slightly lower than the optimal one. In other words, the closed-form suboptimal solution can provide a very close system performance com-

pared with the optimal solution. This can be explained by the fact that the approximation given in (50) is very tight since $I_D \ll I_{j,G}(B)$, i.e., $I_D = 10^{-9}$ while $I_{j,G}(B) \approx 10^{-3}$ . Thus, the optimality loss is negligible. Therefore, it is confirmed that the proposed suboptimal solution has not only low complexity but also high accuracy.

In Fig. 6.12, the illumination in the served area is shown to justify the practicality of the proposed system. Actually, the hybrid RF/VLC system should provide enough illumination for working or studying in the considered office environment.. In this regard, the illuminance can be calculated by a multiplication of the transmitted power and the typical efficacy of a LED. The transmitted power can be calculated by $N_{LED} * V_{LED} * B$ with $B = 0.0085$ A. According to Phi, the typical efficacy is 90 lm/W. By observing Fig. 6.12, it can be seen that the achieved illuminance is approximately 920 lx at the center. Also, the illuminance in most of the area is more than 500 lx, which is the minimum value specified for office workers typing and reading documents by the European lighting standard Eur. Moreover, we can see that (i) different places in the room have different values of illumination, thus, some receivers cannot harvest sufficient energy, and (ii) the harvested energy by solely using VLC is limited.

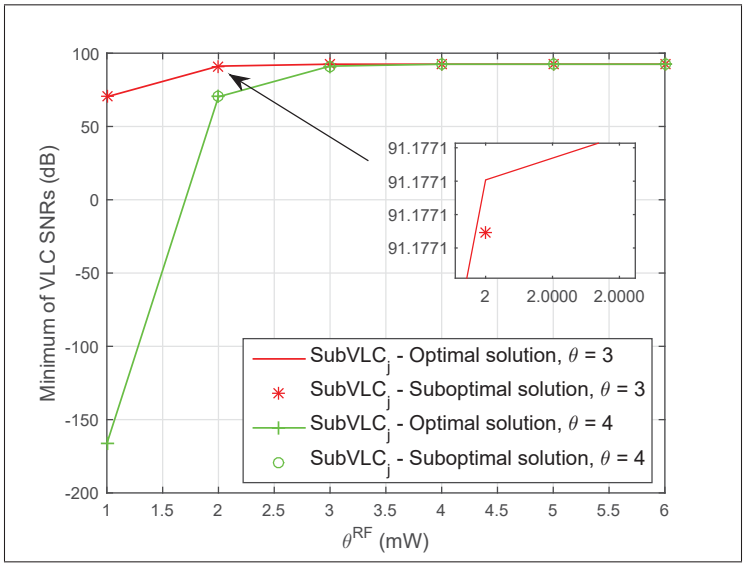


Figure 6.11 Suboptimality of the solution given in Lemma 2 to problem {SubVLC}

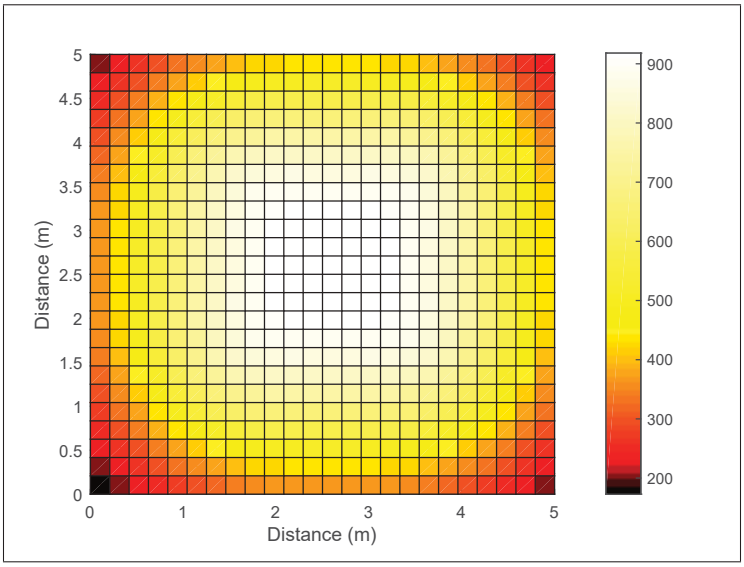


Figure 6.12 Illuminance in the considered area

## 6.6 Conclusion and Future Potential Research

In this work, we proposed a novel collaborative RF and lightwave resource allocation scheme for hybrid RF/VLC ultra-small cell networks. In the proposed scheme, the optical transmitters play the main role and deliver both the lightwave information and energy signals whereas the RF AP is an assistant and transfers wireless power over RF signals. Thus, the minimum of the VLC SNRs is maximized under the constraints of the sum of light and RF EH performances. On this basis, we provide the algorithms to solve the problems associated with the group of the optical transmitters and the RF AP optimally. Further, we derive a simple closed-form suboptimal solution to the optical transmitters' problem to facilitate the solving process. Particularly, the suboptimal solution can be seen as an efficient low-complexity alternative with high accuracy when the network needs to update solutions instantly. The numerical results indicate that the collaborative scheme significantly improves the overall network performance in terms of VLC SNR and EH metrics while maintaining an appropriate illumination in the area.

For future research, an extended scenario, in which multiple RF AFs cooperate with multiple optical transmitters, should be considered to improve both ID and EH performances and reduce

the transmit power. However, this scenario might lead to the increase in the hardness of finding optimal and suboptimal resource allocations. Furthermore, the system model in this work can also be developed with invisible light as an additional energy and information source, such as infrared light. Managing the invisible light band might be more flexbile than the visible one since it does not affect illumination. Nevertheless, resource allocation schemes need to carefully take human eye safety regulations into account.

# CHAPTER 7

# LIGHTWAVE POWER TRANSFER FOR FEDERATED LEARNING-BASED WIRELESS NETWORKS

Ha-Vu Tran[1], Georges Kaddoum[1], Hany Elgala[2], Chadi Abou-Rjeily[3], and Hemani Kaushal[4]

[1] Department of Electrical Engineering, École de Technologie Supérieure, 1100 Notre-Dame west, Montreal, Canada H3C 1K3.
[2] Electrical and Computer Engineering Department, University at Albany-State University of New York, Albany, NY, USA 12222.
[3] Department of Electrical and Computer Engineering of the Lebanese American University, Beirut, Lebanon.
[4] University of North Florida, Jacksonville, FL, USA.

Paper submitted to *OSA Optics Express*, November 2019.

## 7.1 Introduction

Recently, the concept of Federated Learning (FL) has been introduced by Google goo; Konecny, J., McMahan, H. B., Ramage, D. & Richtarik, P. (2016). The main idea behind FL is to build a shared learning model based on data sets that reside across multiple terminal devices while protecting data privacy. In FL networks, each device computes the gradient updates based on its local training data. The updates are then sent to a central server in order to be aggregated in the current global shared model. Afterward, the central server feedbacks the new global model to all devices. By doing so, raw local training data are not leaked.

In the past few years, FL has attracted increasing attention from the research community Konecny *et al.* (2016); Tran, N. H., Bao, W., Zomaya, A., Nguyen, M. N. H. & Hong, C. S. (2019); Yang, Q., Liu, Y., Chen, T. & Tong, Y. (2019). Nevertheless, the following critical issue was overlooked in the literature: in FL-based wireless networks, the mobile devices are energy-constrained and, hence, the energy consumed for executing FL might decrease the devices' lifetime significantly Tran *et al.* (2019). To overcome this issue, prolonging the devices' lifetime performed at the physical layer can be a prominent solution. In this regard, wireless lightwave energy recharging, through visible light (VL) and infrared light (IRL), has recently

gained great interest from both academia and industry Lig; wys (2019). Its high potential in enabling continuous wireless recharging has been confirmed in several reported works Diamantoulakis *et al.* (2018); Fakidis *et al.* (2016); Pan *et al.* (2017).

In this work, we propose the use of lightwave power transfer to enable new possibilities for the sustainability of future FL-based wireless networks. Accordingly, we consider a FL-based network scenario where each terminal device harvests energy from lightwave from from VL and IRL transmitted by an optical transmitter and then uses this energy for: (i) computing the gradient updates based on its local training data and (ii) conveying them to an access point (AP) via radio frequency (RF) uplink communication. On this basis, we aim to derive the resource allocation scheme to handle the power efficiency in the network. In this regard, optimizing the transmit light power from the optical transmitter, the time-slots of computation and uplink transmission at each device and the receive beamformers at the RF AP consitute interesting open research problems. In addition, the total energy consumption for executing FL is restricted by the harvested energy, and the uplink rate and the transmit power budget are constrained by preset thresholds. The resulting optimization problem is difficult to solve because multiple variables are coupled in constraints. Then, we propose a method to tackle the problem in an efficient way. The contributions of our work can be summarized as proposing, for the first time, the application of power transfer through light in FL-based wireless networks and deriving the optimal solution for the resulting problem.

## 7.2 System Model

We consider the network model depicted in Fig. 7.1 where one optical transmitter aims to recharge $J$ terminal devices by using VL and IRL in downlink transmission Lig while the devices communicate with an $M$-antenna RF AP through RF uplink transmissions. Each device is equipped with a single antenna, and a transparent solar panel integrated into the device's screen wys (2019). We consider the FL-based scenario described as follows:

- The terminal devices harvest energy from downlink VL and IRL. This energy will be used for accomplishing the FL tasks of computation and RF uplink transmission,
- Each device computes the gradient update to build a learning shared model based on its local training data. Next, the devices send their updates to the RF AP over the RF uplinks. Since the gradient updates must be synchronously aggregated at the RF AP, the devices need to finish their uplink transmissions at the same time.

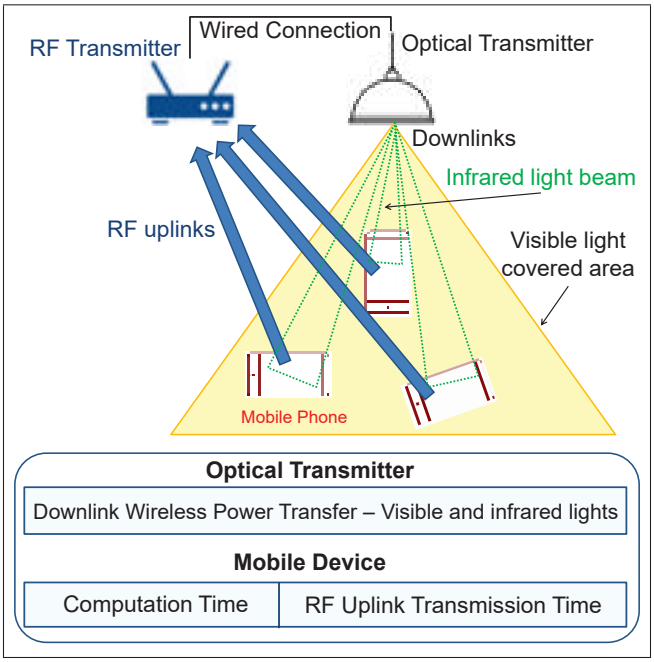


Figure 7.1 Scenario of lightwave power transfer for FL-based networks

### 7.2.1 Optical Downlink Wireless Power Transfer

#### 7.2.1.1 Channel Model

We consider optical channels with only the line-of-sight (LOS) component since the contribution of a non-line-of-sight (NLOS) component to the mission of power transfer could be neglected Diamantoulakis *et al.* (2018); Pan *et al.* (2017). Thus, the optical channel between the optical transmitter and the photodetector of device $j$ $(1 \leq j \leq J)$, denoted by $h_{i,j}$ (i.e.,

$i = \{0;1\}$, where $h_{0,j}$ and $h_{1,j}$ represent the visible light and infrared light channels, respectively), is given by Diamantoulakis *et al.* (2018):

$$h_{i,j} = \frac{A_j(m_i+1)}{2\pi d_j^2}\cos^{m_i}(\phi_{i,j})T_s(\psi_{i,j})g(\psi_{i,j})\cos(\psi_{i,j}), \tag{7.1}$$

where $A_j$ is the photodetector's active area, $m_i$ is the Lambert's mode number, $d_j$ is the distance between the optical transmitter and device $j$, $\phi_{i,j}$ is the irradiation angle, $\psi_{i,j}$ is the angle of incidence, $T_s(\psi_{i,j})$ is the optical band-pass filter gain, and $g(\psi_{i,j})$ is the optical concentrator gain. Moreover, $m_i$ and $g(\psi_{i,j})$ are computed according to the LED semi-angle at half-power, denoted by $\phi_{i,1/2}$, and the field of view (FOV), denoted by $\psi_{i,j,c} \leq \pi/2$, as in Diamantoulakis *et al.* (2018).

#### 7.2.1.2 Lightwave Energy Harvesting

The optical harvested energy at device $j$ is

$$\mathtt{EH}_j = \sum_{i=0,1} \mathtt{EH}_{i,j}, \tag{7.2}$$

where $\mathtt{EH}_{i,j}$ can be computed as Diamantoulakis *et al.* (2018)

$$\mathtt{EH}_{i,j} = f_{\text{opt}} I_{i,j,G} V_{i,j,c}, \tag{7.3}$$

in which $f_{\text{opt}}$ is the fill factor and $I_{i,j,G}$ is the generated DC current which can be calculated as

$$I_{i,j,G} = \nu P_{i,j} h_{i,j}, \tag{7.4}$$

where $\nu$ is the photodetector responsivity, $P_{i,j}$ is the transmit power of the DC component, and $V_{i,j,c}$ is the open circuit voltage computed as

$$V_{i,j,c} = V_t \ln\left(1 + \frac{I_{i,j,G}}{I_d}\right), \tag{7.5}$$

where $V_t$ is the thermal voltage and $I_d$ is the dark saturation current.

### 7.2.2 FL Computation Model

Each device keeps a local data set, denoted by $D$. In the supervised learning setting, the data may include $D$ input-output pairs, so that the task of each device is to find the model parameter that maps an input to an output. We denote the number of CPU cycles needed for each device to process one input-output pair by $c$. In particular, the value of $c$ can be computed offline Miettinen, A. P. & Nurminen, J. K. (2010).

Thus, the CPU energy consumption of each device to process all its data for one local iteration can be expressed as follows Tran *et al.* (2019)

$$E_j^{\text{comp}} = \frac{\alpha}{2} cD (f_j^{\text{CPU}})^2 = \frac{\alpha}{2} (cD)^3 \frac{1}{(T_j^{\text{comp}})^2}. \tag{7.6}$$

where $\frac{\alpha}{2}$ is the effective capacitance coefficient of each device's computing chipset and $f_j^{\text{CPU}}$ is the CPU-cycle frequency. Furthermore, the computation time per local iteration of each device is defined as $T_j^{\text{comp}} = \frac{cD}{f_j^{\text{CPU}}}$.

### 7.2.3 Radio Frequency Uplink Information Transmission

We denote the uplink transmission channel between device $j$ and the RF AP by $\mathbf{g}_j \in \mathbb{C}^M$. Accordingly, for a given transmission time $T_j^{\text{trans}}$, the achievable uplink data rate of device $j$ can be computed as

$$R_{U,j} = T_j^{\text{trans}} B \log_2 \left( 1 + \frac{\left| \mathbf{g}_j^H \mathbf{w}_j \right|^2 P_{U,j}}{\mathbf{w}_j^H \left( \sum\limits_{j' \neq j} \mathbf{g}_{j'} \mathbf{g}_{j'}^H + \sigma_0^2 \mathbf{I} \right) \mathbf{w}_j} \right), \tag{7.7}$$

where $B$ is the bandwidth, $\mathbf{w}_j \in \mathbb{C}^M$ denotes the receive beamforming vector at the RF AP for device $j$, $P_{U,j}$ is the transmit power of device $j$, $\sigma_0^2$ is the variance of the additive white Gaussian

noise (AWGN), $\mathbf{I}$ is the indentity matrix and $(.)^H$ stands for the Hermitian. Furthermore, the transmission energy consumption at user $j$ is

$$E_j^{\text{trans}} = T_j^{\text{trans}} P_{U,j}. \tag{7.8}$$

## 7.3 Problem Formulation and Proposed Solution

### 7.3.1 Problem Formulation

We aim to minimize the IRL transmit power, subject to the constraints of the RF uplink rate, the total energy consumption used for computation and transmission, and the power budget. Particularly, since illumination must be kept constant in the served area, the VL transmit power should not be considered as a variable in the problem formulation. Hence, the corresponding optimization problem can be formulated as follows:

$$\text{OP}_1: \quad \min_{\substack{\mathbf{w}_j, P_{1,j}, P_{U,j}, \\ f_j^{\text{comp}}, T_j^{\text{trans}}}} \quad \sum_{\forall j} P_{1,j} \tag{7.9a}$$

$$\text{s.t.:} \quad R_{U,j} \geq \theta_j, \quad (\forall j) \tag{7.9b}$$

$$E_j^{\text{comp}} + E_j^{\text{trans}} \leq \texttt{EH}_j, \quad (\forall j) \tag{7.9c}$$

$$0 \leq P_{1,j} \leq \texttt{P}_j, \quad (\forall j) \tag{7.9d}$$

$$T_j^{\text{comp}} + T_j^{\text{trans}} = 1, \quad (\forall j) \tag{7.9e}$$

$$f_j^{\min} \leq f_j^{\text{CPU}} \leq f_j^{\max}, \quad (\forall j) \tag{7.9f}$$

$$\left|\mathbf{w}_j\right|^2 = 1, \quad (\forall j) \tag{7.9g}$$

where constraint (7.9b) is set to ensure that the uplink rate of device $j$ is equal or larger than the threshold $\theta_j$. Constraint (7.9c) implies that the energy consumed for the computation and the uplink transmission should be lower than the harvested energy from the downlinks. The IRL transmit power is constrained in (7.9d) by the power budget $\texttt{P}_j$. In constraint (7.9e), the sum of

the computation time and the transmission time is normalized to one for simplicity. Constraint (7.9f) imposes the CPU-frequency range of the devices. Finally, constraint (7.9g) implies that the receive beamforming vectors have unit power.

It can be observed that $\mathrm{OP}_1$ has an intractable form since variables $\mathbf{w}_j, P_{1,j}, P_{U,j}, f_j^{\mathrm{CPU}}$, and $T_j^{\mathrm{trans}}$ are coupled in constraints (7.9b), (7.9c), and (7.9f). Hence, solving $\mathrm{OP}_1$ is challenging.

### 7.3.2 Proposed Optimal Solution

#### 7.3.2.1 Optimal Receive Beamformers $\mathbf{w}_j^\star$

We start by observing constraints (7.9b) and (7.9c). In this regard, we notice that (i) optimizing $\mathbf{w}_j$ does not impact optimizing $\mathbf{w}_{j'}$ $(\forall j' \neq j)$, and (ii) since the procedure for solving problem $\mathrm{OP}_1$ implies minimizing the sum of $E_j^{\mathrm{comp}}$ and $E_j^{\mathrm{trans}}$, the optimal value of $\mathbf{w}_j$ is the one maximizing $R_{U,j}$ to reduce $T_j^{\mathrm{trans}}$ and $P_{U,j}$, following from equations (7.7) and (7.8). In light of this discussion and (7.9g), the optimal value of $\mathbf{w}_j$ can be computed as

$$\mathbf{w}_j^\star = \arg \max_{|\mathbf{w}_j|^2=1} R_{U,j} \quad (\forall j). \tag{7.10}$$

Hence, based on Rayleight-Ritz quotient Parlett (1998), $\mathbf{w}_j^\star$ is the eigenvector corresponding to the largest eigenvalue of the matrix $\mathbf{g}_j\mathbf{g}_j^H \left(\sum_{j'\neq j} \mathbf{g}_{j'}\mathbf{g}_{j'}^H + \sigma_0^2\mathbf{I}\right)^{-1}$.

#### 7.3.2.2 Decomposing problem $\mathrm{OP}_1$ into subproblems

To make problem $\mathrm{OP}_1$ more tractable, we aim to eleminate variables $f_j^{\mathrm{comp}}$ and $T_j^{\mathrm{comp}}$. According to (7.6), and (7.9e), $E_j^{\mathrm{comp}}$ can be derived as

$$E_j^{\mathrm{comp}} = \frac{\frac{\alpha}{2}(cD)^3}{\left(1 - T_j^{\mathrm{trans}}\right)^2}. \tag{7.11}$$

Next, let $\Gamma_j = \frac{\left|\mathbf{g}_j^H \mathbf{w}_j^\star\right|^2}{\mathbf{w}_j^{\star H}\left(\sum\limits_{j' \neq j} \mathbf{g}_{j'} \mathbf{g}_{j'}^H + \sigma_0^2 \mathbf{I}\right)\mathbf{w}_j^\star}$. Hence, (7.7) and (7.9b) can be rewritten as

$$P_{U,j} = \frac{2^{\frac{\theta_j}{T_j^{\text{trans}} B}} - 1}{\Gamma_j}. \tag{7.12}$$

Thus, (7.8) can be rewritten as

$$E_j^{\text{trans}} = T_j^{\text{trans}} \frac{2^{\frac{\theta_j}{T_j^{\text{trans}} B}} - 1}{\Gamma_j}. \tag{7.13}$$

By substituting (7.11) and (7.13) into (7.9c), constraint (7.9c) can be further expressed as

$$\frac{\frac{\alpha}{2}(cD)^3}{\left(1 - T_j^{\text{trans}}\right)^2} + T_j^{\text{trans}} \frac{2^{\frac{\theta_j}{T_j^{\text{trans}} B}} - 1}{\Gamma_j} \leq \texttt{EH}_j. \tag{7.14}$$

Furthermore, in light of (7.6) and (7.9e), constraint (7.9f) can be rewritten as

$$0 < 1 - \frac{cD}{f_j^{\min}} \leq T_j^{\text{trans}} \leq 1 - \frac{cD}{f_j^{\max}} < 1. \quad (\forall j) \tag{7.15}$$

Based on the characteristic of $\text{OP}_1$, one can observe that minimizing the sum of optical powers is equivalent to minimizing the individual ones. This follows from the fact that the variables associated with each user are not coupled. Moreover, it can be seen that $\texttt{EH}_j$ is an increasing function of $P_{1,j}$, seeking to be minimized. Thus, this implies that $P_{1,j}$ reaches its minimum when the part on the left side of (7.14) reaches its minimum over variable $T_j^{\text{trans}}$. Without loss of optimality, we decompose $\text{OP}_1$ into the two following subproblems

$$\begin{aligned} \text{SubOP}_{j1}\text{:} \quad & \min_{T_j^{\text{trans}}} \quad \Psi(T_j^{\text{trans}}) && \text{(7.16a)} \\ & \text{s.t.:} \quad \text{eq. (7.15)}, \end{aligned}$$

$$\text{SubOP}_{j2}: \quad \min_{P_{1,j}} \quad P_{1,j} \tag{7.17a}$$

$$\text{s.t.:} \quad \texttt{EH}_j = \varepsilon_j^{\star}, \tag{7.17b}$$

$$(7.9\text{d}),$$

where $\varepsilon_j^{\star} = \dfrac{\frac{\alpha}{2}(cD)^3}{\left(1-T_j^{\star\text{trans}}\right)^2} + T_j^{\star\text{trans}} \dfrac{2^{\frac{\theta_j}{T_j^{\star\text{trans}}B}}-1}{\Gamma}$, $T_j^{\star\text{trans}}$ is obtained by solving $\text{SubOP}_{j1}$, and

$$\Psi(T_j^{\text{trans}}) = \frac{\frac{\alpha}{2}(cD)^3}{\left(1-T_j^{\text{trans}}\right)^2} + T_j^{\text{trans}} \frac{2^{\frac{\theta_j}{T_j^{\text{trans}}B}}-1}{\Gamma_j}.$$

#### 7.3.2.3 Optimal Transmission Time $T_j^{\star\text{trans}}$

Considering $\text{SubOP}_{j1}$, it is convex in the genernal sense. The convexity of $\text{SubOP}_{j1}$ can be verified by evaluating the second derivative as follows

$$\frac{\mathrm{d}^2\Psi(T_j^{\text{trans}})}{\mathrm{d}(T_j^{\text{trans}})^2} = \frac{3\alpha(cD)^3}{\left(1-T_j^{\text{trans}}\right)^4} + \frac{\theta_j^2 2^{\frac{\theta_j}{T_j^{\text{trans}}B}}}{B^2(T_j^{\text{trans}})^3\Gamma_j}, \tag{7.18}$$

which is larger than 0 under constraint (7.15). $\text{SubOP}_{j1}$ can be solved using the Golden-section search method Press, W. H., Teukolsky, S. A., Vetterling, W. T. & Flannery, B. P. (2007) in which $T_j^{\text{trans}}$ is updated until convergence with the following rule:

| |
|---|
| If $\Psi(a_{n+1}) \leq \Psi(b_{n+1})$ then $T_j^{\text{trans}} \in [a_n, b_{n+1}]$. |
| Else $T_j^{\text{trans}} \in [a_{n+1}, b_n]$. |

Herein, $a_{n+1} = a_n + \rho(b_n - a_n)$, $b_{n+1} = a_n + (1-\rho)(b_n - a_n)$, $\rho = \frac{3-\sqrt{5}}{2}$, $a_0 = 1 - \frac{cD}{f_j^{\min}}$, $b_0 = 1 - \frac{cD}{f_j^{\max}}$.

#### 7.3.2.4 Optimal Power $P_{1,j}^{\star}$

Constraint (7.17b) can be rewritten as

$$\mathtt{EH}_{1,j} = \varepsilon_j^{\star} - \mathtt{EH}_{0,j}, \quad (\forall j) \tag{7.19}$$

Following from (7.3), (7.4), and (7.5), constraint (7.17b) can be further reformulated as

$$\ln\left(1 + \frac{I_{i,j,G}(P_{1,j})}{I_d}\right) \geq \frac{\varepsilon_j^{\star} - \mathtt{EH}_{0,j}}{f_{\text{opt}} V_t I_{i,j,G}(P_{1,j})}, \tag{7.20}$$

where $I_{i,j,G}(P_{1,j})$ denotes that $I_{i,j,G}$ is a function of $P_{1,j}$. Accordingly, replacing (7.17b) by (7.20), problem SubOP$_{j2}$ can be tackled by a bisection-based algorithm Press *et al.* (2007). By setting $P_{\min} = 0$ and $P_{\max} = \mathtt{P}_j$, $P_{1,j}$ is updated until convergence through the rule below:

| |
|---|
| If (7.20) is satisfied with $P_{1,j} = \dfrac{P_{\min} + P_{\max}}{2}$, then $P_{\min} = P_{1,j}$. Else $P_{\max} = P_{1,j}$. |

## 7.4 Numerical Results

Table 7.1 Important parameters

| **Parameters** | **System values** |
|---|---|
| The optical band-pass filter gain, $T_s(\psi_{i,j})$ | 1 |
| The field of view, $\psi_{i,j,c}$ | 70° |
| The LED semiangle at half-power, $\phi_{0,1/2}$ | 60° |
| The photodetector's active area, $A_j$ | 85 cm$^2$ (phone screens) |
| Distances, $[d_1 \quad d_2 \quad d_3]$ | $[2.2 \quad 2.1 \quad 2]$ |
| VL and IRL transmit power, $P_{0,j}$ and $P_{1,j}$ | 28 W **?** and 15 W Lig |

Regarding the uplink RF channels, we set $M = 4$ and the three devices, namely 1, 2, and 3, are located 3.3 m, 3 m, and 2.7 m away from the RF AP, respectively. Further, the uplink RF channels are assumed to have a Rician distribution with the Rician factor equal to 8 dB and the pathloss exponent factor equal to 2.6. For the optical downlink channels, important

parameters are listed in Table 1. For the uplink rate, $B = 1$ MHz, and $\sigma_0^2 = 10^{-10}$ W. For the light EH model, $I_d = 10^{-9}$ mA, $f_{\text{opt}} = 0.75$, and $\nu = 0.4$ A/W (i.e. silicon solar cell). For the computation model, $\alpha = 2 * 10^{-28}$, $c = 20$, $D = 10$ Mb, $f_j^{\max} = 1.5$ GHz, and $f_j^{\min} = 0.3$ GHz Tran *et al.* (2019). The simulation is carried out over 10000 channel realizations.

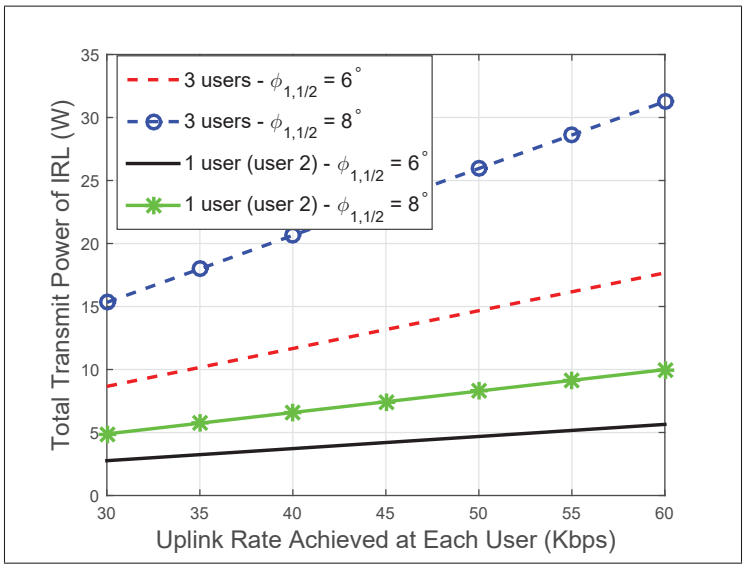


Figure 7.2 Total transmit IRL power versus the uplink rate

Fig. 7.2 presents the variation of the total transmit IRL power with respect to the uplink rate threshold $\{\theta_j\}$ for different values of $\phi_{1,1/2}$. It can be observed that the higher the uplink rate is, the higher the IRL power that needs to be transferred by the optical transmitter. Furthermore, using a lower $\phi_{1,1/2}$ (which implies a narrower IRL beam) reduces the required transmit power while maintaining the same uplink rates. With the used system settings, the uplink rate needed for the FL updates is 36 Kbps Tran *et al.* (2019). Therefore, the proposed approach can support the mobile devices in handling the FL tasks without expending any power from their batteries.

In Fig. 7.3, the optimal ratios of $\{T_j^{\text{trans}}\}$ to $\{T_j^{\text{comp}}\}$ at the devices are shown with different values of the uplink rate. It is observed that device 3, the nearest device to the RF AP, has the shortest transmission time. This can be explained that a longer distance requires a higher $E_j^{\text{trans}}$ and hence a higher $T_j^{\text{trans}}$ following from (7.8). Further, setting a higher $\theta$ requires not only a higher transmit power (as in fig. 7.2) but also a longer transmission time. In these cases,

since the computation tasks are the same for all the devices, the optimal management implies increasing the transmission time rather than the computation time.

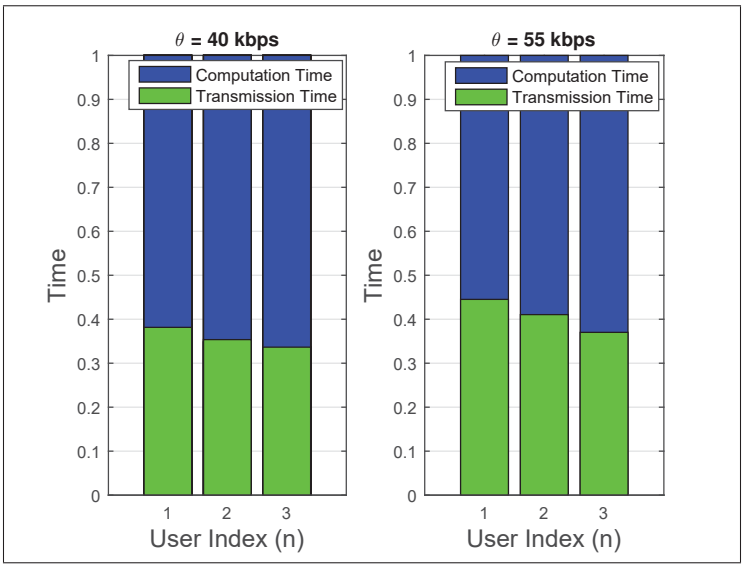


Figure 7.3 Transmission time vs. computation time ($\{\theta_j\} = \theta$)

## 7.5 Conclusion

In this work, we proposed for the first time the application of the lightwave power transfer to the FL-based wireless networks. On this basis, we devised a strategy to manage the power efficiency of the network and formulated the corresponding optimization problem. Moreover, we provided the algorithms to tackle the problem optimally. The numerical results indicate that the proposed scenario can sufficiently replenish energy for the terminal devices to open up new opportunities for sustainable FL-based wireless networks.

# CHAPTER 8

# COLLABORATIVE RF AND LIGHTWAVE POWER TRANSFER FOR NEXT-GENERATION WIRELESS NETWORKS

Ha-Vu Tran[1], Georges Kaddoum[1], and Chadi Abou-Rjeily[2]

[1] Department of Electrical Engineering, École de Technologie Supérieure,
1100 Notre-Dame west, Montreal, Canada H3C 1K3.
[2]Department of Electrical and Computer Engineering of the Lebanese American University,
Beirut, Lebanon.

Paper submitted to *IEEE Communications Magazine*, June 2019.

## 8.1 Introduction

The rise of the information and communication technology (ICT) era has led to the massive deployment of wireless devices in diverse networks, including the fifth generation (5G) cellular, Internet-of-Things (IoT), and E-healthcare networks Kamel, M., Hamouda, W. & Youssef, A. (2016). Generally, a substantial burden is on these devices, where their constant provision of wireless access and the fact that they are battery operated, and thus energy-constrained, severely affects their operational lifetime. Replacing the battery may seem like a simple task; however, given the ever-increasing number of devices and their limited accessibility in some applications (e.g., in hazardous environments), battery replacement is often operationally expensive or infeasible.

To cope with this issue, simultaneous wireless information and power transfer (SWIPT) technology has been proposed, which enables wireless devices to be continuously recharged via electromagnetic waves Clerckx *et al.* (2019); Diamantoulakis *et al.* (2018), and opens new possibilities for the sustainability of future networks. SWIPT based on transmitted radio frequency (RF) waves is an interesting solution; however, due to the inevitable spectrum crunch, solely relying on RF may not be possible due to the need to jointly meet the expectations of (i) 10-fold longer device battery lifetime Gupta, A. & Jha, R. K. (2015a), and (ii) global mo-

bile data traffic in excess of 100 exabytes Ericsson (2017), while respecting the transmit power constraints imposed due to various safety concerns WHO (2007).

Recently, optical wireless communication (OWC) has emerged as a complementary technology to RF for the provisioning of indoor wireless links Pathak *et al.* (2015). On the platform of OWC, wireless energy recharging over lightwave, i.e., visible light (VL) and infrared light (IRL), has recently attracted a surge of attention from both academia and industry. The high potential of lightwave power transfer techonology has been confirmed in several previous works Diamantoulakis *et al.* (2018); Fakidis *et al.* (2016); Pan *et al.* (2017). However, this technology may only be used if a line-of-sight (LoS) is available in order to transfer a sufficient amount of power for energy harvesting (EH). In addition, VL is constrained by the requirement to maintain constant illumination while IRL is restricted by eye- and skin-safety conditions saf (2001).

It is apparent from their relative advantages and disadvantages that RF and lightwave wireless power transfer approaches are complementary rather than competitive technologies. Since the combination of lightwave and RF can entirely exploit the efficacy of both the RF and lightwave bands for wireless power transfer (WPT), it is possible to retain RF pollution lower than the safe limit while increasing the WPT performance. Therefore, the novel combination and the joint optimization of the RF and lightwave power transfer has the potential to efficiently provide safe and reliable WPT technology for next-generation networks.

This article focuses on the applications of the RF and lightwave power transfer for indoor wireless communication networks. Its core contents are described as follows: First, a brief overview of the current RF and lightwave-based WPT techniques are presented and the associated health and safety concerns are discussed. We then present a novel framework for collaborative RF and lightwave power transfer, consisting of a transceiver architecture witcomplementary rather than competitive technologies. Since the combination of lightwave and RF can entirely exploit the efficacy of both the RF and lightwave bands for wireless power transfer (WPT), it is possible to retain RF pollution lower than the safe limit while increasing the WPT performance. There-

fore, the novel combination and the joint optimization of the RF and lightwave power transfer has the potential to efficiently provide safe and reliable WPT technology for next-generation neth four communication and power transfer protocols. Finally, future research directions are comprehensively discussed.

## 8.2 RF and Lightwave Power Transfer and Related Health Concerns

Although both RF and lightwave communications have revolutionized our world, they can have detrimental effects on the health of individuals and hence must be deployed with care. In this section, we provide a brief overview of RF and lightwave power transfer, and discuss some related health concerns.

### 8.2.1 RF Wireless Power Transfer

RF WPT is a technique that wirelessly delivers electrical energy over RF signals to recharge the devices in next-generation cellular, wireless body area, and IoT networks. Deploying RF WPT systems introduces several new concerns for human health due to RF radiation. In RF WPT systems, the operating power level of an EH receiver, i.e., $-10$ dBm, is much higher than that of a conventional information decoding (ID) receiver, i.e., $-60$ dBm Clerckx *et al.* (2019). To enable RF WPT, manufacturers and network operators need to increase the transmit power levels to achieve a reasonable EH performance at the receiver side. In addition, since RF WPT systems are often deployed in buildings where people could be stationary or moving, human bodies may unexpectedly block the transmission. This not only causes a significant EH performance loss at the intended devices but may also result in adverse human health effects due to exposure to RF fields WHO (2007). These effects include localized heating or stimulation of excitable tissue.

More specifically, according to the IEEE C95.1-2005 Standard, regarding the continuous and long-term exposure of individuals to RF signals, the fundamental restriction of the specific absorption rate (SAR) for frequencies between 100 kHz and 3 GHz is 0.08 W/kg, averaged

over any 6-minute-reference-period (IEE, 2005, pp. 20). Concretely, assuming a body mass of 60 kg, there is a SAR limit of 4.8 W averaged over a period of 6 minutes that can be applied on a human body. This limit guarantees that there is no risk of any adverse effects on human health.

Although the RF WPT approach has gained much support from the industry over the past few years, the safety concern is considered by only few companies yet, as shown in Table 8.1. However, it is obvious that addressing the human safety results in a strict limit for the wireless energy beamed to devices. Moreover, in practical scenarios, the actual harvested energy might be much lower than the beamed energy due to energy conversion losses. Thus, novel technologies must be considered for the realistic implementation of WPT in future networks.

Table 8.1 RF and lightwave WPT in industry

| Company | RF WPT | RF EH | Light WPT | Light EH | Health Safety |
|---|---|---|---|---|---|
| Powercast | ✓ | ✓ | | | ✓ |
| Energous Corp | ✓ | ✓ | | | ✓ |
| Samsung Electronics Co Ltd | ✓ | | | | |
| Intel IP Corp | ✓ | | | | |
| Drayson Technologies (europe) Ltd | ✓ | ✓ | | | |
| Qorvo US Inc | ✓ | ✓ | | | |
| RF Micro Devices Inc | ✓ | ✓ | | | |
| BlackBerry Ltd | ✓ | ✓ | | | |
| Rakuvisions LLC | ✓ | | | | ✓ |
| Kim Jae Beom | ✓ | | | | |
| International Business Machines Corp | ✓ | | | | |
| Ossia Inc | ✓ | ✓ | | | |
| Origin Wireless | ✓ | | | | |
| Qualcomm | ✓ | | | | |
| Wi-Charge | | | ✓ | ✓ | ✓ |
| Sunpartner Technologies | | | | ✓ | |

### 8.2.2 Lightwave Power Transfer: Visible and Infrared Light

Inspired by the high potential of OWC technology, lightwave WPT and EH from artificial light is attracting increasing attention. This new approach has already been invested by several companies, as shown in Table 8.1.

There are two main research directions of lightwave power transfer: using VL and using IRL. In the case of visible lightwave power transfer, which uses the $30-770$ THz spectrum band, the achievable EH performance for indoor visible light communication (VLC) networks is quite limited. The reason behind this is twofold: (i) the intensity of LED lights is lower than that of solar light and LED bulbs in buildings are not always turned on, and (ii) the illumination in indoor living environments should be from 200 luminous flux (lx) to 1000 lx to respect the eye safety standard Eur. Meanwhile, the main advantage of VLC is that the indoor light brings *free* energy since there is no extra transmit power needed from the lighting system. Moreover, a recently developed transparent solar panel, Wysips Crystal wys (2019), promises to significantly improve light EH performance. This renders the implementation of lightwave power transfer remarkably practical.

On the other hand, the infrared spectrum ($300-400$ THz band) causes no light pollution to human eyes, and therefore is less constrained. Nonetheless, incautiously handling the light emission in this band could cause injuries to humans. Thus, network operators need to obey the safety standard of the irradiance on eyes and skin, i.e., for example, 0.005 W/m$^2$ at wavelength 905 nm for long-time exposures saf (2001). This limitation is general for IRL-applied wireless networks and not particularly related to IRL power transfer. Meanwhile, since IRL does not cause light pollution to human eyes; to improve the efficiency of EH, the optical transmitter can form very narrow light beams with high intensity over the safety standard but must keep the light beams away from the human body. Particularly, IRL can be interrupted when the link is blocked by using the distributed resonating laser method Liu, Q., Wu, J., Xia, P., Zhao, S., Chen, W., Yang, Y. & Hanzo, L. (2016), which can diminish any possible health risks. Indeed, the high potential of this approach has been demonstrated. For instance, as an impressive progress in the field, the Wi-Charge company has recently developed a product, the LIGHTS transmitter, able to deliver 5 W over 5 meters using IRL Lig.

Rather than the above discussion, the combination of RF and lightwave power transfer is important even when only using RF is sufficient to not provoke any health risks. To this end, it can be seen that the lightwave and RF WPT are complementary technologies. In the next sec-

tion, we will discuss how we can combine them to enable novel safe WPT for next-generation networks.

## 8.3 Enabling Collaborative RF and Lightwave Power Transfer

Since RF, VL, and IRL do not interfere with each other, they may be applied to WPT in a mutually supportive way. In this section, we present a novel architecture for collaborative RF and lightwave power transfer networks as well as four distinct communication and power transfer protocols for different scenarios.

### 8.3.1 Collaborative RF and Lightwave Power Transfer Architectures

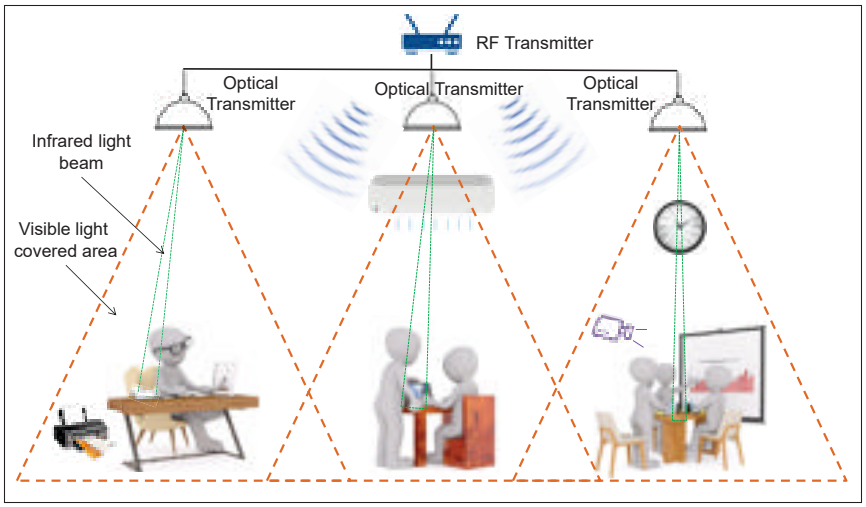


Figure 8.1 An illustration of the proposed collaborative RF and lightwave power transfer network

The combination of RF and lightwave power transfer can fully exploit the multi-band efficacy of RF, VL, and IRL for WPT, while satisfying the safety induced transmit power constraints per band. Fig. 8.1 illustrates a collaborative RF and lightwave power transfer network scenario where terminal devices can accumulate the energy harvested from light and RF.

The transmitter architecture, based on a joint design of optical and RF transmitters, is shown in Fig. 8.2a. In most cases, each optical transmitter, generally an LED bulb, only has a micro-

controller. Therefore, all computational tasks are processed at the RF transmitter, which is often equipped with a powerful digital baseband unit.

The proposed receiver architecture is shown in Fig. 8.2b. In this architecture, the photodetector is responsible of receiving both data and energy from the light which is then conveyed to an alternating current (AC)-to-direct current (DC) separator in order to extract the DC component from the light signals for the EH purpose. The separation can be performed in the time domain or the power domain Diamantoulakis *et al.* (2018) and will be further described in Subsection III.B. Moreover, RF signals, received from antennas, are split into two parts for information decoding (ID) and EH. The part for ID is conveyed to the information receiver, while the one for EH is directed to the EH unit where it is converted to DC form. Based on the harvested energy from both RF and light and concurrent energy consumption, the energy management module decides either to draw energy from the storage or convey excessive energy to the storage for future use.

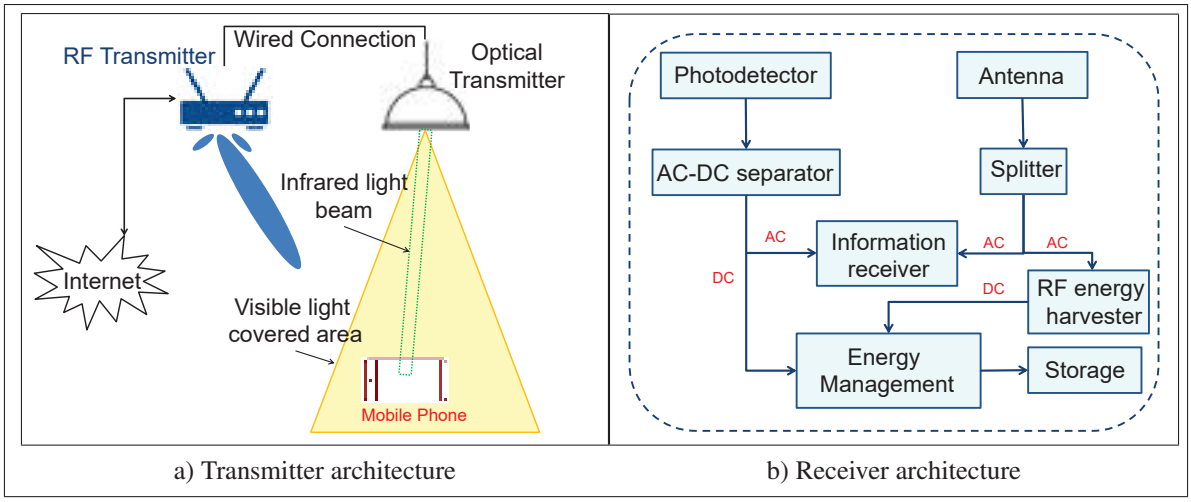


Figure 8.2 Proposed transceiver design

### 8.3.2 Information and Power Transfer Protocols

Indeed, there are many possible combinations of using VL, IRL, and RF according to network requirements. However, to maximize total power transfer performance while maintaining in-

formation transmission, our idea is to allocate the primary function of delivering information and power to IRL, while the RF and the VL act as complimentary wireless power sources. It can be explained by that IRL are able to provide significantly higher data rates than RF Pathak *et al.* (2015). Additionally, the IRL band is more convenient than the VL band for transferring energy because there are no constraints on consistent lighting in covered areas.

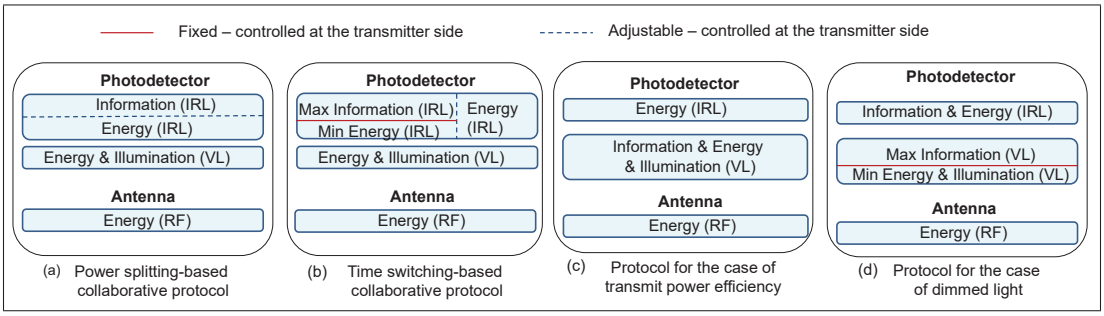


Figure 8.3 Information and power transfer protocols

In this context, motivated by the fact that the ID and EH performances can be managed in the time and power domains, we first introduce two preliminary protocols, namely (a) and (b), as follows.

**Protocol (a):** A power splitting-based collaborative protocol is shown in Fig. 8.3a, where the RF only deliver energy, IRL conveys both information and energy, and VL maintains the illumination in the served area and also contribute to EH performance. In this context, AC and DC-biased components of the IRL signals determine the ID and EH performance, respectively. Thus, managing the ID and EH performances can be achieved by adjusting the ratio between the AC and DC powers.

**Protocol (b):** The IRL carries both information and power whereas the RF and VL convey energy and illumination, respectively. This protocol is quite similar to protocol (a); however, the management of the ID and EH associated to the IRL relies on time switching as shown in Fig. 8.3b. In this context, the time frame is divided into two time-slots for information transmission and power transfer, where the performances of information and energy are maximized,

respectively. Particularly, since IRL signals always include a DC-biased component; the light energy can also be harvested in the time-slot dedicated to information transmission.

Furthermore, on this basis of protocols (a) and (b), we then present two more protocols (c) and (d) to address the specific cases where the served areas have strong background light and dimmed light, respectively, in the following.

**Protocol (c):** This protocol, presented in Fig. 8.3c, is designed for the case of transmit power efficiency. The main motivation behind this protocol is due to the fact that although IRL can deliver data at very high rates as VL, it consumes additional transmit power. However, as mentioned, no extra transmit power needed from the lighting system for VL to convey either information or energy. Hence, in protocol (c), we propose releasing IRL from the task of information transmission. More specifically, IRL and RF is in charge of transferring power while VL is responsible of delivering information, power, and proper illumination by using either the similar power-splitting or time switching manner given in protocols (a) and (b).

**Protocol (d):** In contrast with protocol (c), this protocol addresses the scenario of dimmed light in the served areas, e.g., a bedroom during rest time. The use of VL, in this case, is set in a dimmable configuration that only focuses on maximizing ID performance with low-intensity light. This is mainly due to the fact that although the light intensity can be enough to ensure a reasonable data rate, it might be insufficient for harvesting energy. In this protocol, IRL and RF play a complementary role to improve the ID or EH performance whenever necessary. Also, IRL can be handled by either the power-splitting or time switching manner.

Note that in the proposed protocols, the ratio between AC and DC components and the RF power-splitting factor can be optimized according to various requirements of the network.

### 8.3.3 Performance of Collaborative RF and Lightwave Power Transfer

We simulate a network consisting of a four-antenna RF transmitter, an optical transmitter, and three single-antenna terminal deivces equipped with a solar pannel.

First, in order to visualize the safety level of the standalone RF WPT, a heat map of RF radiation with respect to transmit power levels is shown in Fig. 8.4. In this simulation, the channel model is subjected to the Rician fading with the Rician factor equal to 6 dB and the pathloss exponent equal to 2.6. The devices are 4 meters far from the RF transmitter. For simplicity, maximal ratio transmission (MRT) beamformer is used and the transmit power is equally allocated to each device. According to the IEEE C95.1-2005 Standard, there is a SAR limit applied on a person with 60 kg body mass which implies that only 13.3 mW EH rate can be beamed towards the person. On this basis, in Fig. 8.4, the green areas indicate the safe zones for a person. In practice, the safe zone might be rather small because of the existence of numerous RF transmitters.

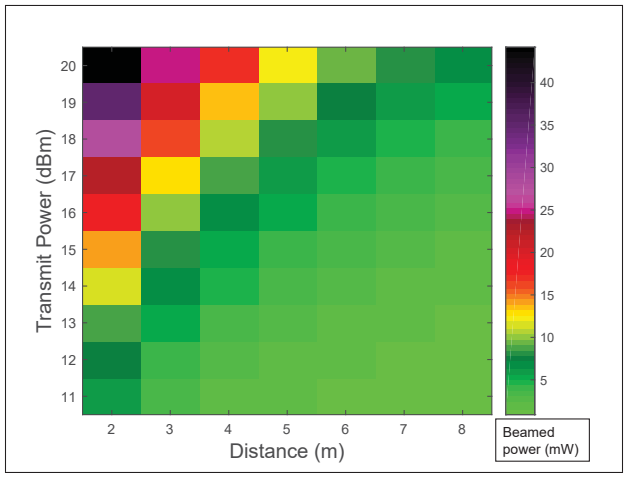


Figure 8.4 Heat map of the RF radiation

As observed in Fig. 8.5a, VL and IRL can offer a much higher data rate than RF. Nevertheless, RF outperforms VL when considering the EH performance. Further, the achievable performance of the four proposed protocols is depicted in Fig. 8.5b. According to LIGHTS transmitter Lig, the IRL can be used to transfer watts of energy. However, in our application, we consider the case of IoT devices where only milliwatts are harvested. In general, the combined use of RF, VL, and IRL expands the rate-energy region significantly compared to the sole use of either of the three resources. In Fig. 8.5b, the RF transmit power is reduced to 16 dB, implying a wider safe zone. However, the achievable EH of any protocol still outperforms

the EH of any individual approaches in Fig. 8.5a. In fact, the collaborative RF and lightwave power transfer approach allows us to reduce the RF radiation while maintaining a decent EH performance.

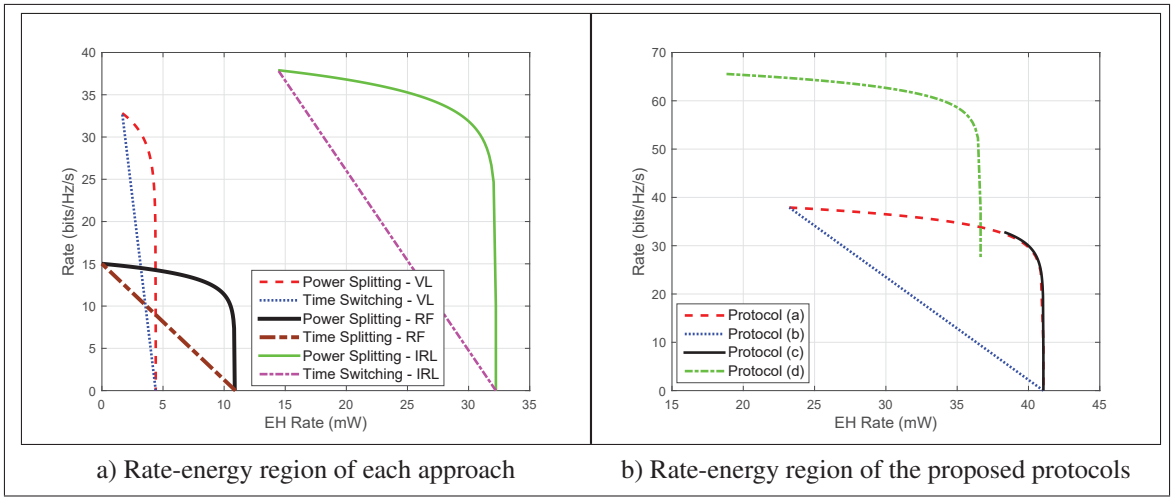


a) Rate-energy region of each approach b) Rate-energy region of the proposed protocols

Figure 8.5 Scenarios of collaborative RF and lightwave power transfer

## 8.4 Future Research Opportunities

Since RF, VL, and IRL are complementary to each other, their combination can be applied to many interesting applications in next-generation networks. In the following, we discuss some future research opportunities.

### 8.4.1 Indoor Applications

#### 8.4.1.1 Secure Wireless Powered Communication Networks

Beside the benefits of data rate, wireless energy transfer, and illumination; the applications of the proposed collaborative approach, in nature, can also offer high security at the physical layer of wireless networks. In other words, the combination of RF, VL, and IRL can be extensively exploited to design new secure WPT scenarios to better protect information while transfering data and wireless energy to devices. More specifically, it is motivated due to the fact that since

light cannot pass through opaque structures, the information it carries is secured from users in other rooms or buildings. However, even though security is one of the main advantages of OWC, dealing with the circumstance when eavesdroppers exist in the covered network area, i.e., in the same room, is challenging. For instance, assume that eavesdroppers are able to detect optical and RF signals. If the eavesdroppers are passive, the design of angle-diversity optical transmitters with color allocation may help improve the network security, whereas RF can play a role as artificial noise to decrease the eavesdropping performance while enhancing the EH performance at the device. If the eavesdroppers are active and jam the network using either RF or IRL (they may not use VL to jam the network since this manner will be able to reveal their position), the network may use VL for secure communications while jamming back the eavesdropper using RF and IRL. Additionally, as a consequence, the EH performance is improved.

#### 8.4.1.2 E-Healthcare

With the development of ICT, doctors can diagnose patients remotely. Thus, data transferred from medical devices to the doctors should be accurate and timely because it might be critical to the lives of patients. The use of the lightwave for downlink can replenish energy for medical or security devices such as handheld medical instruments, sensors, and smart locks for health monitoring, and indoor localization. Indeed, this technology is a promising candidate for E-Healthcare, particularly in Telemedicine and Mobile Health (mHealth) applications where patients can be connected with doctors and nurses in hospitals, at home, or anywhere through one secure platform. Further, in these indoor applications, one of the main challenges is providing high quality services while accounting for human eye safety regulations carefully and maintaining consistent illumination in served areas.

### 8.4.2 Outdoor Applications

#### 8.4.2.1 Unmanned aerial vehicles

In a disaster situation, such as an earthquake, providing continuous wireless communication is vital for rescuing victims. In such situations, unmanned aerial vehicles (UAVs) could act as a relay to convey information as well as to recharge devices over the air. A group of UAVs can maintain communication and simultaneously recharge some devices, while searching for victims in devastated buildings. In this hazardous circumtance, RF can be used to provide continuous transmission for alert and command signals, which are not in need of high data rate communication. Otherwise, lightwave is employed. Regarding wireless power transfer, in the presence of LoS transmission, since narrow light beams can be created more conveniently than narrow RF beams, the lightwave power transfer is preferred. Otherwise, RF is a more suitable option. In this scenario, optimizing the position of the group of UAVs to improve energy transfer efficiency is one of the most crucial challenges. Further, the health safety of victims and rescue staffs should be guaranteed while delivering wireless power.

#### 8.4.2.2 Underwater Communication and Power Transfer

While RF is an efficient approach for terrestrial communications, its use for underwater communications faces many difficulties due to dramatic absorption losses. Generating RF signals for underwater communications requires a considerable antenna size and a tramendous transmit power, namely in hundreds of Watts, to achieve a 100 Mbps data rate. Further, the use of RF for wireless power transfer is very challenging. On the other hand, narrow light beams can be generated at a low cost and only need several Watts to achieve Gbps data rates. Therefore, lightwave outperforms RF for underwater applications. However, this scenario might entail a big challenge in terms of dealing with pointing errors due to bore-sight and jitter effects to maintain a reasonable EH performance under when both transmitters and receiver are moving. Hence, a hybrid scheme, where lightwave is used to transmit power and information at high data rates over shorter range whereas RF is employed to send command and control signals

(i.e., not requiring high data rates) over the longer range, is a promising future direction for this field.

## 8.5 Conclusion

In this article, we presented a brief overview of RF and optical power transfer techniques. Furthermore, we introduced a framework for collaborative RF and lightwave power transfer. In this regard, we developed a transceiver architecture suitable for hybrid RF and optical WPT. Moreover, four communication and power transfer protocols for distinct scenarios were proposed and challenged through simulations. We showed that supplemental performance gains can be achieved by intelligently combining RF and lightwave technologies. Finally, several future research directions have been highlighted to foster continuous advancement in this area. It is firmly believed that this will become a fruitful research topic in the very near future. We hope this article will inspire future research on this topic.

# CONCLUSION AND RECOMMENDATIONS

## 9.1 Conclusion and Learned Lessons

Contemporarily, the world has witnessed the explosive development of ICT where 5G and IoT are the key technologies. Due to the explosive progress of smart devices, such as Android and Apple mobile phones, and the success of social networks, such as Instagram and Facebook, the demands of heterogeneous wireless communication services have been exponentially increasing. Nevertheless, generating sufficient power to supply ICT will produce carbon footprint and then pollute the environment. For example, the electricity consumption by Facebook is equivalent to by New York city. Also, in 2012, the $CO_2$ emission in Quebec is 78.3 metric tons carbon dioxide equivalent (Mt CO2 eq.) and is expected that the emissions achieve 20% below 1990 levels by 2020 Can (2015). Particularly, the ICT industry, one of the topics gaining the top-most priority identified by the government of Quebec, generates a significant amount of $CO_2$. Indeed, the energy cost and $CO_2$ emissions have been promptly growing due to the ICT network operation. The aim to future green networks is not only an emerging issue in Quebec, but also a global trend towards re-greening the world.

Over past few years, green radio communication has attracted much research work on energy saving to reduce the footprint from the ICT. Indeed, regreening future networks can be identified as a crucial element in the action dealing with the climate change because it can facilitate substantial cuts in global greenhouse gas emissions. Generally speaking, this dissertation focuses on four aspects: (i) minimizing power consumption, (ii) extending the lifetime of wireless devices, (iii) exploiting available green natural resources and recyling RF and indoor light signals in order to reduce carbon footprint, (iv) reducing electromagnetic pollution to protect human health. In this vein, various resource allocation approaches for future green wireless networks have been studied. To achieve all the aspects simultaneously, this thesis pro-

posed promising schemes to optimally manage and allocate resources in future networks. To be specific, the thesis contributions are summarized as follows:

- In Chapter 2, we proposed the utilization of the TR technique in femtocell networks and designed a new efficient power allocation scheme for HetNets where the backhaul connection provides only an insufficient capacity for signaling exchange. Numerical results confirm a siginificant transmit power saving in femtocell working environments.
- Chapter 3 presented an overview of some promising trends in future green networks. According to the principles of EH techniques, various concepts such as HetNet, mm-wave, and IoT networks, have been considered. In particular, we concentrated on a promising architecture: the green RF-WPT, which plays a vital role as a bridge between natural energy resources and smart energy-hungry devices.
- Chapter 4 proposed an innovative integrated information and energy receiver architecture based on the AC computing methodology. It was shown that the proposed architecture not only improves the computational ability of IoT devices but also the energy efficiency.
- Chapter 5 introduced a novel approach for allocating resources in SWIPT systems under a nonlinear EH model, where various crucial requirements related to the power consumption minimization, RF EH performance and the effect of calibration error, need to be concurrently operated. Thus, the algorithms and the closed-form solutions to tackle these problems were provided. In order to highlight the effectiveness of our work, the proposed scheme was then compared with existing benchmarks and baseline.
- Chapter 6 proposed a novel collaborative RF and lightwave resource management design for hybrid RF/VLC ultra-small cell networks. Further, we derived optimal solutions and a simple closed-form suboptimal solution to aid the solving process. It was demonstrated that the collaborative scheme significantly enhances the overall power efficiency and reduces RF pollution while supporting an appropriate illumination in the area.

- In Chapter 7, we proposed the employment of lightwave power transfer in FL-based wireless networks. In this vein, we introduced a scheme to handle the network power efficiency. It was indicated that the proposed scheme can sufficiently recharge energy for the terminal devices to execute FL tasks.

- Chapter 8 presented a framework for collaborative RF and lightwave power transfer. In more detail, we developed a transceiver architecture suitable for hybrid RF and optical WPT. Furthermore, four protocols to handle communication and power transfer for different scenarios were introduced through simulations. It was shown that substantial performance gains can be attained by cleverly combining RF and lightwave technologies.

This dissertation aims at proposing novel solutions with the purpose of satisfying all the technical, economic, and environmental perspectives of future networks. Particularly, according to the conducted research, there are some interesting learned lessons as follows:

- Interference management is the key solution to handle the system performance of wireless information transmission and power transfer networks. It is because wisely exploiting interference can improve the EH performance significantly.

- Solely using RF signals may be not sufficient to power wireless devices due to the propagation loss, RF-DC conversion efficiency, and safety threshold.

- Optimal solutions are important but suboptimal ones with low-complexity are more neccessary to wireless networks.

- AI-powered wireless networks where the network could make correct decisions automatically would be the future.

## 9.2 Recommendations: Energy Transfer and Harvesting for 6G networks

According to Saad, W., Bennis, M. & Chen, M. (2019), 6G could be the first cellular network generation that can realize wirelessly recharging energy for terminal devices. Since WPT technology is ripening, it is believable to envision that 6G BSs would be able to provide essential power transfer for devices. Hence, some potential directions for future research are discussed below.

### 9.2.1 Mobile Energy Internet

It is well-known that the evolution from Fixed Internet to Mobile Internet on the 2G to 5G platforms has actualized wireless information propagation and determines the barrier of last-kilometer information transmission. Thus, inspired by this success, the concept of Mobile Energy Internet has been introduced in Liu, M., Xiong, M., Deng, H., Liu, Q., Wu, J. & Xia, P. (2018) to overcome the boundaries of fixed power transfer with the conventional power grid. This approach promises to solve the issue of last-meter power transfer and transition power delivery into a mobile realm.

### 9.2.2 Deep Learning for Resource Allocation in Green Wireless Communications

An innovative deep learning-based approach for wireless resource management is promising. The main idea behind it is to handle a given optimization algorithm as a “black box” and then attempt to determine its input/output relation by adopting a deep neural network (DNN). The key improvement is that the DNN has distinguished real-time computational efficiency compared with conventional iterative optimization algorithms. In more detail, its run-time stage excludes numerical optimization tasks and only requires some basic calculations, such as matrix multiplication/addition. If the training stage can produce an approximator of the algorithm which is accurately sufficient, then simple real-time resource allocation is conceivable.

### 9.2.3 Reinforcement Learning for Self-Organizing Green Wireless Communications

Self-organization is one of the primary features of future cellular networks which is becoming more heterogeneous and densified through the form of small cells. In this vein, reinforcement learning (RL) is a promising solution to support this feature. In principle, RL is a learning strategy where an agent can repeatedly make decisions, analyze the outcomes, and hence automatically modify its policy to achieve a specific goal. One of the main advantages of RL compared with supervised learning methods is that there is no need for correct input/output data in the training phase.

### 9.2.4 New Green Sources: Invisible Light

The utilization of invisible light, such as infrared light, as a supplementary energy and information source will be very promising. Regulating the invisible light band might be more adaptable than the visible one since it does not influence illumination. Nonetheless, resource allocation designs require to thoroughly consider human eye safety standards.

## APPENDIX I

## APPENDIX OF CHAPTER 2

### 1. Proof of Lemma 1

To solve this problem $\mathrm{OP}_1$, we start with introducing a new parameter for the objective function as follows

$$\sum_{j=1}^{N_1}\left(\sum_{n=1}^{N_0}\left\|\sum_{i=1}^{M_1}\mathbf{g}_{ij}*\mathbf{h}_{in}^{10}\right\|^2 p_j^1\right)=\hat{\boldsymbol{\eta}}^T\mathbf{p}^1, \tag{A I-1}$$

where $\hat{\boldsymbol{\eta}}$ are defined in *Lemma* 1.

Next, the expression of $\mathrm{SINR}_j^1$ in (2.14) can be re-written as

$$\begin{aligned}&\mathrm{SINR}_j^1\left(L,\ \mathbf{p}^1,\ \left\{\mathbf{g}_{ij}^1\right\}_{i=1,j=1}^{M_1,N_1},P_{(cross)}{}_j^1\right) \\ &=\frac{\left(\left|\left(\sum_{i=1}^{M_1}\mathbf{g}_{ij}*\mathbf{h}_{ij}^1\right)[L]\right|^2-\gamma_j^1\sum_{\substack{l=1\\l\neq L}}^{2L-1}\left|\left(\sum_{i=1}^{M_1}\mathbf{g}_{ij}*\mathbf{h}_{ij}^1\right)[l]\right|^2\right)p_j^1}{P_{(co)}{}_j^1+P_{(cross)}{}_j^1+\|\mathbf{n}_F[\beta]\|^2}.\end{aligned} \tag{A I-2}$$

Accordingly, in form of matrix-vector notation, the $\mathrm{OP}_1$ can be formulated as follows

$$\begin{aligned}\mathrm{OP}_{1-1}\text{: }\min_{\mathbf{p}^1}\quad&\hat{\boldsymbol{\eta}}^T\mathbf{p}^1\\ \text{s.t.}\quad&\mathbf{p}^1\succeq\mathbf{D}\mathbf{B}\mathbf{p}^1+\mathbf{z},\end{aligned} \tag{A I-3}$$

in which, the structures of $\mathbf{D}$, $\mathbf{B}$, and $\mathbf{z}$ are defined in *Lemma* 1.

Considering the objective function of $\mathrm{OP}_{1-1}$, it is a fact that

$$\hat{\boldsymbol{\eta}}^T\mathbf{p}^1=\|\hat{\boldsymbol{\eta}}\|\,\mathrm{Tr}\left(\mathrm{diag}(\boldsymbol{\eta})\mathbf{p}^1\right), \tag{A I-4}$$

where $\boldsymbol{\eta}$ is the normalized form of $\hat{\boldsymbol{\eta}}$ which can be computed as $\boldsymbol{\eta} = \dfrac{\hat{\boldsymbol{\eta}}}{\|\hat{\boldsymbol{\eta}}\|}$.

On this basis, we aim at deriving the constraint of $\mathrm{OP}_{1-1}$ as a function of $\left(\mathrm{diag}(\boldsymbol{\eta})\mathbf{p}^1\right)$. After some manipulations, the constraint can be shown in a new equivalent formulation as

$$\begin{aligned}
&\mathbf{p}^1 \succeq \mathbf{D}\mathbf{B}\mathbf{p}^1 + \mathbf{z} \\
&\Leftrightarrow \mathrm{diag}(\boldsymbol{\eta})\mathbf{p}^1 \succeq \mathrm{diag}(\boldsymbol{\eta})\mathbf{D}\left(\mathbf{B} \circ (\boldsymbol{\eta}^{-1}\mathbf{1}_{N_1\times 1}^T)\right)\mathrm{diag}(\boldsymbol{\eta})\mathbf{p}^1 + \mathbf{z}.
\end{aligned} \tag{A I-5}$$

Hence, the $\mathrm{OP}_{1-1}$ can be re-formulated as

$$\begin{aligned}
\mathrm{OP}_{1-2}\colon \min_{\mathbf{p}^1} \quad & \|\hat{\boldsymbol{\eta}}\|\mathrm{Tr}\left(\mathrm{diag}(\boldsymbol{\eta})\mathbf{p}^1\right) \\
\text{s.t.} \quad & \mathrm{diag}(\boldsymbol{\eta})\mathbf{p}^1 \succeq \mathrm{diag}(\boldsymbol{\eta})\mathbf{D}\left(\mathbf{B} \circ (\boldsymbol{\eta}^{-1}\mathbf{1}_{N_1\times 1}^T)\right) \\
& \qquad\qquad \times \mathrm{diag}(\boldsymbol{\eta})\mathbf{p}^1 + \mathbf{z}.
\end{aligned} \tag{A I-6}$$

Therefore, the closed-form expression of $\mathbf{p}^{\star 1}$ can be given by

$$\mathbf{p}^{\star 1} = \mathrm{diag}(\boldsymbol{\eta})^{-1}\left[\mathbf{I}_{N_1} - \mathrm{diag}(\boldsymbol{\eta})\mathbf{D}\left(\mathbf{B} \circ (\boldsymbol{\eta}^{-1}\mathbf{1}_{N_1\times 1}^T)\right)\right]^{-1}\mathbf{z}. \tag{A I-7}$$

Relying on Perron-Frobenius theory, the optimal value $\mathbf{p}^{\star 1}$ is guaranteed to be a nonnegative vector if and only if the spectral radius of $\mathrm{diag}(\boldsymbol{\eta})\mathbf{D}\left(\mathbf{B} \circ (\boldsymbol{\eta}^{-1}\mathbf{1}_{N_1\times 1}^T)\right)$ is less than unity.

Furthermore, in a special case where $\eta_1 = \eta_2 = ... = \eta_{N_1} = \eta$, the above problem can be written in a simplified form as

$$\begin{aligned}
\mathrm{OP}_{1-3}\colon \min_{\mathbf{p}^1} \quad & \eta\mathbf{I}_{N_1}^T\mathbf{p}^1 \\
\text{s.t.} \quad & \mathbf{p}^1 \succeq \mathbf{D}\mathbf{B}\mathbf{p}^1 + \mathbf{z}.
\end{aligned} \tag{A I-8}$$

Then, the optimal solution of $\mathrm{OP}_{1-2}$ can be given as

$$\mathbf{p}^{\star 1} = (\mathbf{I} - \mathbf{DB})^{-1}\mathbf{z}. \tag{A I-9}$$

One can see that the result of (A I-9) is in agreement with that of the work in Chandrasekhar *et al.* (2009). In final, the proof is completed.

## 2. Proof of Lemma 2

According to (2.58), we can write down that

$$\begin{aligned}
&\min_{\mathbf{e}_{ij}^1 \in \mathscr{F}_{ij}^1} \left| \sum_{i=1}^{M_1} (\hat{\mathbf{g}}_{ij} * \mathbf{h}_{ij}^1)[L] \right|^2 \\
&= \min_{\mathbf{e}_{ij}^1 \in \mathscr{F}_{ij}^1} \frac{\left| \sum\limits_{i=1}^{M_1} \left( \left\| \mathbf{h}_{ij}^1 \right\|^2 + (\mathbf{e}_{ij}^1)^H \mathbf{h}_{ij}^1 \right) \right|^2}{\sum\limits_{i=1}^{M_1} \left\| \hat{\mathbf{h}}_{ij}^1 \right\|^2} \\
&\overset{(a)}{=} \frac{\left| \sum\limits_{i=1}^{M_1} \left( \left\| \mathbf{e}_{ij}^1 \right\|^2 \left( \dfrac{1-\sqrt{\psi}}{\psi} \right) \right) \right|^2}{\sum\limits_{i=1}^{M_1} \left\| \hat{\mathbf{h}}_{ij}^1 \right\|^2}.
\end{aligned} \tag{A I-10}$$

The equality in $(a)$ is due to the fact that the quantity of $\left( \left\| \mathbf{h}_{ij}^1 \right\|^2 + (\mathbf{e}_{ij}^1)^H \mathbf{h}_{ij}^1 \right)$ reaches the minimum if and only if $\mathbf{e}_{ij}^1 = -\sqrt{\psi}\mathbf{h}_{ij}^1$.

Next, by substituting $\mathbf{e}_{ij}^1 = -\sqrt{\psi}\mathbf{h}_{ij}^1$ to (2.59), we can obtain the following derivation

$$\left\| \mathbf{e}_{ij}^1 \right\|^2 = \frac{\psi}{(1-\sqrt{\psi})^2} \left\| \hat{\mathbf{h}}_{ij}^1 \right\|^2. \tag{A I-11}$$

Thus, we infer that

$$\min_{\mathbf{e}_{ij}^1 \in \mathscr{F}_{ij}^1} \left| \sum_{i=1}^{M_1} (\hat{\mathbf{g}}_{ij} * \mathbf{h}_{ij}^1)[L] \right|^2 = \frac{\sum\limits_{i=1}^{M_1} \left\| \hat{\mathbf{h}}_{ij}^1 \right\|^2}{(1-\psi)^2}. \tag{A I-12}$$

On the other hand, the estimated signal power can be given as

$$\left|\sum_{i=1}^{M_1}(\hat{\mathbf{g}}_{ij} * \hat{\mathbf{h}}_{ij}^1)[L]\right|^2 = \sum_{i=1}^{M_1}\left\|\hat{\mathbf{h}}_{ij}^1\right\|^2. \tag{A I-13}$$

Accordingly, the worst-case lower-bound of signal power component can be constituted as

$$\mathscr{P}l_{(sig)}{}_j^1 = \left|\sum_{i=1}^{M_1}(\hat{\mathbf{g}}_{ij} * \hat{\mathbf{h}}_{ij}^1)[L]\right|^2 \frac{p_j^1}{\left(1-\sqrt{\psi}\right)^2}. \tag{A I-14}$$

This completes the proof of *Lemma* 2.

### 3. Proof of Lemma 3

We consider the worst-case upper-bound of $\left\|\hat{\mathbf{g}}_{ij} * \mathbf{h}_{ij}^1\right\|^2$ for simplicity. To investigate a tighter upper-bound than the value suggested in Beckner (1975); Young (1912), we introduce a novel approach in which we start with letting $\tilde{\mathbf{h}}_{ij}^1$ be a virtual channel, and we aim at investigating the optimal value $\tilde{\mathbf{h}}_{ij}^{\star 1}$ that makes $\left\|\hat{\mathbf{g}}_{ij} * \tilde{\mathbf{h}}_{ij}^1\right\|^2$ achieve maximal quantity. Accordingly, the problem becomes

$$\begin{aligned} \max_{\tilde{\mathbf{h}}_{ij}^1} \quad & \left\|\hat{\mathbf{g}}_{ij} * \tilde{\mathbf{h}}_{ij}^1\right\|^2 \\ \text{s.t.} \quad & \left\|\tilde{\mathbf{h}}_{ij}^1\right\|^2 \leq \max_{\mathbf{e}_{ij}^1 \in \mathscr{F}_{ij}^1} \left\|\mathbf{h}_{ij}^1\right\|^2. \end{aligned} \tag{A I-15}$$

As observed, the problem (A I-15) is hard to solve directly due to the convolution operator. Thus, we factorize (A I-15) into two steps. In the first step, we let $\hat{\mathbf{G}}_{ij}$ to be a $(2L-1)\times L$ Toeplitz matrix form of $\hat{\mathbf{g}}_{ij}$, i.e. (2.65)

Additionally, we let $\mathbf{\Phi}_{ij}^{1} = \dfrac{\tilde{\mathbf{h}}_{ij}^{1}}{\sqrt{\max\limits_{\mathbf{e}_{ij}^{1}\in\mathscr{F}_{ij}^{1}} \left\|\mathbf{h}_{ij}^{1}\right\|^{2}}}$. Based on the representation of convolution with Toeplitz matrix form, the above problem can be equivalently re-formulated as

$$\begin{aligned} \max_{\mathbf{\Phi}_{ij}^{1}} \quad & \left\| \left( \sqrt{\max_{\mathbf{e}_{ij}^{1}\in\mathscr{F}_{ij}^{1}} \left\|\mathbf{h}_{ij}^{1}\right\|^{2}}\, \hat{\mathbf{G}}_{ij} \right) \mathbf{\Phi}_{ij}^{1} \right\|^{2} \\ \text{s.t.} \quad & \left\|\mathbf{\Phi}_{ij}^{1}\right\|^{2} \leq 1. \end{aligned} \tag{A I-16}$$

The closed-form derivation of optimal solution $\mathbf{\Phi}_{ij}^{\star 1}$ can be obtained by computing the orthonormal eigenvector corresponding to the largest eigenvalue of the matrix $\left( \hat{\mathbf{G}}_{ij} \left( \hat{\mathbf{G}}_{ij} \right)^{H} \max\limits_{\mathbf{e}_{ij}^{1}\in\mathscr{F}_{ij}^{1}} \left\|\mathbf{h}_{ij}^{1}\right\|^{2} \right)$. Since the norm of $\mathbf{\Phi}_{ij}^{\star 1}$ is equal to 1, to make a fair normalization, we devise that

$$\tilde{\mathbf{h}}_{ij}^{\star 1} = \frac{\left(\mathbf{\Phi}_{ij}^{\star 1}\right) \left\|\hat{\mathbf{h}}_{ij}^{1}\right\|}{\left(1-\sqrt{\psi}\right)}, \tag{A I-17}$$

where $\tilde{\mathbf{h}}_{ij}^{\star 1}$ is the optimal value regarding to the achievement the maximum of $\left\|\hat{\mathbf{g}}_{ij} * \tilde{\mathbf{h}}_{ij}^{1}\right\|^{2}$, and $\max\limits_{\mathbf{e}_{ij}^{1}\in\mathscr{F}_{ij}^{1}} \left\|\mathbf{h}_{ij}^{1}\right\|^{2} = \dfrac{\left\|\hat{\mathbf{h}}_{ij}^{1}\right\|^{2}}{\left(1-\sqrt{\psi}\right)^{2}}$.

Therefore, we can obtain a new boundary from (A I-17) as

$$\begin{aligned} & \max_{\mathbf{e}_{ij}^{1}\in\mathscr{F}_{ij}^{1}} \left\| \sum_{i=1}^{M_1} \hat{\mathbf{g}}_{ij} * \mathbf{h}_{ij}^{1} \right\|^{2} \\ & = \sum_{i=1}^{M_1} \left\| \hat{\mathbf{g}}_{ij} * \tilde{\mathbf{h}}_{ij}^{\star 1} \right\|^{2} + \left| \sum_{i=1}^{M_1} \sum_{\substack{i=1 \\ i'\neq i}}^{M_1} \left( \hat{\mathbf{g}}_{ij} * \tilde{\mathbf{h}}_{ij}^{\star 1} \right)^{H} \left( \hat{\mathbf{g}}_{i'j} * \tilde{\mathbf{h}}_{i'j}^{\star 1} \right) \right|. \end{aligned} \tag{A I-18}$$

Thus, the proof of *Lemma* 3 is completed.

## APPENDIX II

## APPENDIX OF CHAPTER 4

### 1. Proof of Lemma 1

We assume that there is a value of $\phi_0$ such that

$$\frac{\theta}{(1-\phi_0)\Gamma} = \frac{\bar{\varepsilon}}{\Gamma\phi_0} = \Xi. \tag{A II-1}$$

Next, by increasing $\phi_0$ with $a$ ($a > 0$ and $0 < a + \phi_0 < 1$), it can be observed that

$$\max\left\{\frac{\theta}{\Gamma(1-(\phi_0+a))}, \frac{\bar{\varepsilon}}{\Gamma(\phi_0+a)}\right\} = \frac{\theta}{\Gamma(1-(\phi_0+a))} > \Xi. \tag{A II-2}$$

Furthermore, by decreasing $\phi_0$ with $b$ ($b > 0$ and $0 < \phi_0 - b < 1$)

$$\max\left\{\frac{\theta}{\Gamma(1-(\phi_0-b))}, \frac{\bar{\varepsilon}}{\Gamma(\phi_0-b)}\right\} = \frac{\bar{\varepsilon}}{\Gamma(\phi_0-b)} > \Xi. \tag{A II-3}$$

Thus, (A II-2) and (A II-3) imply that either increasing $\phi$ or decreasing $\phi$ results in a scale up of the objective function of $OP_3$. Therefore, $\phi_0$ is the optimal solution of $OP_3$ (i.e., $\phi^\star = \phi_0$), and the proof of *Lemma* 1 is completed.

## APPENDIX III

## APPENDIX OF CHAPTER 5

### 1. Proof of Lemma 1

To compute an approximation for (5.38), we begin with considering the simplified form (setting $G = N_1 = 1$) as follows

$$\mathscr{P}r\left(-p_1^1\left|(\boldsymbol{\nu}_1^1)^T\mathbf{h}_1^1\right|^2 \geq \frac{\hat{\theta}_1^1}{(\rho_1^1-1)}\right) \leq 1-\alpha_1^{\star 1}. \tag{A III-1}$$

Following the one-sided Chebyshev-inequality, we have

$$\begin{aligned}&\mathscr{P}r\left(-p_1^1\left|(\boldsymbol{\nu}_1^1)^T\mathbf{h}_1^1\right|^2 + \mathbb{E}\left[p_1^1\left|(\boldsymbol{\nu}_1^1)^T\mathbf{h}_1^1\right|^2\right] \geq t\right)\\ &\leq \frac{1}{1+t^2/\mathrm{var}\left[p_1^1\left|(\boldsymbol{\nu}_1^1)^T\mathbf{h}_1^1\right|^2\right]},\end{aligned} \tag{A III-2}$$

where $t \geq 0$. By taking

$$t = \frac{\hat{\theta}_1^1}{(\rho_1^1-1)} + \mathbb{E}\left[p_1^1\left|(\boldsymbol{\nu}_1^1)^T\mathbf{h}_1^1\right|^2\right], \tag{A III-3}$$

one can see that the expression (A III-1) is equivalent to the one (A III-2). On this basis, we obtain

$$\begin{aligned}&\mathscr{P}r\left(-p_1^1\left|(\boldsymbol{\nu}_1^1)^T\mathbf{h}_1^1\right|^2 \geq \frac{\hat{\theta}_1^1}{(\rho_1^1-1)}\right)\\ &\leq \frac{\mathrm{var}\left[p_1^1\left|(\boldsymbol{\nu}_1^1)^T\mathbf{h}_1^1\right|^2\right]}{\mathrm{var}\left[p_1^1\left|(\boldsymbol{\nu}_1^1)^T\mathbf{h}_1^1\right|^2\right] + \left(\frac{\theta_1^1}{\xi_1^1(\rho_1^1-1)} + \mathbb{E}\left[p_1^1\left|(\boldsymbol{\nu}_1^1)^T\mathbf{h}_1^1\right|^2\right]\right)^2}.\end{aligned} \tag{A III-4}$$

As a result, the inequality

$$\frac{\mathrm{var}\left[p_1^1\left|(\boldsymbol{v}_1^1)^T\mathbf{h}_1^1\right|^2\right]}{\mathrm{var}\left[p_1^1\left|(\boldsymbol{v}_1^1)^T\mathbf{h}_1^1\right|^2\right]+\left(\frac{\hat{\theta}_1^1}{(\rho_1^1-1)}+\mathbb{E}\left[p_1^1\left|(\boldsymbol{v}_1^1)^T\mathbf{h}_1^1\right|^2\right]\right)^2} \leq 1-\alpha_1^{\star 1}. \tag{A III-5}$$

implies the probability inequality given in (A III-1).

Additionally, since $t \geq 0$, the expression in (A III-5) can be re-written by

$$\sqrt{\mathrm{var}\left[p_1^1\left|(\boldsymbol{v}_1^1)^T\mathbf{h}_1^1\right|^2\right]\left(1/(1-\alpha_1^{\star 1})-1\right)} \leq \mathbb{E}\left[p_1^1\left|(\boldsymbol{v}_1^1)^T\mathbf{h}_1^1\right|^2\right]+\frac{\hat{\theta}_1^1}{(\rho_1^1-1)}. \tag{A III-6}$$

By generalizing (A III-1)-(A III-6),

$$\sqrt{\left(1/(1-\alpha_n^{\star g})-1\right)\sum_{g'=1}^{G}\sum_{n'=1}^{N_g}\mathrm{var}\left[|(\boldsymbol{v}_{n'}^{g'})^T\mathbf{h}_n^g|^2\right](p_{n'}^{g'})^2} \leq \sum_{g'=1}^{G}\sum_{n'=1}^{N_g}\mathbb{E}\left[\left|(\boldsymbol{v}_{n'}^{g'})^T\mathbf{h}_n^g\right|^2\right]p_{n'}^{g'}+\frac{\hat{\theta}_n^g}{(\rho_n^g-1)}. \tag{A III-7}$$

Also, it is known that

$$\sqrt{\sum_{g'=1}^{G}\sum_{n'=1}^{N_g}\mathrm{var}\left[|(\boldsymbol{v}_{n'}^{g'})^T\mathbf{h}_n^g|^2\right](p_{n'}^{g'})^2} \leq \sum_{g'=1}^{G}\sum_{n'=1}^{N_g}\sqrt{\mathrm{var}\left[|(\boldsymbol{v}_{n'}^{g'})^T\mathbf{h}_n^g|^2\right]}\,p_{n'}^{g'}. \tag{A III-8}$$

Thus, (A III-7) can be approximated as follows

$$\sum_{g'=1}^{G}\sum_{n'=1}^{N_g}\sqrt{\left(1/(1-\alpha_n^{\star g})-1\right)\text{var}\left[|(\boldsymbol{\nu}_{n'}^{g'})^T\mathbf{h}_n^g|^2\right]}p_{n'}^{g'}$$
$$\leq\sum_{g'=1}^{G}\sum_{n'=1}^{N_g}\mathbb{E}\left[\left|(\boldsymbol{\nu}_{n'}^{g'})^T\mathbf{h}_n^g\right|^2\right]p_{n'}^{g'}+\frac{\hat{\theta}_n^g}{(\rho_n^g-1)}. \tag{A III-9}$$

This completes our proof.

## 2. Proof of Lemma 2

To calculate $\mathbb{E}\left[\left|(\boldsymbol{\nu}_{n'}^{g'})^T\mathbf{h}_n^g\right|^2\right]$, it is useful to represent it into a formulation regarding the trace operator as follows

$$\mathbb{E}\left[\left|(\boldsymbol{\nu}_{n'}^{g'})^T\mathbf{h}_n^g\right|^2\right]=\mathbb{E}\left[\text{tr}\left(\mathbf{V}_{n'}^{g'}\mathbf{h}_n^g(\mathbf{h}_n^g)^H\right)\right]. \tag{A III-10}$$

Due to the facts that (i) both $\mathbb{E}[.]$ and tr are linear operators and (ii) $\mathbf{h}_n^g\sim\mathscr{CN}(\mathbf{u}_n^g,\sigma_{cal}^2\mathbf{U}_n^g)$, where $\mathbf{U}_n^g=\text{diag}\{|\mathbf{u}_n^g[1]|^2,...,|\mathbf{u}_n^g[M]|^2\}$, we can derive

$$\mathbb{E}\left[\text{tr}\left(\mathbf{V}_{n'}^{g'}\mathbf{h}_n^g(\mathbf{h}_n^g)^H\right)\right]=\text{tr}\left(\mathbf{V}_{n'}^{g'}\mathbb{E}\left[\mathbf{h}_n^g(\mathbf{h}_n^g)^H\right]\right)$$
$$=\text{tr}\left(\mathbf{V}_{n'}^{g'}\hat{\mathbf{U}}_n^g\sigma_{cal}^2\right)+(\mathbf{u}_n^g)^H\mathbf{V}_{n'}^{g'}\mathbf{u}_n^g. \tag{A III-11}$$

On the other hand, one can observe that computing the variance of $\left|(\boldsymbol{\nu}_{n'}^{g'})^T\mathbf{h}_n^g\right|^2$ is quite complicated. Fortunately, based on the work in [Chapter 2, **?**], after some manipulations, the cumulant generating function (CGF) of $\left|(\boldsymbol{\nu}_{n'}^{g'})^T\mathbf{h}_n^g\right|^2$ can be given by

$$\texttt{CGF}_k\left(|(\boldsymbol{\nu}_{n'}^{g'})^T\mathbf{h}_n^g|^2\right)=(k-1)!\left[\text{tr}\left(\mathbf{V}_{n'}^{g'}\hat{\mathbf{U}}_n^g\sigma_{cal}^2\right)^k\right.$$
$$\left.+k(\mathbf{u}_n^g)^H\mathbf{V}_{n'}^{g'}\left(\sigma_{cal}^2\hat{\mathbf{U}}_n^g\mathbf{V}_{n'}^{g'}\right)^{k-1}\mathbf{u}_n^g\right]. \tag{A III-12}$$

Particularly, by setting $k=2$, the variance of $\left|(\boldsymbol{\nu}_{n'}^{g'})^T\mathbf{h}_n^g\right|^2$ can be shown as

$$\begin{aligned}\text{var}\left[\left|(\boldsymbol{\nu}_{n'}^{g'})^T\mathbf{h}_n^g\right|^2\right] &= \text{tr}\left(\mathbf{V}_{n'}^{g'}\hat{\mathbf{U}}_n^g\sigma_{cal}^2\right)^2 \\ &\quad + 2\sigma_{cal}^2(\mathbf{u}_n^g)^H\mathbf{V}_{n'}^{g'}\hat{\mathbf{U}}\mathbf{V}_{n'}^{g'}\mathbf{u}_n^g. \end{aligned} \tag{A III-13}$$

This completes our proof.

### 3. Proof of Lemma 4

First, we consider constraint (5.52b). According to (5.39), the constraint can be re-expressed as

$$(\boldsymbol{\mu}_n^g-\boldsymbol{\upsilon}_n^g)^T\mathbf{a}(\sigma_0^2+\frac{\sigma_1^2}{\rho})\geq\frac{\hat{\theta}_n^g}{(1-\rho)}, \tag{A III-14}$$

where

$$\mathbf{a}=(\mathbf{I}-\mathbf{L}\boldsymbol{\Upsilon})^{-1}\boldsymbol{\Delta}\mathbf{1}_{NG}, \tag{A III-15a}$$

$$\boldsymbol{\mu}_n^g=[\mu_{1n}^{1g}...\mu_{Nn}^{Gg}]^T, \tag{A III-15b}$$

$$\bar{\alpha}_n^g=(1/(1-\alpha_n^{\star g})-1), \tag{A III-15c}$$

$$\boldsymbol{\upsilon}_n^g=[\sqrt{\bar{\alpha}_n^g\upsilon_{1n}^{1g}}...\sqrt{\bar{\alpha}_n^g\upsilon_{Nn}^{Gg}}]^T. \tag{A III-15d}$$

By inverting both sides, we can obtain the derivation as below

$$\frac{\rho}{\rho(\boldsymbol{\mu}_n^g-\boldsymbol{\upsilon}_n^g)^T\mathbf{a}\sigma_0^2+(\boldsymbol{\mu}_n^g-\boldsymbol{\upsilon}_n^g)^T\mathbf{a}\sigma_1^2}\leq\frac{(1-\rho)}{\hat{\theta}_n^g}. \tag{A III-16}$$

After some manipulations, the constraint can be further transformed into a second-order inequation as

$$(\boldsymbol{\mu}_n^g-\boldsymbol{\upsilon}_n^g)^T\mathbf{a}\sigma_0^2\rho^2-\kappa_n^g\rho-(\boldsymbol{\mu}_n^g-\boldsymbol{\upsilon}_n^g)^T\mathbf{a}\sigma_1^2\leq 0, \tag{A III-17}$$

in which,

$$\kappa_n^g = (\boldsymbol{\mu}_n^g - \boldsymbol{\upsilon}_n^g)^T \mathbf{a}(\sigma_0^2 - \sigma_1^2) - \hat{\theta}_n^g. \tag{A III-18}$$

In particular, according to (A III-14), it can be induced that $(\boldsymbol{\mu}_n^g - \boldsymbol{\upsilon}_n^g)^T \mathbf{a} \geq 0$ to make the problem feasible. This yields that (A III-17) is a convex quadratic constraint Boyd & Vandenberghe (2004). In other words, constraint (5.52b) has been transformed into a convex formulation.

Second, we analyze the convexity of the objective function of problem (5.52). Taking (5.45), (5.50), and (5.51) into account, it can be evaluated that since matrix $(\mathbf{I} - \mathbf{L}\boldsymbol{\Upsilon})^{-1}\boldsymbol{\Delta}$ is positive element-wise Bambos *et al.* (2000), $\Lambda_{g,n}(1/\rho)$ is convex. Thus, the objective function of problem (5.52) can be seen as a summation of convex functions. Therefore, the objective function is convex.

Based on the above discussion, it can be concluded that problem (5.52) is convex.

Next, since the objective function of problem (5.52) is non-increasing, the closed-form solution can be given by

$$\rho^\star = \min_{\substack{1 \leq n \leq N \\ 1 \leq g \leq G}} \left\{ \frac{\kappa_n^g + \sqrt{(\kappa_n^g)^2 + 4((\boldsymbol{\mu}_n^g - \boldsymbol{\upsilon}_n^g)^T \mathbf{a})^2 \sigma_0^2 \sigma_1^2}}{2(\boldsymbol{\mu}_n^g - \boldsymbol{\upsilon}_n^g)^T \mathbf{a} \sigma_0^2} \right\}. \tag{A III-19}$$

This completes our proof.

# APPENDIX IV

# APPENDIX OF CHAPTER 6

## 1. Proof of Proposition 1

For convenience, we use $\mathtt{SNR}^{\mathtt{s}}_{oi,j}(B)$ to denote that the VLC SNR at any user is a function of $B$. Our aim is to maximize the minimum of the VLC SNRs, i.e., max min $\mathtt{SNR}^{\mathtt{s}}_{oi,j}(B)$.

Since $\mathtt{SNR}^{\mathtt{s}}_{oi,j}(B)$ is an increasing function, inreasing $B$ leads to increasing the VLC SNRs at all the users. Thus, maximizing the minimum of VLC SNRs is equivalent to simply maximizing the VLC SNR at the user with the worst VLC SNR, mathematically represented as

$$\max \min \mathtt{SNR}^{\mathtt{s}}_{oi,j}(B) = \max \mathtt{SNR}^{\mathtt{s}}_{oi,\bar{j}}(B), \tag{A IV-1}$$

where $\bar{j}$ denotes the user with the worst VLC SNR.

Furthemore, according to (6.15b), there is a relationship between the VLC SNR and the VLC EH. It can be seen that maximizing the VLC SNR implies minimizing the VLC EH. Hence, we have

$$\max \mathtt{SNR}^{\mathtt{s}}_{oi,\bar{j}}(B) = \min \mathtt{EH}^{VLC}_{\bar{j}}(B). \tag{A IV-2}$$

Next, due to constraint (6.15b), reducing $\mathtt{EH}^{VLC}_{\bar{j}}(B)$ is achieved by adding more $\mathtt{EH}^{RF}_{\bar{j}}$. Generally speaking, increasing the RF EH reduces the contribution of the VLC EH, and increases the achievable amount of the VLC SNRs. Therefore, the RF EH allocated to the user with the worst VLC SNR determines the value of the minimum of the VLC SNRs, and therefore determines $B$ for all the users. This completes the proof.

## 2. Proof of Lemma 1

To demonstrate the rank-one issue, we can have some following expressions based on the Karush-Kuhn-Tucker (KKT) condition as Boyd & Vandenberghe (2004)

$$\mathbf{I} - \gamma_j \mathbf{G}_j - \boldsymbol{\Xi}_j = \mathbf{0}, \tag{A IV-3}$$

$$\mathbf{W}_j \boldsymbol{\Xi}_j = \mathbf{0}, \tag{A IV-4}$$

where $\gamma_j$ and $\boldsymbol{\Xi}_j$ are dual variables associated with constraints (6.35b) and (6.35c), respectively.

On one hand, according to (6.35b), (6.35c), and (A IV-4), it is implied that $\mathbf{W}_j \neq \mathbf{0}$. Thus, we infer that

$$\text{rank}(\boldsymbol{\Xi}_j) \leq M_T - 1. \tag{A IV-5}$$

On the other hand, based on (A IV-3), we have

$$\text{rank}(\boldsymbol{\Xi}_j) = \text{rank}(\mathbf{I} - \gamma_j \mathbf{G}_j) \geq M_T - 1. \tag{A IV-6}$$

Taking (A IV-5) and (A IV-6) into account, it is clear that

$$\text{rank}(\boldsymbol{\Xi}_j) = M_T - 1. \tag{A IV-7}$$

Next, in light of (A IV-4), the rank of $\mathbf{W}_j$ can be calculated by

$$\text{rank}(\mathbf{W}_j) \leq M_T - \text{rank}(\boldsymbol{\Xi}_j). \tag{A IV-8}$$

Since $\text{rank}(\mathbf{W}_j) \neq 0$ due to $\mathbf{W}_j \neq \mathbf{0}$, we conclude that

$$\text{rank}(\mathbf{W}_j) = 1. \tag{A IV-9}$$

This completes our proof.

### 3. Proof of Lemma 2

The key to achieving a closed-form solution for problem (6.30) relies on dealing with constraint (7.20). We recall the constraint as follows

$$fV_0 I_{\bar{j},G}(B)\ln\left(1+\frac{I_{\bar{j},G}(B)}{I_D}\right) \geq \theta - \mathtt{EH}_{\bar{j}}^{\star RF}. \tag{A IV-10}$$

Initially, we aim to transform the constraint into a simplified form of $B$ greater than a constant. Unfortunately, this is difficult to achieve. Then, deriving a closed-form optimal solution is intractable. However, a closed-form suboptimal solution can be obtained by relaxing constraint (7.20). Our method is presented as follows.

Since $I_D \ll I_{\bar{j},G}(B)$ in practice, we can have an approximation as

$$\ln\left(1+\frac{I_{\bar{j},G}(B)}{I_D}\right) \approx \ln\left(\frac{I_{\bar{j},G}(B)}{I_D}\right). \tag{A IV-11}$$

Thus, (A IV-10) becomes

$$I_{\bar{j},G}(B)\ln\left(\frac{I_{\bar{j},G}(B)}{I_D}\right) \geq \frac{\theta - \mathtt{EH}_{\bar{j}}^{\star RF}}{fV_0}, \tag{A IV-12}$$

After some manipulations, $I_{\bar{j},G}(B)$ can be computed as

$$I_{\bar{j},G}(B) \geq \frac{\theta - \mathtt{EH}_{\bar{j}}^{\star RF}}{fV_0 \mathscr{W}\left(\frac{\theta - \mathtt{EH}_{\bar{j}}^{\star RF}}{fV_0 I_D}\right)} \tag{A IV-13}$$

where $\mathscr{W}(.)$ is the Lambert function. Accordingly, we have

$$B \geq \frac{\theta - \mathtt{EH}_{\bar{j}}^{\star RF}}{3\nu N_{LED} V_{LED} f V_0 \mathscr{W}\left(\frac{\theta - \mathtt{EH}_{\bar{j}}^{\star RF}}{f V_0 I_D}\right) \sum\limits_{o}^{\mathscr{O}} \sum\limits_{i}^{M_I} h_{oi,\bar{j}}} = \Upsilon. \tag{A IV-14}$$

Accordingly, problem (6.30) becomes

$$\min_{B} \quad B \tag{A IV-15a}$$

$$\text{s.t.:} \quad B \geq \Upsilon, \tag{A IV-15b}$$

$$\frac{I_H + I_L}{2} \leq B \leq I_H. \tag{A IV-15c}$$

As observed, the closed-form suboptimal solution can be computed as follows

$$B^{\times} = \min\left\{\max\{\Upsilon, I_L\}, I_H\right\}, \tag{A IV-16}$$

$$A_{oi,j}^{\times \mathtt{s}} = B - B^{\times}. \quad (\forall j) \tag{A IV-17}$$

Thus, our proof is completed.

## REFERENCES


The European lighting standard – EN12464-1:2011. Light and lighting – Lighting of work places – Part 1: Indoor work places.

LIGHTS Transmitter. Consulted at https://www.wi-charge.com/product_category/reference-integrations/.

How to Harvest and Store Wind Energy. Consulted at http://www.ctmmagnetics.com/wind-power-basics-how-to-harvest-and-store-wind-energy/.

Philips. All in 1 LED Lighting Solutions Guide. Consulted at PhilipsLumileds.com.

Google. Federated Learning: Collaborative Machine Learning without Centralized Training Data. Consulted at https://ai.googleblog.com/2017/04/federated-learning-collaborative.html.

IEC. (2001). Safety of laser products - Part 1: Equipment classification, requirements and user's guide.

IEEE. (2005). IEEE Standard for Safety Levels With Respect to Human Exposure to Radio Frequency Electromagnetic Fields, 3 kHz to 300 GHz.

(2007). Extremely Low Frequency Fields, Environmental Health Criteria 238. Geneva, Switzerland.

(2014). *Green Power for Mobile*. Consulted at https://www.gsma.com/mobilefordevelopment/wp-content/uploads/2015/01/140617-GSMA-report-draft-vF-KR-v7.pdf.

CBC. (2015). How Canada's provinces are tackling greenhouse gas emissions. Consulted at http://www.cbc.ca/news/canada/how-canada-s-provinces-are-tackling-greenhouse-gas-emissions-1.3030535.

(2019). Wysips Reflect. Consulted at https://sunpartnertechnologies.fr/en/objets-connectes/produits/.

3GPP. (2009). *Hardware calibration requirement for dual layer beamforming* (Report n°R1-091794).

Agarwal, D., Chen, B.-C., Elango, P. & Wang, X. (2012, August). Personalized click shaping through lagrangian duality for online recommendation. *the 35th International ACM SIGIR Conference on Research and Development in Information Retrieval*.

Agiwal, M., Roy, A. & Saxena, N. (2016). Next Generation 5G Wireless Networks: A Comprehensive Survey. *IEEE Communications Surveys & Tutorials*, 18(3), 1617 – 1655.

Ahmed, E., Eltawil, A. M. & Sabharwal, A. (2013). Self-interference cancellation with phase noise induced ICI suppression for full-duplex systems. *in Proc. IEEE Global Commun. Conf. (GLOBECOM)*, pp. 3384–3388.

Al-Fuqaha, A., Guizani, M., Mohammadi, M., Aledhari, M. & Ayyash, M. (2015). Internet of Things: A Survey on Enabling Technologies, Protocols, and Applications. *IEEE Communications Surveys & Tutorials*, 17(4), 2347 – 2376.

Alippi, C. & Galperti, C. (2008). An Adaptive System for Optimal Solar Energy Harvesting in Wireless Sensor Network Nodes. *IEEE Transactions on Circuits and Systems*, 55(6), 742–1750.

Americas, G. (2009). The benefits of son in LTE: Self-optimizing and selforganizing networks. *White Paper*.

Amiri, R., Almasi, M. A., Andrews, J. G. & Mehrpouyan, H. (2019). Reinforcement Learning for Self Organization and Power Control of Two-Tier Heterogeneous Networks. *IEEE Transactions on Wireless Communications*. early access.

Ammar, Y., Buhrig, A., Marzencki, M., Charlot, B., Basrour, S., Matou, K. & Renaudin, M. (2005, October). Wireless sensor network node with asynchronous architecture and vibration harvesting micro power generator. *Proc. of Joint sOc-EUSAI conference*, pp. 287–292.

Andrews, J., Claussen, H., Dohler, M., Rangan, S. & Reed, M. (2012). Femtocells: Past, Present, and Future. *IEEE Journal on Selected Areas in Communications*, 30(3), 497–508.

Arnon, S. (Ed.). (2015). *Visible Light Communication*. Cambridge University Press.

Ayyash, M., Elgala, H., Khreishah, A., Jungnickel, V., Little, T., Shao, S., Rahaim, M., Schulz, D., Hilt, J. & Freund, R. (2016). Coexistence of WiFi and LiFi Toward 5G: Concepts, Opportunities, and Challenges. *IEEE Communications Magazine*, 54(2), 64 – 71.

Bambos, N., Chen, S. C. & Pottie, G. J. (2000). Channel Access Algorithms with Active Link Protection for Wireless Communication Networks with Power Control. *IEEE/ACM Transactions on Networking*, 5(8), 583–597.

Baraniuk, R. (2007). Compressive Sensing. *IEEE Signal Processing Magazine*, 24(4), 118 – 121.

Basnayaka, D. A. & Haas, H. (2017). Design and Analysis of a Hybrid Radio Frequency and Visible Light Communication System. *IEEE Transactions on Communications*, 65(10), 4334 – 4347.

Beck, A., Ben-Tal, A. & Tetruashvili, L. (2010). A sequential parametric convex approximation method with applications to nonconvex truss topology design problems. *Journal of Global Optimization*, 47(1), 29 – 51.

Beckner, W. (1975). Inequalities in Fourier analysis. *Ann. of Math.*, 102(1), 159–182.

Belkhir, L. & Elmeligi, A. (2018). Assessing ICT global emissions footprint: Trends to 2040 & recommendations. *Journal of Cleaner Production*, 177, 448–463.

Bengtsson, M. & Ottersten, B. (2001). *Optimal and Suboptimal Transmit Beamforming*. CRC Press.

Bennis, M., Giupponi, L., Diaz, E., Lalam, M., Maqbool, M., Strinati, E., De Domenico, A. & Latva-aho, M. (2011). Interference management in self-organized femtocell networks: The BeFEMTO approach. *Proc. of 2nd International Conference on Wireless Communication, Vehicular Technology, Information Theory and Aerospace & Electronic Systems Technology (Wireless VITAE)*, pp. 1–6.

Bi, S., Ho, C. K. & Zhang, R. (2014). Recent advances in joint wireless energy and information transfer. *Proc. IEEE Information Theory Workshop (ITW 2014)*, pp. 341–345.

Bi, S., Ho, C. & Zhang, R. (2015). Wireless powered communication: opportunities and challenges. *IEEE Communications Magazine*, 53(4), 117–125.

Bjornson, E. & Jorswieck, E. (2013). Optimal resource allocation in coordinated multi-cell systems. *Foundations and Trends in Communications and Information Theory*, 9(2-3), 113–381.

Bjornson, E., Jorswieck, E. A., Debbah, M. & Ottersten, B. (2014). Multiobjective Signal Processing Optimization: The way to balance conflicting metrics in 5G systems. *IEEE Signal Processing Magazine*, 31(6), 14 – 23.

Bobkov, S., Madiman, M. & Wang, L. (2011). Fractional generalizations of Young and Brunn-Minkowski inequalities. *Contemporary Mathematics*, 545.

Bogachev & I., V. (2007). *Measure Theory I*. New York: Springer-Verlag.

Bonnefoi, R., Moy, C. & Palicot, J. (2018). Power Control and Cell Discontinuous Transmission Used As a Means of Decreasing Small-Cell Networks' Energy Consumption. *IEEE Transactions on Green Communications and Networking*, 2(6), 899 – 914.

Boshkovska, E., Ng, D. W. K., Zlatanov, N. & Schober, R. (2015). Practical Non-Linear Energy Harvesting Model and Resource Allocation for SWIPT Systems. *IEEE Communications Letters*, 19(12), 2082 – 2085.

Boshkovska, E., Ng, D. W. K., Zlatanov, N., Koelpin, A. & Schober, R. (2017). Robust Resource Allocation for MIMO Wireless Powered Communication Networks Based on a Non-linear EH Model. *IEEE Transactions on Communications*, 65(5), 1984 – 1999.

Bottner, H. & et al. (2004). New Thermoelectric Components Using Microsystem Technologies. *Journal of Microelectromechanical Systems*, 13(3), 414–420.

Bouzigues, M.-A., Siaud, I., Helard, M. & Ulmer-Moll, A.-M. (2013). Turn Back the Clock: Time Reversal for Green Radio Communications. *IEEE Vehicular Technology Magazine*, 8(1), 49–56.

Boyd, S. & Vandenberghe, L. (2004). *Convex Optimization*. Cambridge University Press.

Buzzi, S., I, C.-L., Klein, T. E., Poor, H. V., Yang, C. & Zappone, A. (2016). A Survey of Energy-Efficient Techniques for 5G Networks and Challenges Ahead. *IEEE Journal on Selected Areas in Communications*, 34(4), 697–709.

Caramia, M. & Dell'Olmo, P. (2008). *Multi-objective management in freight logistics: Increasing capacity, service level and safety with optimization algorithms*. Springer Science & Business Media.

Carvalho, C. & Paulino, N. (2014). On the Feasibility of Indoor Light Energy Harvesting for Wireless Sensor Networks. *Procedia Technology*, 17, 343–350.

Chandrasekhar, V., Andrews, J. G., Muharemovic, T., Chen, Z. & Gatherer, A. (2009). Power control in two-tier femtocell networks. *IEEE Transactions on Wireless Communications*, 8(8), 4316–4328.

Chen, C., Basnayaka, D. A. & Haas, H. (2016a). Downlink Performance of Optical Attocell Networks. *IEEE/OSA J. Lightw. Technol.*, 34(1), 137 – 156.

Chen, F. & Zhang, Y. (2013). Sparse Hyperspectral Unmixing Based on Constrained lp - l2 Optimization. *IEEE Geoscience and Remote Sensing Letters*, 10(6), 1142 – 1146.

Chen, H. H., Li, Y., Jiang, Y., Ma, Y. & Vucetic, B. (2015). Distributed Power Splitting for SWIPT in Relay Interference Channels Using Game Theory. *IEEE Transactions on Wireless Communications*, 14(1), 410–420.

Chen, Y., Wang, B., Han, Y., Lai, H.-Q., Safar, Z. & Liu, K. R. (2016b). Why Time Reversal for Future 5G Wireless? [Perspectives]. *IEEE Signal Processing Magazine*, 33(2), 17–26.

Chen, Z., Basnayaka, D. A. & Haas, H. (2017). Space Division Multiple Access for Optical Attocell Network Using Angle Diversity Transmitters. *IEEE/OSA J. Lightw. Technol.*, 35(11), 2118 – 2131.

Chiang, P., Guruprasad, R. B. & Dey, S. (2018). Optimal Use of Harvested Solar, Hybrid Storage and Base Station Resources for Green Cellular Networks. *IEEE Transactions on Green Communications and Networking*, 2(3), 707–720.

Chingoska, H., Hadzi-Velkov, Z., Nikoloska, I. & Zlatanov, N. (2016). Resource Allocation in Wireless Powered Communication Networks With Non-Orthogonal Multiple Access. *IEEE Wireless Communications Letters*, 5(6), 684 – 687.

Clerckx, B. & Bayguzina, E. (2016). Waveform Design for Wireless Power Transfer. *IEEE Transactions on Signal Processing*, 64(23), 6313–6328.

Clerckx, B., Zhang, R., Schober, R., Ng, D. W. K., Kim, D. I. & Poor, H. V. (2019). Fundamentals of Wireless Information and Power Transfer: From RF Energy Harvester Models to Signal and System Designs. *IEEE Journal on Selected Areas in Communications*, 37(1), 4–33. Consulted at https://arxiv.org/abs/1803.07123.

Covic, G. A. & Boys, J. T. (2013). Inductive Power Transfer. *Proceedings of the IEEE*, 101(6), 1276–1289.

Diamantoulakis, P. D. & Karagiannidis, G. K. (2017). Maximizing Proportional Fairness in Wireless Powered Communications. *IEEE Wireless Communications Letters*, 6(2), 202 – 205.

Diamantoulakis, P. D., Pappi, K. N., Karagiannidis, G. K., Xing, H. & Nallanathan, A. (2017). Joint Downlink/Uplink Design for Wireless Powered Networks With Interference. *IEEE Access*, 5, 1534 – 1547.

Diamantoulakis, P. D., Karagiannidis, G. K. & Ding, Z. (2018). Simultaneous Lightwave Information and Power Transfer (SLIPT). *IEEE Transactions on Green Communications and Networking*, 2(3), 764–773.

Ding, Z., Krikidis, I., Sharif, B. & Poor, H. V. (2014). Wireless Information and Power Transfer in Cooperative Networks With Spatially Random Relays. *IEEE Transactions on Wireless Communications*, 13(8), 4440–4453.

Ericsson. (2017). *Mobile data traffic growth outlook*. Consulted at https://www.ericsson.com/en/mobility-report/reports/november-2017/mobile-data-traffic-growth-outlook.

Evangelista, J. V. C., Sattar, Z., Kaddoum, G. & Chaaban, A. (2019). Fairness and Sum-Rate Maximization via Joint Subcarrier and Power Allocation in Uplink SCMA Transmission. *IEEE Transactions on Wireless Communications*, 18(12), 5855–5867.

Fakidis, J., Videv, S., Kucera, S., Claussen, H. & Haas, H. (2016). Indoor Optical Wireless Power Transfer to Small Cells at Nighttime. *IEEE/OSA Journal of Lightwave Technology*, 34(13), 3236–3258.

Fehske, A., Fettweis, G., Malmodin, J. & Biczok, G. (2011). The global footprint of mobile communications: the ecological and economic perspective. *IEEE Communications Magazine*, 49(8), 55–62.

Fletscher, L. A., Suarez, L. A., Grace, D., Peroni, C. V. & Maestre, J. M. (2019). Energy-Aware Resource Management in Heterogeneous Cellular Networks With Hybrid Energy Sources. *IEEE Transactions on Network and Service Management*, 16(1), 279–293.

Fouladgar, A. & Simeone, O. (2012). On the Transfer of Information and Energy in Multi-User Systems. *IEEE Communications Letters*, 16(11), 1733–1736.

Fukushima, T. (2013). Precise and fast computation of Lambert W-functions without transcendental function evaluations. *Journal of Computational and Applied Mathematics*, 244, 77–89.

Ge, D., Jiang, X. & Ye, Y. (2011). A Note on the Complexity of Lp Minimization. *Mathematical Programming*, 129(2), 285–299.

Grant, M. & Boyd, S. (2009). *CVX: Matlab software for disciplined convex programming*.

Grover, P. & Sahai, A. (2010). Shannon meets Tesla: Wireless information and power transfer. *IEEE International Symposium on Information Theory Proceedings (ISIT)*, pp. 2363–2367.

Gupta, A. & Jha, R. K. (2015a). A Survey of 5G Network: Architecture and Emerging Technologies. *IEEE Access*, 3, 1206 – 1232.

Gupta, A. & Jha, R. K. (2015b). A Survey of 5G Network: Architecture and Emerging Technologies. *IEEE Access*, 3, 1206 – 1232.

Haas, H. (2017). LiFi is a paradigm-shifting 5G technology. *Reviews in Physics*, 3, 26-31.

Hande, A., Polk, T., Walker, W. & Bhatia, D. (2007). Indoor solar energy harvesting for sensor network router nodes. *Microprocessors and Microsystems*, 31(6), 420–432.

Henty, B. E. & Stancil, D. D. (2004). Multipath-enabled super-resolution for RF and microwave communication using phase-conjugate arrays. *Physical Review Letters*, 93(24), 243904.

Hernandez, M., Li, H.-B., Dotlic, I. & Miura, R. (2012). *Channel models for TG8*. Consulted at https://mentor.ieee.org/802.15/dcn/12/15-12-0459-06-0008-tg8-channel-models.doc.

Hossain, E. & Hasan, M. (2015). 5G Cellular: Key Enabling Technologies and Research Challenges. *IEEE Instrumentation and Measurement Magazine*, 18(3), 11–21.

Hossain, E., Rasti, M., Tabassum, H. & Abdelnasser, A. (2014). Evolution toward 5G multi-tier cellular wireless networks: An interference management perspective. *IEEE Wireless Communications Magazine*, 21(3), 118–127.

Iordache, M.-D., Bioucas-Dias, J. M. & Plaza, A. (2014). Collaborative Sparse Regression for Hyperspectral Unmixing. *IEEE Geoscience and Remote Sensing Letters*, 12(1), 341 – 354.

Jiang, R., Xiong, K., Fan, P., Zhang, Y. & Zhong, Z. (2017). Optimal design of SWIPT systems with multiple heterogeneous users under non-linear energy harvesting model. *IEEE Access*, 5, 11479 – 11489.

Jiang, Y., Zou, Y., Guo, H., Tsiftsis, T. A., Bhatnagar, M. R., de Lamare, R. C. & Yao, Y.-D. (2019). Joint Power and Bandwidth Allocation for Energy-Efficient Heterogeneous Cellular Networks. *IEEE Transactions on Communications*. early access.

Jo, H.-S., Mun, C., Moon, J. & Yook, J.-G. (2010). Self-Optimized Coverage Coordination in Femtocell Networks. *IEEE Transactions on Wireless Communications*, 9(10), 2977–2982.

Joeng, Y., Quek, T. Q. & Shin, H. (2011). Beamforming Optimization for Multiuser Two-Tier Networks. *Journal of Communications and Networks*, 13(4).

Ju, H. & Zhang, R. (2014a). Throughput Maximization for Wireless Powered Communication Networks. *IEEE Transactions Wireless Communications*, 13(1), 418–428.

Ju, H. & Zhang, R. (2014b). User Cooperation in Wireless Powered Communication Networks. *Proc. of IEEE Global Communications Conference (GLOBECOM)*, pp. 1430–1435.

Kaddoum, G., Tran, H.-V., Kong, L. & Atalla, M. (2017). Design of Simultaneous Wireless Information and Power Transfer Scheme for Short Reference DCSK Communication Systems. *IEEE Transactions on Communications*, 65(1), 431 – 443.

Kaiser, T. & Zheng, F. (2010). *Ultra-wideband Systems with MIMO*. Wiley.

Kamel, M., Hamouda, W. & Youssef, A. (2016). Ultra-Dense Networks: A Survey. *IEEE Communications Surveys & Tutorials*, 18(4).

Kashef, M., Ismail, M., Abdallah, M., Qaraqe, K. A. & Serpedin, E. (2016). Energy Efficient Resource Allocation for Mixed RF/VLC Heterogeneous Wireless Networks. *IEEE Journal on Selected Areas in Communications*, 34(4), 883 – 893.

Kavehrad, M. (2010). Sustainable Energy-Efficient Wireless Applications Using Light. *IEEE Communications Magazine*, 48(12), 66–73.

Kim, H., Hirayama, H., Kim, S., Han, K. J., Zhang, R. & Choi, J. (2017). Review of Near-Field Wireless Power and Communication for Biomedical Applications. *IEEE Access*, 5, 21264–21285.

Konecny, J., McMahan, H. B., Ramage, D. & Richtarik, P. (2016). Federated Optimization: Distributed Machine Learning for On-Device Intelligence. *CoRR abs/1610.02527*. Consulted at https://arxiv.org/pdf/1610.02527.pdf.

Krikidis, I., Sasaki, S., Timotheou, S. & Ding, Z. (2014a). A low complexity antenna switching for joint wireless information and energy transfer in MIMO relay channels. *IEEE Transactions on Communications*, 62(5), 1577–1587.

Krikidis, I., Timotheou, S., Nikolaou, S., Zheng, G., Ng, D. W. K. & Schober, R. (2014b). Simultaneous wireless information and power transfer in modern communication systems. *IEEE Communications Magazine*, 52(11), 104 –110.

Ku, M.-L., Li, W., Chen, Y. & Liu, K. J. R. (2016). Advances in Energy Harvesting Communications: Past, Present, and Future Challenges. *IEEE Communications Surveys & Tutorials*, 18(2), 1384 – 1412.

Kurs, A., Karalis, A., Moffatt, R., Joannopoulos, J. D., Fisher, P. & Soljacic, M. (2007). Wireless power transfer via strongly coupled magnetic resonances. *Science*, 317(5834), 83-86.

Lakshminarayana, S., Assaad, M. & Debbah, M. (2015). Transmit Power Minimization in Small Cell Networks Under Time Average QoS Constraints. *IEEE Journal on Selected Areas in Communications*, 33(10), 2087 – 2103.

Lapidoth, A., Moser, S. M. & Wigger, M. A. (2009). On the Capacity of Free-Space Optical Intensity Channels. *IEEE Transactions on Information Theory*, 55(10), 4449–4461.

Larimore, B. (2013). *LED Lighting and DC-DC Conversion Control Integrated on One C2000 Microcontroller* (Report n°SPRABR2).

Le, T., Kaddoum, G. & Shin, O. (2018). Joint Channel Resources Allocation and Beamforming in Energy Harvesting Systems. *IEEE Wireless Communications Letters*, 7(5), 884–887.

Le, T. A., Vien, Q.-T., Nguyen, H. X., Ng, D. W. K. & Schober, R. (2017). Robust Chance-Constrained Optimization for Power-Efficient and Secure SWIPT Systems. *IEEE Transactions on Green Communications and Networking*, 1(3), 333 - 346.

Lee, H., Lee, S., Lee, K., Kong, H. & Lee, I. (2015). Optimal Beamforming Designs for Wireless Information and Power Transfer in MISO Interference Channels. *IEEE Transactions on Wireless Communications*, 14(9), 4810–4821.

Li, C., Jia, W., Tao, Q. & Sun, M. (2011). Solar Cell Phone Charger Performance in Indoor Environment. *IEEE 37th Annual Northeast Bioengineering Conference (NEBEC)*, pp. 1–2.

Liu, L., Zhang, R. & Chua, K.-C. (2013). Wireless Information Transfer with Opportunistic Energy Harvesting. *IEEE Transactions on Wireless Communications*, 12(1), 288–300.

Liu, L., Zhang, R. & Chua, K.-C. (2014). Multi-Antenna Wireless Powered Communication With Energy Beamforming. *IEEE Transactions on Communications*, 62(12), 4349–4361.

Liu, M., Xiong, M., Deng, H., Liu, Q., Wu, J. & Xia, P. (2018). Mobile Energy Internet. *arXiv*. Consulted at https://arxiv.org/abs/1802.01570.

Liu, Q., Wu, J., Xia, P., Zhao, S., Chen, W., Yang, Y. & Hanzo, L. (2016). Charging Unplugged: WillDi stributed Laser Charging for Mobile Wireless Power Transfer Work ? *IEEE Vehicular Technology Magazine*, 2(4), 36–45.

Liu, Y., Zhang, Y., Yu, R. & Xie, S. (2015). Integrated energy and spectrum harvesting for 5G wireless communications. *IEEE Network*, 29(3), 75–81.

Liu, Z., Zhang, P., Chan, K. Y., Ma, K. & Li, L. (2019). Robust Power Allocation for Femtocell Networks Using Fuzzy Estimation of Dynamic Channel States. *IEEE Access*, 7, 22872 – 22883.

Lopez-Perez, D., Chu, X., Vasilakos, A. V. & Claussen, H. (2014). Power Minimization Based Resource Allocation for Interference Mitigation in OFDMA Femtocell Networks. *IEEE Journal on Selected Areas in Communications*, 32(2), 333 – 344.

Lu, X., Wang, P., Niyato, D., Kim, D. I. & Han, Z. (2016). Wireless Charging Technologies: Fundamentals, Standards, and Network Applications. *IEEE Communications Surveys Tutorials*, 18(2), 1413–1452.

Lu, X., Niyato, D., Wang, P., Kim, D. I. & Han, Z. (2015a). Wireless charger networking for mobile devices: fundamentals, standards, and applications. *IEEE Wireless Communications*, 22(2), 126–135.

Lu, X., Wang, P., D., N., Kim, D. I. & Han, Z. (2015b). Wireless Networks With RF Energy Harvesting: A Contemporary Survey. *IEEE Communications Surveys & Tutorials*, 17(2), 757–789.

Ma, H., Lampe, L. & Hranilovic, S. (2015). Coordinated Broadcasting for Multiuser Indoor Visible Light Communication Systems. *IEEE Transactions on Communications*, 63(9), 3313–3324.

Maaz, M., Helard, M., Mary, P. & Liu, M. (2015, May). Performance Analysis of Time-Reversal Based Precoding Schemes in MISO-OFDM Systems. *Proc. IEEE 81st Vehicular Technology Conference (VTC Spring)*, pp. 1–6.

Marler, R. & Arora, J. (2004). Survey of multi-objective optimization methods for engineering. *Structural and Multidisciplinary Optimization*, 26, 369–395.

Mateu, L., Codrea, C., Lucas, N., Pollak, M. & Spies, P. (2006). Energy harvesting for wireless communication systems using thermogenerators. *Proc. of the XXI Conference on Design of Circuits and Integrated Systems (DCIS)*, pp. 22–24.

Mathews, I., King, P. J., Stafford, F. & Frizzell, R. (2016). Performance of III-V Solar Cells as Indoor Light Energy Harvesters. *IEEE J. of Photovoltaics*, 6(1), 230–235.

Miettinen, A. P. & Nurminen, J. K. (2010, Jun.). Energy Efficiency of Mobile Clients in Cloud Computing. *Proceedings of the 2nd USENIX conference on Hot topics in cloud computing (USENIX HotCloud'10)*.

Mishra, D., De, S. & Krishnaswamy, D. (2017). Dilemma at RF Energy Harvesting Relay: Downlink Energy Relaying or Uplink Information Transfer? *IEEE Transactions on Wireless Communications*, 16(8), 4939 – 4955.

Morsi, R., Michalopoulos, D. S. & Schober, R. (2015). Multi-User Scheduling Schemes for Simultaneous Wireless Information and Power Transfer Over Heterogeneous Fading Channels. *IEEE Transactions on Wireless Communications*, 14(4), 1967 –1982.

Mossaad, M. S. A., Hranilovic, S. & Lampe, L. (2015). Visible Light Communications Using OFDM and Multiple LEDs. *IEEE Transactions on Communications*, 63(11), 4304–4313.

Nasir, A. A., Zhou, X., Durrani, S. & Kennedy, R. A. (2013). Relaying protocols for wireless energy harvesting and information processing. *IEEE Transactions on Wireless Communications*, 12(7), 3622–3636.

Nasiri, A., Zabalawi, S. A. & Mandic, G. (2009). Indoor Power Harvesting using Photovoltaic Cells for Low-Power Applications. *IEEE Transactions on Industrial Electronics*, 56(11), 4502–4509.

Ng, D. W. K. & Schober, R. (2015). Secure and Green SWIPT in Distributed Antenna Networks With Limited Backhaul Capacity. *IEEE Transactions on Wireless Communications*, 14(9), 5082–5097.

Ng, D. W. K., Lo, E. S. & Schober, R. (2016). Multiobjective Resource Allocation for Secure Communication in Cognitive Radio Networks With Wireless Information and Power Transfer. *IEEE Transactions on Vehicular Technology*, 65(5), 3166 – 3184.

Ng, D., Lo, E. & Schober, R. (2014). Robust Beamforming for Secure Communication in Systems With Wireless Information and Power Transfer. *IEEE Transactions on Wireless Communications*, 13(8), 4599–4615.

Nguyen, D., Le, L. B. & Le-Ngoc, T. (2015). Multiuser Admission Control and Beamforming Optimization Algorithms for MISO Heterogeneous Networks. *IEEE Access*, 3, 759–773.

Nguyen, H. T., Pedersen, J., Kyritsi, P. & Eggers, P. (2006). Time reversal in wireless communications: a measurement based investigation. *IEEE Transactions on Wireless Communications*, 5(8), 2242–2252.

Niyato, D., Kim, D. I., Maso, M. & Han, Z. (2017). Wireless Powered Communication Networks: Research Directions and Technological Approaches. *IEEE Wireless Communications*, 24(6), 88–97.

Niyato, D., Kim, D. I., Maso, M. & Han, Z. (2017). Wireless Powered Communication Networks: Research Directions and Technological Approaches. *IEEE Wireless Communications Magazine*, 24(6), 88 – 97.

Ozel, O., Shahzad, K. & Ulukus, S. (2014). Optimal Energy Allocation for Energy Harvesting Transmitters With Hybrid Energy Storage and Processing Cost. *IEEE Transactions on Signal Processing*, 62(12), 3232–3245.

Pan, G., Ye, J. & Ding, Z. (2017). Secure Hybrid VLC-RF Systems With Light Energy Harvesting. *IEEE Transactions on Communications*, 65(10), 4348 – 4359.

Parlett, B. N. (1998). *The symmetric eigenvalue problem*. NJ, USA: Prentice-Hall, Inc. Upper Saddle River.

Pathak, P. H., Feng, X., Hu, P. & Mohapatra, P. (2015). Visible Light Communication, Networking, and Sensing: A Survey, Potential and Challenges. *IEEE Communications Surveys & Tutorials*, 17(4), 2047 – 2077.

Peel, C., Hochwald, B. & Swindlehurst, A. (2005). A vector-perturbation technique for near-capacity multiantenna multiuser communication-part I: channel inversion and regularization. *IEEE Transactions on Communications*, 53(1), 195–202.

Peng, M., Zhang, K., Jiang, J., Wang, J. & Wang, W. (2015). Energy-Efficient Resource Assignment and Power Allocation in Heterogeneous Cloud Radio Access Networks. *IEEE Transactions on Vehicular Communications*, 64(11), 5275 – 5287.

Pitarokoilis, A., Mohammed, S. & Larsson, E. (2015). Uplink Performance of Time-Reversal MRC in Massive MIMO Systems Subject to Phase Noise. *IEEE Transactions on Wireless Communications*, 14(2), 711–723.

Popovski, P., Fouladgar, A. & Simeone, O. (2013). Interactive Joint Transfer of Energy and Information. *IEEE Transactions on Communications*, 61(5), 2086–2097.

Press, W. H., Teukolsky, S. A., Vetterling, W. T. & Flannery, B. P. (2007). *Numerical Recipes 3rd Edition: The Art of Scientific Computing*. New York: Cambridge University Press.

Raghunathan, V., Kansal, A., Hsu, J., Friedman, J. & Srivastava, M. (2005, April). Design Considerations for Solar Energy Harvesting Wireless Embedded Systems. *Fourth International Symposium on Information Processing in Sensor Networks*, pp. 457–462.

Rakia, T., Yang, H.-C., Gebali, F. & Alouini, M.-S. (2016). Optimal Design of Dual-Hop VLC/RF Communication System With Energy Harvesting. *IEEE Communications Letters*, 20(10), 1979 – 1982.

Rappaport, T. & Sandhu, S. (1994). Radio-wave propagation for emerging wireless personal-communication systems. *IEEE Antennas and Propagation Magazine*, 36(5), 14–24.

Rozé, A., Hélard, M., Crussière, M. & Langlais, C. (2015). Linear Precoder Performance for Massive MIMO Systems in near LOS Environments: Application to mmWave Transmission. *Proc. of 21th European Wireless Conference*, pp. 1–6.

Saad, W., Bennis, M. & Chen, M. (2019). A Vision of 6G Wireless Systems: Applications, Trends, Technologies, and Open Research Problems. *arXiv*.

Salman, E., Stanaćević, M., Das, S. & Djurić, P. M. (2018). Leveraging RF Power for Intelligent Tag Networks. *Proceedings of the 2018 on Great Lakes Symposium on VLSI*, (GLSVLSI '18), 329–334.

Sha, F., Lin, Y., Saul, L. K. & Lee, D. D. (2007). Multiplicative Updates for Nonnegative Quadratic Programming. *Journal Neural Computation*, 19(8), 2004 – 2031.

Shenck, N. & Paradiso, J. (2001). Energy Scavenging with Shoe-mounted Piezoelectrics. *IEEE Micro*, 21(3), 30–42.

Shi, Q., Liu, L., Xu, W. & Zhang, R. (2014). Joint transmit beamforming and receive power splitting for MISO SWIPT systems. *IEEE Transactions on Wireless Communications*, 13(6), 3269–3280.

Siaud, I., Ulmer-Moll, A.-M., Bouzigues, M.-A. & Cassiau, N. (2015, 4-7 Oct). Adaptive and Spatial Processing for Millimeter Wave Backhaul Architectures. *Proc. IEEE International Conference on Ubiquitous Wireless Broadband (ICUWB)*.

Sorrell, S. (2018). *The Internet of Things: Consumer, Industrial & Public Services 2018-2023*. Juniper. Consulted at https://www.juniperresearch.com/press/press-releases/iot-connections-to-grow-140-to-hit-50-billion.

Starner, T. (1996). Human-powered Wearable Computing. *IBM Systems Journal*, 35(3–4), 618–629.

Sun, Y., Ng, D. W. K., Zhu, J. & Schober, R. (2016). Multi-Objective Optimization for Robust Power Efficient and Secure Full-Duplex Wireless Communication Systems. *IEEE Transactions on Wireless Communications*, 15(8), 5511 – 5526.

Tabassum, H. & Hossain, E. (2018). Coverage and Rate Analysis for Co-Existing RF/VLC Downlink Cellular Networks. *IEEE Transactions on Wireless Communications*, 16(4), 2588 – 2601.

Tabassum, H., Hossain, E., Ogundipe, A. & Kim, D. I. (2015). Wireless-Powered Cellular Networks: Key Challenges and Solution Techniques. *IEEE Communications Magazine*, 53(6), 63 – 71.

Taneja, J., Jeong, J. & Culler, D. (2008). Design, Modeling, and Capacity Planning for Micro-solar Power Sensor Networks. *Proc. 7th International Conference on Information Processing in Sensor Networks*, pp. 407–418.

Timotheou, S., Krikidis, I., Zheng, G. & Ottersten, B. (2014). Beamforming for MISO Interference Channels with QoS and RF Energy Transfer. *IEEE Transactions on Wireless Communications*, 13(5), 2646–2658.

Timotheou, S., Krikidis, I., Karachontzitis, S. & Berberidis, K. (2015). Spatial Domain Simultaneous Information and Power Transfer for MIMO Channels. *IEEE Transactions on Wireless Communications*, 14(8), 4115–4128.

Tolli, A., Pennanen, H. & Komulainen, P. (2011). Decentralized Minimum Power Multi-Cell Beamforming with Limited Backhaul Signaling. *IEEE Transactions on Wireless Communications*, 10(2), 570–580.

Torfs, T., Sterken, T., Brebels, S., Santana, J., van den Hoven, R., Spiering, V., Bertsch, N., Trapani, D. & Zonta, D. (2013). Low power wireless sensor network for building monitoring. *IEEE Sensors Journal*, 13(3), 909–915.

Tran, H.-V. & Kaddoum, G. (2018a). RF Wireless Power Transfer: Regreening Future Networks. *IEEE Potentials*, 37(2), 35 – 41.

Tran, H.-V. & Kaddoum, G. (2018b, Apr.). Green Cell-less Design for RF-Wireless Power Transfer Networks. *Proc. of IEEE Wireless Communications and Networking Conference (WCNC)*, pp. 1–6.

Tran, H. V. & Kaddoum, G. (2019). Robust Design of AC Computing-enabled Receiver Architecture for SWIPT Networks. *IEEE Wireless Communications Letters*, 8(3), 801–804.

Tran, H.-V., Kaddoum, G., Tran, H. & Hong, E.-K. (2017). Downlink Power Optimization for Heterogeneous Networks with Time Reversal-based Transmission under Backhaul Limitation. *IEEE Access*, 5, 755 – 770.

Tran, H.-V., Kaddoum, G. & Truong, K. T. (2018). Resource Allocation in SWIPT Networks Under a Nonlinear Energy Harvesting Model: Power Efficiency, User Fairness, and Channel Nonreciprocity. *IEEE Transactions on Vehicular Technology*, 67(9), 8466 – 8480.

Tran, N. H., Bao, W., Zomaya, A., Nguyen, M. N. H. & Hong, C. S. (2019, 29 April - 2 May). Federated Learning over Wireless Networks: Optimization Model Design and Analysis. *IEEE International Conference on Computer Communications (INFOCOM)*.

Tran-Ha, V., Vu, Q.-D. & Hong, E.-K. (2015). Time Reversal-Based Transmissions with Distributed Power Allocation for Two-Tier Networks. *Proc. of IEEE 29th International Conference on Advanced Information Networking and Applications Workshops (WAINA)*, pp. 181–186.

Trott, M. (2007). *The Mathematica guidebook for symbolics*. Springer Science & Business Media.

Tuan, P. V. & Koo, I. (2017). Optimal Multiuser MISO Beamforming for Power-Splitting SWIPT Cognitive Radio Networks. *IEEE Access*, 5, 14141 – 14153.

Ulukus, S., Yener, A., Erkip, E., Simeone, O., Zorzi, M., Grover, P. & Huang, K. (2015). Energy Harvesting Wireless Communications: A Review of Recent Advances. *IEEE Journal on Selected Areas in Communications*, 33(3), 360–381.

Upton, G. & Cook, I. (2014). *A Dictionary of Statistics* (ed. third). Oxford University Press.

Varshney, L. (2008). Transporting information and energy simultaneously. *Information Theory, 2008. ISIT 2008. IEEE International Symposium on*, pp. 1612–1616.

Venturino, L., Zappone, A., Risi, C. & Buzzi, S. (2015). Energy-Efficient Scheduling and Power Allocation in Downlink OFDMA Networks With Base Station Coordination. *IEEE Transactions on Wireless Communications*, 14(1), 1–14.

Vieira, J., Rusek, F. & Tufvesson, F. (2014, December). Reciprocity calibration methods for massive MIMO based on antenna coupling. *IEEE Global Communications Conference*.

Vijayaraghavan, K. & Rajamani, R. (2007, July). Active Control based Energy Harvesting for Battery-less Wireless Traffic Sensors: Theory and Experiments. *Proc. of American Control Conference*, pp. 4579–4584.

Visser, H. & Vullers, R. (2013). RF Energy Harvesting and Transport for Wireless Sensor Network Applications: Principles and Requirements. *Proceedings of the IEEE*, 101(6), 1410–1423.

Viteri-Mera, C. A., Teixeira, F. L. & Sainath, K. (2015). Interference-Nulling Time-Reversal Beamforming for mm-Wave Massive MIMO Systems. *Proc. IEEE Int. Conf. Microw., Commun., Antennas Electron. Syst. (COMCAS)*, pp. 1–5.

Viteri-Mera, C. A. & Teixeira, F. L. (2016). Space-Time Block Diagonalization for Frequency-Selective MIMO Broadcast Channels. *IEEE Access*, 4, 6602–6613.

Vu, Q.-D., Tran, L.-N., Farrell, R. & Hong, E.-K. (2016). Energy-Efficient Zero-Forcing Precoding Design for Small-cell Networks. *IEEE Transactions on Communications*, 64(2), 790 – 804.

Wan, T., Karimi, Y., Stanacevic, M. & Salman, E. (2017). Perspective Paper–Can AC Computing Be an Alternative for Wirelessly Powered IoT Devices? *IEEE Embedded Systems Letters*, 9(1), 13–16.

Wan, T., Karimi, Y., Stanacevic, M. & Salman, E. (2019). AC Computing Methodology for RF-Powered IoT Devices. *IEEE Transactions on Very Large Scale Integration (VLSI) Systems*, 27(5), 1017–1028.

Wang, Z., Tsonev, D., Videv, S. & Haas, H. (2015). On the Design of a Solar-Panel Receiver for Optical Wireless Communications with Simultaneous Energy Harvesting. *IEEE Journal on Selected Areas in Communications*, 33(8), 1612–1623.

Wu, Q., Li, G. Y., Chen, W., Ng, D. W. K. & Schober, R. (2017). An Overview of Sustainable Green 5G Networks. *IEEE Wireless Communications*, 24(4), 72–80.

Xiong, K., Wang, B. & Liu, K. J. R. (2017). Rate-energy region of SWIPT for MIMO broadcasting under nonlinear energy harvesting model. *IEEE Transactions on Wireless Communications*, 16(8), 5147 – 5161.

Xu, Z., Yang, C., Li, G., Liu, Y. & Xu, S. (2014). Energy-efficient CoMP precoding in heterogeneous networks. *IEEE Transactions on Signal Processing*, 62(4), 1005–1017.

Yang, Q., Liu, Y., Chen, T. & Tong, Y. (2019). Federated Machine Learning: Concept and Applications. *ACM Transactions on Intelligent Systems and Technology*, 10(2), Article 12. 19 pages.

Yang, Y.-H., Wang, B., Lin, W. & Liu, K. (2013). Near-Optimal Waveform Design for Sum Rate Optimization in Time-Reversal Multiuser Downlink Systems. *IEEE Transactions on Wireless Communications*, 12(1), 346–357.

Yoon, E., Kim, S.-Y. & Yun, U. (2015). A Time-Reversal-Based Transmission Using Predistortion for Intersymbol Interference Alignment. *IEEE Transactions on Communications*, 63(2), 455–465.

Young, W. H. (1912). On the multiplication of successions of fourier constants. *Proc. Roy. Soc. Lond. Series A*, 87, 331–339.

Zahir, T., Arshad, K., Nakata, A. & Moessner, K. (2013). Interference management in femtocells. *IEEE Communications Surveys & Tutorials*, 15(1), 293–311.

Zeng, Y. & Zhang, R. (2016). Full-Duplex Wireless-Powered Relay With Self-Energy Recycling. *IEEE Wireless Commun. Lett.*, 4(2), 201–204.

Zhang, H., Jiang, C., Hu, R. Q. & Qian, Y. (2016). Self-Organization in Disaster-Resilient Heterogeneous Small Cell Networks. *IEEE Network*, 116–122.

Zhang, R. & Ho, C. K. (2013). MIMO Broadcasting for Simultaneous Wireless Information and Power Transfer. *IEEE Transactions on Wireless Communications*, 12(5), 1989–2001.

Zhang, Z., Zhang, H., Zhao, Z., Liu, H., Wen, X. & Jing, W. (2013). Low complexity energy-efficient resource allocation in downlink dense femtocell networks. *Proc. IEEE 24th Int. Symp. on PIMRC*.

Zhou, X. (2014). Training-Based SWIPT: Optimal Power Splitting at the Receiver. *IEEE Transactions on Vehicular Technology*, 64(9), 4377–4382.

Zhou, X., Zhang, R. & Ho, C. K. (2013). Wireless Information and Power Transfer: Architecture Design and Rate-Energy Tradeoff. *IEEE Transactions on Communications*, 61(11), 4754–4767.